# Advances in Clinical and Experimental Medicine

MONTHLY ISSN 1899-5276 (PRINT) ISSN 2451-2680 (ONLINE) advances.umw.edu.pl

2024, Vol. 33, No. 3 (March)

Impact Factor (IF) – 2.1
Ministry of Science and Higher Education – 70 pts
Index Copernicus (ICV) – 161.11 pts

Wroclaw Medical University

Advances
in Clinical and Experimental
Medicine

# Advances
# in Clinical and Experimental Medicine

ISSN 1899-5276 (PRINT) ISSN 2451-2680 (ONLINE) advances.umw.edu.pl

**MONTHLY 2024**
**Vol. 33, No. 3**
**(March)**

Advances in Clinical and Experimental Medicine (*Adv Clin Exp Med*) publishes high-quality original articles, research-in-progress, research letters and systematic reviews and meta-analyses of recognized scientists that deal with all clinical and experimental medicine.

**Editorial Office**
ul. Marcinkowskiego 2–6
50-368 Wrocław, Poland
Tel.: +48 71 784 12 05
E-mail: redakcja@umw.edu.pl

**Publisher**
Wroclaw Medical University
Wybrzeże L. Pasteura 1
50-367 Wrocław, Poland

Online edition is the original version of the journal

## Editorial Policy

Advances in Clinical and Experimental Medicine (Adv Clin Exp Med) is an independent multidisciplinary forum for exchange of scientific and clinical information, publishing original research and news encompassing all aspects of medicine, including molecular biology, biochemistry, genetics, biotechnology and other areas. During the review process, the Editorial Board conforms to the "Uniform Requirements for Manuscripts Submitted to Biomedical Journals: Writing and Editing for Biomedical Publication" approved by the International Committee of Medical Journal Editors (www.ICMJE.org). The journal publishes (in English only) original papers and reviews. Short works considered original, novel and significant are given priority. Experimental studies must include a statement that the experimental protocol and informed consent procedure were in compliance with the Helsinki Convention and were approved by an ethics committee.

For all subscription-related queries please contact our Editorial Office: redakcja@umw.edu.pl
For more information visit the journal's website: advances.umw.edu.pl

Pursuant to the ordinance of the Rector of Wroclaw Medical University No. 12/XVI R/2023, from February 1, 2023, authors are required to pay a fee for each manuscript accepted for publication in the journal Advances in Clinical and Experimental Medicine. The fee amounts to 990 EUR for original papers and meta-analyses, 700 EUR for reviews, and 350 EUR for research-in-progress (RIP) papers and research letters.

Advances in Clinical and Experimental Medicine has received financial support from the resources of Ministry of Science and Higher Education within the "Social Responsibility of Science – Support for Academic Publishing" project based on agreement No. RCN/SP/0584/2021.

Ministry of Education and Science
Republic of Poland

Czasopismo Advances in Clinical and Experimental Medicine korzysta ze wsparcia finansowego ze środków Ministerstwa Edukacji i Nauki w ramach programu „Społeczna Odpowiedzialność Nauki – Rozwój Czasopism Naukowych" na podstawie umowy nr RCN/SP/0584/2021.

Ministerstwo
Edukacji i Nauki

Indexed in: MEDLINE, Science Citation Index Expanded, Journal Citation Reports/Science Edition, Scopus, EMBASE/Excerpta Medica, Ulrich's™ International Periodicals Directory, Index Copernicus

Typographic design: Piotr Gil, Monika Kolęda
DTP: Wydawnictwo UMW
Cover: Monika Kolęda
Printing and binding: PRINT PROFIT Sp. z o.o., Koźmin 27, 59-900 Zgorzelec

Advances
in Clinical and Experimental Medicine

MONTHLY 2024, Vol. 33, No. 3 (March)

ISSN 1899-5276 (PRINT)
ISSN 2451-2680 (ONLINE)
advances.umw.edu.pl

# Contents

# The association between hypoglycemia and mortality in sepsis and septic shock: A systematic review and meta-analysis

Yuping Shao[1,A,D,F], Feng Shao[2,B,C,F], Jie Zhou[1,B,C,F], Shunjin Fang[1,B,C,F], Jianfeng Zhu[1,B,C,F], Fangfang Li[3,E,F]

[1] Department of Critical Care Medicine, Huzhou Third Municipal Hospital, Affiliated Hospital of Huzhou University, China
[2] Department of Rheumatology, Huzhou Third Municipal Hospital, Affiliated Hospital of Huzhou University, China
[3] Department of Hospital Infection Management, Huzhou Traditional Chinese Medicine Hospital Affiliated to Zhejiang Chinese Medical University, China

A – research concept and design; B – collection and/or assembly of data; C – data analysis and interpretation;
D – writing the article; E – critical revision of the article; F – final approval of the article

Advances in Clinical and Experimental Medicine, ISSN 1899–5276 (print), ISSN 2451–2680 (online) *Adv Clin Exp Med*. 2024;33(3):197–205

**Address for correspondence**
Fangfang Li
E-mail: lff13587201430@163.com

**Funding sources**
None declared

**Conflict of interest**
None declared

Received on August 24, 2022
Reviewed on April 21, 2023
Accepted on May 30, 2023

Published online on June 30, 2023

## Abstract

Over 48 million cases of sepsis and 11 million sepsis-related deaths were reported in 2017, making it one of the leading causes of mortality. This meta-analysis compared mortality risk among patients with sepsis or septic shock and associated hypoglycemia or euglycemia on admission by searching for observational studies in PubMed, Embase and Scopus databases. The eligible studies included patients with sepsis and/or severe sepsis/septic shock and compared mortality rates between those with hypoglycemia on admission and those who were euglycemic. A stratified analysis based on sepsis or severe sepsis/septic shock and diabetes on admission included 14 studies. Patients with hypoglycemia had a significantly higher risk of in-hospital mortality and mortality during the 1st month after discharge. In addition, hypoglycemic patients with sepsis had a slightly increased risk of in-hospital mortality, but no increase in the mortality risk was observed within 1 month of follow-up. However, in patients with severe sepsis and/or septic shock, hypoglycemia was associated with a higher risk of both in-hospital mortality and mortality during 1 month of follow-up. In patients with diabetes, hypoglycemia was not associated with an increased risk of in-hospital mortality or mortality within 1 month of follow-up. Patients with sepsis or severe sepsis/septic shock and hypoglycemia had an increased mortality risk, and the association was stronger in cases of severe sepsis/septic shock. Hypoglycemia in diabetic patients did not correlate with increased mortality risk. Careful monitoring of blood glucose in sepsis and/or severe sepsis/septic shock patients is required.

**Key words:** sepsis, severe sepsis, septic shock, blood glucose, hypoglycemia, mortality, meta-analysis

**Cite as**
Shao Y, Shao F, Zhou J, Fang S, Zhu J, Li F. The association between hypoglycemia and mortality in sepsis and septic shock: A systematic review and meta-analysis. *Adv Clin Exp Med*. 2024;33(3):197–205. doi:10.17219/acem/166656

**DOI**
10.17219/acem/166656

# Introduction

Over 48 million cases of sepsis and 11 million sepsis-related deaths were reported in 2017, making it one of the leading causes of mortality.[1] Data from Europe, North America and Australia show that 30-day and 90-day mortality rates due to sepsis were 25% and 32%, respectively.[2] The highest sepsis burden and related mortality were found in Sub-Saharan Africa and Southeast Asia.[1]

Due to changes in endocrinal metabolism, patients with sepsis and/or septic shock have fluctuations in blood glucose levels that negatively impact the internal milieu and worsen their clinical condition.[3,4] Sepsis is associated with higher levels of oxidative stress and the secretion of interleukin (IL)-1, IL-6 and tumor necrosis factor alpha (TNF-α) by inflammatory cells. This, in turn, damages pancreatic β-cells,[3–5] affects the production of insulin, and leads to a state of stress hyperglycemia.[5] Hyperglycemia may result in several complications, such as increased predisposition to infections, oxidative stress and increased mortality risk.[6,7] However, studies have also indicated that patients with sepsis and/or septic shock are at an increased risk of hypoglycemia,[5,8] though its mechanisms are still unclear. Some studies suggest that the increased utilization of peripheral glucose, depletion of glycogen reserves, reduction in gluconeogenesis, and a comparatively decreased nutrient supply may play a role in sepsis-induced hypoglycemia.[5,9,10] Another crucial contributor could be the strict measures for blood glucose control in such patients.[11]

The effect of hypoglycemia on the survival of patients with sepsis is still unclear. Although studies have examined the impact of hypoglycemia on the mortality of these patients, only a few have summarized the available data.[12,13] A meta-analysis by Wang et al. pooled findings from 5 studies and found increased mortality in patients with decreased blood glucose levels.[12] Recently, several new studies provided updated clinical evidence, and these findings should also be considered.

# Objectives

The primary objective of this meta-analysis was to synthesize evidence from available studies to estimate the risk of mortality in patients with sepsis and/or septic shock and associated hypoglycemia at the time of hospital admission.

# Materials and methods

## Database search and strategy

We searched PubMed, Embase and Scopus databases for English-language papers published until April 30, 2022, using the following key words: ("hypoglycaemia" OR "hypoglycemia" OR "low blood glucose" OR "low blood sugar") AND ("sepsis" OR "severe sepsis" OR "septic shock" OR "septicemia") AND ("mortality" OR "death" OR "survival"). We based our review on Preferred Reporting Items for Systematic Reviews and Meta-Analyses (PRISMA) guidelines,[14] and the paper was registered at PROSPERO with the number CRD42022336895.

## Study selection criteria and process

Observational studies with either retrospective or prospective designs concerning subjects with sepsis and/or severe sepsis/septic shock were considered. Furthermore, the analyzed studies had to compare the mortality risk among patients with hypoglycemia or euglycemia at the time of hospital admission. We excluded case reports and review articles, as well as studies that did not have the exposure of interest (blood glucose assessment at the time of admission) or did not compare the risk of mortality between hypoglycemic and euglycemic patients.

After removing duplicates, the list of potentially eligible studies was screened by 2 independent reviewers following pre-defined inclusion and exclusion criteria. The articles that met the inclusion criteria were subject to a full-text assessment. Any disagreements between the 2 reviewers were resolved by discussion. The bibliography of the included studies was thoroughly screened for additional relevant publications. The study selection process is shown in Fig. 1.

## Data extraction and statistical analysis

We used a pretest data extraction sheet to fill in relevant data from the included studies. The data extraction process was carried out independently by 2 authors. The quality of the studies was assessed using the Newcastle-Ottawa Quality Assessment Scale for observational studies.[15] Statistical analysis employed STATA software v. 16.0 (StataCorp LLC, College Station, USA). The pooled effect sizes and 95% confidence intervals (95% CIs) were reported as odds ratios (ORs). The selection of the final analytical model was based on the observed $I^2$ value (used to denote the degree of heterogeneity). We used a random effects model for outcomes with $I^2 > 40\%$, and a fixed effects model was used for $I^2 \leq 40\%$.[16] Egger's test assessed publication bias.[17] Wherever reported, we considered a p-value of less than 0.05 to denote statistical significance. We used the method reported by Chyou to calculate the p-value for the reported pooled effect sizes in the meta-analysis.[18] First, we calculated the standardized z statistic using the following formula: z = (b/sb), where b = log (OR) and sb = ln (upper confidence limit/OR)/1.96. Second, we derived p-values corresponding to the obtained z-statistic and reported the z-statistic and its corresponding p-value in the results. A subgroup analysis based on the clinical condition studied, i.e., sepsis or severe sepsis/septic shock, as well as the presence or absence of diabetes on admission, was also carried out.

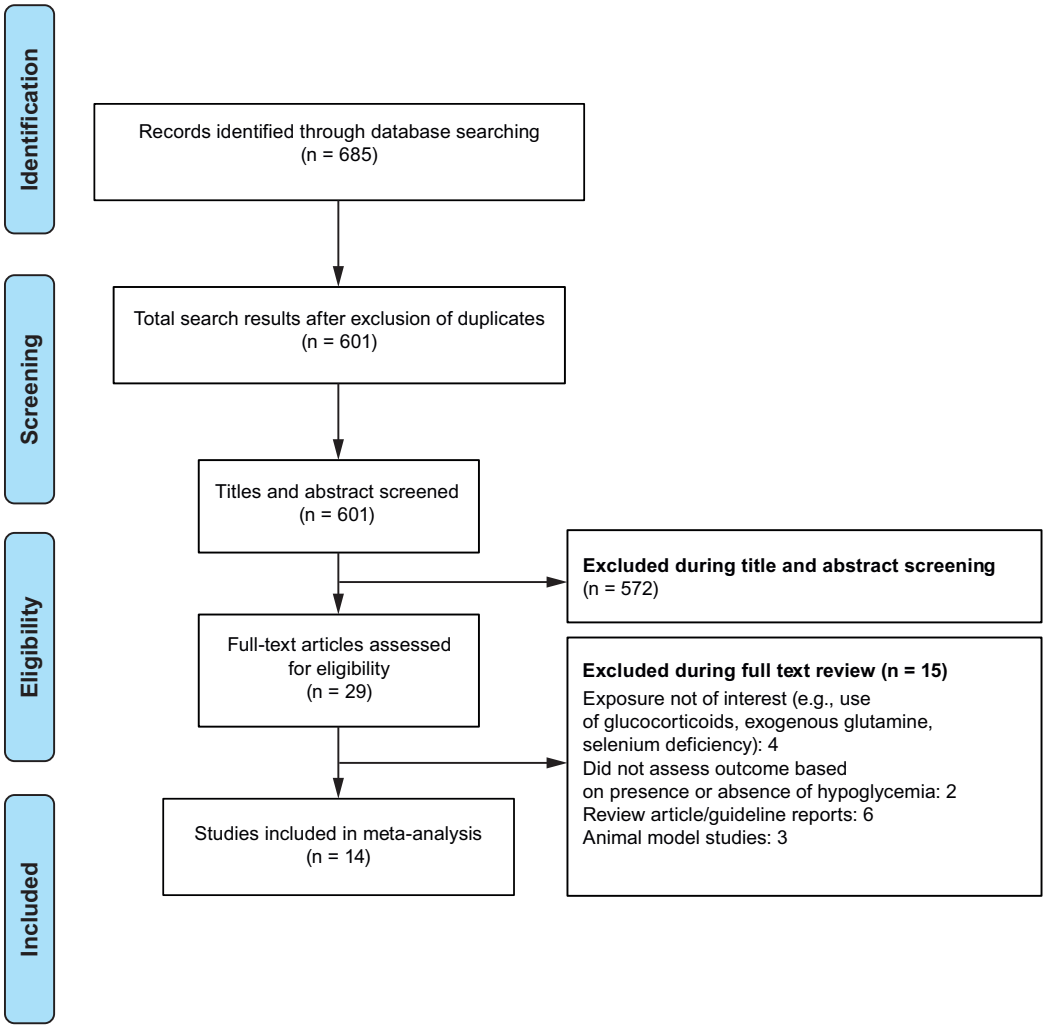


**Fig. 1.** The selection process of the studies included in the review

## Results

A total of 14 studies were selected for this meta-analysis.[19–32] The specific details of the included studies are summarized in Table 1. All studies were observational, including 12 retrospective and 2 prospective in design. Three studies were conducted in Japan and Australia. Two studies were from Taiwan and the USA, and China, Uganda and South Korea conducted 1 study each. Eight studies included patients with severe sepsis and/or septic shock, and 6 included patients with sepsis. There was a difference in the operational definition adopted for the classification of hypoglycemia

**Table 1.** Characteristics of the studies included in the meta-analysis

| Author, year, reference | Study design | Country | Characteristics of the participants | Operational definition for hypoglycemia | Sample size | Outcome (mortality) (hypoglycemia compared to euglycemia) |
|---|---|---|---|---|---|---|
| Furukawa et al. (2019)[19] | retro-spective | Japan | patients included in the study had sepsis; mean age: 74 years; males: 61%; infection focus (pneumonitis: 53%; pyelonephritis: 16%) | blood glucose on admission: <80 mg/dL | 336 | in-hospital: OR: 3.50 (95% CI: 1.78–6.94) |
| Mitsuyama et al. (2022)[20] | retro-spective | Japan | patients included in the study had sepsis; median age: 71 years; males: 63%; infection focus (lung: 38%; abdomen: 23%; skin and soft tissue: 17%); pre-existing diabetes: 26%, hypertension: 34% | blood glucose on admission: ≤70 mg/dL | 265 | day 28: OR: 12.18 (95% CI: 4.35–34.2) |
| Wei et al. (2021)[21] | retro-spective | China | patients included in the study had sepsis; mean age: approx. 65 years; males: 55%; hypertension: 30%, chronic heart disease: 10%, chronic kidney disease: 13% | blood glucose on admission: <70 mg/dL | 2948 | day 30: OR: 1.91 (95% CI: 1.35–2.72); with diabetes on admission, day 30: OR: 1.40 (95% CI: 0.86–2.29) |

Table 1. Characteristics of the studies included in the meta-analysis – cont.

| Author, year, reference | Study design | Country | Characteristics of the participants | Operational definition for hypoglycemia | Sample size | Outcome (mortality) (hypoglycemia compared to euglycemia) |
|---|---|---|---|---|---|---|
| Chan et al. (2016)[22] | retrospective | Taiwan | patients included in the study had severe sepsis; median age: approx. 74 years; males: 79%; primary reason for sepsis (pneumonia: 83%); mean APACHE II score: 27 | blood glucose on admission: <80 mg/dL | 127 | in-hospital: OR: 3.60 (95% CI: 1.24–10.50) day 14: OR: 6.81 (95% CI: 2.43–19.1) with diabetes on admission, day 14: OR: 0.70 (95% CI: 0.10–4.87) |
| Schuetz et al. (2011)[23] | prospective | USA | majority of patients included in the study had sepsis (57.5%); mean age: 59 years; males: 49%; white race: 70%; associated diabetes: 24%; associated prior congestive heart failure: 10% | blood glucose on admission: <100 mg/dL | 7754 | in-hospital: OR: 1.09 (95% CI: 1.03–1.14) with diabetes on admission, in-hospital: OR: 2.30 (95% CI: 1.61–3.30) |
| Ssekitoleko et al. (2011)[24] | prospective | Uganda | patients included in the study had severe sepsis; mean age: approx. 35 years; males: 46%; bacteremia/fungemia present in 21%; HIV-positive: 83% | blood glucose on admission: <80 mg/dL | 418 | in-hospital: OR: 1.60 (95% CI: 0.92–2.78) |
| Park et al. (2012)[25] | retrospective | South Korea | patients included in the study had septic shock (around 60%); mean age: approx. 70 years; males: 53%; associated diabetes: 33%: insulin therapy: 70%; bacteremia/fungemia present in 21%; HIV-positive: 83% | blood glucose on admission: <40 mg/dL | 313 | in-hospital: OR: 6.37 (95% CI: 2.31–17.55) day 30: OR: 5.30 (95% CI: 2.04–13.78) 1 year: OR: 6.48 (95% CI: 1.89–22.21) |
| Magee et al. (2018)[26] | retrospective | Australia | patients included in the study with sepsis; mean age: approx. 66 years; males: 56%; associated chronic renal failure: 6%; immunosuppression: 9%; APACHE III mean score: approx. 66 | blood glucose on admission: <120 mg/dL | 90,644 | in-hospital: OR: 0.99 (95% CI: 0.95–1.04) with diabetes on admission, in-hospital: OR: 1.71 (95% CI: 1.36–2.14) |
| Kushimoto et al. (2020)[27] | retrospective | Japan | majority of patients included in the study had severe sepsis/septic shock; mean age: approx. 73 years; males: 60%; mean BMI: 22 kg/m$^2$; associated diabetes: 23%; site of infection (lung: 31%, abdomen: 26%) | blood glucose on admission: <70 mg/dL | 1158 | in-hospital: OR: 2.06 (95% CI: 1.22–3.50) day 28: OR: 2.37 (95% CI: 1.38–4.08) with diabetes on admission, in-hospital: OR: 1.71 (95% CI: 0.51–5.72) |
| Chao et al. (2017)[28] | retrospective | Taiwan | patients included in the study had sepsis; median age: approx. 66 years; males: 54%; associated diabetes: 58%; chronic kidney disease: 12% | blood glucose on admission: ≤100 mg/dL | 6165 | in-hospital: OR: 1.39 (95% CI: 1.08–1.78) with diabetes on admission, in-hospital: OR: 0.74 (95% CI: 0.59–0.93) |
| Bagshaw et al. (2009)[29] | retrospective | Australia | majority of patients included in the study had severe sepsis/septic shock; mean age: approx. 65 years; males: 59% | blood glucose on admission: <72 mg/dL | 66,184 | in-hospital: OR: 1.60 (95% CI: 1.40–1.80) |
| Liang and Ty (2018)[30] | retrospective | USA | patients included in the study had severe sepsis and/or septic shock; age >18 years; patients with DKA or hyperosmolar hyperglycemic state were excluded from the study | blood glucose on admission: <140 mg/dL | 150 | in-hospital: OR: 0.65 (95% CI: 0.29–1.46) |
| Shahab et al. (2011)[31] | retrospective | no data provided | patients included in the study had severe sepsis and/or septic shock; patients with DKA and/or hyperosmolar nonketotic comma were excluded from the study | blood glucose on admission: <150 mg/dL | 115 | in-hospital: OR: 1.08 (95% CI: 0.48–2.45) |
| Tiruvoipati et al. (2013)[32] | retrospective | Australia | patients included in the study had severe sepsis and/or septic shock; mean age: 67 years; males: 50%; mean APACHE III score: 75; 16% with associated chronic renal failure and 20% with diabetes mellitus | blood glucose on admission: ≤124 mg/dL | 297 | in-hospital: OR: 1.20 (95% CI: 0.64–2.23) |

APACHE II – Acute Physiology and Chronic Health Evaluation II; HIV – human immunodeficiency virus; DKA – diabetic ketoacidosis; OR – odds ratio; 95% CI – 95% confidence interval; BMI – body mass index.

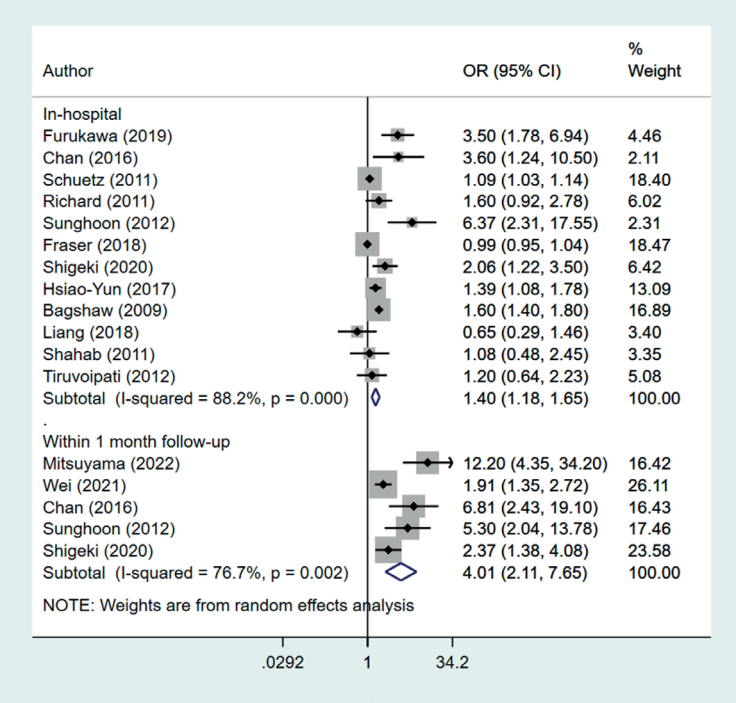


**Fig. 2.** Mortality risk in patients with sepsis or severe sepsis/septic shock and associated hypoglycemia, compared to those with euglycemia at the time of admission

OR – odds ratio; 95% CI – 95% confidence interval.

in the included studies. Supplementary Tables 2 and 3 summarize the findings of the quality assessment of the 14 included studies. All studies were of moderate to good quality.

## Hypoglycemia and mortality risk

The pooled findings suggested an increased risk of in-hospital mortality (OR = 1.40, 95% CI: 1.18–1.65, $I^2$ = 88.2%, n = 12, z-statistic = 4.25, p = 0.0001) and mortality within 1 month of hospital discharge (OR = 4.01, 95% CI: 2.11–7.65, $I^2$ = 76.7%, n = 5, z-statistic = 4.21, p = 0.0001) among patients with hypoglycemia compared to patients with euglycemia (Fig. 2). There was no evidence of publication bias (p > 0.05) for mortality outcomes at either timepoint (Supplementary Table 3).

## Analysis based on the presence of sepsis or severe sepsis/septic shock

In patients with sepsis, hypoglycemia was not significantly correlated with a higher risk of in-hospital mortality (OR = 1.15, 95% CI: 1.00–1.32, $I^2$ = 88.1%, n = 4, z-statistic = 1.99, p = 0.05) or with an increased risk for mortality within 1 month of follow-up (OR = 4.52, 95% CI: 0.74–27.7, $I^2$ = 91.0%, n = 2, z-statistic = 1.64, p = 0.10), compared to euglycemic patients (Fig. 3). In patients with severe sepsis and/or septic shock, hypoglycemia was associated with a significantly higher risk of in-hospital mortality (OR = 1.64, 95% CI: 1.20–2.25, $I^2$ = 58.1%, n = 8, z-statistic = 3.06, p = 0.002) and mortality within 1 month of follow-up (OR = 3.94, 95% CI: 1.96–7.89, $I^2$ = 53.2%, n = 3, z-statistic = 3.88, p = 0.0001) (Fig. 4), with no evident publication bias (p > 0.05) (Supplementary Table 3).

## Analysis of patients with diabetes at the time of admission

In patients who were diabetic at the time of admission, hypoglycemia did not correlate with increased in-hospital mortality risk (OR = 1.45, 95% CI: 0.79–2.66, $I^2$ = 92.3%, n = 4, z-statistic = 1.19, p = 0.23) or mortality within 1 month of follow-up (OR = 1.34, 95% CI: 0.84–2.16, $I^2$ = 0.0%, n = 2, z-statistic = 1.16, p = 0.25) (Fig. 5), with no evident publication bias (p > 0.05) for any of these 2 outcomes (Supplementary Table 3).

# Discussion

The findings of the current review showed a higher mortality risk in patients with hypoglycemia, and this risk was predominant in patients with severe sepsis and/or septic shock. However, hypoglycemia was not associated with a higher mortality risk in patients with pre-existing diabetes. These findings are consistent with a previous review by Wang et al., where a similar association of hypoglycemia with mortality was noted (OR = 1.68).[12] Similarly, the association between mortality and hyperglycemia was stronger in patients with severe sepsis/septic shock (OR = 1.98).

Previous studies showed that patients with severe infection/sepsis usually have elevated blood glucose levels (stress hyperglycemia) due to the enhanced release of glucocorticoids, epinephrine and norepinephrine.[33–35] These higher glucose levels may lead to an inflammatory state, endothelial cell dysfunction, oxidative stress, and immunosuppression.[34–36] Studies have also noted an increased risk

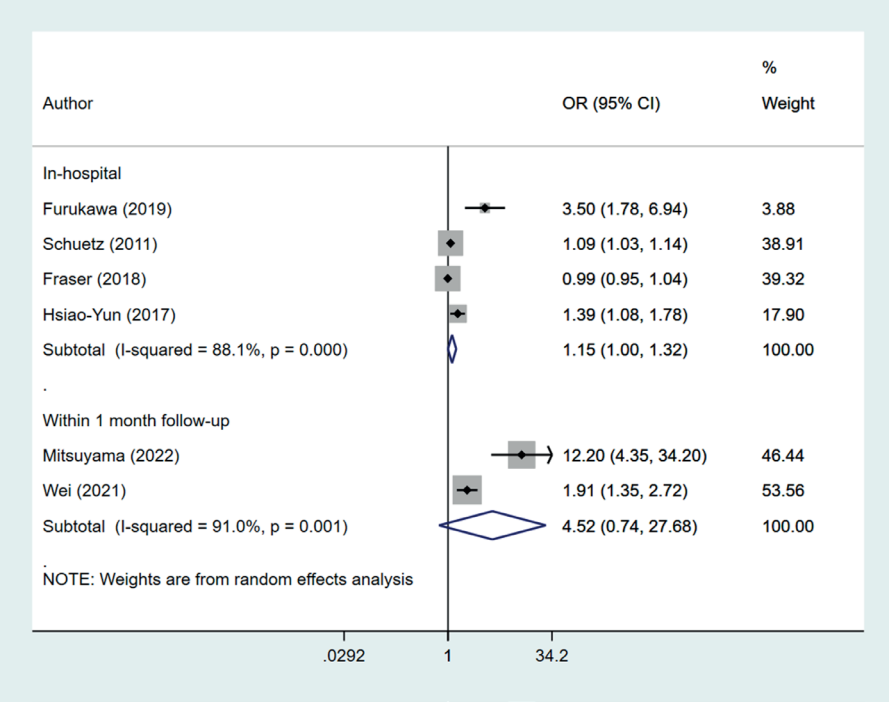


**Fig. 3.** Mortality risk in patients with sepsis and associated hypoglycemia, compared to those with euglycemia at the time of admission

OR – odds ratio; 95% CI – 95% confidence interval.

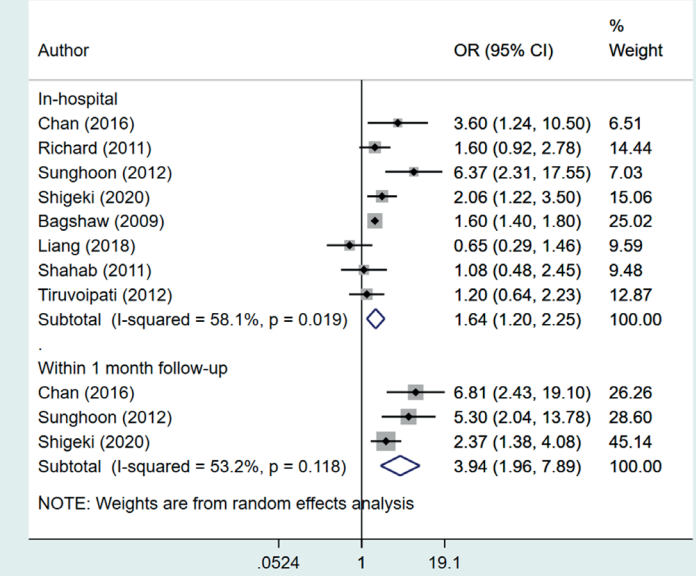


**Fig. 4.** Mortality risk in patients with severe sepsis/septic shock and associated hypoglycemia, compared to those with euglycemia at the time of admission

OR – odds ratio; 95% CI – 95% confidence interval.

of mortality in patients with hyperglycemia and associated sepsis.[6,7,37] However, there is also a possible risk of hypoglycemia due to either strict glycemic control strategies or the upregulation of cytokines that increase the utilization of peripheral blood glucose and downregulate gluconeogenesis.[5,8–11] Additionally, the metabolic rate in patients with sepsis is higher, which may lead to excessive glucose consumption and glycogen reserve depletion.[5,38,39] Another vital pathway through which hypoglycemia may occur in patients with sepsis is the inhibition of the prosecretory effects of adrenocorticotropic hormone (ACTH) on adrenal cortisol production,[39,40] leading to corticosteroid insufficiency.[39,40]

Hypoglycemia may lead to the activation of sympathoadrenal mechanisms, abnormal cardiac repolarization, dysregulation of hemostatic mechanisms such as accelerated thrombogenesis and vasoconstriction, and elevated levels of inflammatory cytokines.[41] All of these processes could worsen the outcome for patients with sepsis. The higher mortality risk, especially in patients with severe sepsis/septic shock, could be due to increased glycemic variability, as documented in some studies.[42,43] The current meta-analysis found no significant association between hypoglycemia and mortality among diabetic patients, which is contrary to the findings of a meta-analysis by Wang et al. showing

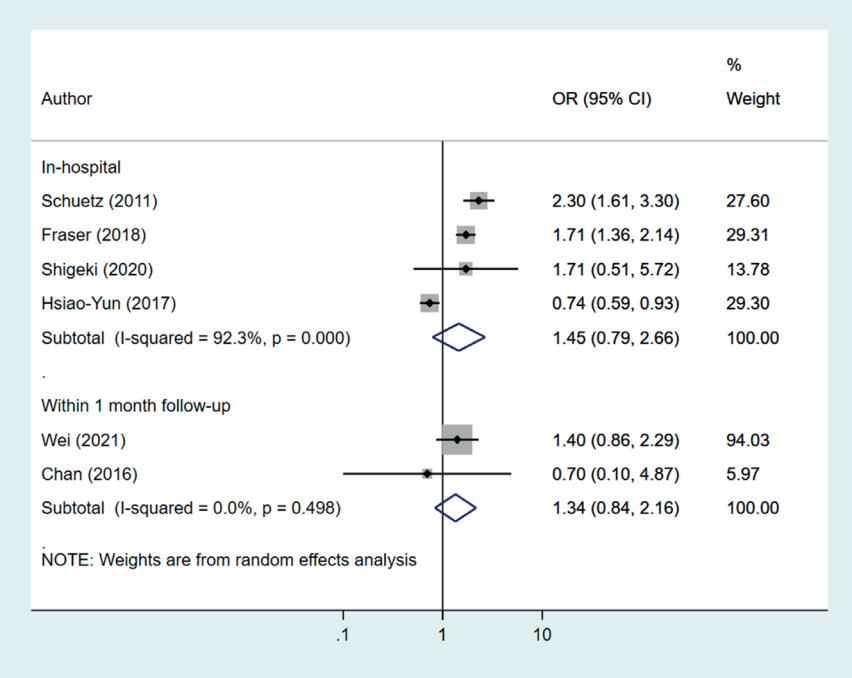


**Fig. 5.** Mortality risk in diabetic subjects with associated hypoglycemia, compared to those with euglycemia on admission

OR – odds ratio; 95% CI – 95% confidence interval.

that hypoglycemia (defined as a blood glucose level of <145 mg/dL) correlated with increased mortality risk in patients with diabetes and associated sepsis.[13] The authors suggested that this could be due to the relative intolerance in diabetic subjects to hypoglycemic episodes.[12,23] The noted difference in the findings could be partially explained by the difference in the cutoff level defining hypoglycemia. Most studies included in the current meta-analysis adopted a comparatively lower cutoff level. These contrasting findings underscore the complex nature of the interactions between blood glucose levels and adverse clinical outcomes among patients with pre-existing diabetes and call for more research on this issue.

## Limitations

Our study had some limitations. First, all included studies were observational, meaning that a causal relationship could not be established between hypoglycemia and mortality. Furthermore, there is a possibility that crucial variables and confounders were not adjusted for, or data on these variables were not collected. Second, there was a high heterogeneity in the findings, which could be due to the differences in methodologies and variation in the participant characteristics. The included studies used various blood sugar cutoff values for hypoglycemia, and there were differences in the operational definitions adopted for sepsis. We conducted our analysis using a random effects model to partly address the high heterogeneity.

# Conclusions

Our findings indicate that hypoglycemia might correlate with increased mortality risk in sepsis and/or severe sepsis/septic shock patients. Therefore, monitoring of blood glucose in these patients may be required. We noted that different blood sugar cutoff values were used to label hypoglycemia for both euglycemic and diabetic patients. It is important to develop harmonized diagnostic criteria that are reliable and practical enough to be implemented routinely in order to avoid such heterogeneity. Such criteria need to be updated when new evidence becomes available, with new developments necessitating changes in the criteria for sepsis informed by findings from prospectively conducted studies. More research is needed to clarify the link between low blood glucose levels and the mortality risk in sepsis patients with diabetes.

## Supplementary data

The supplementary materials are available at https://doi.org/10.5281/zenodo.7967501. The package contains the following files:

Supplementary Table 1. Authors' judgements about study quality using the adapted Newcastle-Ottawa risk of bias assessment tool.

Supplementary Table 2. Authors' judgements about study quality using the adapted Newcastle-Ottawa risk of bias assessment tool.

Supplementary Table 3. Results of Egger's test for the outcomes.

## ORCID iDs

Yuping Shao https://orcid.org/0009-0001-4015-0682
Feng Shao https://orcid.org/0009-0001-7700-841X
Jie Zhou https://orcid.org/0009-0001-6403-7377
Shunjin Fang https://orcid.org/0009-0000-7915-0420
Jianfeng Zhu https://orcid.org/0009-0007-2809-6680
Fangfang Li https://orcid.org/0000-0003-4324-3355


## References


1. Rudd KE, Johnson SC, Agesa KM, et al. Global, regional, and national sepsis incidence and mortality, 1990–2017: Analysis for the Global Burden of Disease Study. *Lancet*. 2020;395(10219):200–211. doi:10.1016/S0140-6736(19)32989-7
2. Bauer M, Gerlach H, Vogelmann T, Preissing F, Stiefel J, Adam D. Mortality in sepsis and septic shock in Europe, North America and Australia between 2009 and 2019: Results from a systematic review and meta-analysis. *Crit Care*. 2020;24(1):239. doi:10.1186/s13054-020-02950-2
3. Ingels C, Gunst J, Van den Berghe G. Endocrine and metabolic alterations in sepsis and implications for treatment. *Crit Care Clin*. 2018;34(1):81–96. doi:10.1016/j.ccc.2017.08.006
4. Khardori R, Castillo D. Endocrine and metabolic changes during sepsis: An update. *Med Clin North Am*. 2012;96(6):1095–1105. doi:10.1016/j.mcna.2012.09.005
5. Wasyluk W, Zwolak A. Metabolic alterations in sepsis. *J Clin Med*. 2021;10(11):2412. doi:10.3390/jcm10112412
6. Yao RQ, Ren C, Wu GS, Zhu YB, Xia ZF, Yao YM. Is intensive glucose control bad for critically ill patients? A systematic review and meta-analysis. *Int J Biol Sci*. 2020;16(9):1658–1675. doi:10.7150/ijbs.43447
7. van Vught LA, Wiewel MA, Klein Klouwenberg PMC, et al. Admission hyperglycemia in critically ill sepsis patients: Association with outcome and host response. *Crit Care Med*. 2016;44(7):1338–1346. doi:10.1097/CCM.0000000000001650
8. Maitra SR, Wojnar MM, Lang CH. Alterations in tissue glucose uptake during the hyperglycemic and hypoglycemic phases of sepsis. *Shock*. 2000;13(5):379–385. doi:10.1097/00024382-200005000-00006
9. Dendoncker K, Libert C. Glucocorticoid resistance as a major drive in sepsis pathology. *Cytokine Growth Factor Rev*. 2017;35:85–96. doi:10.1016/j.cytogfr.2017.04.002
10. Weis S, Carlos AR, Moita MR, et al. Metabolic adaptation establishes disease tolerance to sepsis. *Cell*. 2017;169(7):1263–1275.e14. doi:10.1016/j.cell.2017.05.031
11. Hirasawa H, Oda S, Nakamura M. Blood glucose control in patients with severe sepsis and septic shock. *World J Gastroenterol*. 2009;15(33):4132. doi:10.3748/wjg.15.4132
12. Wang J, Zhu CK, Yu JQ, Tan R, Yang PL. Hypoglycemia and mortality in sepsis patients: A systematic review and meta-analysis. *Heart Lung*. 2021;50(6):933–940. doi:10.1016/j.hrtlng.2021.07.017
13. Wang W, Chen W, Liu Y, et al. Blood glucose levels and mortality in patients with sepsis: Dose–response analysis of observational studies. *J Intensive Care Med*. 2021;36(2):182–190. doi:10.1177/0885066619889322
14. Preferred Reporting Items for Systematic Reviews and Meta-Analyses (PRISMA). PRISMA 2020 checklist. 2020. http://www.prisma-statement.org/. Accessed May 10, 2022.
15. Wells G, Shea B, O'Connell D, et al. The Newcastle-Ottawa Scale (NOS) for assessing the quality of nonrandomized studies in meta-analysis. Ottawa, Canada: Ottawa Hospital Research Institute; 2021. https://www.ohri.ca/programs/clinical_epidemiology/oxford.asp. Accessed May 14, 2022.
16. Higgins JPT, Thomas J, Chandler J, et al., eds. *Cochrane Handbook for Systematic Reviews of Interventions*. 2nd ed. Hoboken, USA: John Wiley & Sons; 2019. doi:10.1002/9781119536604
17. Egger M, Smith GD, Schneider M, Minder C. Bias in meta-analysis detected by a simple, graphical test. *BMJ*. 1997;315(7109):629–634. doi:10.1136/bmj.315.7109.629
18. Chyou PH. A simple and robust way of concluding meta-analysis results using reported p-values, standardized effect sizes, or other statistics. *Clin Med Res*. 2012;10(4):219–223. doi:10.3121/cmr.2012.1068
19. Furukawa M, Kinoshita K, Yamaguchi J, Hori S, Sakurai A. Sepsis patients with complication of hypoglycemia and hypoalbuminemia are an early and easy identification of high mortality risk. *Intern Emerg Med*. 2019;14(4):539–548. doi:10.1007/s11739-019-02034-2
20. Mitsuyama Y, Shimizu K, Komukai S, et al. Sepsis-associated hypoglycemia on admission is associated with increased mortality in intensive care unit patients. *Acute Med Surg*. 2022;9(1):e718. doi:10.1002/ams2.718
21. Wei X, Min Y, Yu J, et al. Admission blood glucose is associated with the 30-days mortality in septic patients: A retrospective cohort study. *Front Med (Lausanne)*. 2021;8:757061. doi:10.3389/fmed.2021.757061
22. Chan MC, Tseng JS, Hsu KH, et al. A minimum blood glucose value less than or equal to 120 mg/dL under glycemic control is associated with increased 14-day mortality in nondiabetic intensive care unit patients with sepsis and stress hyperglycemia. *J Crit Care*. 2016;34:69–73. doi:10.1016/j.jcrc.2016.04.002
23. Schuetz P, Jones AE, Howell MD, et al. Diabetes is not associated with increased mortality in emergency department patients with sepsis. *Ann Emerg Med*. 2011;58(5):438–444. doi:10.1016/j.annemergmed.2011.03.052
24. Ssekitoleko R, Jacob ST, Banura P, et al. Hypoglycemia at admission is associated with inhospital mortality in Ugandan patients with severe sepsis. *Crit Care Med*. 2011;39(10):2271–2276. doi:10.1097/CCM.0b013e3182227bd2
25. Park S, Kim DG, Suh G, et al. Mild hypoglycemia is independently associated with increased risk of mortality in patients with sepsis: A 3-year retrospective observational study. *Crit Care*. 2012;16(5):R189. doi:10.1186/cc11674
26. Magee F, Bailey M, Pilcher DV, Mårtensson J, Bellomo R. Early glycemia and mortality in critically ill septic patients: Interaction with insulin-treated diabetes. *J Crit Care*. 2018;45:170–177. doi:10.1016/j.jcrc.2018.03.012
27. Kushimoto S, Abe T, Ogura H, et al; on behalf of JAAM FORECAST group. Impact of blood glucose abnormalities on outcomes and disease severity in patients with severe sepsis: An analysis from a multicenter, prospective survey of severe sepsis. *PLoS One*. 2020;15(3):e0229919. doi:10.1371/journal.pone.0229919
28. Chao HY, Liu PH, Lin SC, et al. Association of in-hospital mortality and dysglycemia in septic patients. *PLoS One*. 2017;12(1):e0170408. doi:10.1371/journal.pone.0170408
29. Bagshaw SM, Egi M, George C, Bellomo R. Early blood glucose control and mortality in critically ill patients in Australia. *Crit Care Med*. 2009;37(2):463–470. doi:10.1097/CCM.0b013e318194b097
30. Liang M, Ty P. Abstract1511: Impact of varying ICU hyperglycemia severities on sepsis mortality. *Crit Care Med*. 2018;46(1):739. doi:10.1097/01.ccm.0000529513.81407.a4
31. Shahab L, Soufi S, Al-Hamad S, Shibli M. The outcome of glycemic control in critically ill septic patients. *Chest*. 2011;140(4):327A. doi:10.1378/chest.1116700
32. Tiruvoipati R, Chiezey B, Lewis D, et al. Stress hyperglycemia may not be harmful in critically ill patients with sepsis. *Surv Anesthesiol*. 2013;57(1):5–6. doi:10.1097/01.SA.0000424053.09290.f1
33. Bar-Or D, Rael LT, Madayag RM, et al. Stress hyperglycemia in critically ill patients: Insight into possible molecular pathways. *Front Med (Lausanne)*. 2019;6:54. doi:10.3389/fmed.2019.00054
34. Leonidou L, Michalaki M, Leonardou A, et al. Stress-induced hyperglycemia in patients with severe sepsis: A compromising factor for survival. *Am J Med Sci*. 2008;336(6):467–471. doi:10.1097/MAJ.0b013e318176abb4
35. Schmoch T, Uhle F, Siegler BH, et al. The glyoxalase system and methylglyoxal-derived carbonyl stress in sepsis: Glycotoxic aspects of sepsis pathophysiology. *Int J Mol Sci*. 2017;18(3):657. doi:10.3390/ijms18030657
36. Yu WK. Influence of acute hyperglycemia in human sepsis on inflammatory cytokine and counterregulatory hormone concentrations. *World J Gastroenterol*. 2003;9(8):1824. doi:10.3748/wjg.v9.i8.1824
37. Fabbri A, Marchesini G, Benazzi B, et al. Stress hyperglycemia and mortality in subjects with diabetes and sepsis. *Crit Care Explor*. 2020;2(7):e0152. doi:10.1097/CCE.0000000000000152
38. Kreymann G, Grosser S, Buggisch P, Gottschall C, Matthaei S, Greten H. Oxygen consumption and resting metabolic rate in sepsis, sepsis syndrome, and septic shock. *Crit Care Med*. 1993;21(7):1012–1019. doi:10.1097/00003246-199307000-00015
39. Annane D, Maxime V, Ibrahim F, Alvarez JC, Abe E, Boudou P. Diagnosis of adrenal insufficiency in severe sepsis and septic shock. *Am J Respir Crit Care Med*. 2006;174(12):1319–1326. doi:10.1164/rccm.200509-1369OC

40. Annane D. The role of ACTH and corticosteroids for sepsis and septic shock: An update. *Front Endocrinol (Lausanne)*. 2016;7:70. doi:10.3389/fendo.2016.00070
41. Zoungas S, Patel A, Chalmers J, et al. Severe hypoglycemia and risks of vascular events and death. *N Engl J Med*. 2010;363(15):1410–1418. doi:10.1056/NEJMoa1003795
42. Egi M, Bellomo R, Stachowski E, French CJ, Hart G. Variability of blood glucose concentration and short-term mortality in critically ill patients. *Anesthesiology*. 2006;105(2):244–252. doi:10.1097/00000542-200608000-00006
43. Hermanides J, Vriesendorp TM, Bosman RJ, Zandstra DF, Hoekstra JB, DeVries JH. Glucose variability is associated with intensive care unit mortality. *Crit Care Med*. 2010;38(3):838–842. doi:10.1097/CCM.0b013e3181cc4be9

# A meta-analysis of the efficacy of intra-arterial chemotherapy for the management of retinoblastoma patients

Guoxiao Yu[1,A–D], Xiaoqiang Zhou[1,A–D], Juan Li[2,A,D–F]

[1] Department of Ophthalmology, First People's Hospital of Linping District, Hangzhou, China
[2] Department of Radiotherapy, Hangzhou Cancer Hospital, China

A – research concept and design; B – collection and/or assembly of data; C – data analysis and interpretation;
D – writing the article; E – critical revision of the article; F – final approval of the article

Advances in Clinical and Experimental Medicine, ISSN 1899–5276 (print), ISSN 2451–2680 (online) *Adv Clin Exp Med*. 2024;33(3):207–216

**Address for correspondence**
Juan Li
E-mail: Lijuan0086751@outlook.com

**Funding sources**
None declared

**Conflict of interest**
None declared

Received on October 27, 2022
Reviewed on March 10, 2023
Accepted on May 31, 2023

Published online on July 24, 2023

## Abstract

**Background.** Intra-arterial chemotherapy (IAC) is considered a unique technique for retinoblastoma (Rb) management and has widespread applicability as a first-line or second-line treatment due to the high globe survival rates.

**Objectives.** This meta-analysis aimed to assess the efficacy of IAC approach among patients with Rb.

**Materials and methods.** This study outlined the most recent research on IAC effectiveness in Rb treatment. We carried out a systematic search for published papers examining IAC treatment among patients with Rb using electronic search engines, including Embase, Web of Science (WoS), PubMed, OVID, and Google Scholar, until October 2021.

**Results.** This meta-analysis included 39 observational studies with 2604 treated eyes and 3112 individuals who were eligible for inclusion. Enucleation rates varied from 0% to 43.7% in the chosen trials, with an odds ratio (OR) of 0.52 (95% confidence interval (95% CI): 0.41–0.66, $p < 0.0001$). A range of 30–100% was reported for globe salvage across 27 investigations involving 2310 eyes. The estimated OR of globe salvage was 2.41, with 95% CI of 1.6–3.63 and a p-value <0.0001. The combined total effect sizes and the death rate for the proportion of cases with metastatic Rb were as follows: OR = 0.03 (95% CI: 0.03–0.03) and OR = 0.05 (95% CI: 0.04–0.05, $p < 0.0001$), respectively.

**Conclusions.** Retrospective trials have shown that intra-arterial-based therapy for Rb is an effective choice. Intra-arterial chemotherapy also reduced enucleation and metastasis incidence rates. The paucity of evidence in the literature necessitates further high-level studies.

**Key words:** metastases, retinoblastoma, globe salvage

**Cite as**
Yu G, Zhou X, Li J. A meta-analysis of the efficacy of intra-arterial chemotherapy for the management of retinoblastoma patients. *Adv Clin Exp Med*. 2024;33(3):207–216. doi:10.17219/acem/166664

**DOI**
10.17219/acem/166664

# Background

Retinoblastoma (Rb) is an intra-ocular cancer that mainly affects young people throughout the world and carries life-threatening consequences. This type of cancer was identified in about 8000 patients globally.[1] A systemic delivery of intravenous chemotherapy (IVC) was the standard care approach that achieved encouraging results in Rb using laser adjunctive therapy and cryotherapy, while advanced Rb cases showed modest outcomes with IVC.

Since the development of intra-arterial chemotherapy (IAC), the direct intra-arterial delivery of chemotherapy has become the standard of care for salvage therapy at numerous tertiary ocular facilities globally.[2] This method assisted in the treatment of advanced Rb cases that would have otherwise been enucleated.[1,3] Before the emergence of IAC, enucleation was performed in around 80% of advanced Rb cases classified as group D or E, according to the International Classification of Retinoblastoma (ICRB) group.[4]

Compared to intravenously delivered systemic chemotherapy, IAC has achieved higher levels of chemotherapy in tumor tissue and better outcomes. The systemic chemotherapeutic adverse effects of ototoxicity and neurotoxicity were reduced by IAC treatment.[5] Furthermore, IAC can be delivered in 1 day, and the tumor can be controlled with 2 to 3 sessions.

Intra-arterial chemotherapy is beneficial as second-line therapy in refractory Rb that leads to improved globe salvage of eyes that would have otherwise been enucleated. However, patient selection and the procedure's complications have raised many concerns. Intra-arterial chemotherapy is an invasive therapeutic method necessitating an experienced team with multiple specialties, including a neurosurgeon, an interventional radiologist and a pediatric oncologist. In addition, IAC requires specialized centers and advanced techniques. However, through proper application in professional hands, the advantages of IAC outweigh its drawbacks.[6,7]

Although IAC has demonstrated superior efficacy in terms of global salvage rates, the metastasis incidence rate among Rb patients treated with IAC remains unknown. In 2016, Yousef et al. conducted a systematic review of the evidence for IAC use in Rb treatment.[8] Since then, several studies have been carried out. However, most patient cohort reports using comparative data were of insufficient quality, and differences in sample sizes led to challenging critical evaluation of problems and outcomes.[9]

# Objectives

To assess the current research and update the existing evidence on the clinical effectiveness of IAC in patients with Rb, particularly those with advanced disease, we set out to review the studies conducted to date. The information provided by this meta-analysis is expected to help doctors in their clinical work.

# Materials and methods

The current investigation was conducted according to the predetermined procedure based on the Meta-analysis of Observational Studies in Epidemiology (MOOSE) protocol.

## Search strategy

Following the treatment of Rb with IAC, eligible trials assessed a minimum of one of the following outcomes: enucleation rate, metastatic incidence, globe salvage, or mortality. Studies describing the results of combined IAC and intravitreal treatment (IVT) were also included.

We considered research studies published in all languages and conducted in humans. The inclusion was not restricted by study size. Editorials, irrelevant research studies and review articles were all eliminated. The study search procedure is depicted in Table 1. The following criteria were met by the studies included in this meta-analysis: 1) well-designed prospective and retrospective studies; 2) studies that targeted Rb patients; 3) IAC therapy was the interventional procedure; 4) results of IAC therapy, either alone or in conjunction with IVT, were included in the investigation.

The exclusion criteria were as follows: 1) case reports, editorials, review articles, abstracts only, and research with a limited sample size (less than 10 subjects); 2) studies with missing or incomplete data and different outcomes other than the outcomes of interest; 3) studies performed with aims other than examining IAC outcomes in Rb; 4) study articles with therapeutic procedures other than IAC.

## Identification

As shown in Table 1, we first conducted a search using a combination of MeSH terms and keywords related to IAC and Rb in electronic databases, including Embase, PubMed, Google Scholar, OVID, and the Cochrane Library, up until October 2021. After omitting duplicates, the retrieved papers were compiled into a single EndNote file. We examined the titles and abstracts to rule out the articles that did not discuss how IAC affected patients with Rb, enucleation rates, globe salvage, metastasis rate, or mortality. The collected studies were examined for pertinent information.

## Screening

The first author's name, time frame, location, publication year, target patients, research procedure, number of subjects, demographics, and applicable clinical treatment features were all summarized in a predesigned form, as shown in Fig. 1. The assessment period was also related to the statistical analysis of odds ratios (ORs) with 95% confidence intervals (95% CIs) regarding relationships,

Table 1. Search strategy for each database

| Database | Search strategy |
|---|---|
| PubMed | #1 "intra-arterial" [MeSH Terms] OR "chemosurgery procedures" [All Fields] OR "retinoblsatoma" [All Fields]<br>#2 "enucleation" [MeSH Terms] OR "globe salvage" [All Fields] OR "metastasis" [All Fields] OR "mortality" [All Fields]<br>#3 #1 AND #2 |
| Embase | #1 'intra-arterial chemotherapy'/exp OR 'chemosurgery procedures'/exp OR 'retinoblastoma'/exp<br>#2 'enucleation'/exp OR 'ICBG'/exp OR 'globe salvage'/exp OR 'metastasis'/exp OR 'mortality'/exp<br>#3 #1 AND #2 |
| Cochrane Library | #1 (intra-arterial chemotherapy):ti,ab;kw OR (chemosurgery procedures):ti,ab;kw OR (retinoblastoma):ti,ab;kw (Word variations have been searched)<br>#2 (enucleation):ti,ab;kw OR (globe salvage):ti,ab;kw OR (metastasis):ti,ab;kw OR (mortality):ti,ab;kw (Word variations have been searched)<br>#3 #1 AND #2 |
| OVID | #1 "intra-arterial chemotherapy" OR "chemosurgery procedures" [All Fields] OR "retinoblastoma" [All Fields]<br>#2 "enucleation" OR "globe salvage" [All Fields] OR "metastasis" [All Fields] OR "mortality" [All Fields]<br>#3 #1 AND #2 |
| Google Scholar | #1 "intra-arterial chemotherapy" OR "chemosurgery procedures" OR "retinoblastoma"<br>#2 "enucleation" OR "globe salvage" OR "metastasis" OR "mortality"<br>#3 #1 AND #2 |

MeSH – medical subject headings; ti,ab;kw – terms in either title or abstract or keyword fields; exp – exploded indexing term.

| | |
|---|---|
| **Study title/ ID** | |
| **Author's name/ year** | |
| **Time frame** | |
| **Target population (number and characteristics)** | |
| **Country/settings** | |
| **Study design and intervention description** | |
| **Language** | |
| **Number of eyes treated** | |
| **Follow-up duration** | |
| **Outcome assessed** | |
| **Chemotherapy used** | |
| **Analysis method/instruments** | |
| **Results** | |
| **Quality assessment** | |
| **Comments** | |

Fig. 1. Predesigned form for data extraction

information resources, outcome assessment, and quantitative and qualitative review methodologies. Two authors independently evaluated the non-randomized controlled trials for study quality.

Information was gathered independently by 2 authors to determine if a study met the inclusion criteria. In case of a dispute, the corresponding author made the final decision. Data were individually extracted if there was variation in the data obtained from one of the trials. Two authors independently assessed procedural quality to determine the degree of bias in the retrieved studies.

## The risk of bias

The Cochrane risk-of-bias tool was used to assess bias risk and procedural quality (RoB 2; Cochrane Collaboration, London, UK).[10] Following data extraction, the authors evaluated the quality of the eligible studies according to the Cochrane Collaboration criteria. The risk of bias was assessed as low, moderate or high. The bias risk was evaluated based on the randomization technique, blinding of the outcome assessment, missing data, and selective reporting. Any inconsistencies or disputes were addressed by re-examining the original publication.

## Statistical analysis

The estimated ORs and 95% CIs were calculated. We also calculated the $I^2$ index, which was predicted to be between 0% and 100%. The $I^2$ index values of roughly 0% were evaluated as negligible heterogeneity, while those over 25% were perceived as minimal heterogeneity, with 50% and 75% indicating moderate and high heterogeneity, respectively.[11] In order to ascertain the correct model to be used, we analyzed the main discrepancies and similarities between the studies, including the effect size, discrepancies in the population characteristics, number of IAC sessions, follow-up duration, and methods. Based on the discrepancy assessment, all analyses used a random effects model. The stratification of studies per result category was performed for the subgroup analysis. A value of $p < 0.05$ indicated statistical significance for differences between the assessed outcomes in the analyzed studies. The Egger's regression test for quantitative bias assessment was performed (bias was present if $p \leq 0.05$) and funnel plots were used to qualitatively assess bias. The calculated p-values were two-sided. All measurements and graphs were created using Reviewer Manager (RevMan) software v. 5.3 (The Nordic Cochrane Centre Inc., Copenhagen, Denmark).

# Results

## Characteristics of the included studies

Initial search engine results identified 614 potential articles (Fig. 2). Thirty-nine articles[3,12–49] published up until 2021 met the meta-analysis inclusion criteria after full-text evaluation and review. A total of 2604 eyes were treated in the included studies. Only 4 studies were prospective, while most were retrospective (n = 35). The number of participants with Rb in the trials ranged from 10 to 500 at the beginning of the study. The chemotherapeutic drugs used included carboplatin, melphalan and topotecan. Indications for IAC were reported in all trials among Rb patients. Table 2 provides a summary of the major characteristics of the included research.

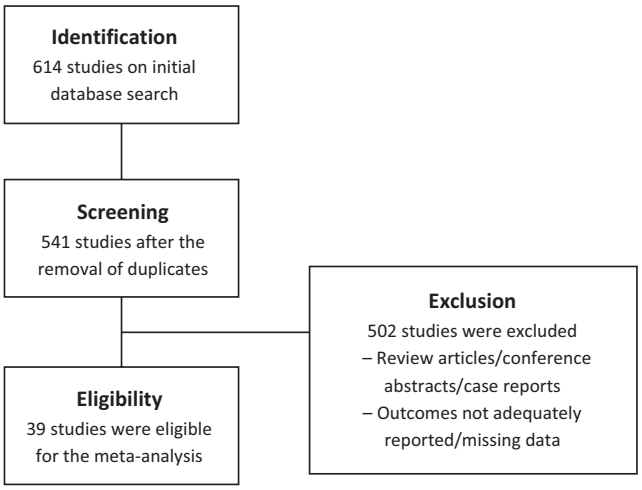


Fig. 2. Flowchart of the study search strategy

## Enucleation rate

Nineteen studies explicitly assessed the enucleation rate with IAC. The rate of enucleation ranged from 0% to 43.7%, with the highest rate (>50%) reported by Hua et al. in 2018.[39] The estimated total pooled OR of enucleation rates was 0.53 (95% CI: 0.42–0.65, p < 0.001) with a considerably high level of heterogeneity ($I^2$ = 98%), as shown in Fig. 3.

## Globe salvage

The globe salvage rate was reported in 27 investigations of 2310 treated eyes and ranged from 30% to 100%. The overall percentage of Rb patients who underwent IAC treatment was 76.4%. With substantial heterogeneity ($I^2$ = 90%), the calculated overall OR for globe salvage was 2.05 (95% CI: 1.62–2.60, p < 0.001), as shown in Fig. 4.

Table 2. The main characteristics of the included studies

| Author's name, publication year | Region, study design | Treated eyes, n | Unilateral eye disease, % | Age [months], median (range) | Sessions, median (range) | Follow-up duration [months], median (range) | Chemotherapeutic agent |
|---|---|---|---|---|---|---|---|
| Abramson et al. (2010)[12] | USA, prospective | 28 | 82 | 11 (3–88) | 3.2 (1–6) | 15 (3–37) | topotecan, melphalan, carboplatin |
| Gobin (2011)[13] | USA, retrospective | 91 | – | – | – | 13 | melphalan, topotecan, carboplatin, methotrexate |
| Munier et al. (2011)[14] | Switzerland, retrospective | 13 | – | – | – | 7 | melphalan |
| Peterson et al. (2011)[15] | USA, retrospective | 17 | 38 | 18 (9–32) | 1.4 (1–2) | 8.6 (3–12) | melphalan (7.5 mg) |
| Suzuki et al. (2011)[16] | Japan, retrospective | 408 | 39 | – | 3.7 (1–18) | 79 (58) | melphalan |
| Marr et al. (2012)[17] | USA, retrospective | 26 | 4 | 18 (0–62) | 2.3 (1–4) | 14 (1–43) | topotecan, carboplatin, melphalan |
| Muen et al. (2012)[18] | UK, prospective | 15 | NA | 17 (11–150) | 1–3 | 9 (3–16) | melphalan |
| Thampi et al. (2013)[19] | USA, retrospective | 20 | 38 | 15 (7–63) | NA | 15 (1–29) | melphalan |
| Venturi et al. (2013)[20] | Italy, retrospective | 41 | – | – | – | 13 | melphalan |
| Ghassemi et al. (2014)[21] | Iran, retrospective | 24 | 58 | 39 (14–120) | NA | 17 (3–36) | topotecan + melphalan |
| Shields et al. (2014)[22] | USA, retrospective | 70 | 63 | 20 (4–392) | 3 (1–6) | – | melphalan + topotecan + carboplatin |
| Taich et al. (2014)[23] | Argentina, retrospective | 27 | – | – | – | 11.7 | melphalan and topotecan |
| Parareda et al. (2014)[24] | Spain, prospective | 12 | 73 | 21 (7–51) | 2.6 (1–5) | 29.5 (6–57) | melphalan (3–5 mg) |

**Table 2.** The main characteristics of the included studies – cont.

| Author's name, publication year | Region, study design | Treated eyes, n | Unilateral eye disease, % | Age [months], median (range) | Sessions, median (range) | Follow-up duration [months], median (range) | Chemotherapeutic agent |
|---|---|---|---|---|---|---|---|
| Akyüz et al. (2015)[25] | Turkey, retrospective | 56 | – | – | – | 11.9 | melphalan |
| Ong et al. (2015)[26] | Taiwan, retrospective | 17 | 42 | 18 (2–50) | 3 (1–6) | 22 (5–43) | – |
| Abramson et al. (2016)[27] | USA, retrospective | 120 | – | – | – | 36 | melphalan, topotecan, carboplatin, methotrexate |
| Chen et al. (2016)[28] | China, retrospective | 13 | – | – | 2.6 (2–4) | 28 (9–65) | melphalan, topotecan, carboplatin |
| Leal-Leal et al. (2016)[29] | Mexico, prospective | 11 | 100 | 22.6 (12–36) | – | 14.3 (1.8–28) | melphalan (4 mg), topotecan (1 mg) |
| Michaels et al. (2016)[30] | USA, retrospective | 19 | 88 | 29 (5–192) | – | – | melphalan or topotecan |
| Tuncer et al. (2016)[31] | Turkey, retrospective | 24 | 77 | NA | – | 29 (6–55) | melphalan |
| Chen et al. (2017)[32] | China, retrospective | 107 | 33 | 20 (4–95) | 3.1 (2–5) | 9.1 (1–26) | melphalan (0.5 mg/kg), topotecan (1 mg) |
| Fabian et al. (2017)[33] | UK, retrospective | 64 | 33 | 11 (0.6–144) | 55 (11–156) | 38.7 | melphalan |
| Munier et al. (2017)[34] | Switzerland, retrospective | 25 | 100 | 33.5 ±25.9 | – | – | melphalan (2.8–7.5 mg) |
| Reddy et al. (2017)[35] | UK, retrospective | 9 | – | – | – | – | melphalan, topotecan |
| Rishi et al. (2017)[36] | India, retrospective | 10 | 20 | 26 (11–59) | 3.8 (3–5) | 21 | melphalan, topotecan |
| Francis et al. (2018)[37] | USA, retrospective | 436 | 38 | 13.4 (0.1–195) | – | 26.5 (0–119.7) | melphalan, topotecan, carboplatin |
| Funes et al. (2018)[38] | Argentina, retrospective | 97 | – | – | 4 (1–14) | 48.7 (12–79) | carboplatin |
| Hua et al. (2018)[39] | China, retrospective | 84 | 65 | 16 (4–96) | – | 14.2 (3–28) | melphalan, topotecan |
| Kiratli et al. (2018)[40] | Turkey, retrospective | 30 | – | – | 2.6 | 4.0 (1–16) | melphalan, topotecan |
| Rojanaporn et al. (2019)[41] | Thailand, retrospective | 27 | – | – | – | 32 | melphalan, topotecan, carboplatin |
| Yassa et al. (2019)[3] | Egypt, retrospective | 30 | – | – | – | 14.2 (6–20) | melphalan |
| Liu et al. (2020)[42] | Malaysia, retrospective | 14 | – | – | – | 17 | melphalan, topotecan, carboplatin |
| Batu Oto et al. (2020)[43] | Turkey, retrospective | 21 | – | – | – | – | melphalan |
| Rishi et al. (2020)[44] | India, retrospective | 24 | – | – | – | 28.6 | melphalan, topotecan |
| González et al. (2021)[45] | Colombia, retrospective | 100 | 39 | 8.70 (4.53–18.55) | – | 29 (16–59) | melphalan + topotecan |
| Linde and Mustak (2021)[46] | South Africa, retrospective | 25 | – | – | – | 47 | melphalan + topotecan |
| Oporto et al. (2021)[47] | Chile, retrospective | 35 | – | – | – | 36.5 | melphalan, topotecan |
| Shields et al. (2021)[48] | USA, retrospective | 341 | – | – | – | – | melphalan, topotecan, carboplatin |
| Li et al. (2022)[49] | China, retrospective | 73 | – | – | – | 7 | melphalan, topotecan, carboplatin |

NA – not applicable.

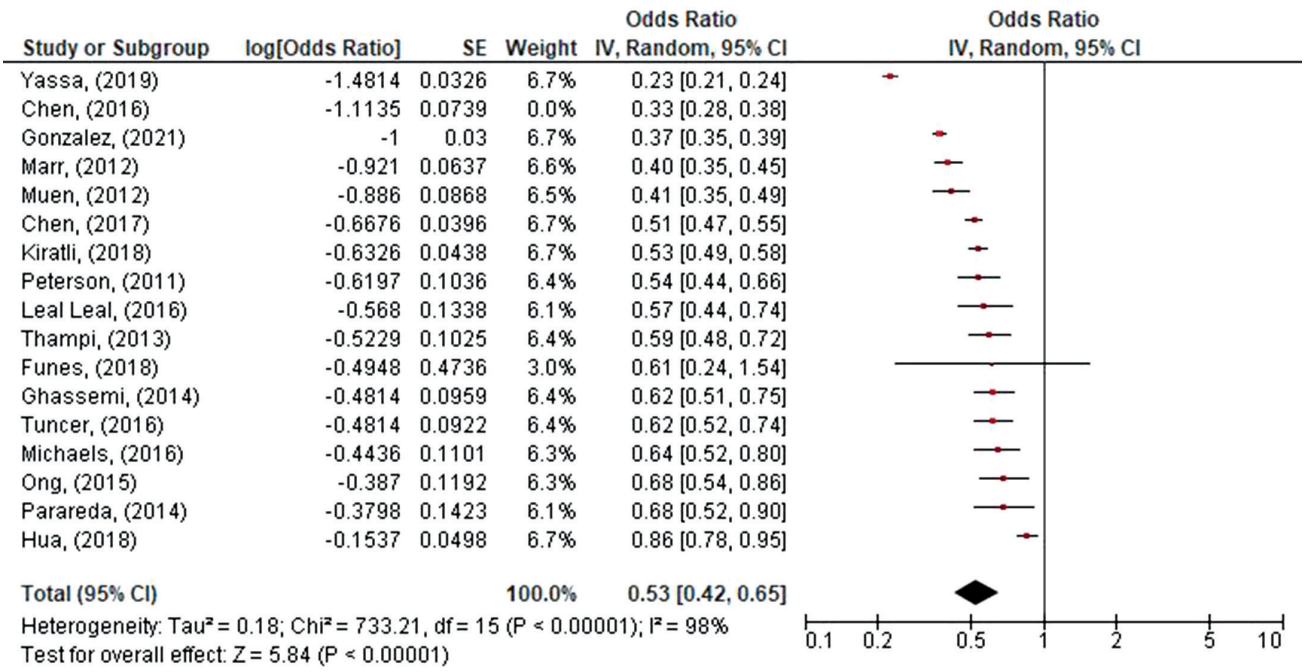


Fig. 3. Forest plot of the overall estimated effect sizes of enucleation rate

OR – odds ratio; 95% CI – 95% confidence interval; SE – standard error; df – degrees of freedom.

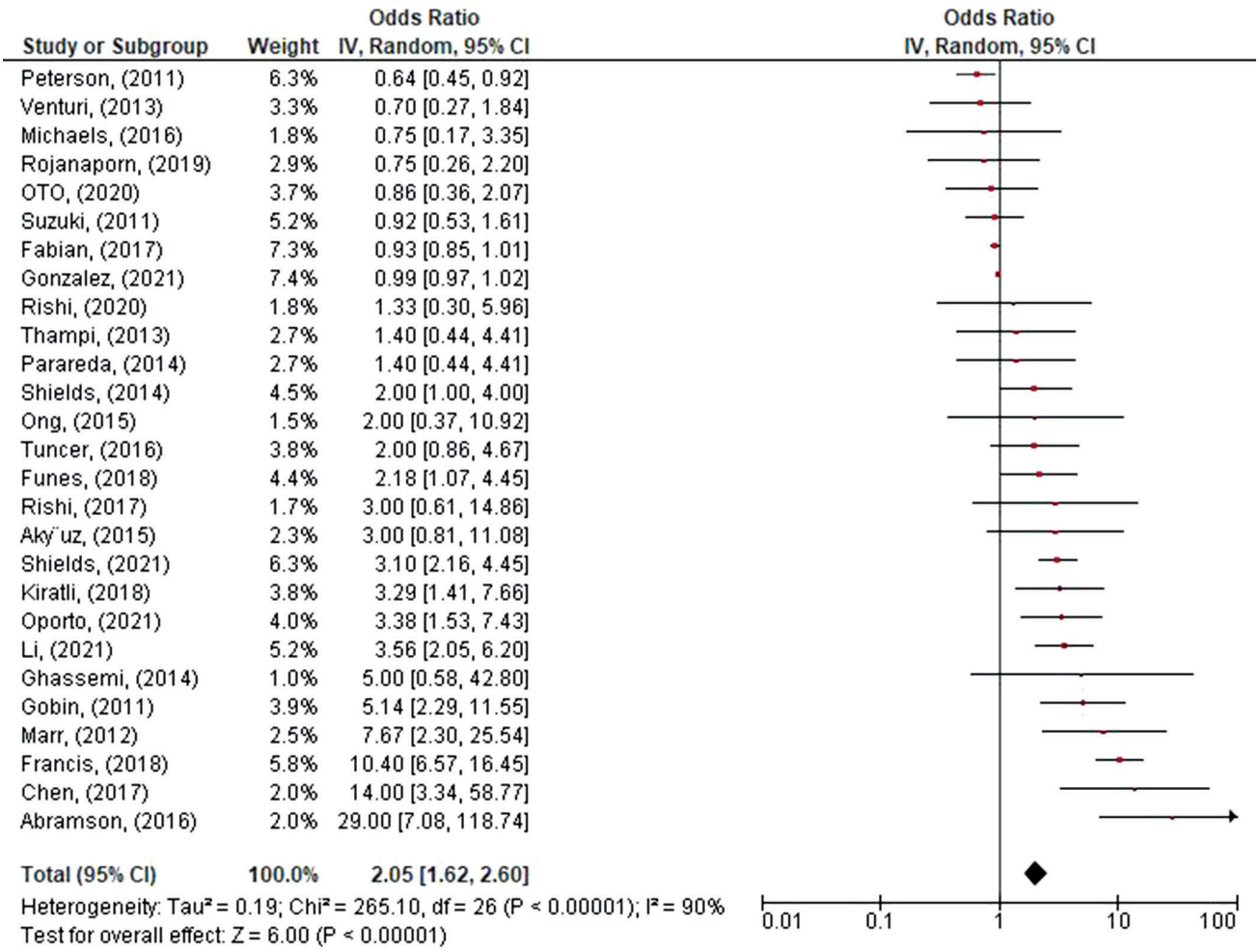


Fig. 4. Forest plot of the overall estimated effect sizes of globe salvage

OR – odds ratio; 95% CI – 95% confidence interval; SE – standard error; df – degrees of freedom.

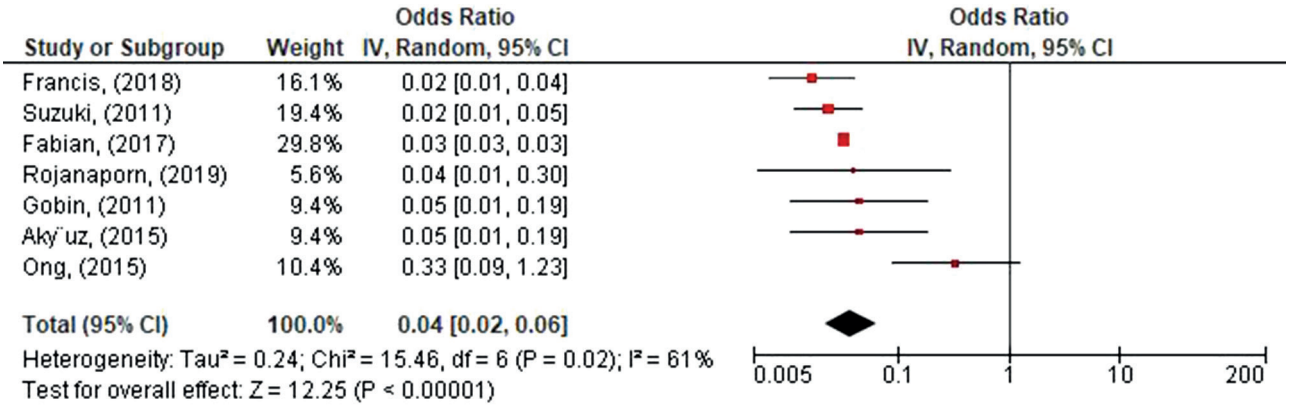


Fig. 5. Forest plot of the overall estimated effect sizes of metastasis

OR – odds ratio; 95% CI – 95% confidence interval; SE – standard error; df – degrees of freedom.

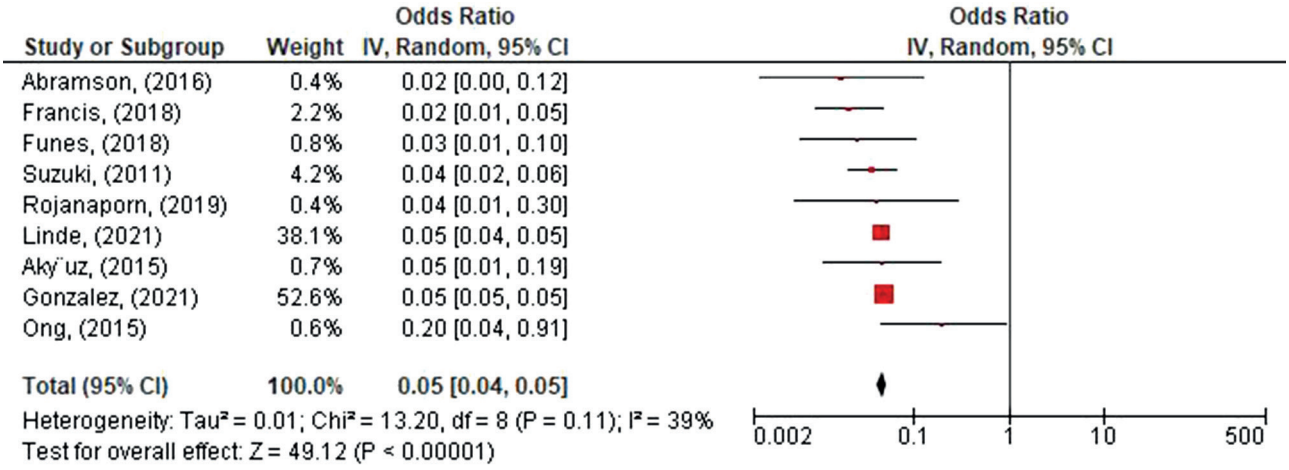


Fig. 6. Forest plot of the overall estimated effect sizes of mortality rate

OR – odds ratio; 95% CI – 95% confidence interval; SE – standard error; df – degrees of freedom.

## Metastasis rate

According to 7 studies, the metastasis rate was 2.4%. The total impact size of the proportion of metastatic disease had an OR = 0.04 (95% CI: 0.02–0.06, p < 0.001). The estimated heterogeneity was 61% (Fig. 5).

## Mortality rate

Nine studies with a total population of 1896 patients reported the mortality rate. The estimated overall mortality rate was 1.3%. The pooled mortality rate effect size had an OR = 0.05 (95% CI: 0.04–0.05, p < 0.001) with a low level of heterogeneity ($I^2$ = 39%) (Fig. 6).

There were no adjustments for age, ethnicity or gender because none of the studies accounted for these factors.

## Publication bias

There was no evidence of publication bias as shown by the symmetrical funnel plots (Fig. 7), where the vertical line represented the summary of the estimated effect size. Moreover, Egger's test did not detect significant publication bias, and the estimated p-values for Fig. 7 were 0.317, 0.294, 0.527, and 0.461. Despite this, most studies included in this meta-analysis had low procedural quality because of the limited size of the study populations. None of the research studies had a selective bias in reporting or inadequate data on outcomes.

# Discussion

Most cancer patients, including those with Rb, are treated with systemic chemotherapy, which has a high frequency of treatment-related adverse effects.[50] Yamane et al. published the first study on targeted intra-arterial ophthalmic chemotherapy for Rb patients in 2004.[51] Despite the difficulties with small blood vessel catheterization, IAC has emerged as the first alternative to Rb treatment, with broad applicability around the globe. Before IAC, around 80% of Rb cases eventually required to be enucleated to minimize hematogenous tumor dissemination and central nervous system involvement.[52]

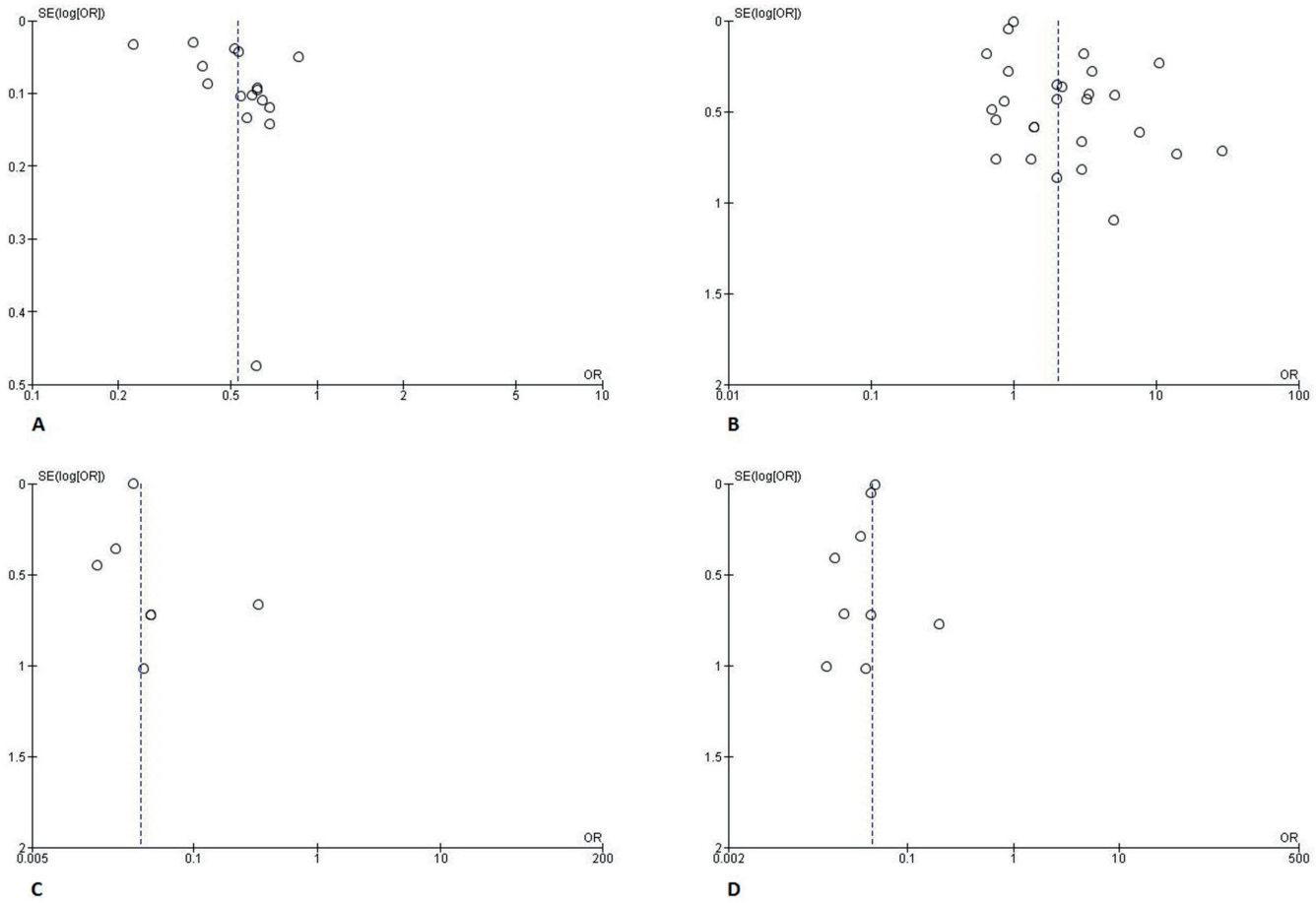


Fig. 7. Funnel plots for qualitative assessment of publication bias. A. Enucleation rate; B. Globe salvage; C. Metastasis rate; D. Mortality rate

OR – odds ratio; SE – standard error.

The current meta-analysis comprised 39 papers that assessed the key outcomes and complications of IAC for subjects with Rb. We conducted this study to provide updated evidence on the utility and effectiveness of the IAC technique by including recent trials that adopted diverse medications for Rb treatment. This study revealed a significantly improved enucleation rate after IAC in Rb patients. The clinical benefits of IAC in globe conservation were reported in several research articles. In the present meta-analysis, the estimated overall globe salvage with IAC was 76.4%, which is in accordance with the rates observed by Yousef et al. in their systematic review of 12 articles.[8]

According to our findings, the overall metastasis rate was estimated to be 2.4%, which is comparable to the estimations of 2.1% from the pooled analysis of Yousef et al.[8] Moreover, Chen et al. showed that patients with advanced Rb had a 2.7% overall metastasis rate with IAC.[53] The likelihood of metastatic eye disease is greatly increased by the presence of histopathologic risk factors. In nations with well-developed hospital facilities, this risk significantly decreases to less than 10%.[54]

Most adverse effects reported after IVC use would effectively disappear with symptomatic treatments. Rational use of IVC is crucial to minimize adverse events. Many systemic and ocular problems have been observed as a result of the high doses of chemotherapy used to treat eyes, despite the potential therapeutic efficacy, and the high rates of globe salvage achieved with IAC. The most frequently reported ocular problems were eyelid edema, retinal ischemia, retinal detachment (in around 25% of patients), vitreous hemorrhages, and retina atrophy. Clinical consequences that are temporary and typically self-limiting include retinal detachment and hemorrhages, though they may have long-term consequences and endanger vision, unlike ischemic attacks. Thus, long-term follow-up is recommended to assess vision. Moreover, IAC-related vascular injuries can be reduced through angiographic analysis and precise micro-catheter placement. Neutropenia and fever were among the commonly observed systemic side effects, with bronchospasm present in about 10% of cases, which required bronchodilators for its management.[9,54]

Kaliki et al. classified metastasis as a high risk in patients with a 4% mortality rate and a low risk in Rb patients with 0% mortality.[55,56] Besides, metastasis incidence rate and secondary malignancies among patients with heritable Rb are higher than in non-heritable Rb patients. Sarcoma, leukemia, melanoma, and brain cancers are the most commonly reported secondary malignancies. Recurrent radiotherapy and melphalan use with IAC have

been associated with mutations and resulted in secondary malignancies. Regarding IVC, carboplatin and etoposide have been linked with an increased risk of secondary malignancies. However, the total drug dose received also plays an important role and needs to be considered when assessing secondary malignancy risk. Moreover, most of the reported cases of metastasis and secondary malignancies received radiotherapy either previously or concomitant to chemotherapy. Therefore, radiotherapy could be the reason for secondary malignancy rather than the chemotherapy used.

## Limitations

There are some limitations to the current meta-analysis. First, it lacks any high-level randomized controlled trials and is based primarily on retrospective data. Second, few studies assessed disease progression and survival rates following IAC. Third, there was significant heterogeneity seen in the published results; and fourth, there was limited stratification of Rb patients according to disease severity factors such as tumor size, vitreous tumor or sub-retinal fluid seeds, and prior treatment.

# Conclusions

In summary, retrospective trials have shown that intra-arterial-based therapy is an effective alternative for treating Rb. This method also reduced enucleation and metastasis rates; however, the paucity of evidence in the literature necessitates further high-level randomized controlled studies.


### ORCID iDs

Guoxiao Yu https://orcid.org/0009-0001-2051-5306
Xiaoqiang Zhou https://orcid.org/0000-0001-7499-6662
Juan Li https://orcid.org/0000-0003-1937-1576


### References


1. Manjandavida F, Stathopoulos C, Zhang J, Honavar S, Shields C. Intra-arterial chemotherapy in retinoblastoma: A paradigm change. *Indian J Ophthalmol*. 2019;67(6):740. doi:10.4103/ijo.IJO_866_19
2. Fabian ID, Puccinelli F, Gaillard MC, Beck-Popovic M, Munier FL. Diagnosis and management of secondary epipapillary retinoblastoma. *Br J Ophthalmol*. 2017;101(10):1412–1418. doi:10.1136/bjophthalmol-2016-309899
3. Yassa G, Hassan F, Zakaria A, Nassef A. The role of intra-arterial chemotherapy in the manegment of advanced retinoblastoma: Group D & E. *Med J Cairo Univ*. 2019;87(9):3393–3400. doi:10.21608/mjcu.2019.65636
4. Abramson DH, Fabius AWM, Francis JH, et al. Ophthalmic artery chemosurgery for eyes with advanced retinoblastoma. *Ophthalmic Genet*. 2017;38(1):16–21. doi:10.1080/13816810.2016.1244695
5. Pekacka A. The role of intraarterial chemotherapy in the management of retinoblastoma. *J Ophthalmol*. 2020;2020:3638410. doi:10.1155/2020/3638410
6. Shields CL, Lally SE, Leahey AM, et al. Targeted retinoblastoma management: When to use intravenous, intra-arterial, periocular, and intravitreal chemotherapy. *Curr Opin Ophthalmol*. 2014;25(5):374–385. doi:10.1097/ICU.0000000000000091
7. Radros J, All-Eriksson C, Pal N, et al. Intra-arterial chemotherapy for retinoblastoma in Sweden: Evaluation of treatment efficacy and complications. *Acta Ophthalmol*. 2018;96(8):e1040–e1041. doi:10.1111/aos.13796
8. Yousef YA, Soliman SE, Astudillo PPP, et al. Intra-arterial chemotherapy for retinoblastoma: A systematic review. *JAMA Ophthalmol*. 2016;134(5):584. doi:10.1001/jamaophthalmol.2016.0244
9. Ravindran K, Dalvin LA, Pulido JS, Brinjikji W. Intra-arterial chemotherapy for retinoblastoma: An updated systematic review and meta-analysis. *J NeuroIntervent Surg*. 2019;11(12):1266–1272. doi:10.1136/neurintsurg-2019-014909
10. Higgins JPT, Altman DG, Gotzsche PC, et al. The Cochrane Collaboration's tool for assessing risk of bias in randomised trials. *BMJ*. 2011;343:d5928. doi:10.1136/bmj.d5928
11. Higgins JPT, Thomas J, Chandler J, et al., eds. *Cochrane Handbook for Systematic Reviews of Interventions*. 2nd ed. Hoboken, USA: John Wiley & Sons; 2019. doi:10.1002/9781119536604
12. Abramson DH, Dunkel IJ, Brodie SE, Marr B, Gobin YP. Superselective ophthalmic artery chemotherapy as primary treatment for retinoblastoma (chemosurgery). *Ophthalmology*. 2010;117(8):1623–1629. doi:10.1016/j.ophtha.2009.12.030
13. Gobin YP. Intra-arterial chemotherapy for the management of retinoblastoma: Four-year experience. *Arch Ophthalmol*. 2011;129(6):732. doi:10.1001/archophthalmol.2011.5
14. Munier FL, Beck-Popovic M, Balmer A, Gaillard MC, Bovey E, Binaghi S. Occurrence of sectoral choroidal occlusive vasculopathy and retinal arteriolar embolization after superselective ophthalmic artery chemotherapy for advanced intraocular retinoblastoma. *Retina*. 2011;31(3):566–573. doi:10.1097/IAE.0b013e318203c101
15. Peterson EC, Elhammady MS, Quintero-Wolfe S, Murray TG, Aziz-Sultan MA. Selective ophthalmic artery infusion of chemotherapy for advanced intraocular retinoblastoma: Initial experience with 17 tumors. *J Neurosurg*. 2011;114(6):1603–1608. doi:10.3171/2011.1.JNS10466
16. Suzuki S, Yamane T, Mohri M, Kaneko A. Selective ophthalmic arterial injection therapy for intraocular retinoblastoma: The long-term prognosis. *Ophthalmology*. 2011;118(10):2081–2087. doi:10.1016/j.ophtha.2011.03.013
17. Marr BP, Brodie SE, Dunkel IJ, Gobin YP, Abramson DH. Three-drug intra-arterial chemotherapy using simultaneous carboplatin, topotecan and melphalan for intraocular retinoblastoma: Preliminary results. *Br J Ophthalmol*. 2012;96(10):1300–1303. doi:10.1136/bjophthalmol-2012-301925
18. Muen WJ, Kingston JE, Robertson F, Brew S, Sagoo MS, Reddy MA. Efficacy and complications of super-selective intra-ophthalmic artery melphalan for the treatment of refractory retinoblastoma. *Ophthalmology*. 2012;119(3):611–616. doi:10.1016/j.ophtha.2011.08.045
19. Thampi S, Hetts S, Cooke DL, et al. Superselective intra-arterial melphalan therapy for newly diagnosed and refractory retinoblastoma: Results from a single institution. *Clin Ophthalmol*. 2013;7:981. doi:10.2147/OPTH.S43398
20. Venturi C, Bracco S, Cerase A, et al. Superselective ophthalmic artery infusion of melphalan for intraocular retinoblastoma: Preliminary results from 140 treatments. *Acta Ophthalmol*. 2013;91(4):335–342. doi:10.1111/j.1755-3768.2011.02296.x
21. Ghassemi F, Ghanaati H, Karkhaneh R, Boujabadi L, ZiaTabatabaie S, Rajabi MT. Outcome of retinoblastoma following limited sessions of intra-arterial chemotherapy in Iran. *Iran J Radiol*. 2014;11(3):e16958. doi:10.5812/iranjradiol.16958
22. Shields CL, Manjandavida FP, Lally SE, et al. Intra-arterial chemotherapy for retinoblastoma in 70 eyes. *Ophthalmology*. 2014;121(7):1453–1460. doi:10.1016/j.ophtha.2014.01.026
23. Taich P, Ceciliano A, Buitrago E, et al. Clinical pharmacokinetics of intra-arterial melphalan and topotecan combination in patients with retinoblastoma. *Ophthalmology*. 2014;121(4):889–897. doi:10.1016/j.ophtha.2013.10.045
24. Parareda A, Català J, Carcaboso AM, et al. Intra-arterial chemotherapy for retinoblastoma: Challenges of a prospective study. *Acta Ophthalmol*. 2014;92(3):209–215. doi:10.1111/aos.12295
25. Akyüz C, Kıratlı H, Şen H, Aydın B, Tarlan B, Varan A. Intra-arterial chemotherapy for retinoblastoma: A single-center experience. *Ophthalmologica*. 2015;234(4):227–232. doi:10.1159/000439357

26. Ong SJ, Chao AN, Wong HF, Liou KL, Kao LY. Selective ophthalmic arterial injection of melphalan for intraocular retinoblastoma: A 4-year review. *Jpn J Ophthalmol*. 2015;59(2):109–117. doi:10.1007/s10384-014-0356-y
27. Abramson DH, Marr BP, Francis JH, et al. Simultaneous bilateral ophthalmic artery chemosurgery for bilateral retinoblastoma (tandem therapy). *PLoS One*. 2016;11(6):e0156806. doi:10.1371/journal.pone.0156806
28. Chen M, Zhao J, Xia J, et al. Intra-arterial chemotherapy as primary therapy for retinoblastoma in infants less than 3 months of age: A series of 10 case-studies. *PLoS One*. 2016;11(8):e0160873. doi:10.1371/journal.pone.0160873
29. Leal-Leal CA, Asencio-López L, Higuera-Calleja J, et al. Globe salvage with intra-arterial topotecan-melphalan chemotherapy in children with a single eye. *Rev Invest Clin*. 2016;68(3):137–142.doi:10.4103/ijo.IJO_843_16.
30. Michaels ST, Abruzzo TA, Augsburger JJ, Corrêa ZM, Lane A, Geller JI. Selective ophthalmic artery infusion chemotherapy for advanced intraocular retinoblastoma: CCHMC early experience. *J Pediatr Hematol Oncol*. 2016;38(1):65–69. doi:10.1097/MPH.0000000000000471
31. Tuncer S, Sencer S, Kebudi R, Tanyıldız B, Cebeci Z, Aydın K. Superselective intra-arterial chemotherapy in the primary management of advanced intra-ocular retinoblastoma: First 4-year experience from a single institution in Turkey. *Acta Ophthalmol*. 2016;94(7):e644–e651. doi:10.1111/aos.13077
32. Chen M, Jiang H, Zhang J, et al. Outcome of intra-arterial chemotherapy for retinoblastoma and its influencing factors: A retrospective study. *Acta Ophthalmol*. 2017;95(6):613–618. doi:10.1111/aos.13333
33. Fabian ID, Naeem Z, Stacey AW, et al. Long-term visual acuity, strabismus, and nystagmus outcomes following multimodality treatment in group D retinoblastoma eyes. *Am J Ophthalmol*. 2017;179:137–144. doi:10.1016/j.ajo.2017.05.003
34. Munier FL, Mosimann P, Puccinelli F, et al. First-line intra-arterial versus intravenous chemotherapy in unilateral sporadic group D retinoblastoma: Evidence of better visual outcomes, ocular survival and shorter time to success with intra-arterial delivery from retrospective review of 20 years of treatment. *Br J Ophthalmol*. 2017;101(8):1086–1093. doi:10.1136/bjophthalmol-2016-309298
35. Reddy MA, Naeem Z, Duncan C, et al. Reduction of severe visual loss and complications following intra-arterial chemotherapy (IAC) for refractory retinoblastoma. *Br J Ophthalmol*. 2017;101(12):1704–1708. doi:10.1136/bjophthalmol-2017-310294
36. Rishi P, Sharma T, Sharma M, et al. Intra-arterial chemotherapy for retinoblastoma: Two-year results from tertiary eye-care center in India. *Indian J Ophthalmol*. 2017;65(4):311. doi:10.4103/ijo.IJO_843_16
37. Francis JH, Levin AM, Zabor EC, Gobin YP, Abramson DH. Ten-year experience with ophthalmic artery chemosurgery: Ocular and recurrence-free survival. *PLoS One*. 2018;13(5):e0197081. doi:10.1371/journal.pone.0197081
38. Funes S, Sampor C, Villasante F, et al. Feasibility and results of an intra-arterial chemotherapy program for the conservative treatment of retinoblastoma in Argentina. *Pediatr Blood Cancer*. 2018;65(8):e27086. doi:10.1002/pbc.27086
39. Hua J, Gang S, Yizhou J, Jing Z. Intra-arterial chemotherapy as second-line treatment for advanced retinoblastoma: A 2-year single-center study in China. *J Can Res Ther*. 2018;14(1):106. doi:10.4103/jcrt.JCRT_722_17
40. Kiratli H, Koç İ, Inam O, Varan A, Akyüz C. Retrospective analysis of primarily treated group D retinoblastoma. *Graefes Arch Clin Exp Ophthalmol*. 2018;256(11):2225–2231. doi:10.1007/s00417-018-4051-4
41. Rojanaporn D, Chanthanaphak E, Boonyaopas R, Sujirakul T, Hongeng S, Na Ayudhaya S. Intra-arterial chemotherapy for retinoblastoma: 8-year experience from a tertiary referral institute in Thailand. *Asia Pac J Ophthalmol (Phila)*. 2019;8(3):211–217. doi:10.22608/APO.2018294
42. Liu CC, Mohmood A, Hamzah N, Lau JH, Khaliddin N, Rahmat J. Intra-arterial chemotherapy for retinoblastoma: Our first three-and-a-half years' experience in Malaysia. *PLoS One*. 2020;15(5):e0232249. doi:10.1371/journal.pone.0232249
43. Batu Oto B, Sarıcı AM, Kızılkılıç O. Superselective intra-arterial chemotherapy treatment for retinoblastoma: Clinical experience from a tertiary referral centre. *Can J Ophthalmol*. 2020;55(5):406–412. doi:10.1016/j.jcjo.2020.04.009
44. Rishi P, Agarwal A, Chatterjee P, et al. Intra-arterial chemotherapy for retinoblastoma: Four-year results from tertiary center in India. *Ocul Oncol Pathol*. 2020;6(1):66–73. doi:10.1159/000500010
45. González ME, Gaviria ML, López M, Escudero PA, Bravo A, Vargas SA. Eye salvage with intra-arterial and intra-vitreal chemotherapy in patients with retinoblastoma: 8-year single-institution experience in Colombia. *Ocul Oncol Pathol*. 2021;7(3):215–223. doi:10.1159/000511980
46. Linde L, Mustak H. The outcomes of intra-arterial chemotherapy in retinoblastoma: A South African perspective. S Afr Ophthalmol J. 2021;16(4):13–17. https://hdl.handle.net/10520/ejc-nm_saoj_v16_n4_a4. Accessed January 20, 2022.
47. Oporto JI, Zúñiga P, Ossandón D, et al. Intra-arterial chemotherapy for retinoblastoma treatment in Chile: Experience and results 2013–2020. *Arch Soc Esp Oftalmol (Engl Ed)*. 2021;96(6):288–292. doi:10.1016/j.oftale.2020.10.003
48. Shields CL, Dockery PW, Yaghy A, et al. Intra-arterial chemotherapy for retinoblastoma in 341 consecutive eyes (1,292 infusions): Comparative analysis of outcomes based on patient age, race, and sex. *J AAPOS*. 2021;25(3):150.e1–150.e9. doi:10.1016/j.jaapos.2020.12.006
49. Li J, Jing C, Hua X, et al. Outcome of salvage intra-arterial chemotherapy for recurrent retinoblastoma. *Eye*. 2022;36(11):2106–2110. doi:10.1038/s41433-021-01693-w
50. Al Saiegh F, Chalouhi N, Sweid A, et al. Intra-arterial chemotherapy for retinoblastoma via the transradial route: Technique, feasibility, and case series. *Clin Neurol Neurosurg*. 2020;194:105824. doi:10.1016/j.clineuro.2020.105824
51. Yamane T, Kaneko A, Mohri M. The technique of ophthalmic arterial infusion therapy for patients with intraocular retinoblastoma. *Int J Clin Oncol*. 2004;9(2):69–73. doi:10.1007/s10147-004-0392-6
52. Sidipratomo P, Pandelaki J, Matondang SBRE, et al. Intra-arterial chemotherapy for retinoblastoma: Our first experience in Indonesia. *Radiol Case Rep*. 2022;17(12):4713–4716. doi:10.1016/j.radcr.2022.09.004
53. Chen Q, Zhang B, Dong Y, et al. Comparison between intravenous chemotherapy and intra-arterial chemotherapy for retinoblastoma: A meta-analysis. *BMC Cancer*. 2018;18(1):486. doi:10.1186/s12885-018-4406-6
54. Xu K, Liu J, Zhang C. Intra-arterial chemotherapy combined with VEC intravenous chemotherapy in the treatment of advanced retinoblastoma. *J BUON*. 2020;25(2):1199–1205. PMID:32521926.
55. Kaliki S. Postenucleation adjuvant chemotherapy with vincristine, etoposide, and carboplatin for the treatment of high-risk retinoblastoma. *Arch Ophthalmol*. 2011;129(11):1422. doi:10.1001/archophthalmol.2011.289
56. Kaliki S, Shields CL, Rojanaporn D, et al. High-risk retinoblastoma based on international classification of retinoblastoma: Analysis of 519 enucleated eyes. *Ophthalmology*. 2013;120(5):997–1003. doi:10.1016/j.ophtha.2012.10.044

# The efficacy of glyceryl trinitrate for acute intracerebral hemorrhage: A systematic review and meta-analysis

Qiangyuan Tian[1,A], Xiangkong Song[2,B], Liqiang Wu[3,C,D], Hongyan Shi[4,E,F]

[1] Department of Cerebrovascular Disease Center, Linyi Traditional Chinese Medical Hospital, China
[2] Department of Internal Neurology, Binzhou People's Hospital, China
[3] Department of Emergency Medicine, Binzhou Medical University Hospital, China
[4] Department of Financial Planning, Central Hospital Affiliated to Shandong First Medical University, Jinan, China

A – research concept and design; B – collection and/or assembly of data; C – data analysis and interpretation; D – writing the article; E – critical revision of the article; F – final approval of the article

Advances in Clinical and Experimental Medicine, ISSN 1899–5276 (print), ISSN 2451–2680 (online) *Adv Clin Exp Med*. 2024;33(3):217–223

**Address for correspondence**
Hongyan Shi
E-mail: shandongyanyan@sina.com

**Funding sources**
None declared

**Conflict of interest**
None declared

Received on November 10, 2022
Reviewed on March 4, 2023
Accepted on June 16, 2023

Published online on July 24, 2023

## Abstract

Current research on the effects of glyceryl trinitrate (GTN) on the lowering of elevated blood pressure (BP) among patients with acute intracerebral hemorrhage (AIH) has not been highly emphasized. The aim of this meta-analysis is to examine the effects of GTN in patients with acute stroke. The lowering of BP was the primary outcome measure in patients treated with GTN compared to no-GTN treatment. A meta-analysis was performed to evaluate the efficacy of GTN in lowering BPs and analyze the outcomes of GTN treatment. Appropriate articles were searched using PubMed, Taylor & Francis Online, Cochrane, Scopus, ScienceDirect, Wiley Online Library, and Springer, with the use of appropriate keywords as per the Preferred Reporting Items for Systematic Reviews and Meta-Analyses (PRISMA) guidelines. Out of 13 articles eligible for this study, 7 studies qualified for the meta-analysis by meeting the inclusion criteria. The PRISMA guidelines and the recommendations of Cochrane Collaboration were followed when conducting this meta-analysis. After subgroup analysis, differences between patients treated with GTN and without GTN were analyzed. The lowering of BP resulted in improved functional outcomes in patients treated with GTN. This meta-analysis showed differences between the 2 groups, with a risk ratio (RR) of 1.01 (95% confidence interval (95% CI): 0.92–10.07, $p = 0.30$, $I^2 = 18\%$). There was a significant improvement in outcome measures in patients treated with GTN by lowering elevated BP after acute stroke.

**Key words:** randomized controlled trials, acute stroke, elevated blood pressure, improved functional outcomes

**Cite as**
Tian Q, Song X, Wu L, Shi H. The efficacy of glyceryl trinitrate for acute intracerebral hemorrhage: A systematic review and meta-analysis. *Adv Clin Exp Med*. 2024;33(3):217–223. doi:10.17219/acem/168430

**DOI**
10.17219/acem/168430

# Introduction

Acute intracerebral hemorrhage (AIH) is a common subtype of hemorrhage. It is estimated to occur annually at a rate of 16 per 100,000 individuals worldwide.[1] However, research on whether the rapid lowering of blood pressure (BP) in patients with AIH improves the outcomes is still ongoing. Anderson et al. conducted a study on the rapid lowering of BP, which indicated no significant reductions in severe disabilities and mortality rate in patients.[2] However, intensive lowering of BP improved the functional outcomes. A clinical trial suggested that the risk of hematoma enlargement may be increased due to elevated BP. However, lowering BP below 150 mm Hg might help reduce the risk of hematoma.[3] The volume of the hematoma is the main predictor of 30-day mortality and poor functional outcomes.[4] The association between the baseline volume of the hematoma and oral anticoagulation has not been clarified. Some of the studies show an increased baseline volume,[5,6] while others[7,8] do not show any increase.

Transdermal glyceryl nitrate (TGN), one of the nitric oxide donors, is a candidate for the treatment of intracerebral hemorrhage (ICH). This agent can lower BP without causing any changes in cerebral blood flow. Moreover, no undesirable outcomes were reported regarding platelet function. In acute stroke patients, TGN did not cause reduction in mortality rate at 90 days. The treatment with TGN benefited patients who were randomized within 6 h of stroke onset.[9] Pre-hospital treatment with glyceryl trinitrate (GTN) resulted in worse outcomes in patients with AIH. In addition, time-by-treatment interaction was related to the negative effects of GTN if it was administered in patients randomized within 1 h of stroke onset. However, patients randomized within more than 2 h benefited from the treatment. Therefore, non-perfusion therapies should not be initiated at an earlier ultra-acute phase, because the brain is stunned, fragile and cannot respond well to the active modulation from external interventions.[10]

This systematic review and meta-analysis aimed to examine recent data in order to determine the efficacy of GTN for treating AIH patients. In the literature, the effects of time-by-treatment interaction from GTN have been studied in AIH patients in comparison to a placebo or control group. A recent review article found that GTN improved outcomes if it was administered within 2–6 h of stroke onset.[11] However, no meta-analyses regarding the safety of lowering elevated BP in ultra-acute stroke patients have been performed. Therefore, this meta-analysis investigates the efficacy of lowering the elevated systolic BP (SBP) using GTN and no GTN in patients with acute stroke.

# Objectives

The objective of this study is to examine the effects of GTN in patients with acute stroke.

# Materials and methods

## Design

Preferred Reporting Items for Systematic Reviews and Meta-Analyses (PRISMA) guidelines[12] and the recommendations of Cochrane Collaboration[13] were followed when conducting this meta-analysis.

## Inclusion and exclusion criteria

The inclusion criteria were as follows: 1) research articles focusing on GTN treatment in AIH; 2) studies including patients aged ≥18 years; and 3) studies published in English until February 10, 2023.

The exclusion criteria included 1) editorials, letters and commentaries; and 2) duplicate research articles with the same study population.

## Search strategy

To perform an electronic search, PRISMA guidelines for a systematic review were followed, and PubMed, Taylor & Francis Online, Cochrane, Scopus, ScienceDirect, Wiley Online Library, and Springer databases were additionally

Table 1. Database search strategy

| Database | Keywords |
|---|---|
| PubMed | (glyceryl trinitrate (title/abstract)) OR (trinitroglycerin (title/abstract)) OR ((nitroglycerine (title/abstract)) AND (intracerebral hemorrhage (title/abstract))) OR (stroke (title/abstract)) |
| Taylor & Francis Online | "hemorrhage" OR "intracerebral hemorrhage" AND "glyceryl nitrate (GTN)" OR "transdermal glyceryl nitrate (TGN)" |
| Cochrane | "glyceryl trinitrate" (title, abstract, keyword) AND "acute intracerebral hemorrhage" (title, abstract, keyword) OR "acute ischemic stroke" (title, abstract, keyword) OR "blood pressure" (title, abstract, keyword) |
| Scopus | "glyceryl trinitrate, acute intracerebral hemorrhage, acute ischemic stroke" OR "blood pressure" |
| ScienceDirect | "glyceryl trinitrate for acute intracerebral hemorrhage" |
| Wiley Online Library | "glyceryl trinitrate" (anywhere) AND "acute intracerebral hemorrhage" (anywhere) AND "acute ischemic stroke" (anywhere) |
| Springer | "glyceryl" AND "trinitrate" AND "for" AND "acute" AND "intracerebral" AND "hemorrhage" |

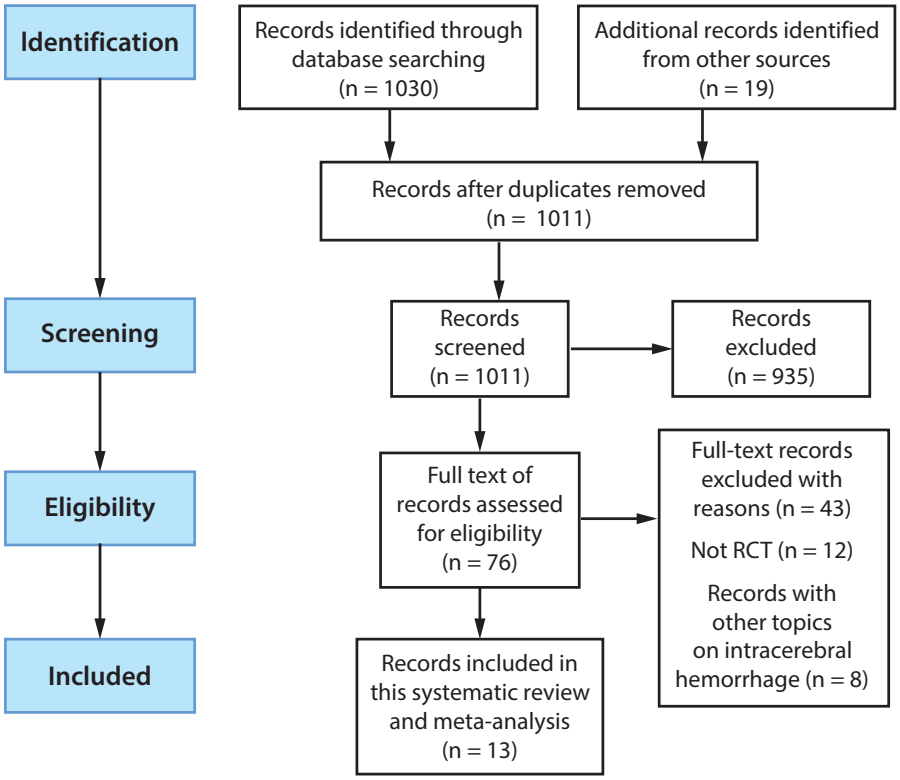


**Fig. 1.** Preferred Reporting Items for Systematic Reviews and Meta-Analyses (PRISMA) flowchart for the selection of research articles

RCT – randomized controlled trial.

searched to identify controlled trials that compared the effects of GTN with non-GTN medications (Table 1). Titles, abstracts and full-text articles were sequentially reviewed (Fig. 1). The quality of the included studies was assessed using the COCHRANE manual.[13]

## Study selection

Endnote™ X9 (Clarivate, London, UK), a referencing package, was used to manage the references of research articles. After the removal of duplicates, 2 authors (QT and XS) independently performed the selection of research articles in 2 phases. Abstracts and titles of the articles were evaluated in order to exclude irrelevant studies. In the next phase, full-text research articles were assessed in detail.

## Data extraction

Data from the eligible studies were independently extracted, including study ID or reference (first author and publication year), study design, and population, intervention, comparison, outcomes and study (PICOS) criteria-based information (Table 2).

## Quality assessment

The Newcastle–Ottawa Scale (NOS)[14] has been jointly developed by the University of Newcastle (Australia) and the University of Ottawa (Canada). The scale is widely used to assess the quality of non-randomized trials in systematic reviews. The methodological quality of this meta-analysis was assessed using NOS. A study with a NOS score ≥7 points was considered of a high quality. Any disagreement between the 2 authors was settled through consensus.

## Statistical analyses

Review Manager (RevMan) v. 5.4.1 (Cochrane, London, UK) was used to perform all statistical analyses in the present study. Data extracted from the included research articles were combined using a random effects model with Begg's and Egger's tests, which deflate the type I error rate and publication bias in a meta-analysis, respectively. Risk ratios (RRs) and 95% confidence intervals (95% CIs) were calculated for the dichotomous data. The $\chi^2$ and $I^2$ tests were used to determine the heterogeneity between included research articles. Heterogeneity was assessed using Cochrane's Q, which is calculated as the weighted sum of squared differences between pooled effects and the individual study effects across the included studies, where Q has distribution as a $\chi^2$ static with k (number of studies) minus 1 degree of freedom. Thus, heterogeneity ($I^2$) is measured as follows (Equation 1):

$$I^2 = \frac{Q - df}{Q} \times 100 \quad (1)$$

where Q expresses Cochrane's homogeneity test static, and df – degrees of freedom.

Table 2. Characteristics of the included studies

| Author of the study, reference | Study design | Population | Intervention | Comparison | Outcomes |
|---|---|---|---|---|---|
| Anderson et al.[2] | RCT | n = 2839, mean age: 63.5 years | topical nitrate | intensive treatment compared to recommended guidelines | lowering BP improved functional outcomes |
| Krishnan et al.[9] | RCT | n = 629, mean age: 67 years, acute stroke | GTN | GTN compared to no GTN | improved functional ability outcomes, lowered BP |
| Bath et al.[10] | prospective randomized trial | n = 145, mean age: 73 years, presumed stroke | GTN and sham | GTN compared to sham | improved functional outcomes |
| Appleton et al.[15] | randomized trial | n = 4011, mean age: 70.3 years, acute stroke | GTN | transdermal GTN compared to no GTN | poor functional and cognitive outcomes |
| Ankolekar et al.[16] | RCT | n = 80, mean age: 79 years | GTN | placebo | improved functional outcomes |
| Woodhouse et al.[17] | RCT | n = 273, mean age: 69 years, acute stroke | GTN | GTN compared to no GTN | improved functional outcomes and lower mortality rate |
| ENOS Trial Investigators[18] | RCT | n = 4011, age ≥18 years, acute stroke | GTN | GTN compared to no GTN | GTN improved safety without improving functional outcomes |
| Qureshi et al.[19] | randomized trial | n = 1000, mean age: 61.9 years, acute cerebral hemorrhage | nicardipine | intensive compared to standard treatment | severe disability or death |
| Tunnage et al.[20] | RCT | n = 1149, mean age: 67 years, stroke mimic | GTN and sham | GTN compared to sham | functional disorder, migraine and seizure |
| Dixon et al.[21] | RCT | n = 1149, mean age: 73 years, hypertensive stroke | GTN and sham | GTN compared to no GTN | rapid delivery of GTN (within 2 h); both distance and time may impede patients to access stroke services |
| van den Berg et al.[22] | RCT | n = 1400, age ≥18 years, acute stroke | GTN | placebo (GTN) | prompt GTN prevents delay to revascularization; lowered BP |
| Bath et al.[23] | RCT | n = 1149, mean age: 73 years, ultra-acute presumed stroke | GTN and sham | GTN compared to sham | no improvement in functional outcomes, increased mortality rate |
| Beishon et al.[24] | RCT | n = 4011, mean age: 70.23 years, acute stroke | GTN | GTN compared to no GTN | poor clinical outcomes |

GTN – glyceryl trinitrate; BP – blood pressure; RCT – randomized controlled trial.

A value of $p < 0.05$ and $I^2 > 0.50$ illustrated the substantial statistical heterogeneity. Therefore, we used a random-effects model. A subgroup analysis was performed in patients treated with GTN and without GTN. A funnel plot was employed to assess the publication bias.

## Risk-of-bias assessment

The review process requires the validation of selected studies by evaluating the risk of bias in the results of the study. The risk of bias evaluates the robustness of the methodology used in the studies and assesses whether conclusions were based on objective and valid evidence. The risk of publication bias was assessed using Begg's rank test and Egger's linear test.

# Results

The selection process of research articles was based on the inclusion and exclusion criteria, as shown in Fig. 1.

## Search results

After performing a digital database search, a total of 1049 research articles were retrieved. Then, 38 duplicates were removed. The titles and abstracts of the remaining 1011 articles were screened. As a result, 935 research articles were excluded. The remaining 76 research articles were read and thoroughly assessed for their relevancy to the research topic. Based on the inclusion and exclusion criteria, 13 research articles were chosen for the final inclusion in this meta-analysis (Table 2).[2,9,10,15–24]

# Characteristics of the included studies

## Primary outcomes

The variability in the modified Rankin Scale (mRS) evaluated for several days was the primary outcome

measure. One study presented SBP variability over 1–7 days on the mRS and death at 90 days.[15] Seven studies were qualified for the meta-analysis based on SBP values.[9,15–18,23,24] Out of the 7 studies, 2 research articles[16,17] favored the use of GTN to improve functional outcomes, while 5 studies[9,15,18,23,24] did not show improvement in functional outcomes after GTN treatment.

We compared the primary outcomes of an acute stroke subgroup based on the variation in SBP between GTN and no-GTN treatments. There was no significant difference in the primary outcome from the subgroup analysis.

The remaining studies compared different treatment agents than the previously mentioned studies.[2,10,19,21–23] For example, Anderson et al. examined the intensive treatment and recommended guidelines in acute stroke.[2] Bath et al.[10] and Tunnage et al.[20] focused on the treatment groups (GTN compared to sham), while Qureshi et al.[19] evaluated intensive compared to standard treatment groups in a randomized controlled trial (RCT). Dixon et al.[21] and van den Berg et al.[22] examined studies on hypertensive stroke and acute stroke, respectively. A study by ENOS Trial Investigators revealed data on ischemic stroke (IS) and ICH.[18] Hence, the same study was represented twice in the forest plot.

The baseline of SBP, based on the SBP level, and subgroups (GTN compared to no GTN) were analyzed. Neutral results ($p < 0.05$) were obtained from 2 group analyses (Fig. 2).

We used a funnel plot and Begg's test to assess the publication bias (Fig. 3). Our study has a low risk of publication bias, as presented in a funnel plot, and the significant p-values of Begg's test[25] are greater than 0.05 (0.628). In addition to the funnel plot and Begg's test results, Egger's test showed significant results ($z = 2.04$, $p = 0.04$).

## Discussion

Intracerebral hemorrhage is a type of stroke with a high mortality rate, accounting for 15–20% of acute strokes.[26–28] An increased risk of ICH is associated with ischemic and hemorrhagic strokes and evolves into chronic lesions causing local microstructural injuries. Data on the treatment with GTN and non-GTN medications come from a low number of studies.[29–32] Also, none of the previous meta-analyses compared GTN and its effects on patients with ICH to patients without GTN treatment.

High BP is common in patients with stroke, and is associated with poor outcomes, including acute stroke and death within a few weeks. Therefore, in most cases, BP control is an essential part of the ICH treatment. Nitrate agents help lower BP in acute stroke. Glyceryl trinitrate is one of the valuable agents, particularly in pre-hospital settings.[33–36] To investigate the effect of GTN administration in patients, a systematic review and meta-analysis of 13 studies recruiting a total of 16,686 participants was conducted. With the inclusion of 4011 patients from a RCT,[24] our systematic review had a greater number of recruited patients compared to other meta-analyses. Thus, our study filled the previously existing research gap. The results of our meta-analysis showed that differences in primary outcomes were significant in GTN compared to non-GTN groups. Our findings are consistent with those of a previous study.[37]

There were 5 previously published systematic reviews and meta-analyses on the topic.[11,38–41] Of these meta-analyses,

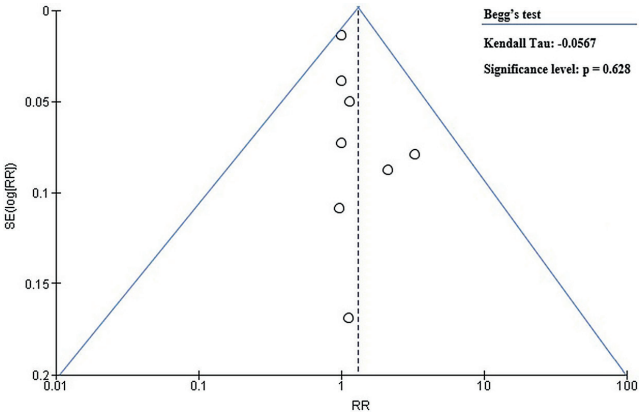


Fig. 3. Funnel plot of publication bias

SE – standard error; RR – risk ratio.

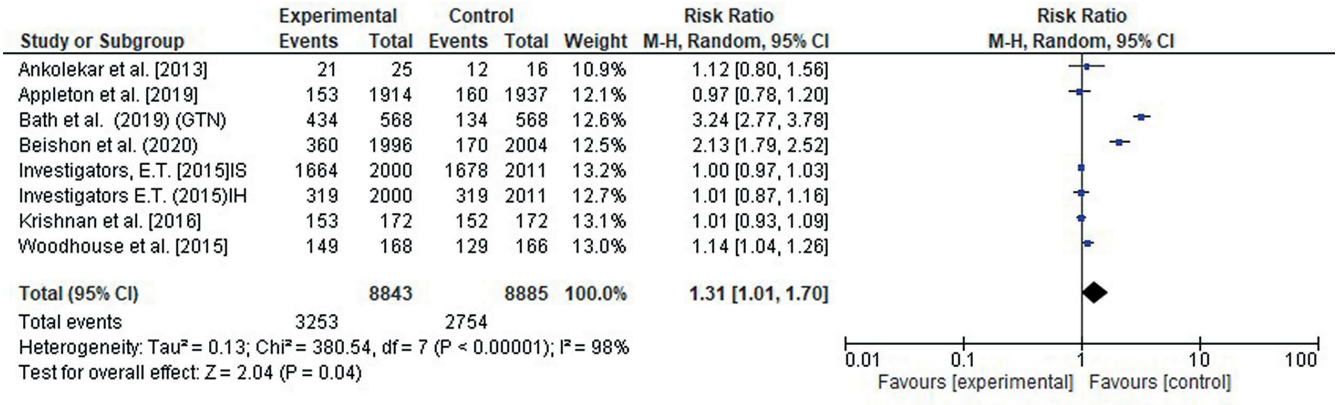


Fig. 2. Forest plot of random effects model

df – degrees of freedom; 95% CI – 95% confidence interval.

only 1 study showed a significant relationship between lowering the elevated BP in acute stroke and improved functional outcomes.[42] Overall, a positive link was observed between lowering BP and a reduction of the risk of acute stroke. The remaining 4 meta-analyses were consistent with the results stating that lowering BP did not show a strong association with the reduction of the risk of acute stroke.

This systematic review showed interesting results regarding the lowering of BP and safety in patients with an acute stroke. However, there were no functional improvements in patients participating in a RCT. This might have been due to the intake of a high concentration of nitric oxide (NO), which might damage brain tissues.[43–45]

The results of the subgroup analysis showed that patients with acute stroke treated with GTN had improved functional outcomes in a few cases with a longer pre-hospital duration or no history of hypertension. In patients with stroke, survival chances did not increase after GTN treatment.[46–48] However, the treatment was effective in pre-hospital conditions, which is consistent with the results of previous analyses.[23,49] These findings play a vital role in the selection of appropriate therapeutic strategies.

## Limitations

This meta-analysis has several limitations. The main limitation is the low number of included research articles. Careful and extensive retrieval of information was performed to minimize the risk of publication bias. We included 7 RCTs that limited the statistical power to find differences. Although strict inclusion and exclusion criteria were followed, selection bias or observer bias may have influenced the research outcomes. To confirm the results of this meta-analysis, more RCTs should be performed with larger sample sizes.

# Conclusions

This meta-analysis demonstrated the efficacy of GTN and its variants in patients with acute stroke. The lowering of SBP is associated with functional improvements in patients with AIH. Due to the small number of included studies, our meta-analysis shows high heterogeneity between the studies. Further research trials should be undertaken to provide stronger evidence and improve outcomes in acute stroke patients.


## ORCID iDs

Hongyan Shi https://orcid.org/0000-0002-2789-9779


## References


1. Wilkinson DA, Pandey AS, Thompson BG, Keep RF, Hua Y, Xi G. Injury mechanisms in acute intracerebral hemorrhage. *Neuropharmacology*. 2018;134(Pt B):240–248. doi:10.1016/j.neuropharm.2017.09.033
2. Anderson CS, Heeley E, Huang Y, et al. Rapid blood-pressure lowering in patients with acute intracerebral hemorrhage. *N Engl J Med*. 2013;368(25):2355–2365. doi:10.1056/NEJMoa1214609
3. Ohwaki K, Yano E, Nagashima H, Hirata M, Nakagomi T, Tamura A. Blood pressure management in acute intracerebral hemorrhage: Relationship between elevated blood pressure and hematoma enlargement. *Stroke*. 2004;35(6):1364–1367. doi:10.1161/01.STR.0000128795.38283.4b
4. Davis SM, Broderick J, Hennerici M, et al. Hematoma growth is a determinant of mortality and poor outcome after intracerebral hemorrhage. *Neurology*. 2006;66(8):1175–1181. doi:10.1212/01.wnl.0000208408.98482.99
5. Cucchiara B, Messe S, Sansing L, Kasner S, Lyden P. Hematoma growth in oral anticoagulant related intracerebral hemorrhage. *Stroke*. 2008;39(11):2993–2996. doi:10.1161/STROKEAHA.108.520668
6. Flaherty ML, Tao H, Haverbusch M, et al. Warfarin use leads to larger intracerebral hematomas. *Neurology*. 2008;71(14):1084–1089. doi:10.1212/01.wnl.0000326895.58992.27
7. Biffi A, Anderson CD, Jagiella JM, et al. APOE genotype and extent of bleeding and outcome in lobar intracerebral haemorrhage: A genetic association study. *Lancet Neurol*. 2011;10(8):702–709. doi:10.1016/S1474-4422(11)70148-X
8. Flibotte JJ, Hagan N, O'Donnell J, Greenberg SM, Rosand J. Warfarin, hematoma expansion, and outcome of intracerebral hemorrhage. *Neurology*. 2004;63(6):1059–1064. doi:10.1212/01.WNL.0000138428.40673.83
9. Krishnan K, Scutt P, Woodhouse L, et al. Glyceryl trinitrate for acute intracerebral hemorrhage: Results from the Efficacy of Nitric Oxide in Stroke (ENOS) trial. A subgroup analysis. *Stroke*. 2016;47(1):44–52. doi:10.1161/STROKEAHA.115.010368
10. Bath PM, Woodhouse LJ, Krishnan K, et al. Prehospital transdermal glyceryl trinitrate for ultra-acute intracerebral hemorrhage: Data from the RIGHT-2 trial. *Stroke*. 2019;50(11):3064–3071. doi:10.1161/STROKEAHA.119.026389
11. Appleton JP, Krishnan K, Bath PM. Transdermal delivery of glyceryl trinitrate: Clinical applications in acute stroke. *Expert Opin Drug Deliv*. 2020;17(3):297–303. doi:10.1080/17425247.2020.1716727
12. Moher D, Liberati A, Tetzlaff J, Altman DG; for the PRISMA Group. Preferred reporting items for systematic reviews and meta-analyses: The PRISMA statement. *BMJ*. 2009;339:b2535. doi:10.1136/bmj.b2535
13. Higgins JPT, Thomas J, Chandler J, et al., eds. Cochrane Handbook for Systematic Reviews of Interventions. 2nd ed. Hoboken, USA: John Wiley & Sons; 2019. doi:10.1002/9781119536604
14. Wells G, Shea B, O'Connell D, et al. The Newcastle-Ottawa Scale (NOS) for assessing the quality of nonrandomized studies in meta-analysis. Ottawa, Canada: Ottawa Hospital Research Institute; 2021. https://www.ohri.ca/programs/clinical_epidemiology/oxford.asp. Accessed March 20, 2022.
15. Appleton JP, Woodhouse LJ, Bereczki D, et al. Effect of glyceryl trinitrate on hemodynamics in acute stroke: Data from the ENOS trial. *Stroke*. 2019;50(2):405–412. doi:10.1161/STROKEAHA.118.023190
16. Ankolekar S, Fuller M, Cross I, et al. Feasibility of an ambulance-based stroke trial, and safety of glyceryl trinitrate in ultra-acute stroke: The rapid intervention with glyceryl trinitrate in Hypertensive Stroke Trial (RIGHT, ISRCTN66434824). *Stroke*. 2013;44(11):3120–3128. doi:10.1161/STROKEAHA.113.001301
17. Woodhouse L, Scutt P, Krishnan K, et al. Effect of hyperacute administration (within 6 hours) of transdermal glyceryl trinitrate, a nitric oxide donor, on outcome after stroke: Subgroup analysis of the Efficacy of Nitric Oxide in Stroke (ENOS) trial. *Stroke*. 2015;46(11):3194–3201. doi:10.1161/STROKEAHA.115.009647
18. ENOS Trial Investigators. Efficacy of nitric oxide, with or without continuing antihypertensive treatment, for management of high blood pressure in acute stroke (ENOS): A partial-factorial randomised controlled trial. *Lancet*. 2015;385(9968):617–628. doi:10.1016/S0140-6736(14)61121-1
19. Qureshi AI, Palesch YY, Barsan WG, et al. Intensive blood-pressure lowering in patients with acute cerebral hemorrhage. *N Engl J Med*. 2016;375(11):1033–1043. doi:10.1056/NEJMoa1603460
20. Tunnage B, Woodhouse LJ, Dixon M, et al. Pre-hospital transdermal glyceryl trinitrate in patients with stroke mimics: Data from the RIGHT-2 randomised-controlled ambulance trial. *BMC Emerg Med*. 2022;22(1):2. doi:10.1186/s12873-021-00560-x

21. Dixon M, Appleton JP, Scutt P, et al. Time intervals and distances travelled for prehospital ambulance stroke care: Data from the randomised-controlled ambulance-based Rapid Intervention with Glyceryl trinitrate in Hypertensive stroke Trial-2 (RIGHT-2). *BMJ Open*. 2022;12(11):e060211. doi:10.1136/bmjopen-2021-060211
22. van den Berg SA, Dippel DWJ, Hofmeijer J, et al. Multicentre Randomised trial of Acute Stroke treatment in the Ambulance with a nitroglycerin Patch (MR ASAP): Study protocol for a randomised controlled trial. *Trials*. 2019;20(1):383. doi:10.1186/s13063-019-3419-z
23. Bath PM, Scutt P, Anderson CS, et al. Prehospital transdermal glyceryl trinitrate in patients with ultra-acute presumed stroke (RIGHT-2): An ambulance-based, randomised, sham-controlled, blinded, phase 3 trial. *Lancet*. 2019;393(10175):1009–1020. doi:10.1016/S0140-6736(19)30194-1
24. Beishon L, Woodhouse LJ, Bereczki D, et al. Relationship between nitrate headache and outcome in patients with acute stroke: Results from the Efficacy of Nitric Oxide in Stroke (ENOS) trial. *Stroke Vasc Neurol*. 2021;6(2):180–186. doi:10.1136/svn-2020-000498
25. Hayashino Y, Noguchi Y, Fukui T. Systematic evaluation and comparison of statistical tests for publication bias. *J Epidemiol*. 2005;15(6):235–243. doi:10.2188/jea.15.235
26. Sun J, Wang Y, Zhang X, He H. The effects of metformin on insulin resistance in overweight or obese children and adolescents: A PRISMA-compliant systematic review and meta-analysis of randomized controlled trials. *Medicine (Baltimore)*. 2019;98(4):e14249. doi:10.1097/MD.0000000000014249
27. Zubair A, Nadeem W, Rasheed S, et al. Meta-analysis of safety effect of nitric oxide drugs on acute cerebral hemorrhage. *Pak J Med Health Sci*. 2022;16(6):178–181. doi:10.53350/pjmhs22166178
28. Gong S, Lin C, Zhang D, et al. Effects of intensive blood pressure reduction on acute intracerebral hemorrhage: A systematic review and meta-analysis. *Sci Rep*. 2017;7(1):10694. doi:10.1038/s41598-017-10892-z
29. Pan C, Hu Y, Liu N, et al. Aggressive blood pressure lowing therapy in patients with acute intracerebral hemorrhage is safe: A systematic review and meta-analysis. *Chin Med J (Engl)*. 2015;128(18):2524–2529. doi:10.4103/0366-6999.164982
30. Tsivgoulis G, Katsanos AH, Butcher KS, et al. Intensive blood pressure reduction in acute intracerebral hemorrhage: A meta-analysis. *Neurology*. 2014;83(17):1523–1529. doi:10.1212/WNL.0000000000000917
31. Ma J, Li H, Liu Y, You C, Huang S, Ma L. Effects of intensive blood pressure lowering on intracerebral hemorrhage outcomes: A meta-analysis of randomized controlled trials. *Turk Neurosurg*. 2015;25(4):544–551. doi:10.5137/1019-5149.JTN.9270-13.0
32. Boulouis G, Morotti A, Goldstein JN, Charidimou A. Intensive blood pressure lowering in patients with acute intracerebral haemorrhage: Clinical outcomes and haemorrhage expansion. Systematic review and meta-analysis of randomised trials. *J Neurol Neurosurg Psychiatry*. 2017;88(4):339–345. doi:10.1136/jnnp-2016-315346
33. Bath PM, Willmot MM, Leonardi-Bee J, Bath-Hextall FJ. Nitric oxide donors (nitrates), L-arginine, or nitric oxide synthase inhibitors for acute stroke. *Cochrane Database Syst Rev*. 2002;2017(4):CD000398. doi:10.1002/14651858.CD000398.pub2
34. Kapil V, Khambata RS, Robertson A, Caulfield MJ, Ahluwalia A. Dietary nitrate provides sustained blood pressure lowering in hypertensive patients: A randomized, phase 2, double-blind, placebo-controlled study. *Hypertension*. 2015;65(2):320–327. doi:10.1161/HYPERTENSIONAHA.114.04675
35. Bonilla Ocampo D, Paipilla A, Marín E, Vargas-Molina S, Petro J, Pérez-Idárraga A. Dietary nitrate from beetroot juice for hypertension: A systematic review. *Biomolecules*. 2018;8(4):134. doi:10.3390/biom8040134
36. Shepherd AI, Wilkerson DP, Dobson L, et al. The effect of dietary nitrate supplementation on the oxygen cost of cycling, walking performance and resting blood pressure in individuals with chronic obstructive pulmonary disease: A double blind placebo controlled, randomised control trial. *Nitric Oxide*. 2015;48:31–37. doi:10.1016/j.niox.2015.01.002
37. Al-Shahi Salman R, Frantzias J, Lee RJ, et al. Absolute risk and predictors of the growth of acute spontaneous intracerebral haemorrhage: A systematic review and meta-analysis of individual patient data. *Lancet Neurol*. 2018;17(10):885–894. doi:10.1016/S1474-4422(18)30253-9
38. Lim BL, Lee WF, Ng WM, et al. Benefits and safety of transdermal glyceryl trinitrate in acute stroke: A systematic review and meta-analysis of randomized trials. *Acad Emerg Med*. 2022;29(6):772–788. doi:10.1111/acem.14408
39. Chang J, Sanossian N. Pre-hospital glyceryl trinitrate: Potential for use in intracerebral hemorrhage. *J Neurol Disord*. 2013;2(1):141. doi:10.4172/2329-6895.1000141
40. Moullaali TJ, Wang X, Woodhouse LJ, et al. Lowering blood pressure after acute intracerebral haemorrhage: Protocol for a systematic review and meta-analysis using individual patient data from randomised controlled trials participating in the Blood Pressure in Acute Stroke Collaboration (BASC). *BMJ Open*. 2019;9(7):e030121. doi:10.1136/bmjopen-2019-030121
41. Krishnan K, Scutt P, Woodhouse L, et al. Continuing versus stopping prestroke antihypertensive therapy in acute intracerebral hemorrhage: A subgroup analysis of the efficacy of nitric oxide in stroke trial. *J Stroke Cerebrovasc Dis*. 2016;25(5):1017–1026. doi:10.1016/j.jstrokecerebrovasdis.2016.01.010
42. De Oliveira MAL, Goffi A, Zampieri FG, et al. The critical care management of spontaneous intracranial hemorrhage: A contemporary review. *Crit Care*. 2016;20:272. doi:10.1186/s13054-016-1432-0
43. Sorby-Adams AJ, Learoyd AE, Bath PM, et al. Glyceryl trinitrate for the treatment of ischaemic stroke: Determining efficacy in rodent and ovine species for enhanced clinical translation. *J Cereb Blood Flow Metab*. 2021;41(12):3248–3259. doi:10.1177/0271678X211018901
44. Cai L, Rajah G, Duan H, et al. Rapid Intravenous Glyceryl Trinitrate in Ischemic Damage (RIGID) after stroke: Rationale, design and protocol for a prospective randomized controlled trial. *Front Neurol*. 2021;12:693330. doi:10.3389/fneur.2021.693330
45. Gao J, Cheng Z, Jiang S, et al. Arterial Glyceryl Trinitrate in Acute Ischemic Stroke after Thrombectomy for Neuroprotection (AGAIN): Rationale, design and protocol for a prospective randomized controlled trial. *BMC Geriatr*. 2022;22(1):804. doi:10.1186/s12877-022-03506-5
46. Lee KB, Lim SH, Kim KH, et al. Six-month functional recovery of stroke patients: A multi-time-point study. *Int J Rehabil Res*. 2015;38(2):173–180. doi:10.1097/MRR.0000000000000108
47. Grefkes C, Fink GR. Recovery from stroke: Current concepts and future perspectives. *Neurol Res Pract*. 2020;2:17. doi:10.1186/s42466-020-00060-6
48. Boysen G, Marott JL, Grønbæk M, Hassanpour H, Truelsen T. Long-term survival after stroke: 30 years of follow-up in a cohort, the Copenhagen City Heart Study. *Neuroepidemiology*. 2009;33(3):254–260. doi:10.1159/000229780
49. Todoroski KB. The timing of administering aspirin and nitroglycerin in patients with STEMI ECG changes alter patient outcome. *BMC Emerg Med*. 2021;21(1):137. doi:10.1186/s12873-021-00523-2

# Immune and allergenic effects of the microalga *Coccomyxa* sp. strain KJ in healthy humans: A pilot study

Satomi Asai[1,A,D], Kyoko Hayashi[1,2,A], Haruyo Atsumi[1,B], Mika Doi[1,B], Hidehumi Kakizoe[1,B], Kazuo Umezawa[3,C], Akihumi Hisada[4,B], Tsukasa Nozaki[4,B], Akiko Kanno[5,A], Satoko Komatsu[5,A], Hitoshi Kuno[5,A], Kentaro Wakamatsu[6,E], Toshio Kawahara[2,E], Yoshiro Yamamoto[7,C], Hayato Miyachi[1,F]

[1] Department of Laboratory Medicine, Tokai University School of Medicine, Isehara, Japan
[2] Department of Clinical Engineering, College of Life and Health Sciences, Chubu University, Kasugai, Japan
[3] Department of Emergency and Critical Care, Tokai University School of Medicine, Isehara, Japan
[4] Clinical Laboratory Center, Tokai University Hospital, Isehara, Japan
[5] DENSO Corporation, Kariya, Japan
[6] National Hospital Organization Omuta National Hospital, Japan
[7] Department of Mathematics, Faculty of Science, Tokai University, Hiratsuka, Japan

A – research concept and design; B – collection and/or assembly of data; C – data analysis and interpretation; D – writing the article; E – critical revision of the article; F – final approval of the article

Advances in Clinical and Experimental Medicine, ISSN 1899–5276 (print), ISSN 2451–2680 (online) *Adv Clin Exp Med*. 2024;33(3):225–232

**Address for correspondence**
Satomi Asai
E-mail: sa@is.icc.u-tokai.ac.jp

**Funding sources**
None declared

**Conflict of interest**
None declared

**Acknowledgements**
We would like to thank Editage (www.editage.com) for English-language editing.

Received on December 14, 2022
Reviewed on February 15, 2023
Accepted on May 31, 2023

Published online on June 30, 2023

**Cite as**
Asai S, Hayashi K, Atsumi H, et al. Immune and allergenic effects of the microalga *Coccomyxa* sp. strain KJ in healthy humans: A pilot study. *Adv Clin Exp Med*. 2024;33(3):225–232. doi: 10.17219/acem/166665

**DOI**
10.17219/acem/166665



## Abstract

**Background.** The *Coccomyxa* sp. strain KJ (*Coccomyxa* KJ), a microalga found in Japan, has a potential function in controlling viral infections. Recently, its dry powder has been marketed as a health food product.

**Objectives.** This pilot study investigated the effects of *Coccomyxa* KJ powder tablet intake on allergic reactions and immune functions in healthy participants.

**Materials and methods.** Nine healthy volunteers (4 males and 5 females) who expressed interest in foods containing *Coccomyxa* KJ, and were willing to undergo blood tests, were recruited. Each individual was asked to take 2 *Coccomyxa* KJ powder tablets (0.3 g) before breakfast once a day for 4 weeks. The salivary immunoglobulin A (IgA) level and blood parameters (white blood cell (WBC) count, eosinophil and lymphocyte counts and percentages, natural killer (NK) cell activity, interleukin (IL)-6 level, and T helper (Th)1/Th2 cell ratio) were evaluated at baseline and weeks 2 and 4.

**Results.** The 4-week intake of *Coccomyxa* KJ did not affect salivary IgA levels, WBC count, eosinophil and lymphocyte counts and percentages, or the Th1/Th2 ratio. There were significant differences in the NK cell activity after 4 weeks, with an average increase of 11.78 (95% confidence interval (95% CI): 6.80–16.76). None of the patients experienced adverse reactions during or after the study.

**Conclusions.** Long-term *Coccomyxa* KJ intake improved NK cell activity without causing adverse effects on the indicators of local immunity, systemic inflammation and immune response balance. This study suggests that *Coccomyxa* KJ powder tablets can induce beneficial immune modifications without causing any adverse effects.

**Key words:** allergic reactions, immune functions, *Coccomyxa* sp. KJ

## Background

Typical representatives of the genus *Coccomyxa* are 6–14 μm × 3–6 μm in size and are irregularly oval or spherical. Moreover, *Coccomyxa* species are characterized by a parietal chloroplast shape without a pyrenoid and the absence of flagella.[1,2] *Coccomyxa*-like organisms of the Trebouxiophyceae class are classified into 3 genera according to their morphology. Only species with massive and partially stratified mucus belong to the genus *Coccomyxa*.[3] In the class Trebouxiophyceae, the genus *Choricystis* represents a unique phylogenetic lineage; however, whether *Coccomyxa* and *Pseudococcomyxa* are 2 distinct genera remains unresolved.[4] According to Jaag (1933), many strains are available in public culture collections.[1]

The genus *Coccomyxa* belongs to the green algae class Trebouxiophyceae and can be subdivided into the Chlorella, Oocystis and Trebouxia lineages using molecular approaches.[5,6] All known strains of *Coccomyxa* belong to the Elliptochloris clade.[7,8] *Coccomyxa* was the first terrestrial green alga to have a fully sequenced genome[7] and be classified by The National Center for Biotechnology Information (NCBI). The following species have been identified, named and registered: *C. melkonianii*, *Coccomyxa cf. olivacea 078*, *C. onubensis*, *C. parasitica*, *C. polymorpha*, *Coccomyxa cf.*, *C. vinatzeri*, and *C. viridis*. Moreover, many unclassified *Coccomyxa* are registered. *Coccomyxa* sp. strain KJ (IPOD FERM BP-22254) (hereafter referred to as "*Coccomyxa* KJ") is also registered in the NCBI.

The nucleotides, proteins, identical protein groups, and taxonomy of *Coccomyxa* KJ have been analyzed. The unicellular algae, belonging to the class Trebouxiophyceae, were found to be a different species from the previously identified *Coccomyxa*. *Coccomyxa* KJ, a microalga found in Japan, has been studied for the extraction and utilization of its intrinsic lipid components as a bioenergy source.[9–11] *Coccomyxa* KJ were isolated by Prof. Hideaki Miyashita in a Rural Biomass Research Project funded by the Ministry of Agriculture, Forestry and Fisheries of Japan.[12] *Coccomyxa* is a genus of algae, approx. 5 μm in size, that inhabits ponds and hot springs. *Coccomyxa* were cultivated in open ponds at a pH between 3.0 and 4.0 to minimize the chance of contamination with other phototrophs and protozoa. *Coccomyxa* KJ can store up to 30% oil and more than 50% protein when the culture conditions are controlled.[9] They can grow rapidly in minimal mineral media and accumulate triacylglycerols with lipid bodies at levels >60% of their dry weight (w/w) at the time of nitrogen decrease. Furthermore, *Coccomyxa* KJ has a high hydrocarbon production capacity and is capable of producing hydrocarbons when the ratio of nitrogen to dry weight is less than 2 wt%. Therefore, the hydrocarbon content per w/w unit of *Coccomyxa* KJ can be increased. It has been proposed to use the produced hydrocarbons as an alternative to fossil fuels (e.g., biodiesel fuel). However, replacing fossil fuels with hydrocarbons from microalgae requires lowering the cost of producing hydrocarbons. For this purpose, microalgae with higher hydrocarbon production capacity are required. *Coccomyxa* KJ is a unicellular green alga with very high triacylglycerol (TAG) productivity isolated from hot spring water (Japanese Patent Application Laid-Open No. 2015-015918), and can be cultured in an open-system culture (Japanese Patent Application Laid-Open No. 2014-117202).

The virucidal action of *Coccomyxa* KJ has been reported.[13–16] Supplementation of *Coccomyxa* KJ in the diet of mice facilitated the induction of neutralizing antibodies against the influenza virus and maintained the antibody titer.[13] Monogalactosyl diacylglyceride (MGDG) isolated from *Coccomyxa* KJ was able to inactivate clinical isolates of severe acute respiratory syndrome coronavirus 2 (SARS-CoV-2) in a time- and concentration-dependent manner. Experimental results showed that *Coccomyxa* KJ helped to advance a potent virus-destructive action factor against SARS-CoV-2, which is an enveloped virus, by causing envelope damage that resulted in the loss of viral host-cell-binding ability. Of the total fatty acids in MGDG, α-linolenic acid (C18:3) accounted for about 72% and 7,10,13-hexadecatrienoic acid (C16:3) for 23%.[14] Moreover, MGDG from *Coccomyxa* KJ showed virucidal activity against herpes simplex virus type 2 (HSV-2), the pathogen that causes genital herpes. Physical changes in the shape of HSV-2 were observed after treatment with MGDG, and electron microscope evaluation revealed a decrease in particle size and possible damage to the viral envelope. Similar to the morphological findings, the viral particles lost their ability to bind to host cells. The HSV-2 treated with high concentrations of MGDG was not pathogenic in animal models, indicating that MGDG exhibits irreversible virus-killing activity against HSV-2 particles. In an animal model of genital herpes caused by HSV-2, mice treated intravaginally with MGDG exhibited prophylactic effects by suppressing viral yield and herpes lesion formation in the genital cavity, and had higher survival rates than solvent-treated control mice. Thus, *Coccomyxa* KJ provides a new prophylactic option against HSV infection. In addition, *Coccomyxa* KJ exhibits an inhibitory effect in viruses, such as norovirus, which have capsids on the external surface. In an animal model, *Coccomyxa* KJ-treated HSV-2 displayed envelope damage and no pathogenicity.

The viral suppression effects of *Coccomyxa* KJ on non-envelope viruses, such as feline calicivirus and murine norovirus, were demonstrated using animal models.[15] Studies in piglets also suggest that *Coccomyxa* may reduce viral infection.[16] The infiltration of chronic diseases that reduce productivity has become an issue in pig farming in Japan, and countermeasures against chronic diseases are being taken, such as improving sanitary environments, thorough cleaning and disinfection, and administration of vaccines and antimicrobial agents. On the other hand, research is being conducted to improve productivity in this area and promote pig farming that does not depend on antimicrobial

agents. Yamada et al. demonstrated the effects of intranasal administration of a polysaccharide solution of microalgae *Coccomyxa* extract (*Coccomyxa* solution) on antibody titers involved in respiratory disease in piglets.[16] Piglets treated with *Coccomyxa* solution showed a trend toward higher body weight ($p < 0.1$) at the 6$^{th}$ week (77–78 days old) and higher average daily body gain from 4 to 6 weeks compared to the non-treated group (control group). Antibody titers for mycoplasma pneumonia (MPS) tended to be higher in the control group than in the treated group ($p < 0.1$), and the positive rate was also higher, suggesting that intranasal administration of *Coccomyxa* solution may reduce MPS infection in piglets. Moreover, *Coccomyxa* sp. enhances antiviral activity, antitumor effects and immune function in animals.[14–18]

*Coccomyxa* KJ has recently gained recognition for inducing neuroprotective effects,[19] enhancing learning and memory,[20] and inhibiting benign prostate hyperplasia.[21] In addition, its ability to regulate the immune system has been shown. The rough polysaccharide isolated from *Coccomyxa* KJ regulated an immune response in chickens[21] and inhibited an inflammatory reaction in RAW 264.7 macrophages after the lipopolysaccharide stimulation. In a study using human leukocytes, a *Coccomyxa* KJ-immunostimulation mechanism was elucidated.[22] *Coccomyxa* KJ coordinated the differentiation of T cells into effector, memory and anergic T cells in response to *Staphylococcus aureus* superantigen infection. The effect of *Coccomyxa* KJ on superantigen-triggered immune responses was investigated. The results revealed that *Coccomyxa* KJ stimulated human peripheral blood-derived mononuclear cells in toxic shock syndrome 1 and moderately decreased the number of activated T cells. Furthermore, the inflammatory cytokine levels remained unchanged; however, the secretions of interleukin (IL)-1β, IL-17, IL-4, and IL-13 increased, while IL-2, tumor necrosis factor alpha (TNF-α), IL-18 and IL-10 decreased. When an immune response was not inhibited by Treg cells, *Coccomyxa* KJ reinforced the expression of the stem cells of T memory cell markers. Therefore, *Coccomyxa* KJ may improve the excessive activation and immunological inhibition of T cells in response to a superantigen by modulating the fate of T cells. According to the currently understood immune mechanism, *Coccomyxa* KJ may act on immune functions to suppress the growth of viruses and bacteria and some cases of cancer.

The demand for food supplements to improve health is increasing.[23] A study conducted by Food Supplements Europe demonstrated that their use has the potential to reduce the incidence of disease-related events and healthcare expenditures.[24] *Coccomyxa* KJ grows in a straightforward manner and has high nutritional value and a positive effect on the immune system. However, no data regarding the reaction of healthy individuals to *Coccomyxa* KJ administration exist. Furthermore, details concerning *Coccomyxa* KJ ingredients are still unknown.

# Objectives

Recently, *Coccomyxa* KJ dry powder has been marketed as a health food product. Therefore, this pilot study aimed to evaluate the potential health hazards and effects of regular *Coccomyxa* KJ consumption over 4 weeks on the immune system of healthy individuals. In addition, the components of *Coccomyxa* KJ were analyzed.

# Materials and methods

## Participants

A poster recruiting volunteers for this study was published and could be accessed via the website of Tokai University Hospital (Isehara, Japan) from June to October 2020. We recruited healthy volunteers in their 30s and 40s who were willing to consume food containing *Coccomyxa* KJ powder tablets. The study involved 9 healthy Japanese adult volunteers (4 males and 5 females with a mean age of 38.2 years, an age range of 37–47 years, and a body mass index (BMI) of 20–25 kg/m$^2$) who were living healthy lifestyles. The exclusion criteria were as follows: smoking, use of antibiotics or pro/prebiotics (as a dietary supplement) within 6 weeks before the study, use of drugs that modify the composition of the gut microbiota (e.g., antidiabetic drugs, cholesterol-lowering drugs and proton pump inhibitors), use of laxatives within 4 weeks of the study, the presence of chronic or intestinal diseases, pregnancy, psychiatric problems, following a special diet (e.g., vegetarian, high-fiber or high-protein diets), and excessive alcohol consumption (over 20 g/day).

## Ethics

The study design was explained to all healthy volunteers before participation in the study using a consent explanation form, and written consent was obtained. To protect the privacy and personal information of the volunteers, all data related to this study were anonymized; each volunteer was assigned a number in the order of their application for participation. The sex and age of the participants were recorded. No personally identifiable information was obtained, and numbers that could be linked to their names or identities were not used. The review board of Tokai University approved the study (approval No. 20R051), which followed the tenets of the Declaration of Helsinki.

## Intervention

We asked the participants to take 2 *Coccomyxa* KJ tablets (0.15 mg/tablet) every day (before breakfast) for 4 consecutive weeks. The dosage was determined based on the quantity administered to mice in a previous study.[15] During

the intake period, the participants were asked to avoid dieting or overeating, i.e., deviating substantially from their lifestyle before participating in the study. Volunteers using foof supplements regularly were requested to stop taking them a month before taking the *Coccomyxa* KJ tablets.

## Outcome measures

Saliva and blood tests were performed at 3 timepoints: before the start of the intake and at 2 and 4 weeks after the intake. Laboratory tests were performed, including general peripheral blood tests, white blood cell (WBC) counts, and eosinophil and lymphocyte counts, using the XE-2100™ Automated Hematology System (Sysmex, Kobe, Japan), as eosinophils reportedly reflect allergic changes.[25] To assess immune function and mucosal immunity, salivary immunoglobulin A (IgA) level was examined using immunonephelometry (JCA-BM8000 series; JEOL Ltd., Tokyo, Japan). In addition, the natural killer (NK) cell activity in the peripheral blood was determined using the $^{51}$Cr release method in a Gamma Counter (PerkinElmer Inc., Waltham, USA). The T helper (Th)1/Th2 (interferon-gamma (IFN-γ)/IL-4/CD4) cell counts were determined with flow cytometry (FACSCanto II™; BD Biosciences, Franklin Lakes, USA). The IL-6 level was measured using an electrochemiluminescence immunoassay system (Lumipulse G1200; Fujirebio Co., Ltd., Tokyo, Japan) to determine if induction of inflammation is a potential adverse effect of the tablet.[26–30]

The participants were questioned every 7 days about their health condition (presence or absence of adverse effects and allergic reactions, including skin rash, anorexia, vomiting, diarrhea, and unpleasantness) to reveal any adverse reactions or health hazards associated with long-term *Coccomyxa* KJ tablet consumption. If adverse effects were observed, the participants were asked to immediately stop taking the tablet and inform us if they felt unwell or developed a rash during intake.

## Statistical analyses

We investigated whether the measured values for each individual exhibited any changes before the consumption of the *Coccomyxa* KJ tablets and 2 and 4 weeks after their intake. The mean and standard deviation (M ±SD) were calculated by setting the difference in value before the intake and 2 weeks after the intake as Δ2w, before the intake and 4 weeks after the intake as Δ4w, and 2 and 4 weeks after the intake as Δ4–2w. We determined whether these values differed from 0 using a two-sided paired t-test with a significance level of 5%. In addition, the 95% confidence interval (95% CI) was calculated for these differences. When the Shapiro–Wilk test rejected the normality of data distribution, the Wilcoxon signed-rank test was used with a significance level of $\alpha = 0.05$ and a multiplicity Bonferroni correction.

## Ingredient analysis of *Coccomyxa* KJ

*Coccomyxa* KJ ingredients were analyzed by Japan Food Research Laboratories (JFRL; Tokyo, Japan).

# Results

Table 1 summarizes the salivary IgA level, WBC count, eosinophil count and percentage, lymphocyte count and percentage, NK cell activity, IL-6 level, and Th1/Th2 ratio before the start of the consumption of food containing *Coccomyxa* KJ, and at weeks 2 and 4 of its intake. Table 2 shows the results of the statistical analysis for Δ2w, Δ4w and Δ4–2w. Additionally, we determined the 95% CIs for the mean of these differences. Only data for which normality was rejected by the Shapiro–Wilk test are shown with medians and 1st and 3rd quartiles.

No significant difference was observed between the salivary IgA level (reference range: 110–410 mg/dL), WBC count (reference range: males: 3900–9800/μL; females: 3500–9100/μL), eosinophil count (70–440/μL) and percentage (0.0–6.0%), or lymphocyte count (630–5782/μL) and percentage (18.9–59.0%) before the start of intake and at weeks 2 and 4 of *Coccomyxa* KJ tablet intake.

No significant change was found in the NK cell activity at baseline (reference range: 18–40%) and at week 2 of *Coccomyxa* KJ tablet intake. However, significant differences were observed in NK cell activity at Δ4w ($p < 0.0167$), with a mean increase of 11.78 (95% CI: 6.80–16.76). Thus, the Δ4w NK cell activity was significantly upregulated, as determined using the paired t-test (Fig. 1). For the NK cell activity, normality was not rejected when analyzed with the Shapiro–Wilk test for the difference between paired data. However, normality was rejected for some differences in the paired data, such as lymphocyte percentage at Δ2w. Therefore, Wilcoxon's signed-rank test assessed all differences. Nonetheless, only Δ4w NK cell activity was significantly different, as shown by the paired t-test. Additionally, we determined the 95% CIs for the average of these differences.

No significant change in the IL-6 level (reference value: <7.0 pg/mL) was observed in the course of this study. Similarly, no significant changes were found in the Th0 $IFN^-$ $IL\text{-}4^-$ or TH0 $IFN^+$ $IL\text{-}4^+$ cell populations, or in the Th1/Th2 ratio before or during the 4-week intake of *Coccomyxa* KJ tablets. Moreover, none of the patients complained of illnesses during the intake period, and no adverse reactions, including allergic reactions, were observed. The results of the component analysis are shown in Table 3.

# Discussion

The effects of *Coccomyxa* KJ consumption were examined in 9 healthy volunteers. The results of the blood tests at week 4

**Table 1.** Comparison between baseline and weeks 2 or 4 and between weeks 2 and 4 of *Coccomyxa* intake

| Intake | WBC [/μL] | Eosinophil count [/μL] | Eosinophil percentage [%] | Lymphocyte count [/μL] | Lymphocyte percentage [%] | Salivary IgA level [mg/dL] | NK cell activity [%] | IL-6 [pg/mL] | Th1 cell count | Th2 cell count | Th1/Th2 ratio [%] | Th0 ($INF\gamma^-$, $IL4^-$) | Th0 ($INF\gamma^+$, $IL4^+$) |
|---|---|---|---|---|---|---|---|---|---|---|---|---|---|
| Before | 5955.56 ±860.38 | 137.11 ±107.78 | 2.22 ±1.47 | 2220.56 ±359.30 | 37.56 ±5.70 | 14.79 ±5.70 | 34.44 ±6.83 | 0.67 ±0.28 | 20.17 ±7.03 | 2.57 ±0.67 | 8.37 ±3.51 | 75.03 ±7.77 | 2.21 ±0.93 |
| Week 2 | 5755.56 ±1088.44 | 146.78 ±134.76 | 2.33 ±1.89 | 2119.22 ±329.45 | 37.44 ±5.14 | 13.84 ±5.07 | 36.78 ±8.47 | 0.63 ±0.18 | 21.21 ±8.08 | 3.67 ±1.22 | 6.13 ±2.29 | 72.04 ±9.97 | 3.07 ±1.63 |
| Week 4 | 5822.22 ±1388.67 | 139.56 ±175.05 | 2.33 ±2.98 | 2093.78 ±333.88 | 37.67 ±8.86 | 15.93 ±4.67 | 46.22 ±9.43 | 0.66 ±0.31 | 21.16 ±8.67 | 3.31 ±1.30 | 7.24 ±3.43 | 72.43 ±10.57 | 3.11 ±1.42 |

Data are reported as mean ± standard deviation (M ±SD) (n = 9). WBC – white blood cell count; NK – natural killer; Th – T helper cell; INF – interferon; IL – interleukin; IgA – immunoglobulin A.

**Table 2.** Differences in the measured value for each individual between before the intake of *Coccomyxa* and 2 (Δ2w) and 4 weeks after the intake (Δ4w)

| Interval | Summary of statistics | WBC [/μL] | Eosinophil count [/μL] | Eosinophil percentage [%] | Lymphocyte count [/μL] | Lymphocyte percentage [%] | Salivary IgA [mg/dL] | NK cell activity [%] | IL-6 [pg/mL] | Th1 cell count | Th2 cell count | Th1/Th2 ratio [%] | Th0 ($INF\gamma^-$, $IL4^-$) | Th0 ($INF\gamma^+$, $IL4^+$) |
|---|---|---|---|---|---|---|---|---|---|---|---|---|---|---|
| Δ2w | M ±SD | −200.00 ±487.62 | 9.67 ±111.88 | 0.11 ±1.79 | −101.33 ±353.16 | −0.11 ±5.88 | −0.94 ±3.88 | 2.33 ±10.28 | −0.03 ±0.20 | 1.04 ±1.67 | 1.10 ±1.24 | −2.23 ±3.01 | −2.99 ±2.65 | 0.86 ±0.91 |
| | 95% CI | (−597.56, 197.56) | (−81.55, 100.88) | (−1.35, 1.57) | (−389.26, 186.59) | (−4.90, 4.68) | (−4.11, 2.22) | (−6.05, 10.72) | (−0.20, 0.13) | (−0.32, 2.41) | (0.09, 2.11) | (−4.68, 0.22) | (−5.15, −0.83) | (0.11, 1.60) |
| | median | – | – | – | – | 4.0 | 0.0 | – | – | – | – | – | – | – |
| | 1st and 3rd quartile | – | – | – | – | −6.0, 5.0 | −0.2, 1.1 | – | – | – | – | – | – | – |
| Δ4w | M ±SD | −133.33 ±985.45 | 2.44 ±197.41 | 0.11 ±3.41 | −126.78 ±289.86 | 0.11 ±8.12 | 1.14 ±4.23 | 11.78 ±6.11* | −0.01 ±0.30 | 0.99 ±2.08 | 0.74 ±1.25 | −1.12 ±3.88 | −2.60 ±3.56 | 0.90 ±0.99 |
| | 95% CI | (−936.77, 670.10) | (−158.50, 163.39) | (−2.67, 2.89) | (−363.10, 109.54) | (−6.51, 6.73) | (−2.30, 4.59) | (6.80, 16.76) | (−0.25, 0.23) | (−0.70, 2.68) | (−0.27, 1.76) | (−4.28, 2.04) | (−5.50, 0.30) | (0.09, 1.71) |
| Δ4–2w | M ±SD | 66.67 ±742.37 | −7.22 ±119.46 | 0.00 ±2.21 | −25.44 ±237.23 | 0.22 ±6.68 | 2.09 ±3.47 | 9.44 ±10.08 | 0.02 ±0.26 | −0.06 ±2.21 | −0.36 ±0.66 | 1.11 ±2.66 | 0.39 ±1.92 | 0.04 ±0.93 |
| | 95% CI | (−538.58, 671.92) | (−104.61, 90.17) | (−1.80, 1.80) | (−218.86, 167.97) | (−5.22, 5.67) | (−0.74, 4.92) | (1.23, 17.66) | (−0.19, 0.23) | (−1.86, 1.75) | (−0.89, 0.18) | (−1.06, 3.28) | (−1.17, 1.95) | (−0.71, 0.80) |
| | median | – | – | – | – | – | – | – | 0.0 | 0.9 | – | – | 0.0 | – |
| | 1st and 3rd quartile | – | – | – | – | – | – | – | −0.1, 0.0 | −0.8, 1.6 | – | – | −0.7, 0.2 | – |

* $p < 0.05$ (significance $\alpha = 0.05$ using a paired t-test). Each test was conducted in triplicate; Bonferroni revision ($p < 0.0167$) was adopted. WBC – white blood cell; NK – natural killer; IL – interleukin; Th – T helper cell; 95% CI – 95% confidence interval M ±SD – mean ± standard deviation. Values with significant differences confirmed using the paired t-test and Wilcoxon's signed-rank test are indicated by an asterisk beside the M ±SD.

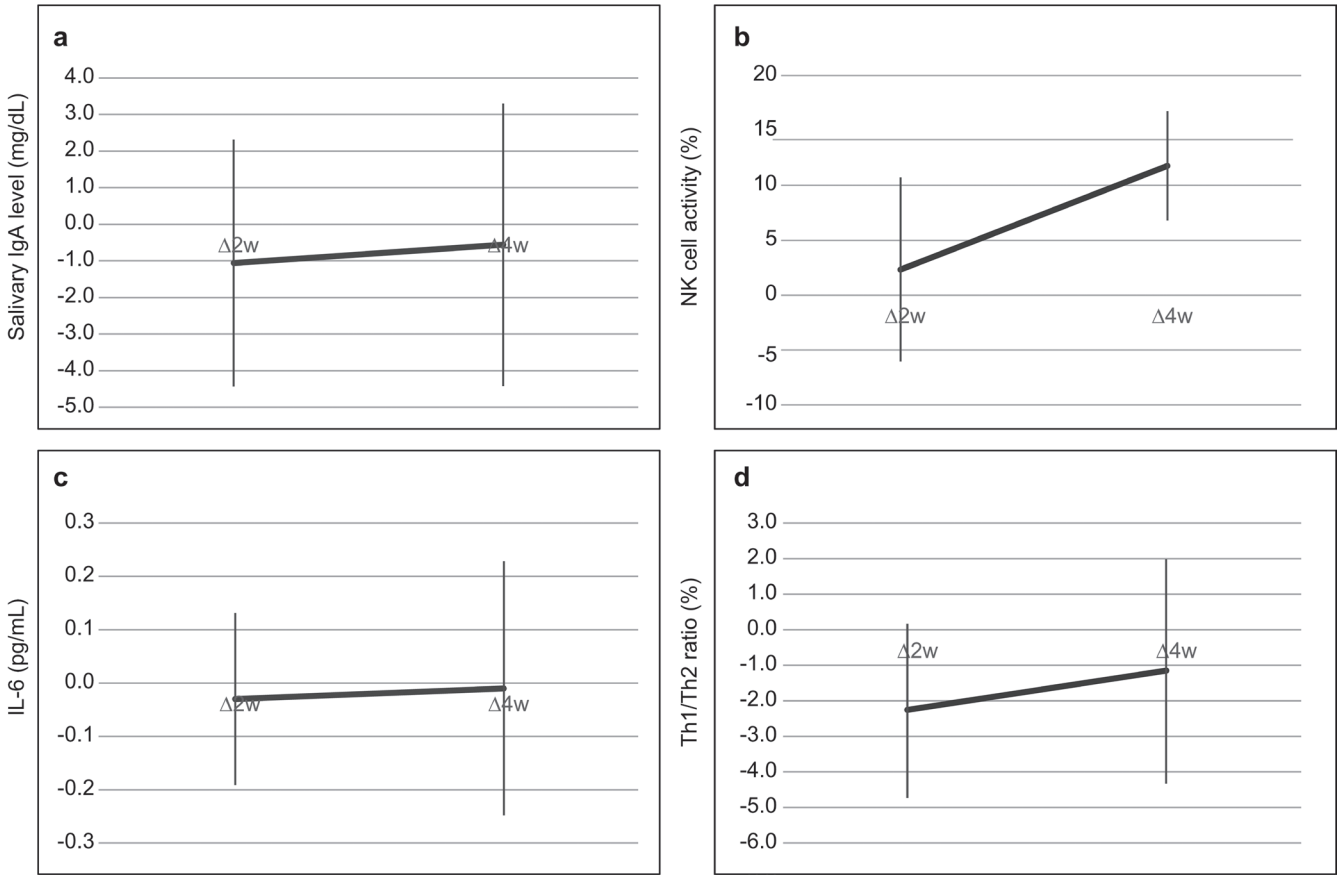


Fig. 1. Plot of 95% confidence interval (95% CI) of the mean for the difference between the 2 timepoints of *Coccomyxa* KJ intake. The 95% CI of the mean for the differences in the salivary immunoglobulin A (IgA) level (A), natural killer (NK) cell activity (B), interleukin (IL)-6 level (C), and T helper cell (Th)1/Th2 ratio (D) were shown. Only NK cell activity after 4 weeks (Δ4w) showed a significant increase in *Coccomyxa* KJ intake

showed upregulated NK cell activity, indicating an improved immune function, and increased attacking cancer cells and virus-infected cells.[26] Natural killer cells play an essential role in immunological surveillance, infection prevention and immune function regulation, and are therefore regarded as immune function indicators.[29] Thus, our findings suggest that long-term *Coccomyxa* KJ intake may help prevent viral and bacterial infections as well as cancer. In contrast, the WBC count, eosinophil count and percentage, lymphocyte count and percentage, Th1/Th2 ratio, and salivary IgA level remained unchanged throughout the 4 weeks of *Coccomyxa* KJ tablet intake. No allergic changes were suspected from the long-term intake. Thus, the results of the salivary IgA and IL-6 analysis implied no adverse effects on mucosal immunity or the systemic inflammatory response.[25,29]

The Th1 cells are responsible for cellular immunity via T-cell activation and enhancement of cytotoxic activity, whereas Th2 cells are involved in B-cell activation and humoral immunity. The immune function is normally regulated via the Th1/Th2 balance in living organisms.[30] Disruption of this balance may cause various diseases, such as cancer and allergies, due to the decrease in antitumor activity and excessive IgE production. Therefore, by measuring the Th1/Th2 balance, the quality of the body's immune response can be estimated in the context of these conditions. Our results suggest that long-term intake of *Coccomyxa* KJ may improve NK cell activity without affecting local immunity, causing systemic inflammation or damaging the immune response balance. *Coccomyxa* KJ exerts antiviral and anti-inflammatory effects during viral infections.[13–16] However, the *Coccomyxa* KJ components responsible for these beneficial effects have not yet been indentified and require further investigation. Nonetheless, according to the component analysis, *Coccomyxa* KJ contains many nutrients and may be suitable for human consumption with many advantages when used as a food.

## Limitations

This pilot study was conducted before initiating a large-scale study. The number of healthy volunteers was small, and the search for indicators of allergic reactions and immune function was limited. In addition, healthy volunteers were only adults in their 30s and 40s to minimize potential bias. This age range was selected as most adults in their 20s are not particularly concerned about their health, and only a few show interest in healthy food.[31] Also, many people in their 50s and above regularly use medications or supplements, which could interfere with the results. Therefore, adults in their 30s and 40s with no underlying diseases and an interest in health maintenance were targeted.

Table 3. Component analysis of *Coccomyxa* sp. strain KJ

| Main substances | Nutrition composition | Value |
|---|---|---|
| Basic ingredients (6) | water (g/100 g) | 2.9 |
| | protein (g/100 g) | 54.9 |
| | fat (g/100 g) | 15.7 |
| | ash (g/100 g) | 5.2 |
| | carbohydrate (g/100 g) | 21.3 |
| | sodium (mg/100 g) | 47.3 |
| Amino acids (20) | threonine (g/100 g) | 2.24 |
| | lysine (g/100 g) | 2.56 |
| | histidine (g/100 g) | 1.03 |
| | phenylalanine (g/100 g) | 2.38 |
| | tryptophan (g/100 g) | 0.87 |
| | leucine (g/100 g) | 3.92 |
| | isoleucine (g/100 g) | 1.96 |
| | methionine (g/100 g) | 0.9 |
| | valine (g/100 g) | 2.66 |
| | alanine (g/100 g) | 3.6 |
| | glycine (g/100 g) | 2.62 |
| | proline (g/100 g) | 2.18 |
| | glutamic acid (g/100 g) | 5.4 |
| | serine (g/100 g) | 2.02 |
| | tyrosine (g/100 g) | 1.65 |
| | aspartic acid (g/100 g) | 4.56 |
| | cystine (g/100 g) | 0.5 |
| | arginine (g/100 g) | 3.65 |
| | hydroxyproline (mg/100 g) | 90 |
| | GABA gamma-aminobutyric acid (mg/100 g) | 795 |
| Minerals (9) | phosphorus (mg/100 g) | 472 |
| | iron (mg/100 g) | 128 |
| | calcium (mg/100 g) | 71.2 |
| | potassium (mg/100 g) | 1450 |
| | magnesium (mg/100 g) | 149 |
| | copper (mg/100 g) | 2.05 |
| | zinc (mg/100 g) | 9.27 |
| | manganese (mg/100 g) | 3.75 |
| | selenium (µg/100 g) | 8 |
| Vitamins (13) | vitamins A (mg/100 g) | 4.84 |
| | vitamins B1 (mg/100 g) | 0.54 |
| | vitamins B2 (mg/100 g) | 3.59 |
| | vitamins B6 (mg/100 g) | 1.46 |
| | vitamins B12 (µg/100 g) | 2.7 |
| | vitamins C (mg/100 g) | 216 |
| | vitamins E (mg/100 g) | 20.5 |
| | vitamins K1 (mg/100 g) | 0.163 |
| | folic acid (mg/100 g) | 4.1 |
| | pantothenic acid (mg/100 g) | 1.41 |
| | biotin (mg/100 g) | 0.154 |
| | inositol (mg/100 g) | 71 |
| | niacin (mg/100 g) | 23.5 |
| Unsaturated fatty acids (10) | myristoleic acid | qualitative analysis |
| | palmitoleic acid | qualitative analysis |
| | oleic acid (g/100 g) | 0.92 |
| | eicosenoic acid (g/100 g) | 0.16 |
| | hexadecadienoic acid (g/100 g) | 0.14 |
| | linoleic acid (g/100 g) | 1.02 |
| | eicosadienoic acid (g/100 g) | 0.01 |
| | hexadecatrienoic acid (g/100 g) | 1.49 |
| | linolenic acid (g/100 g) | 3.53 |
| | 11,14,17-eicosatrienoic acid (g/100 g) | 0.01 |
| Others (9) | polyphenols (g/100 g) | 0.42 |
| | spermidine (mg/100 g) | 17 |
| | α-carotene (mg/100 g) | 5.8 |
| | β-carotene (mg/100 g) | 55.2 |
| | lutein (mg/100 g) | 178 |
| | zeaxanthin (mg/100 g) | 36 |
| | stigmasterol | qualitative analysis |
| | campesterol | qualitative analysis |
| | β-sitosterol | qualitative analysis |

## Conclusions

*Coccomyxa* KJ intake significantly upregulated NK cell activity, thereby improving immune function. No adverse reactions occurred during the intake period. To identify the specific effects of *Coccomyxa* KJ, a comparative study between placebo and intake groups with a larger number of healthy volunteers from different age groups is required.


### ORCID iDs

Satomi Asai https://orcid.org/0000-0002-4075-3141
Kyoko Hayashi https://orcid.org/0000-0002-9582-1201
Haruyo Atsumi https://orcid.org/0000-0002-8713-0902
Mika Doi https://orcid.org/0000-0002-3598-0761
Kazuo Umezawa https://orcid.org/0000-0001-5875-7645
Akihumi Hisada https://orcid.org/0000-0003-3817-122X
Tsukasa Nozaki https://orcid.org/0000-0001-7578-1284
Akiko Kanno https://orcid.org/0000-0003-4983-4092
Satoko Komatsu https://orcid.org/0000-0002-5250-5137
Hitoshi Kuno https://orcid.org/0000-0003-4267-8648
Kentaro Wakamatsu https://orcid.org/0000-0002-9285-880X
Toshio Kawahara https://orcid.org/0000-0003-0168-5825
Yoshiro Yamamoto https://orcid.org/0000-0002-9067-1208
Hayato Miyachi https://orcid.org/0000-0002-5343-6751

## References


1. Jaag A. *Coccomyxa Schmidle: Monographie einer Algengattung*. Band 8, Heft 1. Zurich, Switzerland: Cryptogamica Helvetica; 1933. https://www.e-periodica.ch/digbib/view?pid=cry-001%3A1933%3A8%3A%3A4#4. Accessed January 1, 2023.
2. Abe K, Ishiwatari T, Wakamatsu M, Aburai N. Fatty acid content and profile of the aerial microalga *Coccomyxa* sp. isolated from dry environments. *Appl Biochem Biotechnol*. 2014 Nov;174(5):1724–1735. doi:10.1007/s12010-014-1181-y
3. Thienemann A, Komárek J, Thienemann A. *Chlorophyceae (Grünalgen) Ordnung, 7, 1. Hälfte: Chlorococcales*. Stuttgart, West Germany: Schweizerbart; 1983. ISBN:978-3-510-40023-2.
4. Pröschold T, Darienko T, Silva PC, Reisser W, Krienitz L. The systematics of *Zoochlorella* revisited employing an integrative approach. *Environ Microbiol*. 2011;13(2):350–364. doi:10.1111/j.1462-2920.2010.02333.x
5. Darienko T, Gustavs L, Mudimu O, et al. *Chloroidium*, a common terrestrial coccoid green alga previously assigned to *Chlorella* (Trebouxiophyceae, Chlorophyta). *Eur J Phycol*. 2010;45(1):79–95. doi:10.1080/09670260903362820
6. Darienko T, Gustavs L, Eggert A, Wolf W, Pröschold T. Evaluating the species boundaries of green microalgae (Coccomyxa, Trebouxiophyceae, Chlorophyta) using integrative taxonomy and DNA barcoding with further implications for the species identification in environmental samples. *PLoS One*. 2015;10(6):e0127838. doi:10.1371/journal.pone.0127838
7. Blanc G, Agarkova I, Grimwood J, et al. The genome of the polar eukaryotic microalga *Coccomyxa subellipsoidea* reveals traits of cold adaptation. *Genome Biol*. 2012;13(5):R39. doi:10.1186/gb-2012-13-5-r39
8. Yahr R, Florence A, Škaloud P, Voytsekhovich A. Molecular and morphological diversity in photobionts associated with *Micarea* s. str. (Lecanorales, Ascomycota). *Lichenologist*. 2015;47(6):403–414. doi:10.1017/S0024282915000341
9. Yoshimitsu Y, Abe J, Harayama S. Cas9-guide RNA ribonucleoprotein-induced genome editing in the industrial green alga *Coccomyxa* sp. strain KJ. *Biotechnol Biofuels*. 2018;11(1):326. doi:10.1186/s13068-018-1327-1
10. Satoh A, Kato M, Yamato K, et al. Characterization of the lipid accumulation in a new microalgal species, *Pseudochoricystis ellipsoidea* (Trebouxiophyceae). *J Jpn Inst Energy*. 2010;89(9):909–913. doi:10.3775/jie.89.909
11. Kasai Y, Oshima K, Ikeda F, Abe J, Yoshimitsu Y, Harayama S. Construction of a self-cloning system in the unicellular green alga *Pseudochoricystis ellipsoidea*. *Biotechnol Biofuels*. 2015;8(1):94. doi:10.1186/s13068-015-0277-0
12. Yasui H, Kurano N, Fukuda H, Miyashita H. New microalgae. Japanese patent JP6088375B2. March 1, 2017. https://patents.google.com/patent/JP6088375B2/en. Accessed January 1, 2023.
13. Hayashi K, Asai S, Umezawa K, et al. Virucidal effect of monogalactosyl diacylglyceride from a green microalga, *Coccomyxa* sp. KJ, against clinical isolates of SARS-CoV-2 as assessed by a plaque assay. *Clin Lab Anal*. 2022;36(1):e24146. doi:10.1002/jcla.24146
14. Hayashi K, Lee JB, Atsumi K, et al. In vitro and in vivo anti-herpes simplex virus activity of monogalactosyl diacylglyceride from *Coccomyxa* sp. KJ (IPOD FERM BP-22254), a green microalga. *PLoS One*. 2019;14(7):e0219305. doi:10.1371/journal.pone.0219305
15. Hayashi K, Komatsu S, Kuno H, et al. Virucidal and immunostimulating activities of monogalactosyl diacylglyceride from *Coccomyxa* sp. KJ, a green microalga, against murine norovirus and feline calicivirus. *Marine Drugs*. 2022;20(2):131. doi:10.3390/md20020131
16. Yamada M, Koguchi M, Sugano M, Effects of intranasal mist of polysaccharide solution from *Coccomyxa gloeobotrydiformis*, a green alga, on the growth, blood components and immune-related gene expression levels of piglets [In Japanese]. *J Farm Animal Infect Dis*. 2018;7(1):9–17.
17. Navarro F, Forján E, Vázquez M, et al. Microalgae as a safe food source for animals: Nutritional characteristics of the acidophilic microalga *Coccomyxa onubensis*. *Food Nutr Res*. 2016;60(1):30472. doi:10.3402/fnr.v60.30472
18. Sun L, Jin Y, Dong L, Sumi R, Jahan R, Li Z. The neuroprotective effects of *Coccomyxa gloeobotrydiformis* on the ischemic stroke in a rat model. *Int J Biol Sci*. 2013;9(8):811–817. doi:10.7150/ijbs.6734
19. Sun L, Jin Y, Dong L, et al. *Coccomyxa gloeobotrydiformis* improves learning and memory in intrinsic aging rats. *Int J Biol Sci*. 2015;11(7):825–832. doi:10.7150/ijbs.10861
20. Dong LM, Jin Y, Liu YL, Wang P. Inhibitory effect of *Cocoomyxa gloeobotrydifomis* on benign prostate hyperplasia in aged rats and its action mechanism [in Chinese]. *Zhonghua Nan Ke Xue*. 2013;19(6):506–510. PMID:23862227.
21. Guo Q, Shao Q, Xu W, et al. Immunomodulatory and anti-IBDV activities of the polysaccharide AEX from *Coccomyxa gloeobotrydiformis*. *Marine Drugs*. 2017;15(2):36. doi:10.3390/md15020036
22. Ohshima S, Komatsu S, Kashiwagi H, et al. *Coccomyxa* sp.KJ extract affects the fate of T cells stimulated by toxic shock syndrome toxin-1, a superantigen secreted by *Staphylococcus aureus*. *Microbiol Immunol*. 2022;66(8):394–402. doi:10.1111/1348-0421.12982
23. Izukura S, Ishibasi Y, Ampo Y, Kigawa M, Horiguchi I. The actual status of users of supplements and health foods: Questionnaire-based study in Japan. *Jpn J Health Hum Ecol*. 2022;88(3):84–96. doi:10.3861/kenko.88.3_84
24. Coppens P. The importance of food supplements for public health and well-being. In: Biesalski HK, ed. *World Review of Nutrition and Dietetics*. Vol. 121. Basel, Switzerland: S. Karger AG; 2020:66–72. doi:10.1159/000507524
25. Stone KD, Prussin C, Metcalfe DD. IgE, mast cells, basophils, and eosinophils. *J Allergy Clin Immunol*. 2010;125(2):S73–S80. doi:10.1016/j.jaci.2009.11.017
26. Shereck E, Satwani P, Morris E, Cairo MS. Human natural killer cells in health and disease. *Pediatr Blood Cancer*. 2007;49(5):615–623. doi:10.1002/pbc.21158
27. Brandtzaeg P. The role of humoral mucosal immunity in the induction and maintenance of chronic airway infections. *Am J Respir Crit Care Med*. 1995;151(6):2081–2086. doi:10.1164/ajrccm.151.6.7767561
28. Del Giudice M, Gangestad SW. Rethinking IL-6 and CRP: Why they are more than inflammatory biomarkers, and why it matters. *Brain Behav Immun*. 2018;70:61–75. doi:10.1016/j.bbi.2018.02.013
29. Camous X, Pera A, Solana R, Larbi A. NK cells in healthy aging and age-associated diseases. *J Biomed Biotechnol*. 2012;2012:195956. doi:10.1155/2012/195956
30. Wilczyński JR. Th1/Th2 cytokines balance: Yin and yang of reproductive immunology. *Eur J Obstet Gynecol Reprod Biol*. 2005;122(2):136–143. doi:10.1016/j.ejogrb.2005.03.008
31. Ministry of Agriculture, Forestry and Fisheries of Japan. Policies for the Promotion of Shokuiku (White Paper on Shokuiku) The Fiscal Year 2015 Edition. Tokyo, Japan: Ministry of Agriculture, Forestry and Fisheries of Japan; 2016. https://www.maff.go.jp/e/data/publish/attach/pdf/index-187.pdf. Accessed January 1, 2023.

# The long non-coding RNA BDNF-AS induces neuronal cell apoptosis by targeting miR-125b-5p in Alzheimer's disease models

*Haiyan Ren[1,A–F], *Weibin Qiu[2,A–F], Benju Zhu[1,B,C,F], Qiang Li[1,B,C,F], Chen Peng[1,B,C,F], Xu Chen[1,E,F]

[1] Department of Neurology, Shanghai Eighth People's Hospital, China
[2] Department of Neurology, Shanghai Xuhui Central Hospital, China

A – research concept and design; B – collection and/or assembly of data; C – data analysis and interpretation; D – writing the article; E – critical revision of the article; F – final approval of the article

Advances in Clinical and Experimental Medicine, ISSN 1899–5276 (print), ISSN 2451–2680 (online) *Adv Clin Exp Med*. 2024;33(3):233–245

**Address for correspondence**
Xu Chen
E-mail: hbpetrel@163.com

**Funding sources**
This study was funded by Jiangsu University Clinical Medical Science and Technology Development Fund Project (grant No. JLY2021104).

**Conflict of interest**
None declared

*Haiyan Ren and Weibin Qiu contributed equally to this work.

Received on September 28, 2022
Reviewed on February 3, 2023
Accepted on June 12, 2023

Published online on July 24, 2023

## Abstract

**Background.** At least 55 million individuals suffer from dementia globally, of which Alzheimer's disease (AD) accounts for 60–70% of cases. Alzheimer's disease is the only major cause of death that is still growing. However, the molecular mechanisms are largely unknown in the progress of AD.

**Objectives.** The goal of the study was to assess whether lncRNA brain-derived neurotrophic factor antisense (BDNF-AS) could affect processes underlying the regulation of neuronal cell apoptosis in rat and cellular models of AD by directing the expression of miR-125b-5p.

**Materials and methods.** The amyloid-β $(Aβ)_{1–42}$-induced rat and cellular models of AD were established. Changes in learning and memory in rats were detected with the use of the Morris water maze. Cell viability and apoptosis were determined using the 3-(4,5-dimethylthiazol-2-yl)-2,5 diphenyl tetrazolium bromide (MTT) test and flow cytometry. Reverse transcription-quantitative polymerase chain reaction (RT-qPCR) was applied to detect the expression of lncRNA BDNF-AS and miR-125b-5p, and western blotting was utilized to examine proteins. The correlations between *lncRNA BDNF-AS* and *miR-125b-5p* were demonstrated using dual-luciferase reporter gene assays.

**Results.** Our results showed that BDNF-AS was upregulated and miR-125b-5p was downregulated in the rat and cellular AD models. The addition of si-BDNF-AS and miR-125b-5p mimics shortened the escape latency and swimming distance in the rat model. Furthermore, the knockdown of BDNF-AS or the administration of miR-125b-5p mimic significantly suppressed cell apoptosis, cell inflammatory, and inflammatory pathway-related proteins, while these cellular activities were promoted in rat and cellular models of AD. Additionally, *miR-125b-5p* was found to be a BDNF-AS target gene that was linked negatively with BDNF-AS in AD.

**Conclusions.** Through regulation of miR-125b-5p, lncRNA BDNF-AS suppressed cell death, inflammation and inflammatory pathway-related proteins in AD models, which provides a potential biomarker and therapeutic target in the clinical treatment of AD.

**Key words:** lncRNA BDNF-AS, miR-125b-5p, $Aβ_{1–42}$, apoptosis, Alzheimer's disease

**Cite as**
Ren H, Qiu W, Zhu B, Li Q, Peng C, Chen X. The long non-coding RNA BDNF-AS induces neuronal cell apoptosis by targeting miR-125b-5p in Alzheimer's disease models. *Adv Clin Exp Med*. 2024;33(3):233–245. doi:10.17219/acem/168241

**DOI**
10.17219/acem/168241

# Background

Alzheimer's disease (AD) is a common neurodegenerative disease that results in progressive memory loss, neurocognitive dysfunction, and personality and behavioral changes that have a significant impact on disability-adjusted life years.[1,2] Neurodegeneration, the main pathological feature of AD, is an irreversible and incurable process in which neurons gradually atrophy and lose function in specific parts of the brain, eventually leading to neuron death.[3–5] Neuronal injury and death disrupt the connections between neuronal networks, causing multiple brain regions to atrophy. In AD patients, the atrophy of the hippocampal and medial temporal lobe areas is the structural feature detected with magnetic resonance imaging (MRI).[6]

Histopathologically, the progressive neurodegenerative disorder is distinguished by amyloid-β (Aβ) peptide and tau.[7,8] The toxic Aβ aggregates and assembles into extracellular amyloid plaques that are deposited in specific areas of the brain and cause a reduction in synapses.[9,10] This occurs first in the temporal cortex region, containing the hippocampus, which is implicated in the formation of memories.[8,11] The neuronal toxicity of Aβ manifests itself by binding to a variety of receptors, including α7 nicotinic acetylcholine receptor (α7nAChR), p75 neurotrophin receptor (p75NRT) and N-methyl-D-aspartate receptor (NMDAR).[12,13] The interactions between Aβ and these receptors have been proposed to cause hyperphosphorylation of tau, endoplasmic reticulum (ER) stress responses, mitochondrial dysfunction and inflammatory responses, and, ultimately, lead to synaptic dysfunction and neuronal death.[14,15] Hyperphosphorylated tau constitutes neurofibrillary tangles (NFTs) that can initiate the disassembly of microtubules in the medial temporal lobe, thereby playing a significant role in episodic memory function.[14,16,17] At the same time, the cytotoxicity of tau can lead to synaptic dysfunction and neuronal cell cycle re-entry.[7,18] Many studies focusing on Aβ and tau have had limited success, indicating that the late timing of intervention and focus on a single target are insufficient to block the cascade responses in the neural network system.

MicroRNAs (miRNAs) are a class of small non-coding RNAs that play an important role in regulating the post-transcriptional expression of target genes.[19] Circulating miRNAs are easily detectable and highly stable; thus, many studies have investigated circulating miRNAs in human body fluids such as serum, breast milk, saliva, bile, and urine.[20,21] In recent years, many studies have confirmed the relevance of the aberrant expression of miRNAs in a variety of diseases, such as cardiovascular disease (CVD), diabetes, tumors, and neurodegenerative diseases.[22] Both the type and expression pattern of miRNAs can be used as indicators of the type, progression and pathology of disease.[23,24] For example, overexpressed miR-124 causes hyperphosphorylation of insoluble tau protein by targeting PTPN1, while the tau protein shifts from axon to dendrite, resulting in AD-like tau pathology.[25] Furthermore, upregulated miR-146a promotes M2 polarization of microglia stimulated by inflammation, inhibits the secretion of inflammatory factors, and enhances the phagocytotic capacity.[26] The miR-24-3p/STING pathway can reduce neuroinflammation caused by excessive Aβ deposition in the brains of patients with AD.[27] MicroRNA-125b has an irreplaceable role in many intracellular activities or pathological states, but its effect on AD is, to date, rather controversial.

Long non-coding RNAs (lncRNAs) play a significant role in neurodegenerative illnesses such as AD, Parkinson's disease (PD) and Huntington's disease (HD). Similar to AD, the death of dopamine-secreting neurons and the deposition of Lewy bodies formed by alpha-synuclein are found in PD, and these trigger motor symptoms, including slowness of movement, tremors, stiffness, and postural instability, as well as non-motor symptoms including cognitive changes, fatigue, mood disorders, and sleep disorders.[28–32] A study by Guo et al. demonstrated that low-level expression of brain-derived neurotrophic factor antisense (BDNF-AS) protected neurons from $A\beta_{25-35}$ neurotoxicity by enhancing cell viability and inhibiting apoptosis.[33] Meanwhile, in MPTP-induced PD models, a low expression of BDNF-AS may improve cell viability and suppress autophagy and apoptosis in the SH-SY5Y cell line by modulating miR-125b-5p.[34] However, the link between BDNF-AS and miR-125b-5p in the pathological processes of AD remains unknown.

# Objectives

The current study aims to confirm the involvement of BDNF-AS and miR-125b-5p in the pathogenesis of AD, focusing on inflammation and apoptosis. The influence of BDNF-AS and miR-125b-5p on spatial learning and long-term memory was assessed by constructing AD rat models and conducting Morris water maze experiments. The effects on inflammation and apoptosis were studied at both the animal and cellular levels using AD rat tissues and AD cell models.

# Materials and methods

## Animal model

A total of 120 male Sprague Dawley rats of specific pathogen-free rank were obtained from the Shanghai Laboratory Animal Center at the Chinese Academy of Sciences (Shanghai, China) at the age of 8–12 weeks, weighing 22–30 g. The rats were raised in a standard environment with a 21–22°C temperature, 60–70% relative humidity, natural light, and free access to food and drink. The rats had 1 week to acclimatize to the conditions. The animals

were randomly assigned to one of 6 groups: sham, AD, AD+siRNA-negative control (si-NC), AD+si-BDNF-AS, AD+miR-NC, and AD+miR-125b-5p.

The AD rat model was constructed using human $A\beta_{1-42}$ peptide. With the use of phosphate-buffered saline (PBS), $A\beta_{1-42}$ peptides were dissolved at a concentration of 1 μg/μL, and the solution was incubated at 37°C for 1 week to generate Aβ aggregation. The prepared $A\beta_{1-42}$ solution (10 μL/rat) or PBS (3 μL/rat) was administered into the brain ventricles through stereotactic injection using a Hamilton microsyringe (designated coordinates: anteroposterior = 0.2 mm, mediolateral = 1.0 mm and dorsoventral = 2.5 mm) under anesthesia. A week after the $A\beta_{1-42}$ injection, si-NC, si-BDNF-AS, miR-NC, and miR-125b-5p mimics were injected into the tail vein of the rats in the corresponding group. The tail vein of the rats in the sham group or AD group received an injection of PBS. All the experiments met the requirements of Shanghai Eighth People's Hospital's Ethics Committee (approval No. 2021-0510) for animal experiments.

## Morris water maze

The Morris water maze experiment is used to measure spatial learning and memory in AD models.[35,36] This test is divided into 2 sections: place navigation and spatial probing. A circular pool (diameter: 120 cm) was full of water, with a depth of 35 cm and at a temperature of 22–25°C, and an escape platform (diameter: 9 cm) was immersed approx. 1 cm below the surface of the water. Rats were individually trained 3 times a day for 7 days after the animal model was generated, and every time the rat was put in the water at different starting points. Each experiment lasted 90 s unless the rat touched the platform, and the time of first reaching the platform (escape latency) was recorded. In the probe trial (day 9), the rat had 90 s to search for the escape platform that had been removed. The amount of time the rat spent in the target quadrant, the previous location of the platform, and the number of times the rat crossed the platform location were recorded.

## Primary cerebral cortex neuron culture and PC12 cell culture

As previously stated, the primary cerebral cortex neurons were isolated from the rat embryos (embryonic day 18 (E18)).[37] To separate cells, the cerebral cortex was taken from the E18 rat embryos, treated with papain (10 U/mL) for 10 min and rinsed with Dulbecco's modified Eagle medium (DMEM) containing 10% PBS. Neurons were plated at $1\times10^5$ cells/mL on a poly-L-lysine-coated dish with a neurobasal medium containing B27 supplement, penicillin, streptomycin, insulin, and L-glutamine. The cells were cultured in a B27-supplemented neurobasal medium (Gibco, Waltham, USA). The PC12 cells were cultured in DMEM with 5% horse serum and 10% fetal bovine serum (FBS; Gibco). Additionally, 100 ng/mL of nerve growth factor (NGF) (Sigma-Aldrich, St. Louis, USA) was added to the medium of the PC12 cells to induce neuronal differentiation. All cells were grown in a humidified atmosphere with 5% $CO_2$ at 37°C.

Primary cerebral cortex neurons (NEU) and PC12 cells, stimulated by NGF, were cultured with different proportions of aggregated $A\beta_{1-42}$ (0, 10, 20, and 40 μM) for 24 h to test cell viability.

## Reverse transcription-quantitative polymerase chain reaction (RT-qPCR)

Total RNAs were separated from rat serum or cell samples using TRIzol Reagent (Invitrogen, Waltham, USA) and quantified using Nanodrop (Thermo Fisher Scientific, Waltham, USA). The PrimeScript™ RT Reagent Kit (Takara, Kusatsu, Japan) was then implemented to reverse transcribe RNA into complementary DNA. The PCR conditions were 95°C for 5 min, followed by 40 cycles of 95°C for 5 s and 60°C for 30 s. The RT-qPCR findings were quantified using the $2^{-\Delta\Delta Ct}$ method with U6 or GAPDH as an internal reference.[38] The primers were generated by Sangon Biotech Co., Ltd. (Shanghai, China) and are listed in Supplementary Table 1.

## Western blot

Total protein samples were extracted from the tissues or cells of each group using radioimmunoprecipitation assay (RIPA) lysis buffer (Sigma-Aldrich), and protein quantification was performed with a bicinchoninic acid (BCA) assay kit (Pierce Biotechnology, Waltham, USA). Protein samples (20 μg) underwent electrophoresis in a 15% sodium dodecyl sulfate-polyacrylamide gel electrophoresis (SDS-PAGE) before being transferred to polyvinylidene fluoride (PVDF) membranes (Millipore, Burlington, USA). After 2 h of blocking with 5% non-fat milk, the membranes were incubated with the matching primary antibody at 4°C overnight. Then, they were incubated for 2 h at room temperature with horseradish peroxidase (HRP)-conjugated goat anti-mouse or goat anti-rabbit immunoglobulin G (IgG) as secondary antibodies. The ECL Chemiluminescent Substrate Reagent Kit (Invitrogen) was used to visualize the protein. The used rabbit monoclonal or polyclonal primary antibodies were as follows: Bcl-2 (1:2000, ab182858; Abcam, Cambridge, UK), Bax (1:1000, ab32503; Abcam), cleaved caspase-3 (1:500, ab2302; Abcam), TLR3 (1:3000, ab137722; Abcam), TLR4 (1:300, ab217274; Abcam), MyD88 (1:2000, ab133739; Abcam), TRIF (1:1000, #4596; Cell Signaling Technology, Danvers, USA), NF-kB p65 (1:5000, ab32536; Abcam), and GAPDH (1:2500, ab9485; Abcam). Goat anti-rabbit IgG H&L (1:2000, ab6721; Abcam) was used as a secondary antibody.

## MTT assay

The Cell Proliferation Reagent Kit I (3-(4,5-dimethylthiazol-2-yl)-2,5 diphenyl tetrazolium bromide (MTT)) (Sigma-Aldrich) was used to determine cell proliferation according to the manufacturer's protocol. Following suitable transfections, the 2 cell lines were maintained in 96-well plates. Each well received a total of 20 µL of MTT solution (concentration: 5 mg/mL) and was treated in darkness for 4 h at 37°C. Then, 150 µL of dimethyl sulfoxide (DMSO) was added to each well to dissolve the blue crystals. Finally, the absorbance value of each well was assessed on a microplate reader at 450 nm.

## Cell apoptosis assay

The Annexin V-FITC kit (BD Biosciences, Franklin Lakes, USA) was used to assess cell apoptosis. After the transfection for 48 h, the 2 cell lines at a concentration of $1\times10^6$/mL were collected and resuspended. Then, the cells were treated with 200 µL of Annexin V-FITC for 10 min, after which propidium iodide (PI) was added to the mixture. Finally, flow cytometry (BD Biosciences) was used to determine the cell apoptosis rate.

## Enzyme-linked immunosorbent assay

Using an enzyme-linked immunosorbent assay (ELISA) kit and following the manufacturer's instructions, the expression of interleukin 6 (IL-6), interleukin-1β (IL-1β) and tumor necrosis factor alpha (TNF-α) in tissues or cell supernatant was assessed.

## Cell transfection

Small interfering RNA (siRNA) was synthesized by GenePharma (Shanghai, China). The 2 cell lines were transfected with si-NC, si-BDNF-AS, miR-NC, and miR-125b-5p mimic, according to the manufacturer's guidelines for Lipofectamine™ 3000 (Invitrogen).

## Luciferase reporter assay

StarBase 3.0 (http://starbase.sysu.edu.cn/) was utilized to evaluate the targeted sites for potential interactions between *BDNF-AS* and *miR-125b-5p*. Full-length sequences and fragments of *BDNF-AS* that contained the potential binding site for *miR-125b-5p* were cloned into the pmirGLO vector (Promega, Madison, USA). The 2 cell lines were co-transfected with the luciferase reporters, along with the miR-125b-5p mimic and the miR-NC. After 48 h, relative luciferase activity was measured using the Dual-Luciferase® Reporter Assay System (Promega).

## Statistical analyses

The statistical analyses were conducted using IBM Statistical Package for Social Sciences (SPSS) v. 26.0 software (IBM Corp., Armonk, USA), with data presented as mean ± standard deviation (M ±SD). To confirm normality, we employed the Shapiro–Wilk test, while Levene's test was used to check the homogeneity of variance (Supplementary Tables 2 and 3 present the statistical results). Student's t-test was used to compare data from 2 groups for normally distributed and homogenous data, while one-way analysis of variance (ANOVA) followed by Tukey's post hoc test was applied to analyze 3 or more groups (Supplementary Tables 4 and 5 present the statistical results). In cases where the data were non-normal or violated homogeneity, or for small sample sizes (such as n = 3), we used the Mann–Whitney (M–W) U test for 2-group data analysis and Kruskal–Wallis (K–W) test followed by Dunn's post hoc test for analyzing 3 or more groups (Supplementary Table 6 presents the statistical results). Repeated measures ANOVA (RM ANOVA) followed by Tukey's post hoc test were used for analyzing the data related to escape distance and escape latency. A p-value of less than 0.05 was deemed statistically significant.

# Results

## Effects of lncRNA BDNF-AS and miR-125b-5p on spatial learning and long-term memory in the AD rat model

Repeated measures ANOVA demonstrated that escape distance and escape latency over 5 days varied substantially across groups in the Morris water maze experiment ($F = 14.29$, degrees of freedom (df) = 20, $p < 0.001$; $F = 22.69$, df = 20, $p < 0.001$). The experiment also revealed that the swimming distance and escape latency of rats in the sham group became shorter as the number of training days increased, indicating that the rats had gradually acquired the ability to find a platform during training (Fig. 1A,B). Compared to the sham group, rats in the AD group displayed considerably greater swimming distance and escape latency ($p < 0.001$). Compared to the control groups, the addition of si-BDNF-AS and miR-125b-5p mimics shortened the swimming distance and escape latency by improving the learning ability and memory of rats (both $p < 0.001$). On day 9, a probe test was performed to measure the time spent in the target area in order to test memory maintenance. The AD group spent substantially less time in the target quadrant than the sham group ($p < 0.001$), and the time values for the AD+si-BDNF-AS and AD+miR-125b-5p mimic groups were longer than for their respective control groups (both $p < 0.001$) (Fig. 1C). The above findings indicate that reduced expression of BDNF-AS and higher expression of miR-125b-5p mitigated the learning and memory impairment in the AD rat model caused by the injection of $A\beta_{1-42}$.

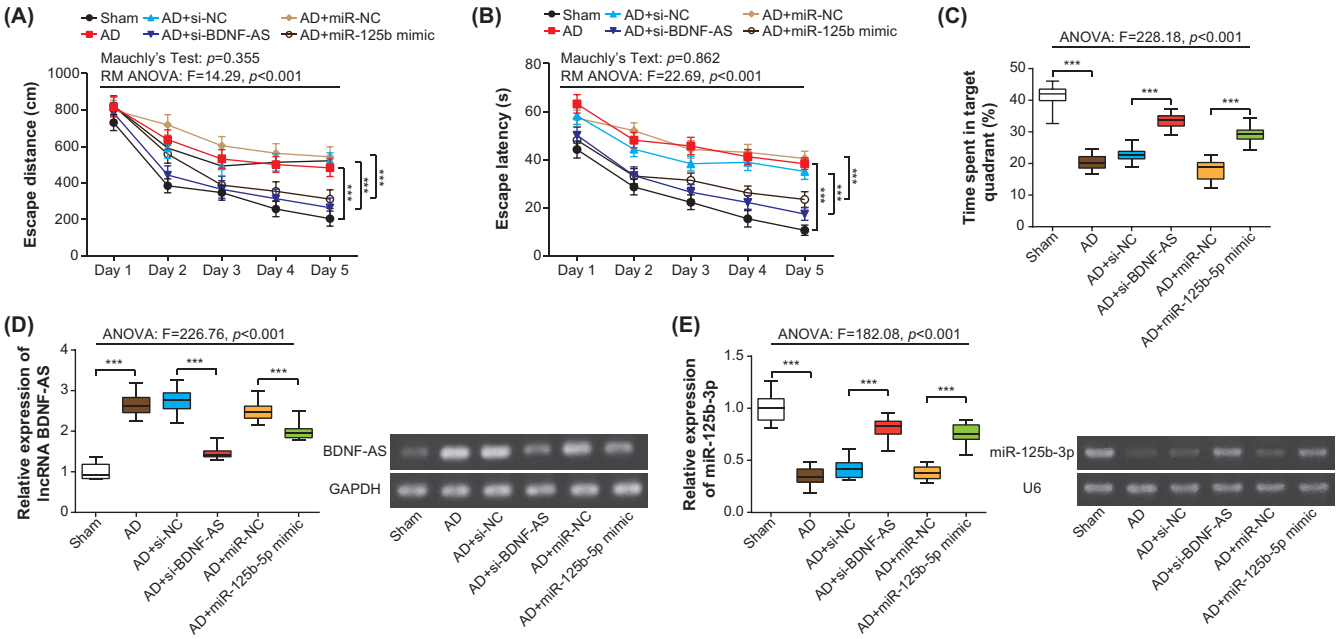


Fig. 1. Effects of lncRNA brain-derived neurotrophic factor antisense (BDNF-AS) and miR-125b-5p on memory impairment in the amyloid-β ($A\beta_{1-42}$)-treated Alzheimer's disease (AD) rat model. Escape distance (A) and latency (B) to arrive at the platform, as well as the amount of time (C) spent in the target quadrant and site within 60 s were automatically recorded. The expression levels of BDNF-AS (D) and miR-125b-5p (E) were examined in the sham, AD, AD+si-NC, AD+si-BDNF-AS, AD+miR-NC, and AD+miR-125b-5p mimic groups. A,B. ***p < 0.001 (Tukey's post hoc test following repeated measures analysis of variance (RM ANOVA)); C–E. ***p < 0.001 (Tukey's post hoc test following ANOVA). Data are presented using the median value as the middle line, with the 25th to 75th percentiles represented by the box. The minimum and maximum values are indicated with whiskers

## Effects of lncRNA BDNF-AS and miR-125b-5p on the expression of BDNF-AS and miR-125b-5p in the AD rat model

We discovered that the expression level of BDNF-AS was 2.66 times greater in the AD group than in the sham group through the detection in the rat serum, while the expression level of miR-125b-5p was only 35% of the sham group's level (both p < 0.001) (Fig. 1D,E). The low-level expression of BDNF-AS and high-level expression of miR-125b-5p had a significant adverse effect on the expression levels of the 2 RNAs, when compared with their corresponding control groups (both p < 0.001) (Fig. 1D,E).

## Effects of lncRNA BDNF-AS and miR-125b-5p on apoptosis in the AD rat model

The hippocampus tissue from the AD group showed a higher rate of apoptosis compared to the sham group (p < 0.001) (Fig. 2A). In the AD+si-BDNF-AS and AD+miR-125b-5p mimic groups, the apoptosis rate was effectively suppressed, and the apoptosis rate in these 2 groups was only 60.38–72.62% of that of their corresponding control group (both p < 0.001). At the same time, the levels of expression of apoptosis-related proteins differed among the groups ($F_{(5,114)} = 283.60$, p < 0.001; $F_{(5,114)} = 96.94$, p < 0.001; $F_{(5,114)} = 94.06$, p < 0.001). The AD group had higher levels of Bax and cleaved caspase-3 and lower levels of Bcl-2 when compared with the sham group (both p < 0.001) (Fig. 2B). However, compared with the respective control groups, the low-level expression of BDNF-AS and high-level expression of miR-125b-5p were able to successfully reduce Bax and cleaved caspase-3 expression while increasing Bcl-2 expression (both p < 0.001).

## Effects of lncRNA BDNF-AS and miR-125b-5p on inflammation and inflammatory pathway-related proteins in the AD rat model

In terms of inflammatory factors, the AD group released higher levels of IL-1β, IL-6 and TNF-α than the sham group (both p < 0.001) (Fig. 3A). Conversely, these levels were considerably suppressed in the AD+si-BDNF-AS and AD+miR-125b-5p mimic groups when compared to the control groups (both p < 0.001). The expression levels of TLR3, TLR4, MyD88, TRIF, and NF-kB p65 were significantly increased in the AD group, and were 1.83–3.15 times higher than that of the sham group (both p < 0.001) (Fig. 3B,C). Compared to the corresponding control groups, adding si-BDNF-AS or miR-125b-5p mimic inhibited the production of these proteins (both p < 0.001).

## Construction of AD cellular models

The MTT results revealed that in both the NGF-PC12 cells and primary cerebral cortex neurons, cell viability was considerably reduced in the $A\beta_{1-42}$ treated group compared to the NC group, which reflects the cytotoxic effect

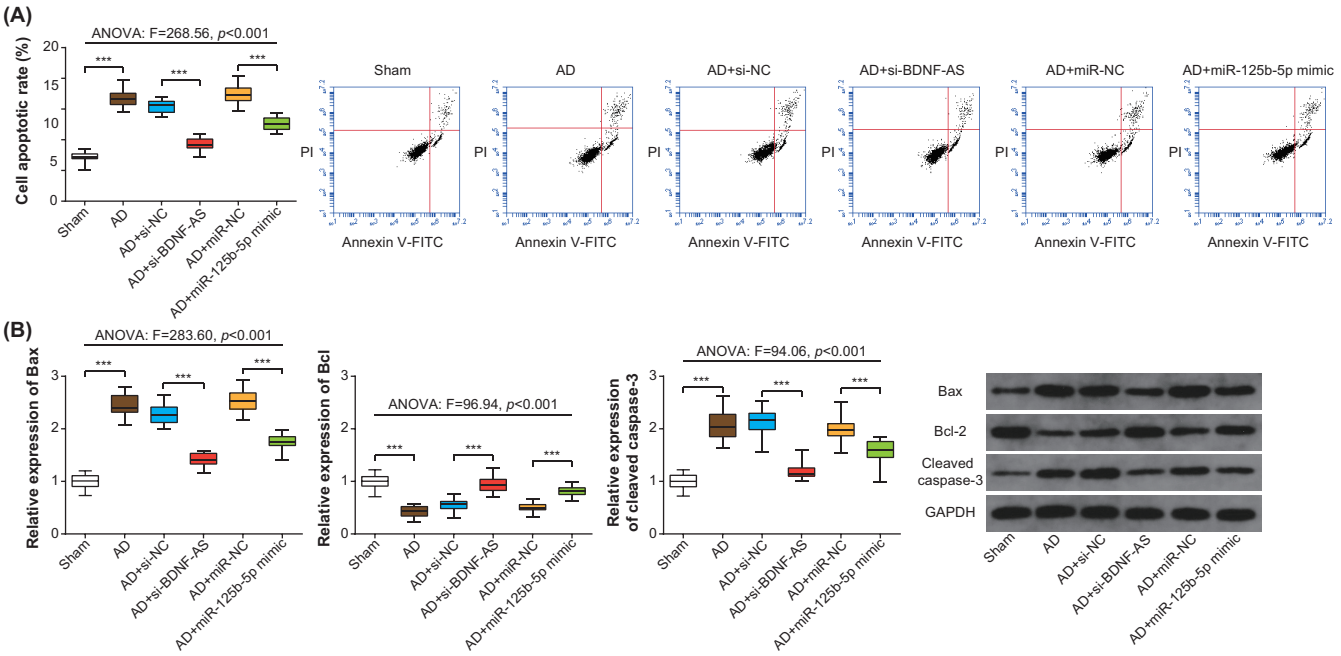


Fig. 2. Effects of lncRNA brain-derived neurotrophic factor antisense (BDNF-AS) and miR-125b-5p on apoptosis in the amyloid-β $(Aβ)_{1–42}$-treated Alzheimer's disease (AD) rat model. A. Cell apoptosis rate and apoptotic-related proteins were evaluated in the sham, AD, AD+si-NC, AD+si-BDNF-AS, AD+miR-NC, and AD+miR-125b-5p mimic groups. A,B. ***p < 0.001 (Tukey's post hoc test following analysis of variance (ANOVA)). Data are presented using the median value as the middle line, with the 25th to 75th percentiles represented by the box. The minimum and maximum values are indicated with whiskers

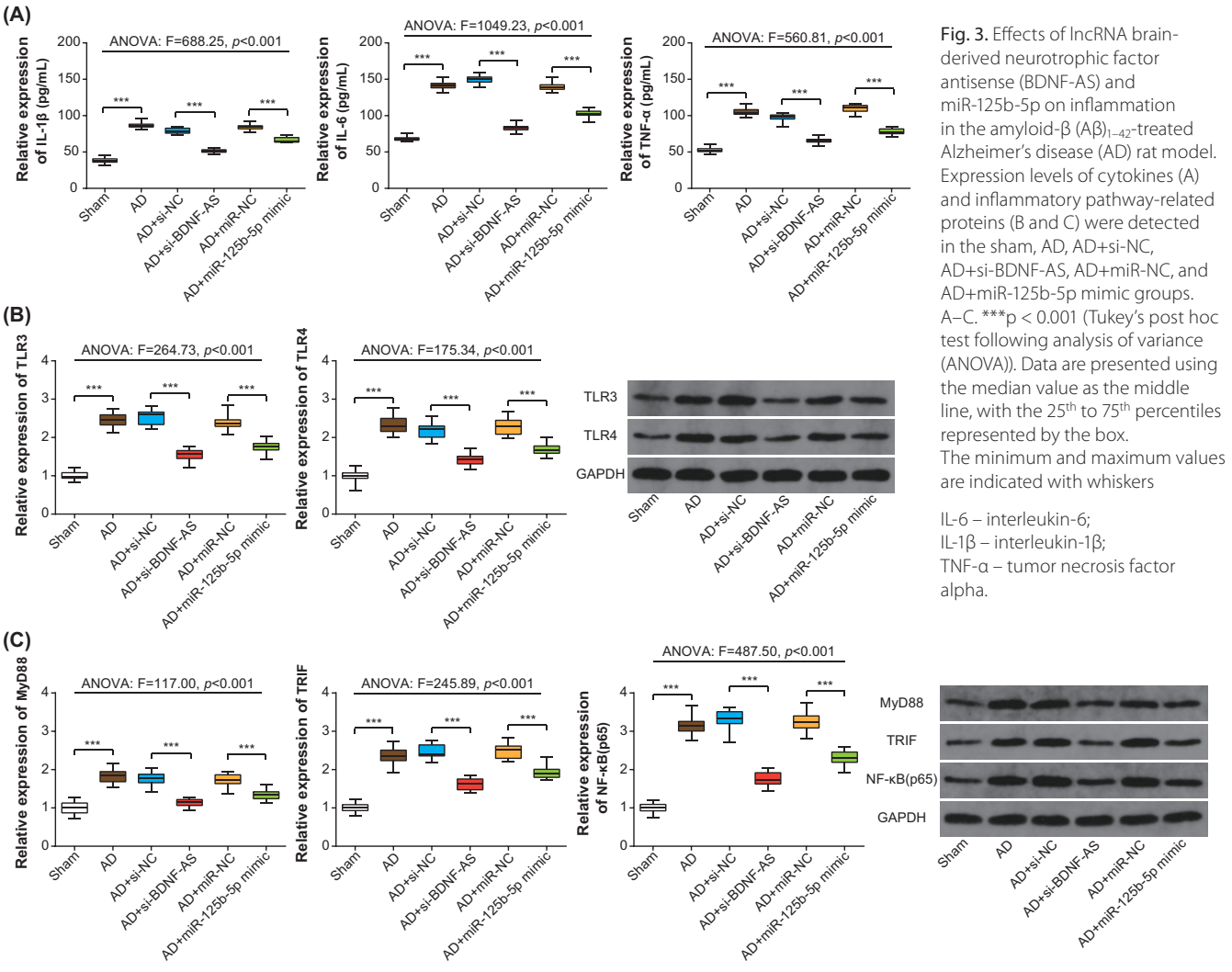


Fig. 3. Effects of lncRNA brain-derived neurotrophic factor antisense (BDNF-AS) and miR-125b-5p on inflammation in the amyloid-β $(Aβ)_{1–42}$-treated Alzheimer's disease (AD) rat model. Expression levels of cytokines (A) and inflammatory pathway-related proteins (B and C) were detected in the sham, AD, AD+si-NC, AD+si-BDNF-AS, AD+miR-NC, and AD+miR-125b-5p mimic groups. A–C. ***p < 0.001 (Tukey's post hoc test following analysis of variance (ANOVA)). Data are presented using the median value as the middle line, with the 25th to 75th percentiles represented by the box. The minimum and maximum values are indicated with whiskers

IL-6 – interleukin-6;
IL-1β – interleukin-1β;
TNF-α – tumor necrosis factor alpha.

of $A\beta_{1-42}$, as well as a gradual decrease in cell viability with increasing concentrations of $A\beta_{1-42}$, and reflects the existence of a dose-dependent effect (K–W: H = 9.97, p = 0.019; H = 10.39, p = 0.016) (Fig. 4A). The above results confirmed the successful construction of 2 AD cellular models. Meanwhile, with an increase in $A\beta_{1-42}$ concentration, the expression level of BDNF-AS increased and miR-125b-5p level decreased (K–W: H = 10.39, p = 0.016) (Fig. 4B,C). The NGF-PC12 cells and primary cerebral cortex neurons were treated with a 20-μM dose of $A\beta_{1-42}$ for 24 h to construct 2 AD cellular models for the following experiments.

After the transfection with si-BDNF-AS, the expression level of BDNF-AS was notably reduced compared to the NC group, while the addition of miR-125b-5p mimic promoted the expression of miR-125b-5p in both cellular models of AD (M–W U: Z = –2.12, p = 0.034) (Fig. 4D,E), reflecting successful transfections.

## Effects of lncRNA BDNF-AS and miR-125b-5p on cell apoptosis in the cellular models of AD

In the 2 cellular models of AD, $A\beta_{1-42}$ was capable of significantly elevating the rate of apoptosis compared to the NC group (PC12 cell: $p < 0.05$; NEU: $p < 0.005$). However, both low-level expression of BDNF-AS and high-level expression of miR-125b-5p were effective in inhibiting apoptosis induced by $A\beta_{1-42}$ (both $p < 0.05$) (Fig. 5A). Western blot results for apoptotic-related proteins revealed that the expression of Bax and cleaved caspase-3 were reportedly elevated, while the expression of Bcl-2 was dramatically lowered in the $A\beta_{1-42}$ group compared to the NC group (both $p < 0.05$) (Fig. 5B). However, the treatment with si-BDNF-AS or miR-125b-5p mimic suppressed the levels of Bax and cleaved caspase-3, and elevated the level of Bcl-2 compared to the corresponding control groups (both $p < 0.05$).

## Effects of lncRNA BDNF-AS and miR-125b-5p on inflammation and inflammatory pathway-related proteins in the cellular models of AD

The ELISA results showed that the $A\beta_{1-42}$ group secreted higher IL-1β, IL-6 and TNF-α levels than the NC group (both $p < 0.05$) (Fig. 6A), while lower expression levels of inflammatory factors were detected in the $A\beta_{1-42}$ +si-BDNF-AS or $A\beta_{1-42}$+miR-125b-5p mimic groups compared to the $A\beta_{1-42}$+si-NC or $A\beta_{1-42}$+miR-NC groups (both $p < 0.05$).

In contrast, the treatment with $A\beta_{1-42}$ promoted the expression levels of TLR3, TLR4, MyD88, TRIF, and NF-kB p65 in the 2 AD cellular models significantly more than in the NC group (both $p < 0.05$) (Fig. 6B,C). Both low-level expression of BDNF-AS and high-level expression of miR-125b-5p inhibited the promotion of inflammatory pathway-related proteins stimulated by $A\beta_{1-42}$ (both $p < 0.05$).

## *miR-125b-5p* is the target gene of lncRNA BDNF-AS

The binding location for *lncRNA BDNF-AS* and *miR-125b-5p* was predicted using StarBase 3.0 (http://starbase.sysu.edu.cn/) (Fig. 7A). The luciferase activity in 2 AD cellular models was lowered in the pmirGLO-BDNF-AS-Wt+miR-125b-5p mimic group when compared to the pmirGLO-BDNF-AS-Wt+miR-NC group (M–W U: Z = –2.12, p = 0.034) (Fig. 7A). Furthermore, the expression of miR-125b-5p was considerably higher in the si-BDNF-AS group compared to the NC group (PC12 cell: U: Z = –2.14, p = 0.032; NEU: U: Z = –2.12, p = 0.034) (Fig. 7B).

# Discussion

This study demonstrated that lncRNA BDNF-AS was substantially upregulated, and miR-125b-3p was decreased in an AD rat model. In addition, decreasing expression of BDNF-AS inhibited neuronal apoptosis, inflammation and inflammatory pathway-related proteins. Further evidence revealed that the knockdown of BDNF-AS could exert a neuroprotective effect by targeting *miR-125b-5p*.

A massive loss of neurons is one of the characteristic pathological changes in AD, especially in the cortex, hippocampus, and other brain areas related to learning and memory, and is closely associated with the onset of impairments in memory and cognition.[39,40] The Aβ can change the Bcl-2/Bax ratio and activate caspase-3, triggering a downstream apoptotic cascade, promoting reactive oxygen species (ROS) accumulation, and resulting in cell death.[41] In the study by Chu et al., the caspase family was shown to directly participate in the cleavage of Aβ and, after being cleaved by caspase-3, the Aβ with an abnormal C-terminal had a cytotoxic effect that could induce cell apoptosis.[42] Meanwhile, caspase-3 is also involved in the cleavage of tau protein into truncated amino acid fragments, 19 of which are effectors of cell apoptosis. Moreover, caspase-3 is related to the cleavage of PS-1 and PS-2, which promotes the hydrolysis of amyloid precursor protein (APP) to release more Aβ and leads to neuronal apoptosis.

The above results are consistent with the present study demonstrating that cell apoptotic rates were promoted after Aβ treatment in the rat and cell models, and this promotion could be inhibited by si-BDNF-AS and miR-125b5p mimics (Fig. 2A, Fig. 5A). The knockdown of BDNF-AS has been shown to increase the mitochondrial membrane potential and prevent the release of cytochrome c from the mitochondria.[43] Therefore, the Bcl-2/Bax ratio, caspase-3 activation and apoptotic rate were reversed due to the effect of BDNF-AS siRNA on protection against mitochondrial damage. While miR-125b-5p regulates the synaptic protein synapsin-2 (SYN-2) and 15-lipoxygenase (15-LOX), it causes synaptic and neurotrophic deficits that are linked to neuronal apoptosis.[44,45]

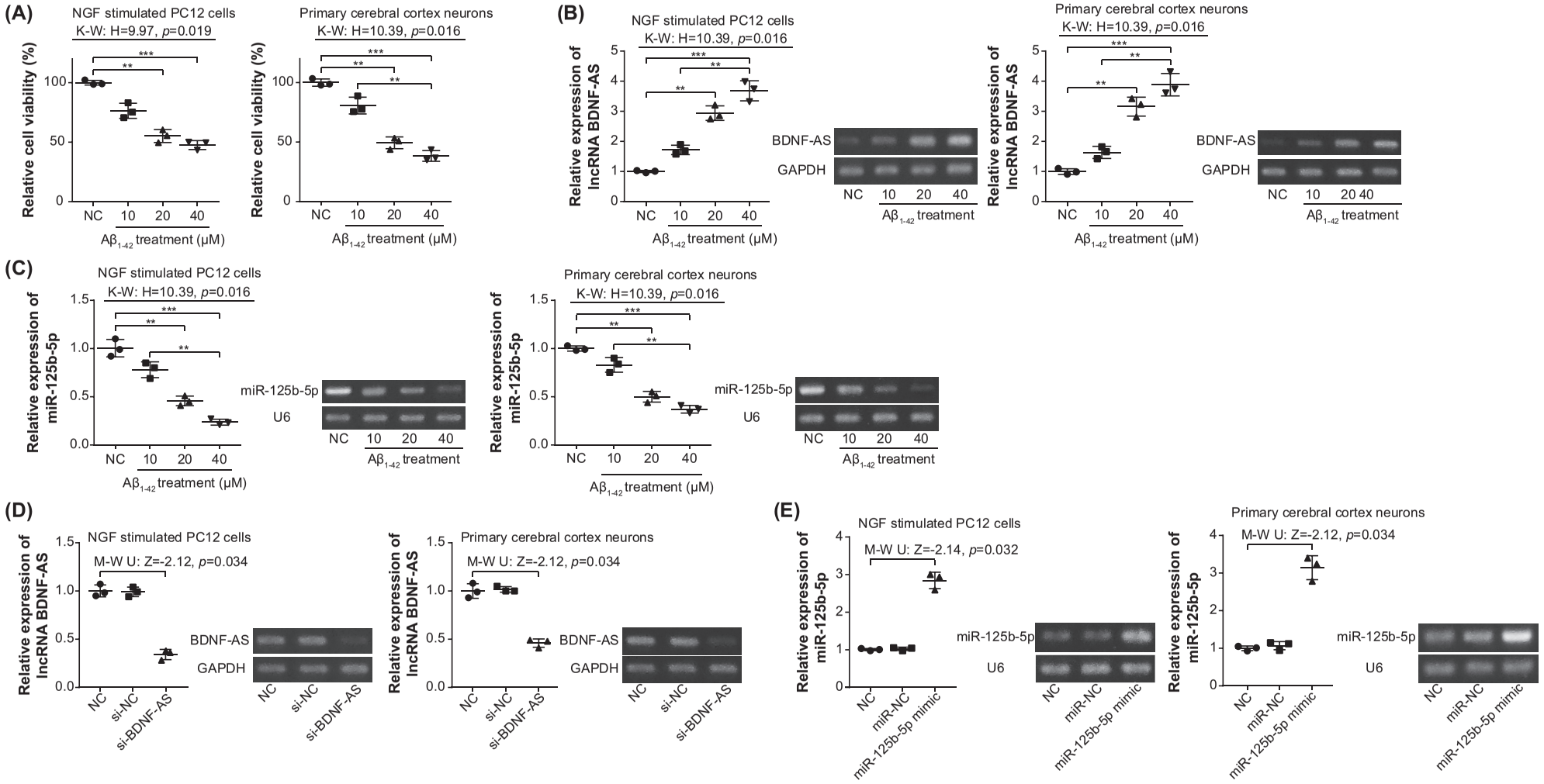


Fig. 4. Construction of cellular models of Alzheimer's disease (AD). The cell viabilities of nerve growth factor (NGF)-stimulated PC12 cells and primary cerebral cortex neurons were monitored after treatment with amyloid-β $(Aβ)_{1-42}$ at different concentrations (A). The expression levels of brain-derived neurotrophic factor antisense (BDNF-AS) (B) and miR-125b-5p (C) were determined after the treatment with $Aβ_{1-42}$ at different concentrations. After transfection of si-NC and si-BDNF-AS, the expression level of lncRNA BDNF-AS was evaluated (D). The level of miR-125b-5p expression was determined in the NC, miR-NC and miR-125b-5p mimic groups (E). A–C. ***p < 0.005 (Dunn's post hoc test following Kruskal–Wallis (K–W) test), and **p < 0.05 (Dunn's post hoc test following K–W test); D–E. The results were statistically analyzed using the Mann–Whitney (M–W) U test. Data are presented as median with range

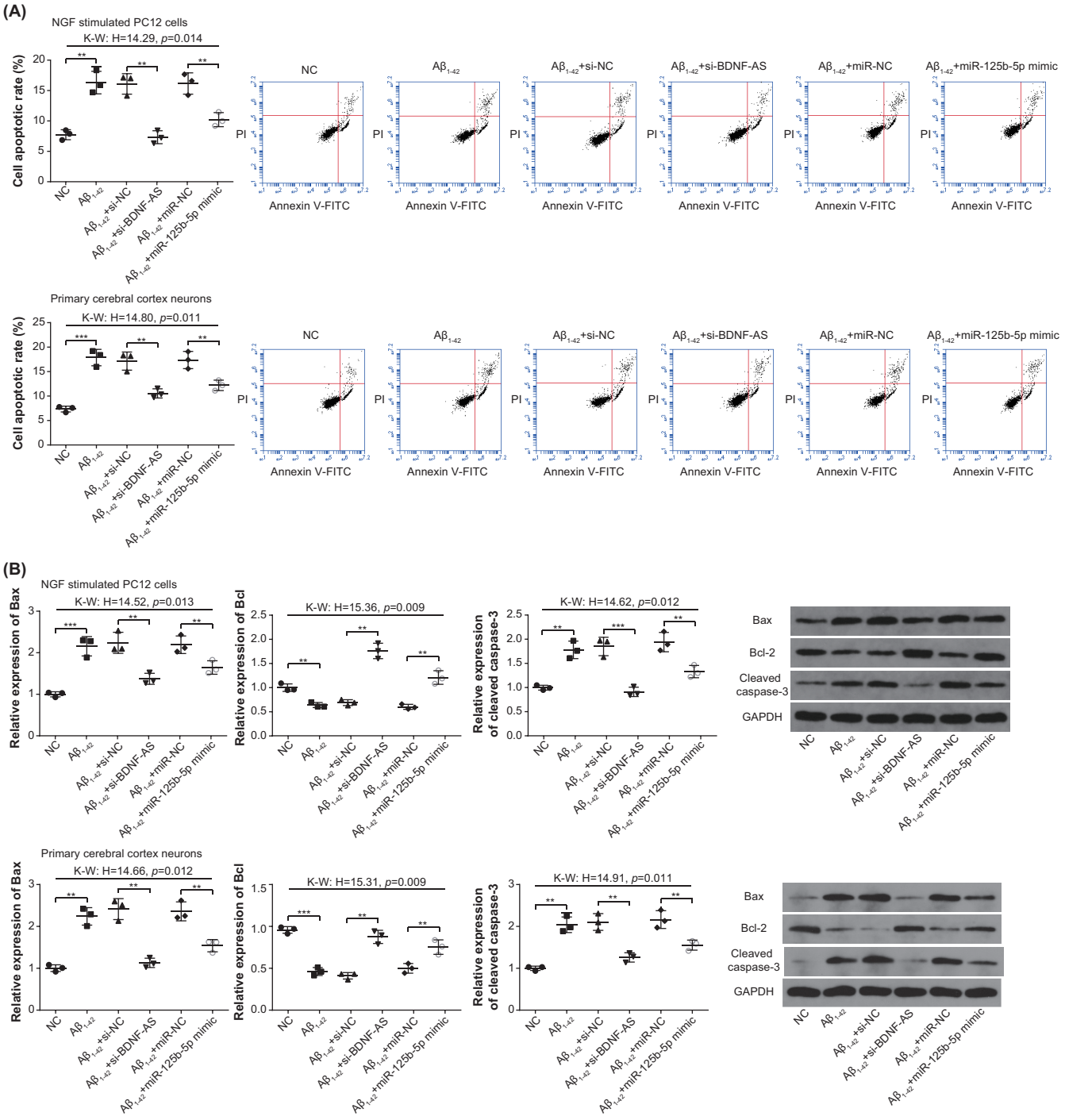


Fig. 5. Effects of lncRNA brain-derived neurotrophic factor antisense (BDNF-AS) and miR-125b-5p on apoptosis in the 2 cellular Alzheimer's disease (AD) models. Cell apoptosis rate (A) and apoptotic-related proteins (B) were detected in the NC, amyloid-β $(Aβ)_{1–42}$, $Aβ_{1–42}$+si-NC, $Aβ_{1–42}$+si-BDNF-AS, $Aβ_{1–42}$+miR-NC, and $Aβ_{1–42}$+miR-125b-5p mimic groups. A,B. ***p < 0.005 (Dunn's post hoc test following Kruskal–Wallis (K–W) test); **p < 0.05 (Dunn's post hoc test following K–W test). Data are presented as median with range

NGF – nerve growth factor.

In the process of AD, Aβ deposition and abnormal phosphorylation of tau protein are the main mechanisms leading to microglial inflammation.[46,47] The Aβ can be recognized by complement receptors and cytokine receptors on the membranes of microglia and astrocytes, thereby promoting the synthesis and secretion of inflammatory factors such as ROS, TNF-α, IL-1β, and IL-6.[48] As shown in Fig. 3A and Fig. 6A, elevated expression of TNF-α, IL-1β, and IL-6 was found after stimulation of Aβ. Continuous microglial activation and the release of inflammatory factors can aggravate neuronal damage and lead to exacerbated NFTs.[49] At the same time, this process can decrease the ability of microglia to clear Aβ, raise the levels of Aβ, and aggravate pathological damage. On the other hand, Aβ can directly activate TLRs to cause microglia-mediated inflammation.[50] Studies have found that in the AD model, the expression levels

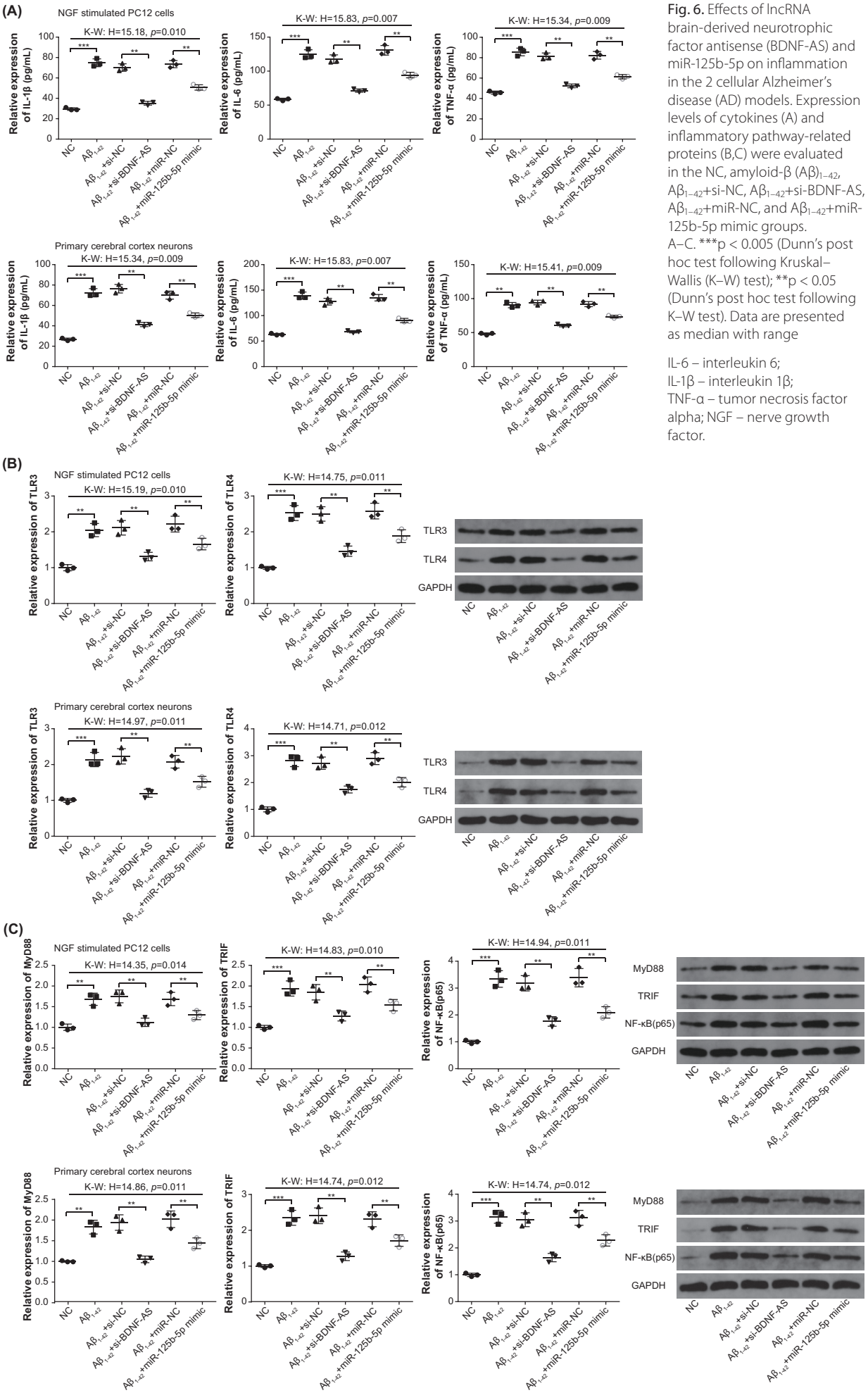


Fig. 6. Effects of lncRNA brain-derived neurotrophic factor antisense (BDNF-AS) and miR-125b-5p on inflammation in the 2 cellular Alzheimer's disease (AD) models. Expression levels of cytokines (A) and inflammatory pathway-related proteins (B,C) were evaluated in the NC, amyloid-β $(Aβ)_{1–42}$, $Aβ_{1–42}$+si-NC, $Aβ_{1–42}$+si-BDNF-AS, $Aβ_{1–42}$+miR-NC, and $Aβ_{1–42}$+miR-125b-5p mimic groups. A–C. ***p < 0.005 (Dunn's post hoc test following Kruskal–Wallis (K–W) test); **p < 0.05 (Dunn's post hoc test following K–W test). Data are presented as median with range

IL-6 – interleukin 6; IL-1β – interleukin 1β; TNF-α – tumor necrosis factor alpha; NGF – nerve growth factor.

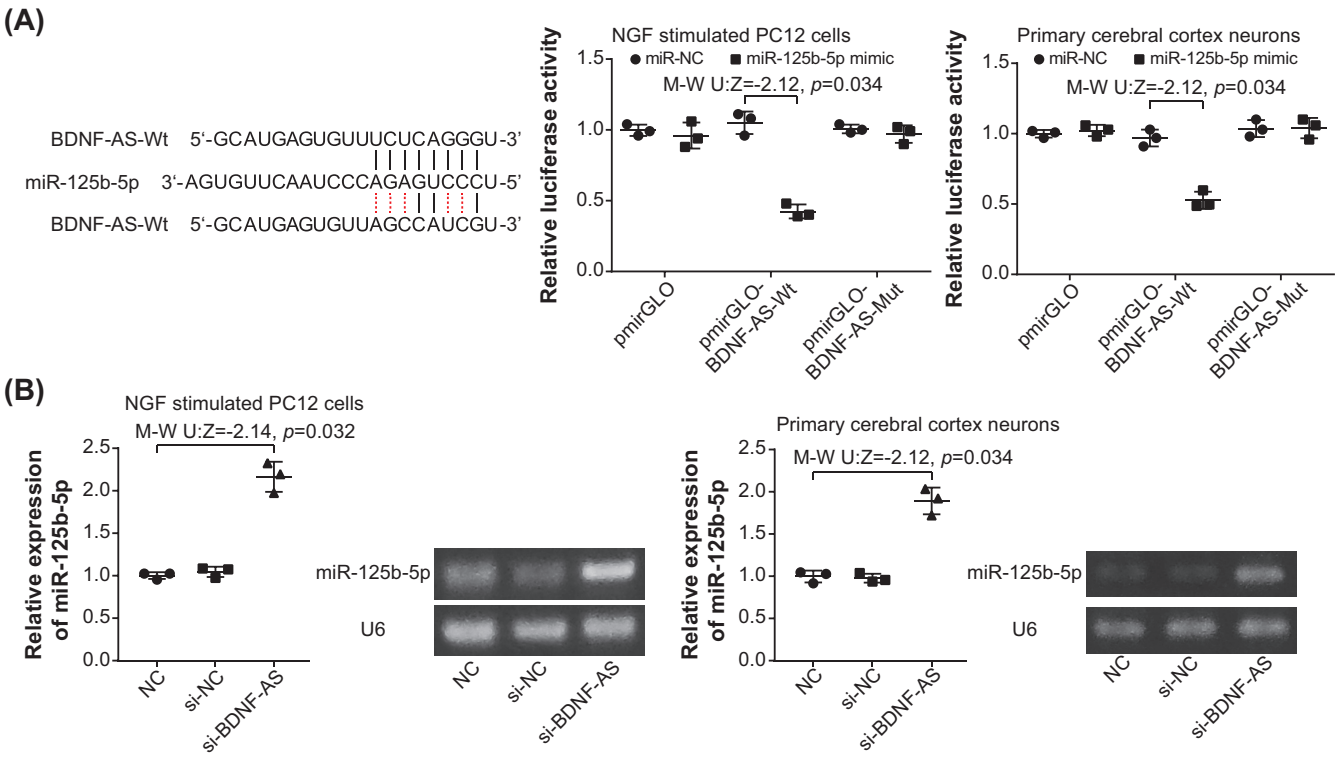


Fig. 7. *miR-125b-5p* is the target gene of the lncRNA brain-derived neurotrophic factor antisense (BDNF-AS). A. *miR-125b-5p* targeted BDNF-AS at specific sites, and luciferase activities were compared between groups of BDNF-AS-Wt+miR-125b-5p mimic, BDNF-AS-Wt+miR-NC, and BDNF-AS-Mut+miR-125b-5p mimic; B. MiR-125b-5p expression was altered after si-BDNF-AS transfection. The results were statistically analyzed using the Mann–Whitney (M–W) U test. Data are presented as median with range

NGF – nerve growth factor.

of TLR3 and TLR4 are increased, and these may be the main subtypes of TLRs activated by Aβ.[51] In the present study, the expression levels of TLR3, TLR4, MyD88, TRIF, and NF-kB p65 were all increased in the Aβ group but were decreased in the $A\beta_{1-42}$+si-BDNF-AS or $A\beta_{1-42}$+miR-125b-5p mimic groups. Elevated TLR3 and TLR4 can trigger NF-κB after activating the downstream signaling pathway by binding to MyD88 or TRIF.[52]

As the most common cause of dementia, there are no specific, standard treatment options for AD, which is often diagnosed late and has a significant impact on a patient's quality of life.[53,54] Compared to established diagnostic methods, such as structural MRI of the hippocampal and molecular neuroimaging utilizing positron emission tomography (PET), the detection of miRNAs in bodily fluids is a relatively simple procedure. The ability of prospective biomarkers to detect the disease at an early stage and track the development of brain function would be a significant contribution. Current drugs, such as donepezil, rivastigmine and galantamine, can temporarily relieve dementia symptoms, but cannot terminate the progression of the disease. The fact that miRNAs are implicated in amyloid peptide aggregates, hyperphosphorylated tau protein aggregation, synaptic loss, neuroinflammation, and defective autophagy favors the development of miRNA-based therapeutic strategies.[55]

## Limitations

Because of a limited budget, this study only focused on cell apoptosis and inflammation. Therefore, limited experiments were conducted on the AD rat and cellular models. The effects of BDNF-AS and miR-125b-5p on neurite outgrowth and oxidative stress are still unknown. Further exploration of the relationship between molecular regulation and neuropathological changes will be useful in future AD research.

# Conclusions

To conclude, lncRNA BDNF-AS siRNA represses cell apoptosis and inflammation via targeting of *miR-125b-5p* in AD, which suggests a strong association between BDNF-AS and the pathological mechanism of AD. The investigation of BDNF-AS and its downstream targets helps to expand our understanding of BDNF as a key molecule involved in neuronal changes related to learning and memory, laying the groundwork for new biomarkers or promising therapeutic targets for AD treatment.

## Supplementary data

The supplementary materials are available at https://doi.org/10.5281/zenodo.7990783. The package contains the following files:

Supplementary Table 1. Primer sequences used in RT-qPCR of this study.

Supplementary Table 2. The results of normality test in the AD rat model.

Supplementary Table 3. The results of Levene's test in the AD rat model.

Supplementary Table 4. The means and 95% CI of ANOVA in the AD rat model.

Supplementary Table 5. The results of ANOVA in the AD rat model.

Supplementary Table 6. The statistical analysis results of the AD cellular model.

### ORCID iDs

Haiyan Ren https://orcid.org/0009-0007-7531-779X
Weibin Qiu https://orcid.org/0009-0009-0731-4399
Benju Zhu https://orcid.org/0009-0007-2455-5384
Qiang Li https://orcid.org/0009-0009-8978-0333
Chen Peng https://orcid.org/0009-0008-1807-4207
Xu Chen https://orcid.org/0000-0003-3465-6932

### References

1. Sengoku R. Aging and Alzheimer's disease pathology. *Neuropathology*. 2020;40(1):22–29. doi:10.1111/neup.12626
2. Gunn-Moore D, Kaidanovich-Beilin O, Iradi MCG, Gunn-Moore F, Lovestone S. Alzheimer's disease in humans and other animals: A consequence of postreproductive life span and longevity rather than aging. *Alzheimers Dement*. 2018;14(2):195–204. doi:10.1016/j.jalz.2017.08.014
3. Dugger BN, Dickson DW. Pathology of neurodegenerative diseases. *Cold Spring Harb Perspect Biol*. 2017;9(7):a028035. doi:10.1101/cshperspect.a028035
4. Tanaka M, Toldi J, Vécsei L. Exploring the etiological links behind neurodegenerative diseases: Inflammatory cytokines and bioactive kynurenines. *Int J Mol Sci*. 2020;21(7):2431. doi:10.3390/ijms21072431
5. Hashimoto A, Matsuoka K, Yasuno F, et al. Frontal lobe function in elderly patients with Alzheimer's disease and caregiver burden. *Psychogeriatrics*. 2017;17(4):267–272. doi:10.1111/psyg.12231
6. Dhikav V, Duraiswamy S, Anand KS. Correlation between hippocampal volumes and medial temporal lobe atrophy in patients with Alzheimer's disease. *Ann Indian Acad Neurol*. 2017;20(1):29–35. doi:10.4103/0972-2327.199903
7. Rajmohan R, Reddy PH. Amyloid-beta and phosphorylated tau accumulations cause abnormalities at synapses of Alzheimer's disease neurons. *J Alzheimers Dis*. 2017;57(4):975–999. doi:10.3233/JAD-160612
8. Battaglia S, Garofalo S, Di Pellegrino G. Context-dependent extinction of threat memories: Influences of healthy aging. *Sci Rep*. 2018;8(1):12592. doi:10.1038/s41598-018-31000-9
9. Takahashi RH, Nagao T, Gouras GK. Plaque formation and the intraneuronal accumulation of β-amyloid in Alzheimer's disease. *Pathol Int*. 2017;67(4):185–193. doi:10.1111/pin.12520
10. Battaglia S, Garofalo S, Di Pellegrino G, Starita F. Revaluing the role of vmPFC in the acquisition of Pavlovian threat conditioning in humans. *J Neurosci*. 2020;40(44):8491–8500. doi:10.1523/JNEUROSCI.0304-20.2020
11. Nobakht M, Hoseini SM, Mortazavi P, et al. Neuropathological changes in brain cortex and hippocampus in a rat model of Alzheimer's disease. *Iran Biomed J*. 2011;15(1–2):51–58. PMID:21725500.
12. Chen GF, Xu TH, Yan Y, et al. Amyloid beta: Structure, biology and structure-based therapeutic development. *Acta Pharmacol Sin*. 2017;38(9):1205–1235. doi:10.1038/aps.2017.28
13. Sharma K, Pradhan S, Duffy LK, Yeasmin S, Bhattarai N, Schulte MK. Role of receptors in relation to plaques and tangles in Alzheimer's disease pathology. *Int J Mol Sci*. 2021;22(23):12987. doi:10.3390/ijms222312987
14. Bloom GS. Amyloid-β and tau: The trigger and bullet in Alzheimer disease pathogenesis. *JAMA Neurol*. 2014;71(4):505–508. doi:10.1001/jamaneurol.2013.5847
15. Iloside attenuate amyloid-beta pathology by reversing BDNF/TrkB signaling deficits and mitochondrial dysfunction. *Mol Neurobiol*. 2022;59(5):3091–3109. doi:10.1007/s12035-022-02728-3
16. Harrison TM, Maass A, Adams JN, Du R, Baker SL, Jagust WJ. Tau deposition is associated with functional isolation of the hippocampus in aging. *Nat Commun*. 2019;10(1):4900. doi:10.1038/s41467-019-12921-z
17. Liang SY, Wang ZT, Tan L, Yu JT. Tau toxicity in neurodegeneration. *Mol Neurobiol*. 2022;59(6):3617–3634. doi:10.1007/s12035-022-02809-3
18. Wu M, Zhang M, Yin X, et al. The role of pathological tau in synaptic dysfunction in Alzheimer's diseases. *Transl Neurodegener*. 2021;10(1):45. doi:10.1186/s40035-021-00270-1
19. Beylerli O, Gareev I, Sufianov A, Ilyasova T, Zhang F. The role of microRNA in the pathogenesis of glial brain tumors. *Noncoding RNA Res*. 2022;7(2):71–76. doi:10.1016/j.ncrna.2022.02.005
20. Miya Shaik M, Tamargo I, Abubakar M, Kamal M, Greig N, Gan S. The role of microRNAs in Alzheimer's disease and their therapeutic potentials. *Genes (Basel)*. 2018;9(4):174. doi:10.3390/genes9040174
21. O'Brien J, Hayder H, Zayed Y, Peng C. Overview of microRNA biogenesis, mechanisms of actions, and circulation. *Front Endocrinol (Lausanne)*. 2018;9:402. doi:10.3389/fendo.2018.00402
22. Paul P, Chakraborty A, Sarkar D, et al. Interplay between miRNAs and human diseases. *J Cell Physiol*. 2018;233(3):2007–2018. doi:10.1002/jcp.25854
23. Cardoso AL, Guedes JR. Quantifying miRNA deregulation in Alzheimer's disease. In: Perneczky R, ed. *Biomarkers for Alzheimer's Disease Drug Development*. Vol. 1750. Methods in Molecular Biology. New York, USA: Springer New York; 2018:307–319. doi:10.1007/978-1-4939-7704-8_21
24. Chang WS, Wang YH, Zhu XT, Wu CJ. Genome-wide profiling of miRNA and mRNA expression in Alzheimer's disease. *Med Sci Monit*. 2017;23:2721–2731. doi:10.12659/MSM.905064
25. Hou T, Zhou Y, Zhu L, et al. Correcting abnormalities in miR-124/PTPN1 signaling rescues tau pathology in Alzheimer's disease. *J Neurochem*. 2020;154(4):441–457. doi:10.1111/jnc.14961
26. Ma Y, Ye J, Zhao L, Pan D. MicroRNA-146a inhibition promotes total neurite outgrowth and suppresses cell apoptosis, inflammation, and STAT1/MYC pathway in PC12 and cortical neuron cellular Alzheimer's disease models. *Braz J Med Biol Res*. 2021;54(5):e9665. doi:10.1590/1414-431x20209665
27. Liu L, Liu L, Lu Y, Zhang T, Zhao W. Serum aberrant expression of miR-24-3p and its diagnostic value in Alzheimer's disease. *Biomark Med*. 2021;15(16):1499–1507. doi:10.2217/bmm-2021-0098
28. Battaglia S, Thayer JF. Functional interplay between central and autonomic nervous systems in human fear conditioning. *Trends Neurosci*. 2022;45(7):504–506. doi:10.1016/j.tins.2022.04.003
29. Battaglia S, Orsolini S, Borgomaneri S, Barbieri R, Diciotti S, Di Pellegrino G. Characterizing cardiac autonomic dynamics of fear learning in humans. *Psychophysiology*. 2022;59(12):e14122. doi:10.1111/psyp.14122
30. Atik A, Stewart T, Zhang J. Alpha-synuclein as a biomarker for Parkinson's disease. *Brain Pathol*. 2016;26(3):410–418. doi:10.1111/bpa.12370
31. Li KL, Huang HY, Ren H, Yang XL. Role of exosomes in the pathogenesis of inflammation in Parkinson's disease. *Neural Regen Res*. 2022;17(9):1898–1906. doi:10.4103/1673-5374.335143
32. Ellena G, Battaglia S, Làdavas E. The spatial effect of fearful faces in the autonomic response. *Exp Brain Res*. 2020;238(9):2009–2018. doi:10.1007/s00221-020-05829-4
33. Guo CC, Jiao CH, Gao ZM. Silencing of LncRNA BDNF-AS attenuates $A\beta_{25-35}$-induced neurotoxicity in PC12 cells by suppressing cell apoptosis and oxidative stress. *Neurol Res*. 2018;40(9):795–804. doi:10.1080/01616412.2018.1480921
34. Fan Y, Zhao X, Lu K, Cheng G. LncRNA BDNF-AS promotes autophagy and apoptosis in MPTP-induced Parkinson's disease via ablating microRNA-125b-5p. *Brain Res Bull*. 2020;157:119–127. doi:10.1016/j.brainresbull.2020.02.003

35. Hu J, Huang HZ, Wang X, et al. Activation of glycogen synthase kinase-3 mediates the olfactory deficit-induced hippocampal impairments. *Mol Neurobiol*. 2015;52(3):1601–1617. doi:10.1007/s12035-014-8953-9
36. Wang X, Wang LP, Tang H, et al. Acetyl-l-carnitine rescues scopolamine-induced memory deficits by restoring insulin-like growth factor II via decreasing p53 oxidation. *Neuropharmacology*. 2014; 76(Pt A):80–87. doi:10.1016/j.neuropharm.2013.08.022
37. Kudoh SN, Kiyohara A, Taguchi T. The heterogeneous distribution of functional synaptic connections in rat hippocampal dissociated neuron cultures. *Electron Comm Jpn*. 2009;92(6):41–49. doi:10.1002/ecj.10063
38. Livak KJ, Schmittgen TD. Analysis of relative gene expression data using real-time quantitative PCR and the 2(–Delta Delta C(T)) method. *Methods*. 2001;25(4):402–408. doi:10.1006/meth.2001.1262
39. Kwon MJ, Kim S, Han MH, Lee SB. Epigenetic changes in neurodegenerative diseases. *Mol Cells*. 2016;39(11):783–789. doi:10.14348/molcells.2016.0233
40. Candini M, Battaglia S, Benassi M, Di Pellegrino G, Frassinetti F. The physiological correlates of interpersonal space. *Sci Rep*. 2021; 11(1):2611. doi:10.1038/s41598-021-82223-2
41. Cui J, Shan R, Cao Y, Zhou Y, Liu C, Fan Y. Protective effects of ginsenoside Rg2 against memory impairment and neuronal death induced by Aβ25-35 in rats. *J Ethnopharmacol*. 2021;266:113466. doi:10.1016/j.jep.2020.113466
42. Chu J, Lauretti E, Praticò D. Caspase-3-dependent cleavage of Akt modulates tau phosphorylation via GSK3β kinase: Implications for Alzheimer's disease. *Mol Psychiatry*. 2017;22(7):1002–1008. doi:10.1038/mp.2016.214
43. Ebrahim K, Vatanpour H, Zare A, Shirazi FH, Nakhjavani M. Anticancer activity a of Caspian cobra (*Naja naja oxiana*) snake venom in human cancer cell lines via induction of apoptosis. *Iran J Pharm Res*. 2016;15(Suppl):101–112. PMID:28228809.
44. Basavaraju M, De Lencastre A. Alzheimer's disease: Presence and role of microRNAs. *Biomol Concepts*. 2016;7(4):241–252. doi:10.1515/bmc-2016-0014
45. Van den Hove DL, Kompotis K, Lardenoije R, et al. Epigenetically regulated microRNAs in Alzheimer's disease. *Neurobiol Aging*. 2014; 35(4):731–745. doi:10.1016/j.neurobiolaging.2013.10.082
46. Anwar S, Rivest S. Alzheimer's disease: Microglia targets and their modulation to promote amyloid phagocytosis and mitigate neuroinflammation. *Expert Opin Ther Targets*. 2020;24(4):331–344. doi:10.1080/14728222.2020.1738391
47. Battaglia S. Neurobiological advances of learned fear in humans. *Adv Clin Exp Med*. 2022;31(3):217–221. doi:10.17219/acem/146756
48. Heppner FL, Ransohoff RM, Becher B. Immune attack: The role of inflammation in Alzheimer disease. *Nat Rev Neurosci*. 2015;16(6): 358–372. doi:10.1038/nrn3880
49. Sung PS, Lin PY, Liu CH, Su HC, Tsai KJ. Neuroinflammation and neurogenesis in Alzheimer's disease and potential therapeutic approaches. *Int J Mol Sci*. 2020;21(3):701. doi:10.3390/ijms21030701
50. Abulfadl Y, El-Maraghy N, Ahmed AE, Nofal S, Abdel-Mottaleb Y, Badary O. Thymoquinone alleviates the experimentally induced Alzheimer's disease inflammation by modulation of TLRs signaling. *Hum Exp Toxicol*. 2018;37(10):1092–1104. doi:10.1177/0960327118755256
51. Mazarati A, Maroso M, Iori V, Vezzani A, Carli M. High-mobility group box-1 impairs memory in mice through both toll-like receptor 4 and Receptor for Advanced Glycation End Products. *Exp Neurol*. 2011; 232(2):143–148. doi:10.1016/j.expneurol.2011.08.012
52. Zhao BS, Liu Y, Gao XY, Zhai HQ, Guo JY, Wang XY. Effects of ginsenoside Rg1 on the expression of toll-like receptor 3, 4 and their signalling transduction factors in the NG108-15 murine neuroglial cell line. *Molecules*. 2014;19(10):16925–16936. doi:10.3390/molecules191016925
53. Graham WV, Bonito-Oliva A, Sakmar TP. Update on Alzheimer's disease therapy and prevention strategies. *Annu Rev Med*. 2017;68: 413–430. doi:10.1146/annurev-med-042915-103753
54. Valenza M, Scuderi C. How useful are biomarkers for the diagnosis of Alzheimer's disease and especially for its therapy? *Neural Regen Res*. 2022;17(10):2205–2207. doi:10.4103/1673-5374.335791
55. Walgrave H, Zhou L, De Strooper B, Salta E. The promise of microRNA-based therapies in Alzheimer's disease: Challenges and perspectives. *Mol Neurodegener*. 2021;16(1):76. doi:10.1186/s13024-021-00496-7

# miR-214-5p increases the radiosensitivity of cervical cancer by targeting ROCK1 expression

Junqin Zhang[1,A,B], Yaxing Li[2,C], Yanan Ren[1,C], Jie Li[1,C], Hua Han[1,C], Ping Yan[1,A,F]

[1] Department of Gynecology, Hebei General Hospital, Shijiazhuang, China
[2] The 3rd Department of Oncology, Hebei General Hospital, Shijiazhuang, China

A – research concept and design; B – collection and/or assembly of data; C – data analysis and interpretation; D – writing the article; E – critical revision of the article; F – final approval of the article

Advances in Clinical and Experimental Medicine, ISSN 1899–5276 (print), ISSN 2451–2680 (online) *Adv Clin Exp Med*. 2024;33(3):247–259

**Address for correspondence**
Ping Yan
E-mail: yanping6368@126.com

**Funding sources**
The study was supported by the Medical Science Research Project Plan of the Hebei Provincial Health Commission (grant No. 20210333).

**Conflict of interest**
None declared

Received on January 5, 2023
Reviewed on April 13, 2023
Accepted on May 31, 2023

Published online on July 24, 2023

## Abstract

**Background.** The tolerance of cervical cancer to radiotherapy is a major factor affecting treatment outcomes. The miR-214-5p is involved in the regulation of biological processes such as tumor proliferation and metastasis.

**Objectives.** The aim of the study was to explore the role of miR-214-5p and Rho-associated coiled-coil containing protein kinase 1 (ROCK1) in cervical cancer and their response to radiotherapy in cervical cancer patients.

**Materials and methods.** Fifty-three cervical cancer tissue samples were collected to analyze the level of miR-214-5p in patients with different responses to radiotherapy. Cervical cancer cell lines with radiation resistance were selected to explore the role of miR-214-5p in radiosensitivity. The wound healing, transwell migration, clone formation assay, and in vivo analysis were utilized to evaluate the effect of miR-214-5p on the radiation sensitivity of cervical cancer cells.

**Results.** Patients with poor radiotherapy responses demonstrated low levels of miR-214-5p. The upregulation of miR-214-5p decreased migration and invasion ability of radiotherapy-resistant cells. The bioinformatic analysis showed that *ROCK1* is a candidate target gene of miR-214-5p, and this was confirmed with dual luciferase reporter assay showing that miR-214-5p directly interacts with the 3'untranslated region (3'UTR) of ROCK1. Decreased ROCK1 improved the radiosensitivity of cervical cancer in vitro and in vivo, and the over-expression of ROCK1 decreased the radiosensitivity effect of miR-214-5p in cervical cancer cells.

**Conclusions.** The miR-214-5p can regulate the radiation sensitivity of cervical cancer cells by targeting the mRNA of ROCK1 and regulating its expression.

**Key words:** radiosensitivity, ROCK1, cervical cancer, microRNA-214-5p

**Cite as**
Zhang J, Li Y, Ren Y, Li J, Han H, Yan P. miR-214-5p increases the radiosensitivity of cervical cancer by targeting ROCK1 expression. *Adv Clin Exp Med*. 2024;33(3):247–259. doi:10.17219/acem/166673

**DOI**
10.17219/acem/166673

# Background

Cervical cancer is ranked as the 4th leading cancer in females worldwide, although early detection of the disease can significantly affect treatment efficacy and prolong the survival time of patients.[1] Currently, radiotherapy is the main treatment strategy for cervical cancer. However, the radiotherapy tolerance of cervical cancer affects the treatment outcomes. The failure of radiotherapy in cervical cancer is correlated with many factors, such as the different clinicopathological characteristics of patients, the hypoxic state of cancer cells and the intrinsic sensitivity of the tumor cells to radiotherapy.[2] MicroRNAs (miRNAs) participate in the progression of a wide array of tumors. They regulate the malignant behavior of tumor cells by reducing the stability and translation of targeted mRNA. Specifically, miR-214 participates in tumor progression, acting as a tumor suppressor gene or oncogene.[3–7] Moreover, miR-214 is involved in the radiosensitivity response of nasopharyngeal carcinoma and skin injury caused by radiation.[8,9] In clinical practice, the enhanced effect of radiotherapy by exogenous miRNA in solid tumors has entered the exploration stage.

The Rho family, also called Rho GTPases, is a class of GTP-binding proteins with GTP enzyme activity that are associated with the Ras superfamily. The Rho GTPases are important signal transduction molecules and participate in the regulation of cytoskeletal reorganization. Working as "molecular switches" in the process of cell signal transduction, Rho GTPases control many signal transduction pathways. The Rho-associated coiled-coil containing protein kinase 1/2 (ROCK1/2) belongs to the Rho family and is expressed in multiple tissues, including the lung, liver, spleen, kidneys, testes, brain, and heart, and acts in several subcellular locations.[10] The ROCK1 promotes tumor cell proliferation, invasion and metastasis by activating the Rho/ROCK signaling pathway. After interacting with activated Rho protein, the active center of ROCK1 is catalyzed and induces the reorganization of the actin cytoskeleton of cancer cells, thereby enhancing the movement ability of cancer cells.[11] The ROCK inhibitor, fasudil, induces terminal adipocyte differentiation of chemoresistant osteosarcoma cells.[12] Epithelial-to-mesenchymal transition (EMT) contributes to therapy resistance in cancers,[13] a process the ROCK is frequently associated with in human ovarian cancer cells.[14] This inspired us to further explore the role of ROCK1 and its attenuating miRNA in radiotherapy resistance in cervical cancer cells.

# Objectives

This study aims to evaluate the miR-214-5p expression and the response to radiotherapy in patients with cervical cancer. In addition, the role of miR-214-5p in radiation sensitivity was investigated in vivo and in vitro. Finally, we explored the mechanism of action of miR-214-5p and its relationship with ROCK1 in cervical cancer following radiotherapy.

# Materials and methods

## Samples

The medical data of patients with cervical cancer were screened to estimate the gene expression of *miR-214-5p* and *ROCK1*. The samples included in the current analysis were collected in Hebei General Hospital (Shijiazhuang, China) from patients who did not receive radiotherapy or chemotherapy before surgery in the years 2017–2020. All patients signed informed consent for sample and data analyses. Fifty-three tissue samples with postoperative pathological reports and complete medical records were included. The International Federation of Gynecology and Obstetrics (FIGO) stage of collected samples ranged from IB to IIIA, based on the 2009 FIGO staging system,[15] and the severities ranged from a relatively early stage to an advanced stage (para-aortic lymph node involvement). Patients' demographic data, including age, menopause state, tumor diameter, lymph node metastasis, and pathological type, were also recorded. Exclusion criteria were patients who received preoperative radiotherapy and chemotherapy, cervical surgery, and hysterectomy, patients with an incomplete cervix, those suffering from other malignant tumors, pregnant patients, and patients with reproductive tract inflammatory diseases. Another 30 samples from normal adjacent cervical tissue and 30 samples of cervical intraepithelial neoplasia (all confirmed by pathological examination) were selected for the analysis. All specimens were collected and stored at –80°C.

## Evaluation of radiotherapy response in patients

The radiotherapy sensitivity in patients was determined according to the response evaluation criteria in solid tumors (RECIST) developed by the World Health Organization (WHO),[16] based on their medical records: 1) the short-term efficacy includes an uncontrolled tumor and disappearance of the tumor; an uncontrolled tumor refers to the persistence or emergence of new lesions within 3 months after radiotherapy; tumor disappearance indicates that the tumor disappears within 3 months following radiotherapy; 2) the long-term efficacy includes tumor recurrence and the tumor being cured; tumor recurrence refers to the disappearance of the tumor after radiotherapy, while a pelvic or distant tumor is found upon re-examination 6 months after radiotherapy; tumor cured refers to the disappearance of the tumor without recurrence; tumor uncontrolled and tumor recurrence were defined as radiotherapy resistance; tumor cured, being neither tumor uncontrolled nor tumor recurrence, was defined as radiotherapy sensitivity.

## In vivo tumor model and inhibition evaluation

The animal study was approved by the ethics committee of Hebei General Hospital (approval No. 2020-256), and all protocols followed the guidelines of Institutional Animal Care and Use Committee (IACUC) issued by the Chinese Academy of Medical Sciences. A total of 24 female BALB/c nude mice (age: 5 weeks; weight: 19–22 g; provided by the Animal Experiment Center of Hebei Medical University, Shijiazhuang, China) housed in an specific pathogen-free (SPF) laboratory animal room, were used to construct a cervical tumor-bearing model. A liposomal delivery system (MaxSuppressor™ In Vivo RNA-LANCEr II; Bioo Scientific, Austin, USA) was used to deliver miR-214-5p mimic and the negative control sequence (miR-214-5p NC), according to the manufacturer's instructions (RiboBio Co., Ltd., Guangzhou, China). Briefly, RNA oligos were diluted to 10 mg/mL, and a total of 500 µL of RNA solution mixture (RNA solution: 11 µL, phosphate-buffered saline (PBS) (10×): 55 µL, and RNase-free water: 434 µL) was mixed with 50 µL of neutral lipid emulsion. The solution was mixed in an ultrasonic water bath for 5 min prior to intravenous administration. Hela cells (200 µL at a concentration of $5\times10^6$ cells/mL) were inoculated into the flank of mice. Radiotherapy (total dose of 20 Gy) was performed 1 week after inoculation. The mice were anesthetized by 5% chloral hydrate (300 mg/kg, intraperitoneal injection) during radiation. Then, the animals were fixed and irradiated by 6MV X-ray (X-RAD 225XL irradiator; Precision X-Ray, Inc., Madison, USA). The irradiated dose was 2 Gy daily, performed 10 times over 2 weeks. Accordingly, the mice were allocated to the model group, the radiation group, the miR-214-5p mimic group, and the miR-214-5p mimic + radiation group (n = 6 mice per group). The miRNA mimics were administered in a 40 µg per mouse bolus, which started on day 7 post-inoculation, and continued every 3 days. The radiation was performed when the tumor volume in the model group reached approx. 200 $mm^3$, and the mice were sacrificed by decapitation when the tumor was over 1000 $mm^3$ in the model group. The growth and the inhibited rate of tumor growth in each group were calculated. The diameter of the tumor by the longest (L) and the shortest diameter (W) were measured, and the transplanted tumor volume (V) was calculated as $0.5\times L\times W^2$.

## RT-qPCR analysis

The total RNA was extracted from tissues and cultured cells using Trizol reagent (#R0016; Beyotime Biotechnology, Shanghai, China), following the manufacturer's instructions. A total of 1 mL of Trizol and 0.2 mL of chloroform were added to the tubes containing homogenized tissues or cell pellets. Five minutes after the lysis, the samples were centrifuged for 15 min at 4°C and 12,000 g. The upper colorless solution containing the total RNA was loaded into a new centrifuge tube, and 0.5 mL of isopropanol was added for 10 min to precipitate the RNA. After the centrifugation for 10 min at 4°C and 12,000 g, the RNA was precipitated with 75% ethanol, centrifuged again and dissolved with diethyl pyrocarbonate (DEPC) water. The integrity of extracted RNAs was measured using a 1% agarose electrophoresis gel. A 30-ng RNA sample was reverse transcribed with PrimeScript RT reagent kit (#RR037B; Takara Bio Inc., Shiga, Japan), following the previously described method.[17] The reverse transcriptional reaction system (10-µL volume) contained 2 µL of PrimeScript buffer, 0.5 µL of RT enzyme mix, 0.5 µL of oligo dT primer, 0.5 µL of random hexamers, total RNA, and RNase free water. The two-step TB Green-based quantitative real-time reverse transcription polymerase chain reaction (RT-qPCR) was performed according to the manufacturer's instruction.[18] The expression of miR-214-5p was normalized and quantified using the small RNA U6.[19–21] The mRNA expression of ROCK1 was also measured and calculated as the relative expression to β-actin.[22,23] The ABI StepOnePlus™ Real-Time PCR system (Thermo Fisher Scientific, Waltham, USA) was used to perform RT-qPCR analysis,[24,25] and the applied thermal cycling parameters were recommended by the manufacturer. All used primers are listed in Table 1. The relative expression of target genes was evaluated by the $2^{-\Delta\Delta Ct}$ method. All measurements were performed in triplicate.

Table 1. Quantitative real-time reverse transcription-polymerase chain reaction (qRT-PCR) primer sequence

| Gene | Sequence |
|---|---|
| *miR-214-5p* | F: 5′-GCCGAGTGCCTGTCTACACT-3′ |
| | R: 5′-GCAGGGTCCGAGGTAT-3′ |
| *U6* | F: 5′-GAGGGCCTATTTCCCATGATT-3′ |
| | R: 5′-TAATTAGAATTAATTTGACT-3′ |
| *ROCK1* | F: 5′-TGAAAGCCGCACTGATGGAT-3′ |
| | R: 5′-GCCATGAGAAAACACATTGCAG-3′ |
| *β-actin* | F: 5′-CACCATTGGCAATGAGCGGTTC-3′ |
| | R: 5′-AGGTCTTTGCGGATGTCCACGT-3′ |

## Cell lines and tissue samples

Six human cervical cancer cell lines were used, namely C4-1, C33A, MS751, Hela, Siha, and CaSki (Cell Bank of the Chinese Academy of Sciences, Shanghai, China). The C4-1 and C33A were cultured in RPMI-1640 medium (#R8758; Sigma-Aldrich, Burlington, USA) containing 10% fetal bovine serum (FBS), while MS751, Hela, Siha, and CaSki cells were cultured in Dulbecco's modified Eagle's medium (DMEM) (#D5796; Sigma-Aldrich), supplemented with 10% FBS, 100 U/mL of penicillin and 100 µg/mL of streptomycin. All cells were cultured at 37°C in 5% $CO_2$.

## RNA oligoribonucleotides, plasmid construction and transfection

To verify the function of miR-214-5p in vitro and in vivo, the following sequence or mutant sequence was prepared: miR-214-5p mimic (#miR10004564-1-5), miR-214-5p NC (#miR1N0000002-1-5), wild type ROCK1 (ROCK1-WT) 3'untranslated region (3'UTR), and mutant ROCK1 (ROCK1-mut) 3'-UTR (all purchased from RiboBio Co., Ltd.). To overexpress ROCK1 in vitro, the full-length coding sequence of ROCK1 was cloned and amplified. The enzymatic digestion sites KpnI and XbaI on the pcDNA3.1(+) vector (#VT1001; YouBio Tec. Inc., Changsha, China) were used for *ROCK1* gene insertion. After recovery and purification, the plasmid was connected by T4 DNA ligase (#T1410; Solarbio Life Science, Beijing, China) with PCR products to obtain the recombinant plasmid. The DH5α was selected for transformation screening of competent cells, and a small amount of recombinant plasmid was extracted, identified and sequenced with double enzyme digestion. The empty plasmid was used as a control to compare the expression of ROCK1 (ROCK1 OE).

A total of $2\times10^5$ cells were cultured in 12-well plates, and transfection was performed after the cells reached 70–90% confluence. The culture medium was replaced by a fresh non-antibiotic medium 2 h before the transfection. Lipofectamine 3000 reagent (#L3000015; Thermo Fisher Scientific) and DNA were diluted by Opti-MEM medium (#11058021; Gibco, Carlsbad, USA) according to the manufacturer's instruction, and then added to the diluted Lipofectamine 3000 in a 1:1 proportion. The mixture was incubated at room temperature for 20 min. The obtained DNA-liposome complex was loaded into target cells, mixed gently and cultured at 37°C for further experiments.

## Cell proliferation measurement

Cell proliferation was assessed using the Cell Counting Kit-8 (CCK-8) method. Fifty microliters of cells treated by miR-214-5p NC or miR-214-5p mimic (75% density, $5\times10^5$ cells at exponential growth phase) were trypsinized and loaded onto a 96-well plate containing the same volume of culture medium. Cells were cultured for 24 h, 48 h and 72 h, and then 10 µL of CCK-8 reagent (#C0038; Beyotime Biotechnology) was loaded into the wells. The cells were cultured for another 2 h, and the optical density (OD) of the target well was measured at 450 nm. The average value from 3 wells was calculated.

## Wound healing assay

Cells with a concentration of $5\times10^5$ were evenly loaded onto a 6-well plate. The cells were washed twice with PBS after 12-h culture to remove any non-adherent cells. A straight scratch was generated using a sterile 20-µL pipette tip across the monolayer of cells. The debris on the plate was washed twice with PBS and replaced with a fresh serum-free medium. The migration ability of cells was observed under an optical microscope (Nikon Labophot 2 Microscope; Nikon Corp., Tokyo, Japan) at 24 h and 48 h. The image was captured, and the width of the scratch wound was evaluated using ImageJ software (National Institutes of Health (NIH), Bethesda, USA).

## Transwell migration

After Matrigel was diluted and spread across the bottom of the upper chamber of the Transwell, 100 µL of cells ($5\times10^5$/mL) were loaded to the upper chamber of a 24-well transwell (8-µm pore, #3422, Transwell®; Corning Life Science, Tewksbury, USA). Medium supplemented with 10% serum (600 µL) was loaded into the lower chamber. The plate was cultured for 24 h, and unmigrated cells in the chamber were swabbed after discarding the medium. The remaining cells were fixed with 4% paraformaldehyde for 15 min and stained with crystal violet for 10 min. The filter membrane was photographed under a light microscope (Nikon Labophot 2 Microscope). Image-Pro Plus v. 6 software (Media Cybernetics, Rockville, USA) was used to count the migrated cells. Five fields of view from each well were randomly analyzed to evaluate the average number of migrated cells.

## Clone formation assay

Logarithmic growth staged cells were added to 60-mm culture dishes. According to the results of a pre-experiment, about 250 cells were loaded to each plate. The cells were dispersed evenly. A single dose of 4 Gy and 6 Gy (5 min per day with a dose rate of 300 cGy/min) was generated ($^{60}$Co medical irradiation device; China Nuclear Power Technology Research Institute, Beijing, China) and absorbed by the cells. The irradiation was performed for 10 consecutive days, and the cells were continued to be cultured for another 10 days. Any clones that were formed were fixed with paraformaldehyde and stained with 0.1% crystal violet solution for 20 min. The number of clones was counted in each group under a low power microscope (Nikon Labophot 2 Microscope). The average number of clones from 3 dishes was calculated for each dose.

## Luciferase reporter assay

To verify the binding effect of miR-214-5p to ROCK1, starBase v. 3.0 (https://rnasysu.com/encori/) and TargetScan (https://www.targetscan.org/vert_80/) online databases were used to predict putative binding sites for miR-214-5p. Briefly, the wild type or mutant (MUT) fragments for ROCK1 3'UTR were amplified. The fragment was inserted into the SpeI and HindIII sites of the pMIR-REPORT luciferase reporter vector following the methods mentioned

above and previously.[26] The pMIR-β-galactosidase reporter plasmid was used to normalize the transfection. The HEK-293T cells were then co-transfected with reporter vectors and duplexes of small interfering RNAs (miR-214-5p mimic or miR-214-5p NC) with Lipofectamine 3000 reagent. Twenty-four hours after the transfection, the cells were harvested, and luciferase assays and β-galactosidase enzyme assays were used to measure relative luminescence units in each well, following the manufacturer's protocol. The luciferase activity of firefly was normalized to β-galactosidase expression. Three parallel wells were measured for each condition.

### Western blot

Radioimmunoprecipitation assay (RIPA) lysis buffer (200 μL) (#R0010; Solarbio Life Science) was used to lyse the cells. The suspension was centrifuged for 4 min at 4°C and 12,000 rpm, and the supernatant was retained to separate targeted proteins. The total protein amount was determined using the bicinchoninic acid (BCA) method. Fifty milligrams of protein were loaded onto a 10% sodium dodecyl sulfate-polyacrylamide gel (SDS-PAGE) for electrophoresis and transferred to polyvinylidene fluoride (PVDF) membranes (Millipore, Burlington, USA). The membrane was blocked using 5% skimmed milk at 37°C for 1 h, and the primary antibodies (Invitrogen, Waltham, USA) for ROCK1 (#MA5-27779, 1:1000 diluted), Rho (#1B8-1C7, 1:1000 diluted), LIMK1 and Phospho-LIMK1 antibody (#MA5-37486, 1:1000 diluted; #PA5-104925, 1:200 diluted) were added overnight at 4°C. The membrane was washed thrice with 1× Tris-Buffered Saline with Tween (TBST) and then incubated with a goat anti-rabbit IgG HRP (#31460, 1:5000 dilution; Thermo Fisher Scientific) for 2 h. The membrane was then washed with 1× TBST, and the electrochemiluminescence (ECL) luminous working solution was added to obtain images of the proteins.[27,28]

### Statistical analyses

Quantitative data are presented as mean ± standard deviation (M ±SD) and were analyzed using GraphPad Prism v. 9.4 software (GraphPad Software, San Diego, USA) and IBM Statistical Package for Social Science (SPSS) v. 24.0 software (IBM Corp., Armonk, USA). The expression levels of miR-214-5p and ROCK1 mRNA in clinical samples are presented as the relative expression. The Shapiro–Wilk test was used to confirm the normal data distribution, and the Brown–Forsythe test was used to confirm the homogeneity of variance. Data that passed normality and homogeneity of variance tests were compared using bootstrap one-way analysis of variance (ANOVA) followed by Tukey's post hoc test to analyze the differences among multiple groups, or Student's t-test for differences between 2 groups. If the data were not normally distributed, Kruskal–Wallis test with Dunn's post hoc test was applied for statistical differences among multiple groups, and the Mann–Whitney U test was used for the comparison between 2 groups. For an in vitro analysis, all experiments were performed in triplicate, and the repeated measurement data in the proliferation assay were completed at different time points and performed in triplicate. The in vitro data and repeated measurements were compared using unpaired Student's t-test or bootstrap one-way ANOVA, followed by a Tukey's post hoc test. The correlation between miR-214-5p and ROCK1 mRNA levels was analyzed with SPSS v. 24.0 statistical software using Spearman's correlation method. The test level of $\alpha = 0.05$ and the value of $p < 0.05$ were considered significant.

## Results

### Decreased miR-214-5p expression in patients with cervical cancer

In this study, 53 tissue samples (Table 2) obtained from patients with cervical cancer, 30 samples from normal cervical tissues and 30 samples from cervical intraepithelial neoplasia were collected for the analysis. Compared with normal tissue, the expression of miR-214-5p was decreased in cervical intraepithelial neoplasia and cervical cancer tissues. In addition, miR-214-5p expression was lower in cervical cancer compared to cervical intraepithelial neoplasia (Fig. 1A). The expression of miR-214-5p was also decreased in more advanced clinical stages (Fig. 1B and Table 2) and in patients with lymph node metastasis (Fig. 1C and Table 2). The analysis of patients who responded to radiotherapy revealed that miR-214-5p expression in radiotherapy-resistant patients was also significantly lower compared with radiotherapy-sensitive patients (Fig. 1D).

### Upregulation of miR-214-5p decreases the proliferation ability of cervical cancer cells

We further analyzed the expression of miR-214-5p in 6 cervical cancer cell lines. This analysis demonstrated that miR-214-5p expression in C4-1, Hela and Siha cells was relatively low (Fig. 2A). The radiosensitivity evaluation of a single dose of 2 Gy showed that Hela and Siha cell lines demonstrated radiation resistance (Fig. 2B), and therefore these 2 cell lines were used in a further analysis. To explore the role of miR-214-5p in the radiosensitivity of cervical cancer, we first upregulated its expression using its mimic, and RT-qPCR demonstrated that the mimic was successfully transfected (Fig. 2C). The CCK-8 assay was used to analyze cell proliferation, showing a significant decrease following increased expression of miR-214-5p (Fig. 2D).

Table 2. Demographic data and miR-214-5p expression of 53 samples obtained from cervical cancer patients

| Parameter | Category | n (53) | Relative expression | Mann–Whitney U | p-value |
|---|---|---|---|---|---|
| Age [years] | ≥45 | 35 | 0.722 ±0.248 | 255 | 0.267 |
| | <45 | 18 | 0.657 ±0.219 | | |
| Menopause state | yes | 32 | 0.733 ±0.267 | 273 | 0.256 |
| | no | 21 | 0.650 ±0.191 | | |
| Tumor size [cm] | ≥4 | 15 | 0.620 ±0.181 | 192.5 | 0.0682 |
| | <4 | 38 | 0.731 ±0.253 | | |
| FIGO stage | IB | 8 | 1.005 ±0.289 | NA | <0.0001* |
| | IIA | 15 | 0.804 ±0.205 | | |
| | IIB | 18 | 0.654 ±0.128 | | |
| | IIIA | 12 | 0.498 ±0.055 | | |
| Lymph node metastasis | yes | 13 | 0.502 ±0.058 | 34 | <0.0001 |
| | no | 40 | 0.764 ±0.240 | | |
| Pathological type | squamous cell carcinoma | 45 | 0.691 ±0.238 | 140.5 | 0.336 |
| | adenocarcinoma | 8 | 0.751 ±0.250 | | |

Data were expressed as mean ± standard deviation (M ±SD) and analyzed using the Mann–Whitney U test; * data were analyzed using the Kruskal–Wallis one-way analysis of variance (ANOVA). The results of multiple group comparisons are also demonstrated in Fig. 1B. NA – not applicable; FIGO – International Federation of Gynecology and Obstetrics.

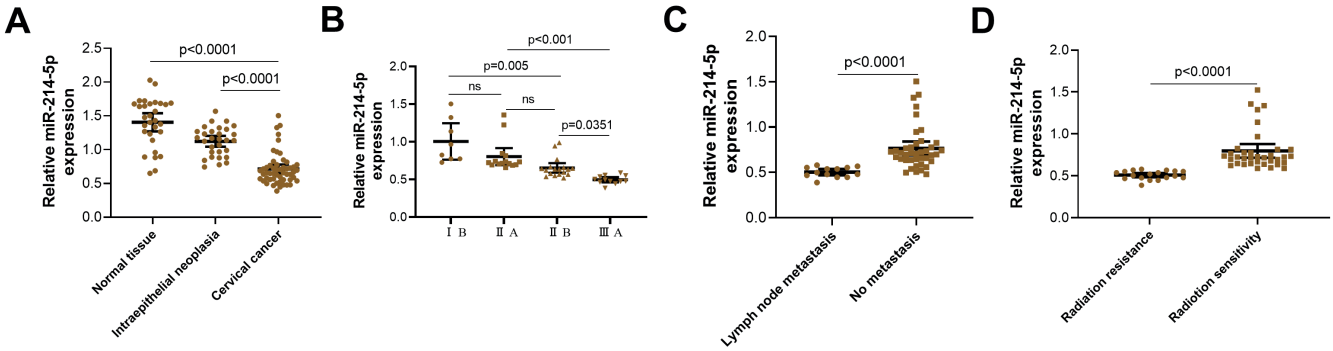


Fig. 1. Expression of miR-214-5p is downregulated in patients with cervical cancer. A. The expression of miR-214-5p in cervical carcinoma tissue (n = 53), cervical intraepithelial neoplasia (n = 30) and normal control (n = 30); B. The expression of miR-214-5p is downregulated along with the increasing clinical stage; data were analyzed using the Kruskal–Wallis test for multiple comparisons (A,B); C. Patients with lymph node metastasis have a significantly lower miR-214-5p expression; D. The expression of miR-214-5p in radiotherapy-sensitive patients is higher than in radiotherapy-resistant patients; data were analyzed using the Mann–Whitney U test (C,D). Whiskers represent the 95% confidence interval (95% CI) values

ns – not significant.

## Upregulation of miR-214-5p decreases the migration and invasion ability, and increases the radiosensitivity of cervical cancer cells

We measured the migration and invasion ability of 2 cell lines after increasing miR-214-5p expression. These data showed that migration and invasion decreased in both cell lines after the upregulation of miR-214-5p (Fig. 3A,B). Two single doses of 4 Gy and 6 Gy were used to test radiosensitivity, and after upregulating miR-214-5p, the radiation resistance of the 2 cell lines decreased significantly (Fig. 3C).

## miR-214-5p regulates radiation sensitivity by targeting ROCK1

To clarify the functions of miR-214-5p, it was important to identify its target genes. We used online bioinformatics tools to analyze the potential binding partners of miR-214-5p, identifying *ROCK1* as a potential target gene of miR-214-5p. A sequence at the 3'UTR region of ROCK1 was selected to construct a mutant variant (Fig. 4A). Dual-luciferase reporter analysis indicated a significant reduction in luciferase activity in cells containing the ROCK1-WT sequence when miR-214-5p was exogenously increased. Moreover, the relative luciferase activity in cells containing ROCK1-mut was consistent after the transfection (Fig. 4B). The RT-qPCR analysis also indicated a significantly decreased ROCK1 expression when miR-214-5p was

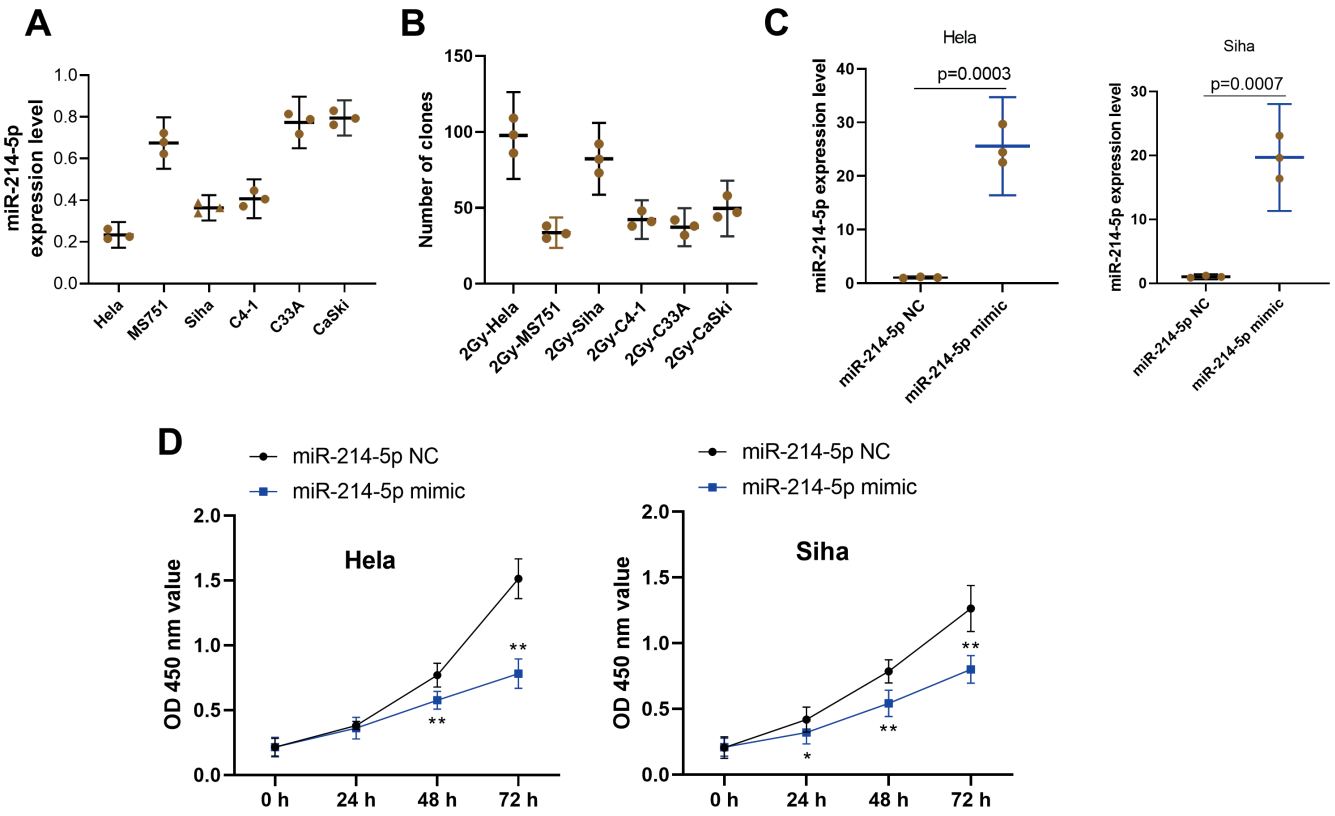


Fig. 2. Upregulation of miR-214-5p decreases the proliferation of cervical cancer cells. A. The expression of miR-214-5p in cervical cancer cell lines C4-1, MS751, Hela, Siha, C33A, and CaSki; B. The radiosensitivity of the above cell lines at 2 Gy; C. The expression of miR-214-5p in Hela and Siha cells after transfection; D. Cell proliferation of Hela and Siha cells after the transfection with a mimic of miR-214-5p; three biological replicates were performed, and the results are shown as a mean with 95% confidence interval (95% CI). The results were analyzed using Student's t-test

OD – optical density; * $p < 0.05$; ** $p < 0.01$, compared with the same time point.

exogenously upregulated (Fig. 4C). We further analyzed the correlation between miR-214-5p and ROCK1 expression in the collected tissues, and found that miR-214-5p was negatively correlated with ROCK1 expression (Fig. 4D). Moreover, we observed a relative increase in ROCK1 expression in patients with poor radiation response (Fig. 4E).

## Overexpression of ROCK1 abolishes the enhanced miR-214-5p-dependent radiosensitivity

To clarify whether radiosensitivity and growth inhibition of cervical cancer cells brought about by miR-214-5p were dependent on ROCK1 regulation, we upregulated the expression of ROCK1 in Hela cells through a ROCK1 overexpression plasmid (ROCK1 OE). The reduction in cell proliferation produced by miR-214-5p was partially reversed by ROCK1 OE (Fig. 5A). In addition, the radiation resistance of Hela cells containing the miR-214-5p mimic was partially restored with the upregulation of ROCK1 (Fig. 5B). The protein expression of ROCK1, Rho and phosphorylated LIMK1 (p-LIMK1) the proteins that sit upstream and downstream in ROCK1 signaling,[29] were also measured. The results of western blot analysis showed that the expression of upstream Rho was not affected, while its downstream kinase p-LIMK1 decreased upon ROCK1 upregulation (Fig. 5C).

## miR-214-5p improves the radiotherapy effect of cervical cancer model in nude mice

Compared with the model group, the miR-214-5p mimic group demonstrated a limited inhibiting effect on the tumor ($p = 0.244$, compared to the model group). As expected, miR-214-5p significantly increased the radiosensitivity of tumors in nude mice (Fig. 6A,B). Compared with the radiation group alone, the tumor inhibition rate in the miR-214-5p mimic + radiation group increased from 45.03 ±5.8% to 64.39 ±4.9% ($p < 0.0001$). These results confirmed that miR-214-5p has a remarkable sensitizing effect on radiotherapy. The protein expressions of Rho, ROCK1 and p-LIMK1 are consistent with the in vitro analysis (Fig. 6C), which revealed that the upregulation of miR-214-5p decreased expressions of ROCK1 and p-LIMK1 while not affecting Rho.

# Discussion

Herein, we evaluated the expression of miR-214-5p in patients who received radiotherapy, and we found that patients with unsatisfactory responses to treatment have relatively lower miR-214-5p expression levels. Based

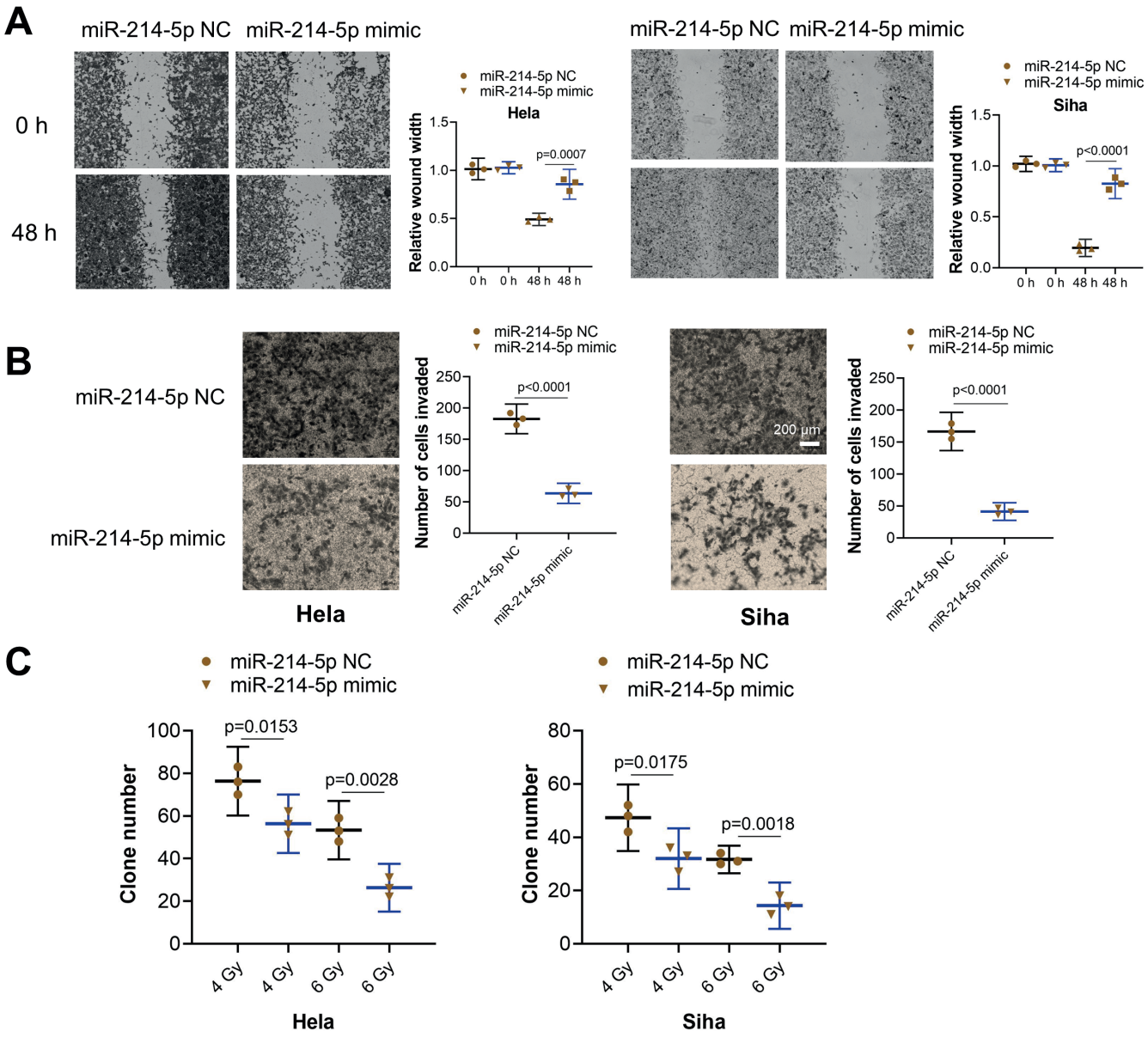


Fig. 3. Upregulation of miR-214-5p decreases the migration and invasion ability, and increases the radiosensitivity of cervical cancer cells. A. The migration ability of Hela and Siha cell lines after being transfected with miR-214-5p; B. The invasion ability of Hela and Siha cell lines decreased after the upregulation of miR-214-5p; C. The radiosensitivity of both cell lines decreased significantly after upregulating miR-214-5p measured using 2 single absorbed doses of 4 Gy and 6 Gy. Three biological replicates were performed, and the results are shown as a mean with 95% confidence interval (95% CI). The results were analyzed using Student's t-test

on the differences in miR-214-5p expression profiles, we found that miR-214-5p expression remained relatively low in several cervical cancer cell lines. The sample analysis suggested that miR-214-5p expression was significantly downregulated in cervical cancer tissues, especially in patients resistant to radiotherapy. Further studies revealed that upregulating the expression of miR-214-5p could inhibit the growth and proliferation of radiation-resistant cervical cancer cells. Intriguingly, in vivo studies showed that the administration of miR-214-5p mimics alone had little effect on tumor growth, but in combination with radiotherapy could significantly inhibit tumor growth, better than radiation treatment alone, indicating that miR-214-5p has a certain sensitizing effect.

Radiotherapy is one of the main therapies for cervical cancer due to the tumor's relatively high sensitivity to radiation therapy.[30,31] Radiotherapy can also induce changes in the expression of many genes and proteins, leading to the reduction of tumor sensitivity to radiotherapy and the development of radiation resistance.[32] Radiation resistance is the main reason for the failure of radiotherapy.[33] Furthermore, radiation resistance is a process involving multiple genes and mechanisms, including cancer stem cells (CSCs) with high tumorigenicity, which repair apoptosis by activating DNA damage responses; increased glucose uptake and decreased mitochondrial oxidative phosphorylation in tumor cells could also efficiently repair DNA. In addition, cell survival is promoted by providing energy through autophagy and

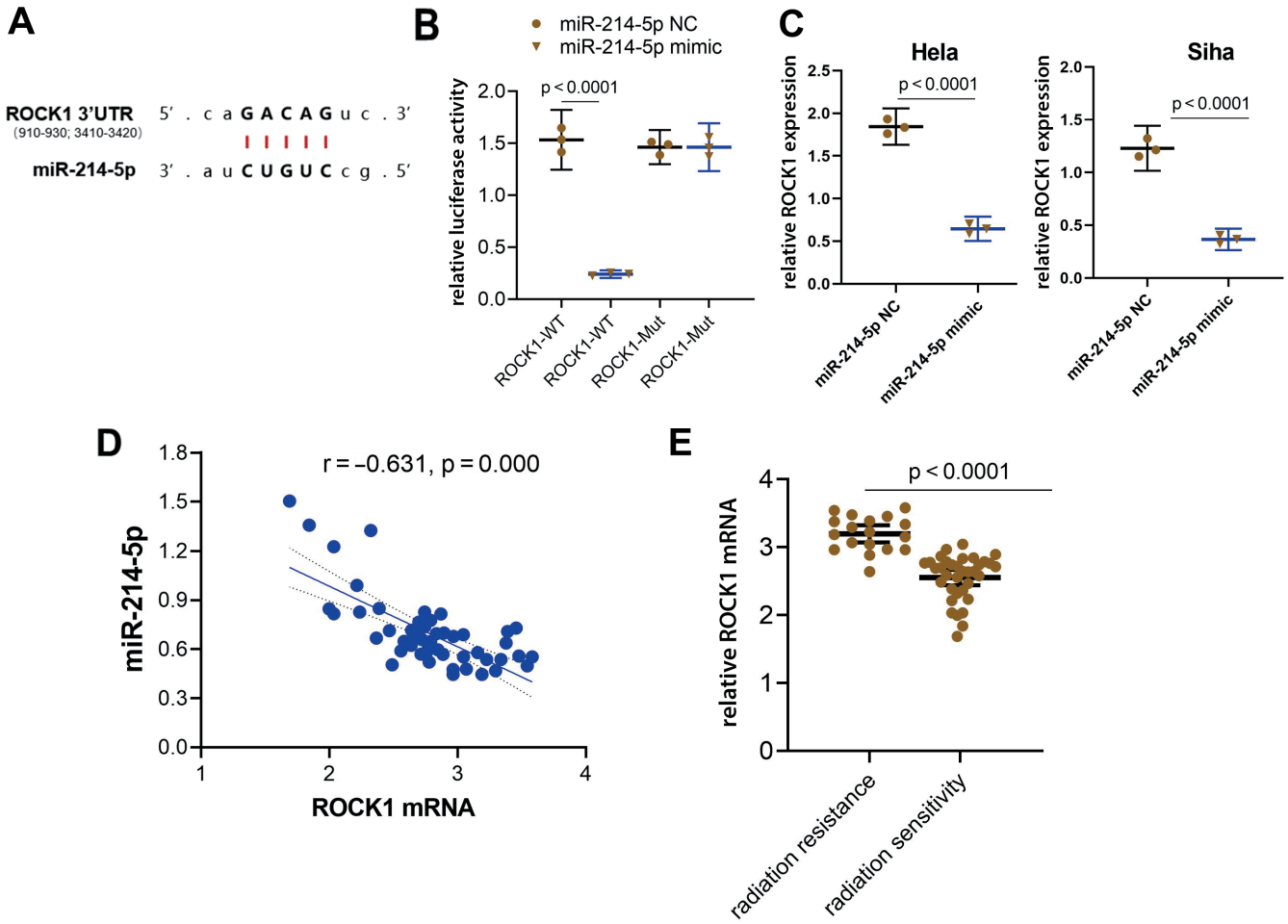


Fig. 4. miR-214-5p regulates radiation sensitivity of cervical cancer cell expression by targeting the expression of ROCK1. A. The selected binding sequence at the 3'untranslated region (3'UTR) region of ROCK1; B. The relative luciferase activity of cells transfected with ROCK1 sequence; C. The ROCK1 expression after miR-214-5p mimics were transfected into cervical cancer cells; three biological replicates were performed and data were analyzed using Student's t-test; D. The correlation analysis showed that the expression of ROCK1 was negatively correlated with the expression of miR-214-5p in cervical cancer tissues; data were analyzed with Spearman's correlation; E. Relative higher ROCK1 expression in patients has poor radiation response; data were analyzed using the Mann–Whitney U test. Whiskers represent the 95% confidence interval (95% CI) values

eliminating proteins that have been damaged by radiation. The regulation of the redistribution of the cell cycle could weaken the sensitivity to radiotherapy of tumor cells.[31,34]

Cell damage caused by different agents can facilitate different miRNA responses, which, in the process, will show expression disorder.[35] The regulation of miRNA expression ensures that miRNA can respond to injury both at the transcriptional and post-transcriptional levels. Generally, the direct target genes of miRNA molecules with oncogene effect are mostly tumor suppressor genes. Conversely, if the miRNA molecule has a tumor suppressor function, it mainly targets multiple oncogenes.[36] In addition, the expression of miRNA is tissue- and tumor stage-specific, which leads to obvious differences in miRNA expression profiles in different tissues. A variety of miRNA molecules are involved in the progression of cancer. For example, the decreased expression of miR-15 in B-cell lymphomas is caused by the deletion of chromosome 13q14,[37] while miR-17/92 is related to the expansion of chromosome 13q31.[38] Moreover, trans-regulatory elements, such as transcription factors, may change the level of gene expression through the interaction of protein and DNA. For example, C-myc and Twist can regulate the expression of miRNAs and contribute to tumor progression.[39,40] Since the expression level and activity of these transcription factors are changed in tumor tissues, the expression of the target gene of miRNA molecules is naturally affected. Finally, studies have found that this transcriptional activation of oncogenes and transcriptional silencing of tumor suppressor genes existed in almost all cancer tissues.[41]

The Rho/ROCK expression is mainly limited to the cytoplasm and is involved in regulating cell morphology, cytoskeletal remodeling, cell migration, and other cellular functions.[42] In the process of cell signal transduction, Rho GTPases mainly act on the cytoskeleton or target proteins. They regulate a variety of biological effects, including cell membrane transport, cell migration, adhesion, and proliferation, among others.[43] The ROCK is a serine/threonine protein kinase with 2 highly homologous isomers, ROCK1 and ROCK2. Liang et al. reported that increased expression

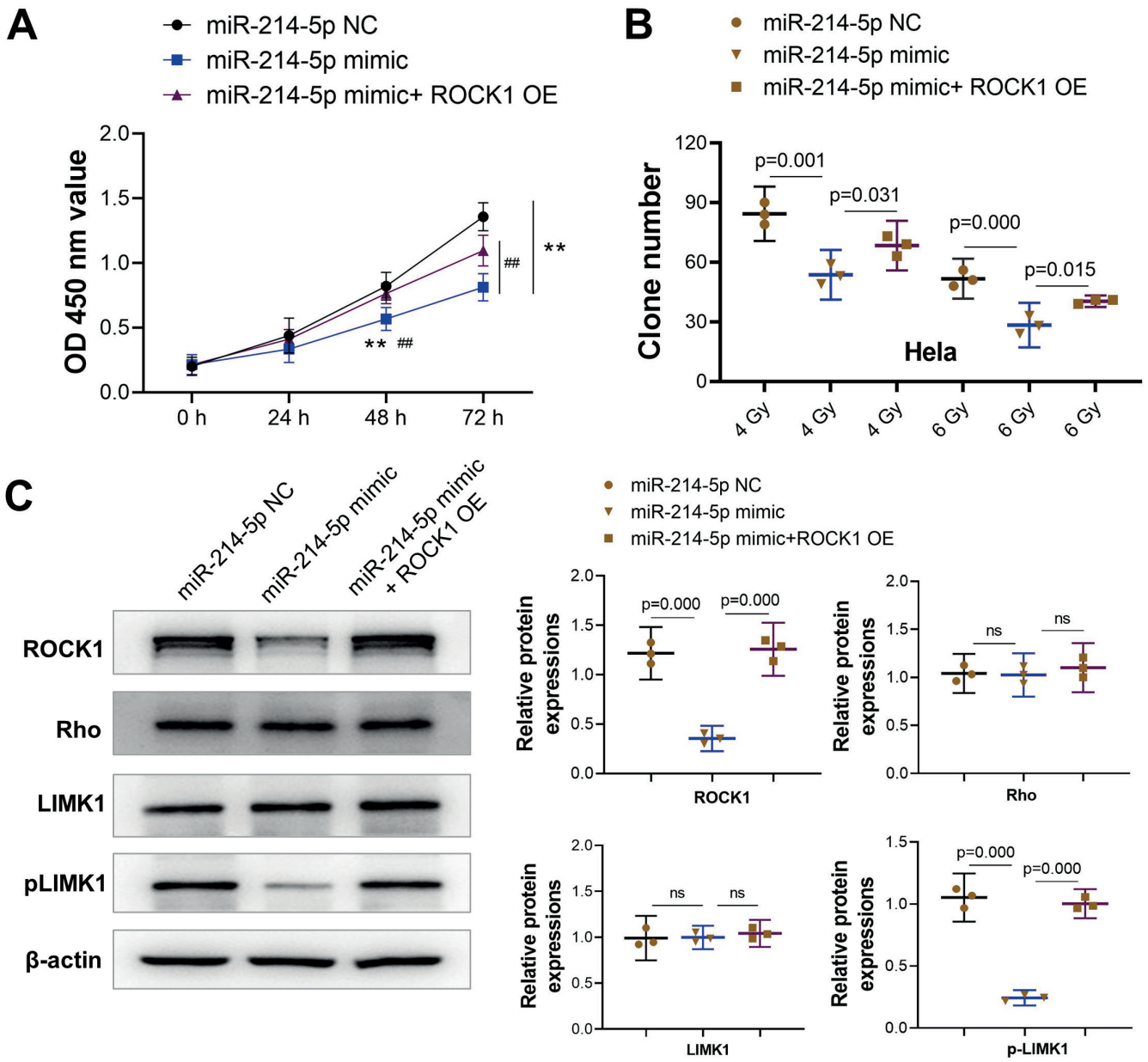


Fig. 5. Overexpression of ROCK1 abolishes the enhanced radiosensitivity brought by miR-214-5p. A. The downregulation of Hela cell proliferation brought by miR-214-5p inhibition was partially reversed after the upregulation of ROCK1 (ROCK1 OE); B. The radiation resistance of miR-214-5p-transfected Hela cell was restored partially by ROCK1 OE; C. Protein expressions of ROCK1, Rho, LIMK1, and phosphorylated LIMK1 (p-LIMK1) were measured with western blot analysis; the expression of Rho and LIMK1 was not affected, while p-LIMK1 expression decreased after the overexpression of ROCK1; three biological replicates were performed, and data were analyzed with bootstrap analysis of variance (ANOVA) analysis, based on 1000 bootstrap samples. The Tukey's multiple comparison test was used for post hoc analysis. Whiskers represent the 95% confidence interval (95% CI) values

ns – not significant; OD – optical density; ** $p < 0.01$, compared to miR-214-5p NC; ## $p < 0.01$, compared to miR-214-5p mimic + ROCK1 OE.

of ROCK1 can promote EMT in cervical cancer cells.[44] Through online database analysis, we identified ROCK1 as a potential target of miR-214-5p. In vitro and in vivo studies show that upregulating miR-214-5p downregulates ROCK1 expression and enhances the sensitivity to radiotherapy. Our analysis showed that ROCK1 was highly expressed in both radiation-resistant cells and radiotherapy-resistant patients with cervical cancer. Moreover, we demonstrated that ROCK1 participates in the radiation resistance of cervical cancer, and that mir-214-5p decreases the resistance of ROCK1 to radiation by targeting its expression.

An anoxic microenvironment exists in most of the solid tumors, which affects the genetic phenotype of tumor cells.[45] Consequently, hypoxic microenvironments of tumors are closely related to the occurrence, development, prognosis, metastasis, and therapeutic response of the tumor to treatment. Leong and Chambers indicated hypoxia-induced migration of tumor cells through Rho/ROCK1 signaling pathways,[46] and Liu et al. observed that ROCK1 is related to cisplatin resistance in lung cancers.[47] These results demonstrate that the Rho/ROCK1 pathway broadly participates in the occurrence and development of tumors,

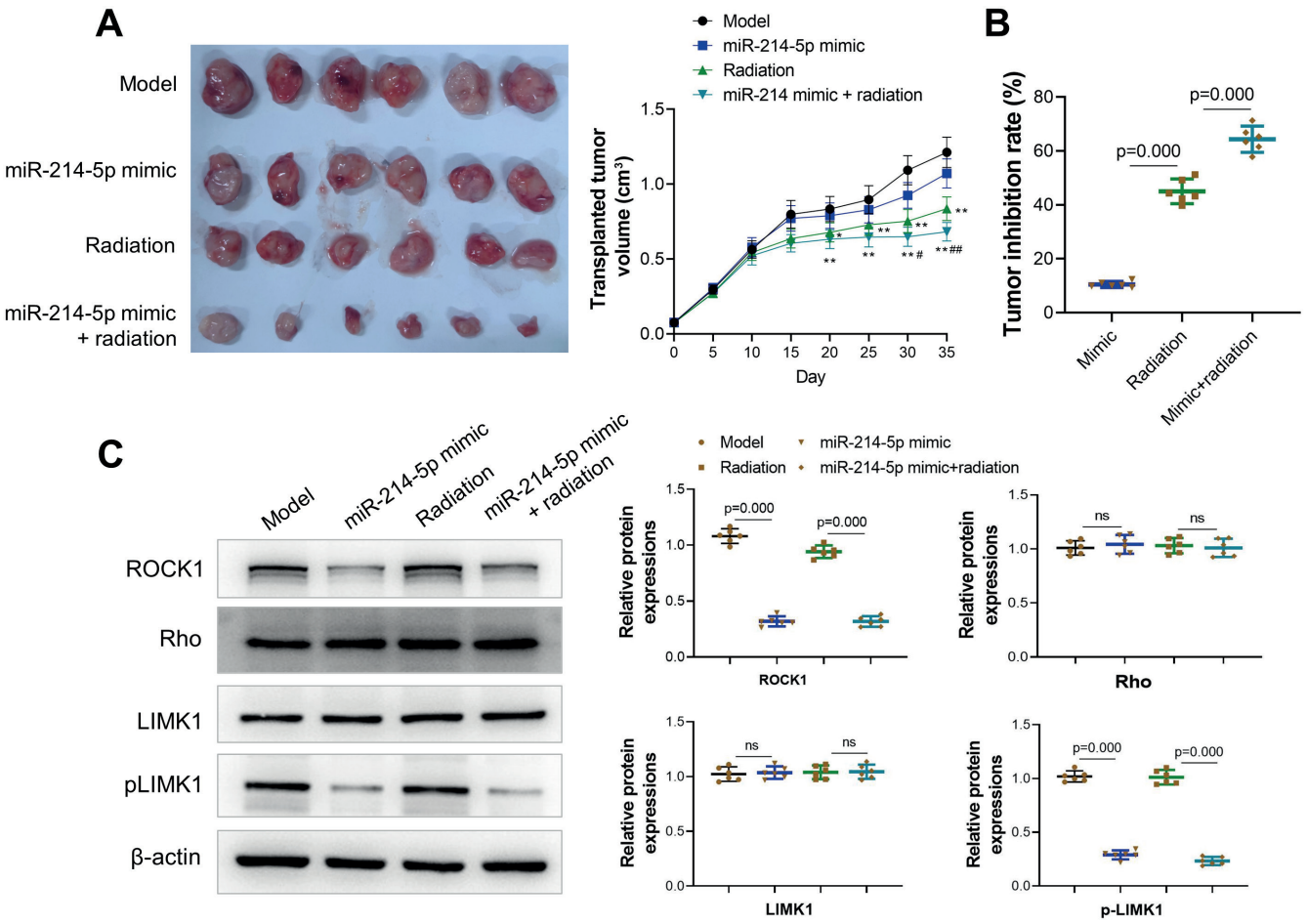


**Fig. 6.** miR-214-5p improves the radiotherapy effect of the cervical cancer model in nude mice. A. Stripped tumor and tumor volume in each group; n = 6, data were analyzed using analysis of variance (ANOVA); B. Tumor inhibition rate in each group; n = 6, results were analyzed with bootstrap ANOVA, based on 1000 bootstrap samples; the Tukey's multiple comparisons test was used for the intercomparison of groups; C. Consistent with in vitro analysis, the protein expressions of Rho, the upstream protein of ROCK1, did not change. The expression of ROCKs and phosphorylated LIMK1 (p-LIMK1) decreased after the upregulation of miR-214-5p, especially when combined with radiation. Measurements were performed in triplicate. Data were analyzed using bootstrap ANOVA analysis, based on 1000 bootstrap samples. The Tukey's multiple comparisons test was used for post hoc analysis. Whiskers represent the 95% confidence interval (95% CI) values

ns – not significant; * $p < 0.05$, ** $p < 0.01$, compared to the model group; # $p < 0.05$, ## $p < 0.01$, compared to the radiation group.

especially in the process of creating therapy resistance. As for the high expression of ROCK1 in radiation resistance, we speculate that ionizing radiation leads to sustained oxidative stress and mitochondrial dysfunction, inducing the upregulation of ROCK1 expression, adjusting the reconstruction of the damaged tumor cytoskeleton and causing tumor cells to resist radiotherapy.[48,49] The miR-214-5p prevents the reconstruction of the cervical cancer cell cytoskeleton by downregulating ROCK1 expression and improving the tolerance of cervical cancer cells to radiation. Unfortunately, due to the previous research design, we only verified the change of ROCK1 expression in radiotherapy sensitivity. We look forward to further explore and verify the upstream influencing factors in subsequent studies.

The LIMK1 is phosphorylated by upstream kinases ROCK1, and its activation continually phosphorylates downstream target proteins, thereby regulating actin and tubulin remodeling.[50] The p-LIMK1 is an important executive protein of ROCK1 during tumor cell migration. Our analysis indicated that with the reduction of ROCK1 regulated by miR-214-5p, Rho expression did not change and the expression level of p-LIMK1 decreased, indicating that ROCK1 is a key protein regulating radiosensitivity in cervical cancer radiotherapy, and is specifically arranged by miR-214-5p.

## Limitations

Our study has some limitations. First, the inhibition of miR-214-5p in tumor cells in vivo and in vitro is inconsistent, and it is not clear whether the reduction of inhibition efficiency in vivo is due to the insufficient miRNA dose, or if the effect itself is limited. These questions need to be further clarified. In addition, whether the sensitizing effect of miR-214-5p on radiotherapy is simply added to radiation or is a synergistic effect requires further analysis.

# Conclusions

Herein, we demonstrated decreased miR-214-5p expression and increased ROCK1 expression in patients with radiotherapy-resistant/insensitive cervical cancer. Exogenously increasing miR-214-5p specifically regulates ROCK1 and improves the sensitivity of cervical cancer to radiotherapy. This suggests that the upregulation of miR-214-5p or decreasing ROCK1 expression may help to improve the treatment response in cervical cancer patients treated with radiotherapy, although this conclusion needs to be verified in further follow-up studies.

## ORCID iDs

Junqin Zhang https://orcid.org/0000-0003-0603-4028
Yaxing Li https://orcid.org/0000-0002-0586-1016
Yanan Ren https://orcid.org/0009-0009-4526-3844
Jie Li https://orcid.org/0000-0002-9622-0889
Hua Han https://orcid.org/0009-0003-4631-0899
Ping Yan https://orcid.org/0000-0001-7397-2255

## References

1. Fuzzell LN, Perkins RB, Christy SM, Lake PW, Vadaparampil ST. Cervical cancer screening in the United States: Challenges and potential solutions for underscreened groups. *Prevent Med*. 2021;144:106400. doi:10.1016/j.ypmed.2020.106400
2. Masadah R, Rauf S, Pratama MY, Tiribelli C, Pascut D. The role of microRNAs in the cisplatin- and radio-resistance of cervical cancer. *Cancers (Basel)*. 2021;13(5):1168. doi:10.3390/cancers13051168
3. Zhang Y, Li M, Hu C. Exosomal transfer of miR-214 mediates gefitinib resistance in non-small cell lung cancer. *Biochem Biophys Res Commun*. 2018;507(1–4):457–464. doi:10.1016/j.bbrc.2018.11.061
4. Penna E, Orso F, Taverna D. miR-214 as a key hub that controls cancer networks: Small player, multiple functions. *J Invest Dermatol*. 2015;135(4):960–969. doi:10.1038/jid.2014.479
5. Zheng C, Guo K, Chen B, Wen Y, Xu Y. miR-214-5p inhibits human prostate cancer proliferation and migration through regulating CRMP5. *Cancer Biomark*. 2019;26(2):193–202. doi:10.3233/CBM-190128
6. Pan L, Du M, Liu H, et al. LncRNA FTX promotes the malignant progression of colorectal cancer by regulating the miR-214-5p–JAG1 axis. *Ann Transl Med*. 2021;9(17):1369–1369. doi:10.21037/atm-21-2755
7. Guo R, Zou B, Liang Y, et al. LncRNA RCAT1 promotes tumor progression and metastasis via miR-214-5p/E2F2 axis in renal cell carcinoma. *Cell Death Dis*. 2021;12(7):689. doi:10.1038/s41419-021-03955-7
8. Qi YF, Yang Y, Zhang Y, Liu S, Luo B, Liu W. Downregulation of lactotransferrin enhanced radio-sensitivity of nasopharyngeal carcinoma. *Comput Biol Chem*. 2021;90:107426. doi:10.1016/j.compbiolchem.2020.107426
9. Zhang S, Wang W, Gu Q, et al. Protein and miRNA profiling of radiation-induced skin injury in rats: The protective role of peroxiredoxin-6 against ionizing radiation. *Free Radic Biol Med*. 2014;69:96–107. doi:10.1016/j.freeradbiomed.2014.01.019
10. Porazinski S, Parkin A, Pajic M. Rho-ROCK signaling in normal physiology and as a key player in shaping the tumor microenvironment. In: Birbrair A, ed. *Tumor Microenvironment*. Vol 1223. Advances in Experimental Medicine and Biology. Cham, Switzerland: Springer International Publishing; 2020:99–127. doi:10.1007/978-3-030-35582-1_6
11. Shin JY, Kim YI, Cho SJ, et al. MicroRNA 135a suppresses lymph node metastasis through down-regulation of ROCK1 in early gastric cancer. *PLoS One*. 2014;9(1):e85205. doi:10.1371/journal.pone.0085205
12. Takahashi N, Nobusue H, Shimizu T, et al. ROCK inhibition induces terminal adipocyte differentiation and suppresses tumorigenesis in chemoresistant osteosarcoma cells. *Cancer Res*. 2019;79(12):3088–3099. doi:10.1158/0008-5472.CAN-18-2693
13. Dudás J, Ladányi A, Ingruber J, Steinbichler TB, Riechelmann H. Epithelial to mesenchymal transition: A mechanism that fuels cancer radio/chemoresistance. *Cells*. 2020;9(2):428. doi:10.3390/cells9020428
14. Peng J, Zhang G, Wang Q, et al. ROCK cooperated with ET-1 to induce epithelial to mesenchymal transition through SLUG in human ovarian cancer cells. *Biosci Biotechnol Biochem*. 2012;76(1):42–47. doi:10.1271/bbb.110411
15. Lewin SN. Revised FIGO staging system for endometrial cancer. *Clin Obstet Gynecol*. 2011;54(2):215–218. doi:10.1097/GRF.0b013e318218 5baa
16. Miller AB, Hoogstraten B, Staquet M, Winkler A. Reporting results of cancer treatment. *Cancer*. 1981;47(1):207–214. doi:10.1002/1097-0142(19810101)47:1<207::AID-CNCR2820470134>3.0.CO;2-6
17. Wu L, Zheng K, Yan C, et al. Genome-wide study of salivary microRNAs as potential noninvasive biomarkers for detection of nasopharyngeal carcinoma. *BMC Cancer*. 2019;19(1):843. doi:10.1186/s12885-019-6037-y
18. Takara Bio Inc. Takara PrimeSciptTM RT Reagent Kit (Perfect Real Time). Shiga, Japan: Takara Bio Inc.; 2020. https://www.takarabiomed.com.cn/DownLoad/RR037A.pdf. Published June 7, 2020.
19. Zhu Y, Zhang X, Wang L, et al. FENDRR suppresses cervical cancer proliferation and invasion by targeting miR-15a/b-5p and regulating TUBA1A expression. *Cancer Cell Int*. 2020;20(1):152. doi:10.1186/s12935-020-01223-w
20. Causin R, Pessôa-Pereira D, Souza K, et al. Identification and performance evaluation of housekeeping genes for microRNA expression normalization by reverse transcription-quantitative PCR using liquid-based cervical cytology samples. *Oncol Lett*. 2019;18(5):4753–4761. doi:10.3892/ol.2019.10824
21. Iempridee T, Wiwithaphon S, Piboonprai K, et al. Identification of reference genes for circulating long noncoding RNA analysis in serum of cervical cancer patients. *FEBS Open Bio*. 2018;8(11):1844–1854. doi:10.1002/2211-5463.12523
22. Lesnikova I, Lidang M, Hamilton-Dutoit S, Koch J. Rapid, sensitive, type specific PCR detection of the E7 region of human papillomavirus type 16 and 18 from paraffin embedded sections of cervical carcinoma. *Infect Agents Cancer*. 2010;5(1):2. doi:10.1186/1750-9378-5-2
23. Schrevel M, Gorter A, Kolkman-Uljee SM, Trimbos JBMZ, Fleuren GJ, Jordanova ES. Molecular mechanisms of epidermal growth factor receptor overexpression in patients with cervical cancer. *Mod Pathol*. 2011;24(5):720–728. doi:10.1038/modpathol.2010.239
24. Wang W, Sheng L, Chen Y, et al. Total coumarin derivates from *Hydrangea paniculata* attenuate renal injuries in cationized-BSA induced membranous nephropathy by inhibiting complement activation and interleukin 10-mediated interstitial fibrosis. *Phytomedicine*. 2022;96:153886. doi:10.1016/j.phymed.2021.153886
25. Zhang Y, Li Z, Wu H, Wang J, Zhang S. Esculetin alleviates murine lupus nephritis by inhibiting complement activation and enhancing Nrf2 signaling pathway. *J Ethnopharmacol*. 2022;288:115004. doi:10.1016/j.jep.2022.115004
26. Shen Q, Cicinnati VR, Zhang X, et al. Role of microRNA-199a-5p and discoidin domain receptor 1 in human hepatocellular carcinoma invasion. *Mol Cancer*. 2010;9(1):227. doi:10.1186/1476-4598-9-227
27. Zhang S, Xin H, Li Y, et al. Skimmin, a coumarin from *Hydrangea paniculata*, slows down the progression of membranous glomerulonephritis by anti-inflammatory effects and inhibiting immune complex deposition. *Evid Based Complement Alternat Med*. 2013;2013:819296. doi:10.1155/2013/819296
28. Sen Z, Weida W, Jie M, Li S, Dongming Z, Xiaoguang C. Coumarin glycosides from *Hydrangea paniculata* slow down the progression of diabetic nephropathy by targeting Nrf2 anti-oxidation and smad2/3-mediated profibrosis. *Phytomedicine*. 2019;57:385–395. doi:10.1016/j.phymed.2018.12.045
29. Rath N, Olson MF. Rho-associated kinases in tumorigenesis: Re-considering ROCK inhibition for cancer therapy. *EMBO Rep*. 2012;13(10):900–908. doi:10.1038/embor.2012.127
30. Chino J, Annunziata CM, Beriwal S, et al. Radiation therapy for cervical cancer: Executive summary of an ASTRO clinical practice guideline. *Pract Radiat Oncol*. 2020;10(4):220–234. doi:10.1016/j.prro.2020.04.002
31. Akilli H, Tohma YA, Bulut AN, et al. Comparison of no adjuvant treatment and radiotherapy in early-stage cervical carcinoma with intermediate risk factors. *Int J Gynecol Obstet*. 2020;149(3):298–302. doi:10.1002/ijgo.13147
32. Galeaz C, Totis C, Bisio A. Radiation resistance: A matter of transcription factors. *Front Oncol*. 2021;11:662840. doi:10.3389/fonc.2021.662840

33. Tang L, Wei F, Wu Y, et al. Role of metabolism in cancer cell radioresistance and radiosensitization methods. *J Exp Clin Cancer Res*. 2018; 37(1):87. doi:10.1186/s13046-018-0758-7
34. Liu Y, Zheng C, Huang Y, He M, Xu WW, Li B. Molecular mechanisms of chemo- and radiotherapy resistance and the potential implications for cancer treatment. *MedComm*. 2021;2(3):315–340. doi:10.1002/mco2.55
35. Gulyaeva LF, Kushlinskiy NE. Regulatory mechanisms of microRNA expression. *J Transl Med*. 2016;14(1):143. doi:10.1186/s12967-016-0893-x
36. Esquela-Kerscher A, Slack FJ. Oncomirs: MicroRNAs with a role in cancer. *Nat Rev Cancer*. 2006;6(4):259–269. doi:10.1038/nrc1840
37. Calin GA, Dumitru CD, Shimizu M, et al. Frequent deletions and down-regulation of micro-RNA genes *miR15* and *miR16* at 13q14 in chronic lymphocytic leukemia. *Proc Natl Acad Sci U S A*. 2002;99(24): 15524–15529. doi:10.1073/pnas.242606799
38. Rinaldi A, Poretti G, Kwee I, et al. Concomitant *MYC* and microRNA cluster miR-17-92 (*C13orf25*) amplification in human mantle cell lymphoma. *Leuk Lymphoma*. 2007;48(2):410–412. doi:10.1080/10428190601059738
39. O'Donnell KA, Wentzel EA, Zeller KI, Dang CV, Mendell JT. c-Myc-regulated microRNAs modulate E2F1 expression. *Nature*. 2005;435(7043): 839–843. doi:10.1038/nature03677
40. Yin G, Chen R, Alvero AB, et al. TWISTing stemness, inflammation and proliferation of epithelial ovarian cancer cells through MIR199A2/214. *Oncogene*. 2010;29(24):3545–3553. doi:10.1038/onc.2010.111
41. Perri F, Longo F, Giuliano M, et al. Epigenetic control of gene expression: Potential implications for cancer treatment. *Crit Rev Oncol Hematol*. 2017;111:166–172. doi:10.1016/j.critrevonc.2017.01.020
42. Huang Z, Mao X, Wu R, et al. RhoA/ROCK pathway mediates the effect of oestrogen on regulating epithelial-mesenchymal transition and proliferation in endometriosis. *J Cell Mol Med*. 2020;24(18): 10693–10704. doi:10.1111/jcmm.15689
43. Singh V, Davidson AC, Hume PJ, Humphreys D, Koronakis V. Arf GTPase interplay with Rho GTPases in regulation of the actin cytoskeleton. *Small GTPases*. 2019;10(6):411–418. doi:10.1080/21541248.2017.1329691
44. Liang H, Zhang C, Guan H, Liu J, Cui Y. LncRNA DANCR promotes cervical cancer progression by upregulating ROCK1 via sponging miR-335-5p. *J Cell Physiol*. 2019;234(5):7266–7278. doi:10.1002/jcp.27484
45. Gilkes DM, Semenza GL, Wirtz D. Hypoxia and the extracellular matrix: Drivers of tumour metastasis. *Nat Rev Cancer*. 2014;14(6):430–439. doi:10.1038/nrc3726
46. Leong HS, Chambers AF. Hypoxia promotes tumor cell motility via RhoA and ROCK1 signaling pathways. *Proc Natl Acad Sci U S A*. 2014; 111(3):887–888. doi:10.1073/pnas.1322484111
47. Liu Y, Fu Y, Hu X, et al. Caveolin-1 knockdown increases the therapeutic sensitivity of lung cancer to cisplatin-induced apoptosis by repressing Parkin-related mitophagy and activating the ROCK1 pathway. *J Cell Physiol*. 2020;235(2):1197–1208. doi:10.1002/jcp.29033
48. Yoshida T, Goto S, Kawakatsu M, Urata Y, Li TS. Mitochondrial dysfunction, a probable cause of persistent oxidative stress after exposure to ionizing radiation. *Free Radic Res*. 2012;46(2):147–153. doi:10.3109/10715762.2011.645207
49. Wang W, Wang Y, Long J, et al. Mitochondrial fission triggered by hyperglycemia is mediated by ROCK1 activation in podocytes and endothelial cells. *Cell Metab*. 2012;15(2):186–200. doi:10.1016/j.cmet.2012.01.009
50. Lee MH, Kundu JK, Chae JI, Shim JH. Targeting ROCK/LIMK/cofilin signaling pathway in cancer. *Arch Pharm Res*. 2019;42(6):481–491. doi:10.1007/s12272-019-01153-w

# Circular RNA ANKIB1 alleviates hypoxia-induced cardiomyocyte injury by modulating miR-452-5p/SLC7A11 axis

Gang Li[1,D], Xiaolei Tang[2,C], Huaping Tang[1,A,B]

[1] Department of Geriatric Medicine, Maanshan People's Hospital, China
[2] Department of Clinical Laboratory, The Second Affiliated Hospital of Wannan Medical College, Wuhu, China

A – research concept and design; B – collection and/or assembly of data; C – data analysis and interpretation;
D – writing the article; E – critical revision of the article; F – final approval of the article

Advances in Clinical and Experimental Medicine, ISSN 1899–5276 (print), ISSN 2451–2680 (online) *Adv Clin Exp Med*. 2024;33(3):261–272

**Address for correspondence**
Gang Li
E-mail: gs_yz@163.com

**Funding sources**
The study was funded by Maanshan Science and Technology Plan Project No. YL-2021-03.

**Conflict of interest**
None declared

Received on February 14, 2023
Reviewed on April 4, 2023
Accepted on June 12, 2023

Published online on August 7, 2023

## Abstract

**Background.** Acute myocardial infarction (AMI) is a common cardiovascular disease worldwide. Circular RNAs (circRNAs) have been shown to exert essential roles in the progression of AMI. However, it remains unclear whether *circANKIB1* protects cardiomyocytes from hypoxia-induced injury.

**Objectives.** The aim of the study was to elucidate the function and mechanisms of *circANKIB1* in AMI.

**Materials and methods.** The expression of RNA was estimated using a quantitative real-time polymerase chain reaction (qPCR) assay, and the level of protein was determined with the use of western blot analysis. Methyl thiazolyl tetrazolium (MTT) assay was introduced to test cell viability, and a terminal deoxynucleotidyl transferase dUTP nick end labeling (TUNEL) assay was used to detect apoptosis. The relative levels of ferrous ion ($Fe^{2+}$), reactive oxygen species (ROS) and malondialdehyde (MDA) were measured with their corresponding detection kits. The potential target of *circANKIB1* and *miR-452-5p* was predicted using the StarBase database and verified by employing a dual luciferase reporter assay.

**Results.** This study showed a significant decrease in *circANKIB1* in hypoxia-treated H9c2 cells. Hypoxic exposure significantly reduced the viability of H9c2 cells and the expression of GPX4, and increased the content of $Fe^{2+}$, ROS and MDA. These effects were reversed by the overexpression of *circANKIB1*. Additionally, *miR-452-5p* was found to be a direct target of *circANKIB1*, and the *miR-452-5p* mimic significantly eliminated the protective effect of *circANKIB1* overexpression in hypoxia-induced cells. In addition, *miR-452-5p* could bind to *SLC7A11* and negatively regulate its expression. The knockdown of *SLC7A11* abolished the effect of *circANKIB1* overexpression on hypoxia-induced cardiomyocyte injury.

**Conclusions.** This investigation revealed for the first time that *circANKIB1* regulated signaling of the *miR-452-5p/SLC7A11* axis, thereby ameliorating hypoxia-induced cardiomyocyte injury. These findings suggest that *circANKIB1* might be a useful adjunct in the treatment of AMI.

**Key words:** cardiomyocyte, *SLC7A11*, acute myocardial infarction, *miR-452-5p*, *circANKIB1*

**Cite as**
Li G, Tang X, Tang H. Circular RNA ANKIB1 alleviates hypoxia-induced cardiomyocyte injury by modulating miR-452-5p/SLC7A11 axis [published online as ahead of print on August 7, 2023]. *Adv Clin Exp Med*. 2024;33(3):261–272. doi:10.17219/acem/168242

**DOI**
10.17219/acem/168242

## Background

Acute myocardial infarction (AMI), as a cardiovascular disease, is associated with cardiomyocyte injury caused by acute ischemia and hypoxia. Acute myocardial infarction causes severe damage to the myocardium, resulting in high mortality.[1,2] Previous findings suggest that AMI could induce oxidative stress in cardiomyocytes, ultimately leading to their dysfunction.[3,4] Exploring the molecular network of cardiomyocyte injury and revealing target genes that protect them from acute ischemia and hypoxia are essential for the treatment of AMI patients.

Circular RNA (circRNA) is highly stable and displays a novel circular structure without 5' or 3' ends.[5–7] CircRNAs are involved in the regulation of various intracellular activities[8] and are considered markers in a variety of human diseases. Additionally, scientists have demonstrated that multiple circRNAs play an important role in the progression of AMI.[9,10] For example, Ren et al. demonstrated that *circ_0023461* knockdown mitigated hypoxia-induced cardiomyocyte injury by mediating the *miR-370-3p*/*PDE4D* signaling axis.[11] Wang et al. discovered that *circUBXN7* improved hypoxia/reoxygenation (H/R)-induced apoptosis and the inflammatory responses in cardiomyocytes by modulating the *miR-622*/*MCL1* axis signaling.[12] The circRNA ankyrin repeats and IBR domain containing 1 (*circANKIB1*) have been reported to be a splicing product of ANKIB1 mRNA that regulate the development of multiple cells.[13,14] Mao et al. revealed that *circANKIB1* was closely related to the process of peripheral nerve injury.[15] However, the role of *circANKIB1* in hypoxia-induced cardiomyocyte injury remains unclear.

MicroRNAs (miRNAs) are another widely studied non-coding RNAs that have been implicated in diverse biological functions, such as cell proliferation.[16] Current investigations have verified that circRNAs could serve as competitive endogenous RNA (ceRNAs) of miRNAs to influence the expression of downstream mRNA.[17] Here, we examined the connection between *circANKIB1* and *miR-452-5p* and explored the effects of *circANKIB1*/*miR-452-5p* in hypoxia-induced cardiomyocyte injury.

Iron accumulation has been reported to increase the risk of cardiovascular disease (CVD).[18] Ferroptosis is a recently discovered mode of cell death characterized by iron-dependent lipid peroxides increased into the toxic range.[19,20] In addition, Fang et al. reported that ferroptosis can modulate ischemia–reperfusion-induced cardiomyopathy.[19] Therefore, revealing the regulators of ferroptosis is crucial for finding the appropriate therapeutic measures for AMI. The SLC7A11 is a multichannel transmembrane protein that prevents the development of ferroptosis by increasing glutathione (GSH) synthesis and reducing the accumulation of lipid oxide.[21,22] Our previous study found that *SLC7A11* is an important potential target for *miR-452-5p*. However, whether *circANKIB1*/*miR-452-5p* mediates ferroptosis of cardiomyocytes under hypoxia conditions by *SLC7A11* is yet to be explored.

## Objectives

We hypothesized that *circANKIB1* plays a key role in hypoxia-induced cardiomyocyte injury by regulating *SLC7A11*-associated ferroptosis, which would provide a promising therapeutic network for the treatment of AMI.

## Materials and methods

### Cell culture

Rat H9c2 cardiomyocytes (BNCC337726) were obtained from the BeNa Culture Collection (Beijing, China) and maintained in Dulbecco's modified Eagle's medium (DMEM; SH30022.LS; Hyclone, Logan, USA) with 10% fetal bovine serum (FBS; F8318; Sigma-Aldrich, St. Louis, USA) and 1× Penicillin-Streptomycin (P1400; Solarbio, Beijing, China) at 37°C and 5% $CO_2$.[23]

### Hypoxia model

The hypoxia model was completed as described in the previous report.[11] The H9c2 cells were subjected to hypoxic conditions ($O_2$:$CO_2$:$N_2$ = 1:5:94) for 24 h, 48 h and 72 h, and then cultured under normoxia conditions ($O_2$:$CO_2$:$N_2$ = 21:5:74) for an additional 6 h to simulate AMI in vitro. The H9c2 cells cultured for 30 h under normoxia conditions ($O_2$:$CO_2$:$N_2$ = 21:5:74) were considered control cells.

### Cell transfection

The vector with circANKIB1 (oe-circANKIB1) and the empty vector (vector) were obtained from Hunan Fenghui Biotechnology Co. Ltd. (Hunan, China). Small interfering RNA (siRNA) targeting the SLC7A11 sequence (si-SLC7A11) and the corresponding scrambled control (si-NC) were synthesized by Sangon Biotech (Shanghai, China). The miR-452-5p mimic/inhibitor and its control (mimic/inhibitor)-NC were obtained from Guangzhou Ruibo Biotechnology Co. Ltd. (Guangzhou, China). Lipofectamine™ 2000 Transfection Reagent (L7800; Solarbio) was used to transfect all vectors (4 μg) and oligonucleotides (50 nM) into H9c2 cells.[24]

### qPCR assay

Total RNA was extracted from H9c2 cells using Trizol™ reagent (Invitrogen, Waltham, USA). NanoDrop™ 2000 nucleic acid analyzer (Thermo Fisher Scientific, Waltham, USA) was used to detect the concentration and purity of RNA to confirm that the A260/A280 ratio was 1.9–2.1, according to the Minimum Information for Publication of Quantitative Real-Time PCR Experiments

Table 1. Quantitative real-time polymerase chain reaction (qPCR) primers

| Genes | Primers (forward) | Primers (reverse) |
|---|---|---|
| *circANKIB1* | 5′-AGACCGCAGACATGCTCC-3′ | 5′-AGTCCCTAATATCCTATTCATTCCA-3′ |
| *miR-452-5p* | 5′-GCGCAACTGTTTGCAGAG-3′ | 5′-GTGCAGGGTCCGAGGT-3′ |
| *SLC7A11* | 5′-GCTGACACTCGTGCTATT-3′ | 5′-ATTCTGGAGGTCTTTGGT-3′ |
| *U6* | 5′-CTCGCTTCGGCAGCACA-3′ | 5′-AACGCTTCACGAATTTGCGT-3′ |
| *GAPDH* | 5′-GGGAGCCAAAAGGGTCAT-3′ | 5′-GAGTCCTTCCACGATACCAA-3′ |

(MIQE) guidelines.[25] The RNA was reverse-transcribed into complementary DNA (cDNA) utilizing the Evo M-MLV RT Master Mix (AG11706; Accurate Biology, Hunan, China). Then, a quantitative polymerase chain reaction (qPCR) analysis was performed using the qPCR kit (RK02001; BioMarker Technologies, Beijing, China) on the QuantStudio 5 RT fluorescence qPCR instrument system (BJ005277; ABI, Hunan, China). The following parameters were used for qPCR: 1 cycle at 98°C for 3 min, followed by 40 cycles for 15 s at 94°C, 30 s at 60°C and 1 min at 72°C. The U6 served as the internal reference for *miR-452-5p*, while glyceraldehyde-3-phosphate dehydrogenase (GAPDH) was the internal reference for *circANKIB1*. The $2^{-\Delta\Delta Ct}$ method was utilized to estimate the levels of *miR-452-5p* and *circANKIB1*.[23] All primers (synthesized by BGI Group, Shenzhen, China) are shown in Table 1.

## RNase R assay

The extracted RNA was treated with 1 U/μg RNase R (14606ES72; YESEN, Shanghai, China) for 30 min, followed by quantitative real-time polymerase chain reaction (qPCR) analysis to detect the expression of *circANKIB1* and liner ANKIB1. A sample of non-processed RNA was considered the control group.[26]

## Subcellular localization assay

A PARIS kit (AM1921; Invitrogen) was used to isolate cytoplasmic and nuclear RNA from H9c2 cells. The qPCR was then performed to determine the content of *circANKIB1* distributed in the cytoplasm or nucleus in H9c2 cells. The *GAPDH* and *U6* served as the housekeeping genes for the cytoplasm and nucleus, respectively.[27]

## Methyl thiazolyl tetrazolium (MTT) assay

Cell viability was tested by employing the MTT Cell Proliferation Assay Kit (40206ES76; YESEN). Briefly, the transfected H9c2 cells were cultured overnight in 96-well plates ($3\times10^3$ cells/well), and cell transfection was performed for 48 h. Then 10 μL of MTT was added to each well for 4 h. The optical density (OD) was recorded at 570 nm with a microplate reader (SpectraMax Mini; Molecular Devices Ltd., Shanghai, China).[28]

## Reactive oxygen species and malondialdehyde detection

For the detection of reactive oxygen species (ROS), cells were incubated with a 2'-7'-dichlorofluorescin diacetate (DCFH-DA) probe (10 μM; Beyotime Biotechnology, Shanghai, China) for 30 min in darkness at room temperature. Then, the cells were rinsed twice with phosphate-buffered saline (PBS) and imaged with a fluorescent microscope (Leica DM1000; Leica Camera, Wetzlar, Germany). The fluorescence intensity was examined using a fluorescent microplate reader (Epoch2; BioTek, Vermont, USA; excitation/emission 488/525 nm). The level of ROS and malondialdehyde (MDA) in H9c2 cells was estimated using the ROS assay kit (CA1410; Solarbio) or the MDA assay kit (BC0025; Solarbio), respectively.[29]

## Iron detection

The ferrous ion ($Fe^{2+}$) in H9c2 cells was monitored using a $Fe^{2+}$ assay kit (BC5415; Solarbio), following the manufacturer's protocol. Briefly, supernatants of conditioned media from cells were placed onto 96-well plates and then incubated with a 5-microliter iron reducer at 25°C for 30 min to detect total iron content. Then, in a dark environment, samples were incubated with 100 μL of the iron probe for 60 min at 25°C. Finally, the OD was measured at 594 nm with a microplate reader (SpectraMax Mini; Molecular Devices Ltd.).[29]

## Luciferase activity

The *circANKIB1* or *SLC7A11* fragments containing wild-type (WT) or mutant-type (MUT) binding sites with miR-452-5p were cloned into pmirGLO vectors (VT1439; YouBio, China). Four luciferase vectors (circANKIB1-WT, circANKIB1-MUT, SLC7A11-WT, and SLC7A11-MUT) were then obtained. The H9c2 cells ($4\times10^5$ cells/well) were transfected with miR-452-5p mimic/NC (25 nM final concentration) and circANKIB1-WT/circANKIB1-MUT (2 μg) or SLC7A11-WT/SLC7A11-MUT (2 μg) using Lipofectamine™ 2000 Transfection Reagent (L7800; Solarbio). Then, the luciferase activity of Renilla (normalized as the control) and Firefly was tested with a Dual-Lucy Assay Kit (D0010; Solarbio) on a microplate reader (SpectraMax Mini; Molecular Devices Ltd.).[23]

## Western blotting analysis

The total protein of H9c2 cells was collected using radioimmunoprecipitation assay (RIPA) lysis buffer (R0020; Solarbio) and isolated on a sodium dodecyl sulfate-polyacrylamide gel electrophoresis (SDS-PAGE), and then transferred to polyvinylidene fluoride (PVDF) membranes (YA1701; Solarbio). The membranes were treated using Tris-buffered saline (TBS) containing 3% skim milk (T476445-10EA; Aladdin, Shanghai, China) at 4°C for 1 h and then incubated with the primary antibodies, including anti-GPX4 (1:1000, 14432-1-AP; Proteintech, Rosemont, USA), anti-SLC7A11 (1:1000, 26864-1-AP; Proteintech) and anti-β-actin (1:1000, ab8227; Abcam, Cambridge, UK). Finally, the membrane was treated with the secondary antibody (1:2000, goat anti-rabbit IgG antibody, bs-0295G; Bioss, Beijing, China) for 2 h and enhanced chemiluminescence (ECL) detection solutions (HR0340, E266188; Aladdin) to observe the protein bands.[24]

## TUNEL assay

Cells were fixed in 4% paraformaldehyde for 30 min, followed by incubation with 0.3% Triton X-100 for 5 min. Then, the cells were incubated using terminal deoxynucleotidyl transferase dUTP nick end labeling (TUNEL) detection buffer (Beyotime Biotechnology) for 1 h. The 4',6-diamidino-2-phenylindole (DAPI) was applied to counterstain the nuclei. The cells were observed under a fluorescence microscope (Leica DM1000; Leica Camera), and the TUNEL-positive cells were counted.[30]

**Table 2.** The results of t-test and ANOVA

| Figure | Method | F (DFn, DFd) | t | df | $p_{Sk}$ | $p_L$ |
|---|---|---|---|---|---|---|
| Figure 1A | ANOVA | F (3,8) = 230.4 | – | – | >0.1 | 0.6704 |
| Figure 1B | ANOVA | F (3,8) = 123.3 | – | – | >0.1 | 0.9921 |
| Figure 1C | ANOVA | F (1,8) = 494.8 | – | – | >0.1 | 0.8131 |
| Figure 1D | ANOVA | F (2,12) = 939.9 | – | – | >0.1 | 0.7471 |
| Figure 2A | Student's t-test | – | 57.88 | 4 | >0.1 | 0.9988 |
| Figure 2B | ANOVA | F (3,8) = 148.2 | – | – | >0.1 | 0.9846 |
| Figure 2C | ANOVA | F (3,8) = 230.3 | – | – | >0.1 | 0.9163 |
| Figure 2D | ANOVA | F (3,8) = 358.5 | – | – | >0.1 | 0.9535 |
| Figure 2E | ANOVA | F (3,8) = 342.0 | – | – | >0.1 | 0.9003 |
| Figure 2F | ANOVA | F (3,8) = 131.7 | – | – | >0.1 | 0.9024 |
| Figure 3B | Student's t-test | – | 35.18 | 4 | >0.1 | 0.9968 |
| Figure 3C | ANOVA | F (1,8) = 168.1 | – | – | >0.1 | 0.6943 |
| Figure 3D | ANOVA | F (3,8) = 294.2 | – | – | >0.1 | 0.7502 |
| Figure 3E | ANOVA | F (3,8) = 164.1 | – | – | >0.1 | 0.9279 |
| Figure 4A | ANOVA | F (3,8) = 202.4 | – | – | >0.1 | 0.7200 |
| Figure 4B | ANOVA | F (3,8) = 427.5 | – | – | >0.1 | 0.9888 |
| Figure 4C | ANOVA | F (3,8) = 291.3 | – | – | >0.1 | 0.9603 |
| Figure 4D | ANOVA | F (3,8) = 240.9 | – | – | >0.1 | 0.8582 |
| Figure 4E | ANOVA | F (3,8) = 147.3 | – | – | >0.1 | 0.9645 |
| Figure 5B | ANOVA | F (1,8) = 197.4 | – | – | >0.1 | 0.6893 |
| Figure 5C | ANOVA | F (3,8) = 60.41 | – | – | >0.1 | 0.9097 |
| Figure 5D | ANOVA | F (3,8) = 57.63 | – | – | >0.1 | 0.9688 |
| Figure 5E | ANOVA | F (3,8) = 164.7 | – | – | >0.1 | 0.9932 |
| Figure 5F | ANOVA | F (3,8) = 215.5 | – | – | >0.1 | 0.8702 |
| Figure 6A | Student's t-test | – | 13.63 | 4 | >0.1 | 0.8026 |
| Figure 6B | ANOVA | F (3,8) = 234.7 | – | – | >0.1 | 0.8439 |
| Figure 6D | ANOVA | F (3,8) = 182.8 | – | – | >0.1 | 0.8641 |
| Figure 7B | ANOVA | F (3,8) = 242.3 | – | – | >0.1 | 0.6751 |
| Figure 7C | ANOVA | F (3,8) = 87.08 | – | – | >0.1 | 0.4217 |
| Figure 7D | ANOVA | F (3,8) = 126.6 | – | – | >0.1 | 0.3352 |
| Figure 7E | ANOVA | F (3,8) = 91.43 | – | – | >0.1 | 0.9008 |

ANOVA – analysis of variance; df – degrees of freedom; t – Student's t-test results; $p_{SK}$ – Shapiro–Wilk test; $p_L$ – Levene's test; DFd – degrees of freedom denominator; DFn – degrees of freedom numerator.

## Statistical analyses

The analysis was conducted using GraphPad Prism v. 8.0 software (GraphPad Software, San Diego, USA), and all data were presented as mean ± standard deviation (M ±SD). Student's t-test or one-way analysis of variance (ANOVA) followed by Tukey's post hoc test were used to analyze differences between 2 groups or multiple groups, respectively. The normality of the data and the homogeneity of variance between groups were tested using the Shapiro–Wilk test and Levene's test, respectively. The value of $p > 0.05$ indicated that the assumption of normality of data and homogeneity of variance were consistent, and further parameter testing could be performed. Statistical significance was set at $p < 0.05$.[13] The results of the statistical analyses are presented in Table 2 and Table 3.

# Results

## Overexpression of *circANKIB1* ameliorates hypoxia-induced cardiomyocyte injury and ferroptosis

The expression levels of HIF1α, which is an indicator of hypoxia,[31] were detected in H9c2 cells following hypoxia treatment. The expression of HIF1α was significantly increased in H9c2 cells after hypoxia treatment for 24 h, 48 h and 72 h compared with normoxic H9c2 cells (Fig. 1A). The results indicated that the hypoxia-induced cardiomyocyte model was successfully established. As hypoxia treatment over a long duration may result in irreversible damage to H9c2 cells, 24 h timepoint was selected for subsequent experiments (Fig. 1A). We demonstrated that *circANKIB1* expression was significantly decreased in a time-dependent manner under hypoxic conditions

**Table 3.** Tukey's post hoc test results of ANOVA

| Figure | Method | $p_S$ | $p_{T1}$ | $p_{T2}$ | $p_{T3}$ |
|---|---|---|---|---|---|
| Figure 1A | ANOVA | 0.0001 | 0.0002 | 0.0001 | 0.0001 |
| Figure 1B | ANOVA | 0.0001 | 0.0045 | 0.0001 | 0.0001 |
| Figure 1C | ANOVA | 0.0001 | 0.0665 | 0.0001 | – |
| Figure 1D | ANOVA | 0.0001 | 0.0001 | 0.0001 | 0.0001 |
| Figure 2B | ANOVA | 0.0001 | 0.0001 | 0.0001 | – |
| Figure 2C | ANOVA | 0.0001 | 0.0001 | 0.0001 | – |
| Figure 2D | ANOVA | 0.0001 | 0.0001 | 0.0001 | – |
| Figure 2E | ANOVA | 0.0001 | 0.0001 | 0.0001 | – |
| Figure 2F | ANOVA | 0.0001 | 0.0001 | 0.0001 | – |
| Figure 3C | ANOVA | 0.0001 | 0.9425 | 0.0001 | – |
| Figure 3D | ANOVA | 0.0001 | 0.0011 | 0.0001 | 0.0001 |
| Figure 3E | ANOVA | 0.0001 | 0.0001 | 0.0001 | – |
| Figure 4A | ANOVA | 0.0001 | 0.0001 | 0.0001 | 0.0001 |
| Figure 4B | ANOVA | 0.0001 | 0.0001 | 0.0001 | 0.0001 |
| Figure 4C | ANOVA | 0.0001 | 0.0001 | 0.0001 | 0.0001 |
| Figure 4D | ANOVA | 0.0001 | 0.0001 | 0.0001 | 0.0001 |
| Figure 4E | ANOVA | 0.0001 | 0.0001 | 0.0001 | 0.0001 |
| Figure 5B | ANOVA | 0.0001 | 0.0001 | 0.7740 | – |
| Figure 5C | ANOVA | 0.0001 | 0.0193 | 0.0002 | 0.0001 |
| Figure 5D | ANOVA | 0.0001 | 0.0001 | 0.0001 | – |
| Figure 5E | ANOVA | 0.0001 | 0.0001 | 0.0001 | – |
| Figure 5F | ANOVA | 0.0001 | 0.0001 | 0.0001 | – |
| Figure 6B | ANOVA | 0.0001 | 0.0001 | 0.0001 | 0.0001 |
| Figure 6D | ANOVA | 0.0001 | 0.0001 | 0.0001 | 0.0001 |
| Figure 7B | ANOVA | 0.0001 | 0.0001 | 0.0001 | 0.0001 |
| Figure 7C | ANOVA | 0.0001 | 0.0001 | 0.0001 | 0.0002 |
| Figure 7D | ANOVA | 0.0001 | 0.0001 | 0.0001 | 0.0001 |
| Figure 7E | ANOVA | 0.0001 | 0.0001 | 0.0001 | 0.0001 |

ANOVA – analysis of variance; $p_S$ – p-value summary of ANOVA; $P_T$ – Tukey's post hoc test results. The p-values of the comparison results between the different groups were divided into $P_{T1/2/3}$, respectively.

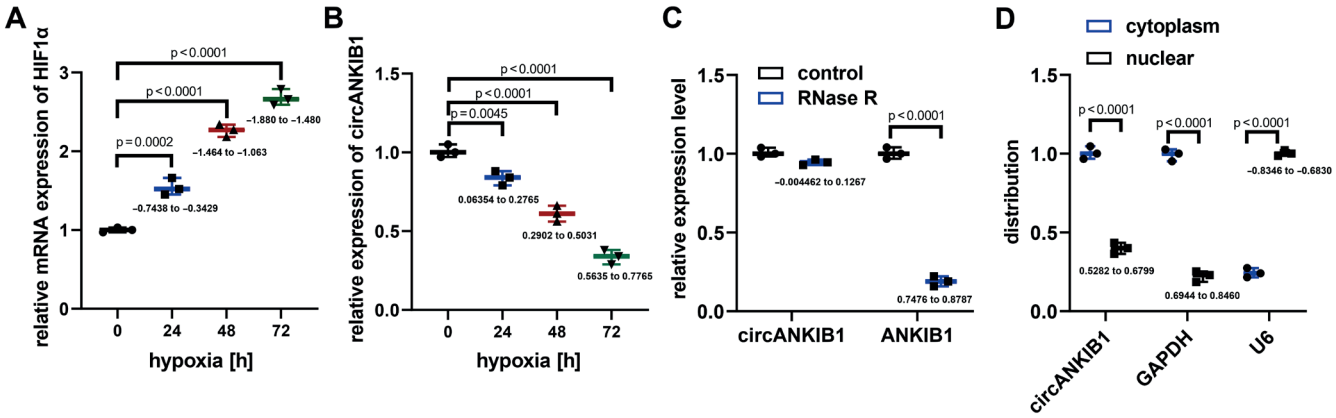


Fig. 1. The overexpression of *circANKIB1* ameliorates hypoxia-induced cardiomyocyte injury and ferroptosis. A. Hypoxia-inducible factor (HIF)1α mRNA expression level in H9c2 cells was increased after hypoxia treatment for 24 h, 48 h or 72 h tested with quantitative real-time polymerase chain reaction (qPCR) assay (p = 0.001, n = 3, analysis of variance (ANOVA) test); B. *CircANKIB1* expression level was decreased in H9c2 cells after hypoxia treatment for 0 h, 24 h, 48 h, or 72 h (p = 0.001, n = 3, ANOVA test); C. RNase R assay and qPCR assay were used to test the expression level of *circANKIB1* or liner and it was found that there was no significant change in *circANKIB1* expression, while liner ANKIB1 expression was decreased (p = 0.001, n = 3, ANOVA test); D. The distribution of *circANKIB1* was confirmed using subcellular localization assay (p = 0.001, n = 3, ANOVA test)

compared to normoxic H9c2 cells (Fig. 1B). To reveal the properties of *circANKIB1*, we carried out an RNase R assay and discovered that *circANKIB1* effectively blocked the degradation of RNase R, implying that *circANKIB1* was more stable than liner ANKIB1 (Fig. 1C). Furthermore, subcellular localization assays demonstrated that *circANKIB1* was localized in the cytoplasm of H9c2 cardiomyocytes more than in the nucleus (Fig. 1D). These data indicated that *circANKIB1* was a stable circRNA that might be involved in the progression of hypoxia-induced cardiomyocyte injury.

## Overexpression of *circANKIB1* inhibited hypoxia-induced cardiomyocyte injury and ferroptosis

To investigate the effect of *circANKIB1* on hypoxia-triggered cardiomyocyte injury, we performed overexpression experiments in H9c2 cells (Fig. 2A). Cell viability was estimated using the MTT assay, which showed that hypoxia suppressed the viability of H9c2 cells, which was notably restored by *circANKIB1* overexpression (Fig. 2B). Interestingly, the level of iron was significantly reduced in H9c2 cells with *circANKIB1* overexpression compared with control cells, which implied that *circANKIB1* was likely to be associated with the progression of ferroptosis (Fig. 2C). Notably, the accumulation of ROS and lipid peroxidation (MDA) is considered an important factor in ferroptosis.[32] Therefore, the levels of ROS and MDA in H9c2 cells after the overexpression of *circANKIB1* were detected. The data demonstrated that hypoxia dramatically increased the accumulation of ROS and MDA, which was effectively reversed by the overexpression of *circANKIB1* (Fig. 2D,E). The GPX4, an inhibitor of ferroptosis,[33] was also investigated. After H/R treatment, GPX4 was decreased in H9c2 cells, whereas overexpressed *circANKIB1* significantly upregulated GPX4 (Fig. 2F). Taken together, these data suggest that the overexpression of *circANKIB1* inhibited ferroptosis from alleviating hypoxia-induced cardiomyocyte injury.

## *miR-452-5p* negatively interacts with *circANKIB1* in hypoxic H9c2 cells

We used the starBase database (http://starbase.sysu.edu.cn/) to predict the target miRNA of *circANKIB1*. We found that *miR-452-5p* contains binding sequences of *circANKIB1* (Fig. 3A). The *miR-452-5p* mimics were obtained to upregulate *miR-452-5p* expression in H9c2 cells, and functional analyses were performed (Fig. 3B). The luciferase assay showed that *miR-452-5p* mimics decreased the luciferase activity of circANKIB1-WT but not circANKIB1-MUT (Fig. 3C). Additionally, the expression level of *miR-452-5p* was significantly upregulated in hypoxia-treated cells, compared with normoxic H9c2 cells (Fig. 3D). Furthermore, to observe the regulatory influence of *circANKIB1* on *miR-452-5p* expression, H9c2 cells were transfected with oe-*circANKIB1* or a vector, followed by the examination of *miR-452-5p* expression using qPCR. The results demonstrated a decrease in *miR-452-5p* expression after the overexpression of *circANKIB1* in H9c2 cells under both normoxic and hypoxic conditions (Fig. 3E).

## miR-452-5p mimic reversed the regulation of *circANKIB1* on hypoxia-induced cardiomyocyte injury and ferroptosis

To verify whether *miR-452-5p* was associated with the protective effect of *circANKIB1* in cardiomyocyte injury, we transfected a miR-452-5p mimic into H9c2 cells with *circANKIB1* overexpression and performed a series of functional experiments. The MTT assay indicated that the miR-452-5p mimic effectively counteracted *circANKIB1* overexpression regarding the viability

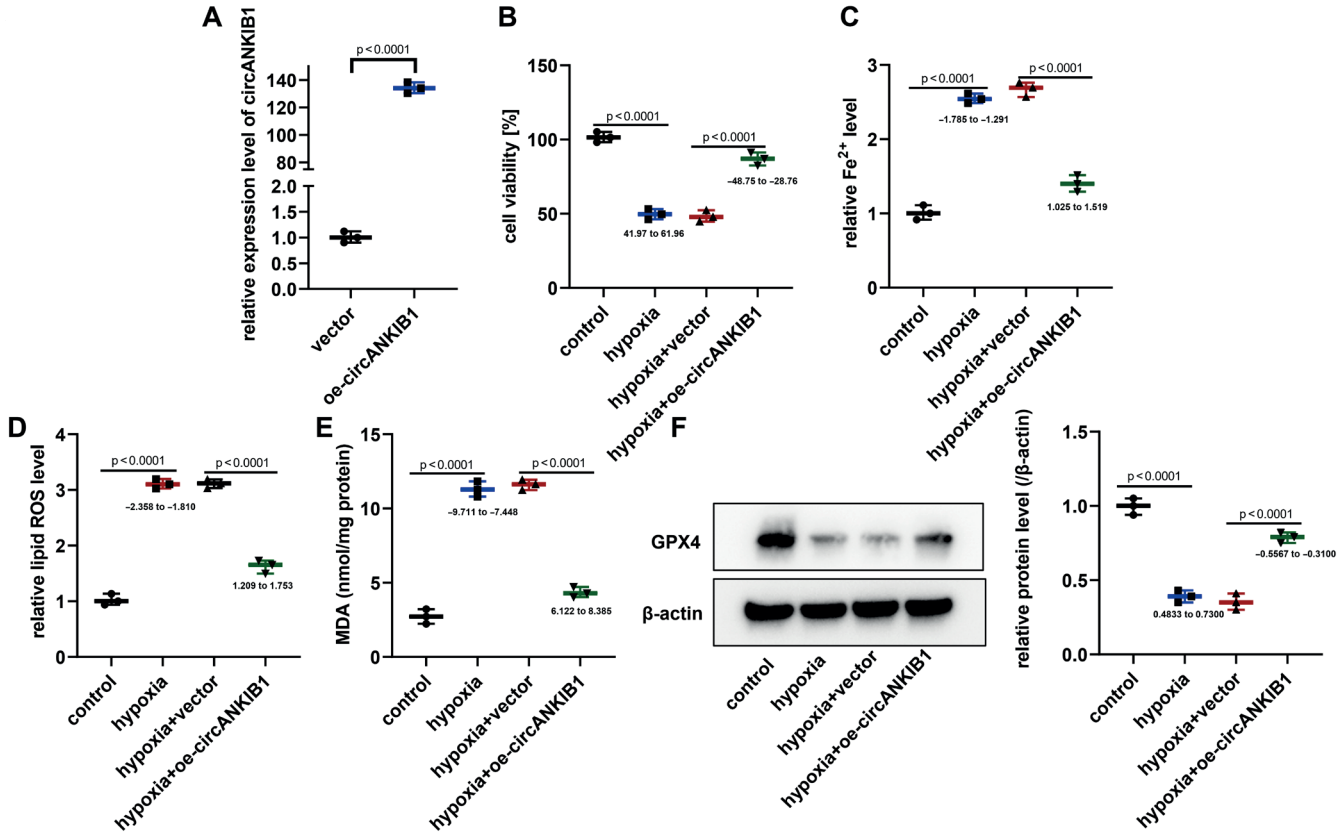


Fig. 2. The overexpression of *circANKIB1* improved hypoxia-induced cardiomyocyte injury and ferroptosis. A. The expression level of *circANKIB1* was increased and tested with quantitative real-time polymerase chain reaction (qPCR) assay (p = 0.001, n = 3, Student's t-test); B. Methyl thiazolyl tetrazolium (MTT) assay monitored that cell viability was suppressed by hypoxia and could be restored by *circANKIB1* overexpression (p = 0.001, n = 3, analysis of variance (ANOVA) test); C–E. The reduced expression of ferrous ion ($Fe^{2+}$) (C), reactive oxygen species (ROS) (D) and malondialdehyde (MDA) (E) was analyzed using corresponding kits (p = 0.001, n = 3, ANOVA test); F. The increased GPX4 expression was examined with western blotting analysis (n = 3, ANOVA test)

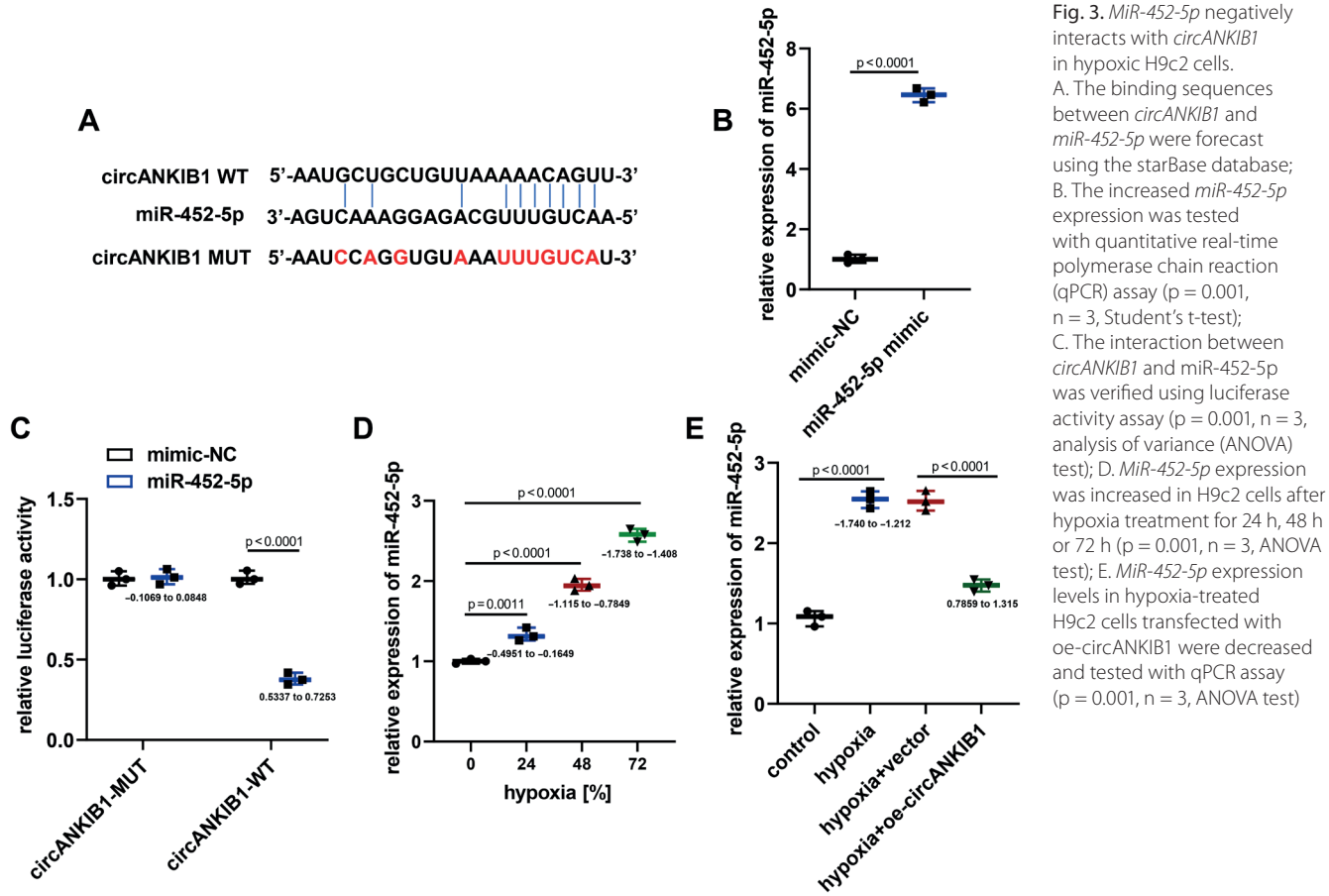


Fig. 3. *MiR-452-5p* negatively interacts with *circANKIB1* in hypoxic H9c2 cells. A. The binding sequences between *circANKIB1* and *miR-452-5p* were forecast using the starBase database; B. The increased *miR-452-5p* expression was tested with quantitative real-time polymerase chain reaction (qPCR) assay (p = 0.001, n = 3, Student's t-test); C. The interaction between *circANKIB1* and miR-452-5p was verified using luciferase activity assay (p = 0.001, n = 3, analysis of variance (ANOVA) test); D. *MiR-452-5p* expression was increased in H9c2 cells after hypoxia treatment for 24 h, 48 h or 72 h (p = 0.001, n = 3, ANOVA test); E. *MiR-452-5p* expression levels in hypoxia-treated H9c2 cells transfected with oe-circANKIB1 were decreased and tested with qPCR assay (p = 0.001, n = 3, ANOVA test)

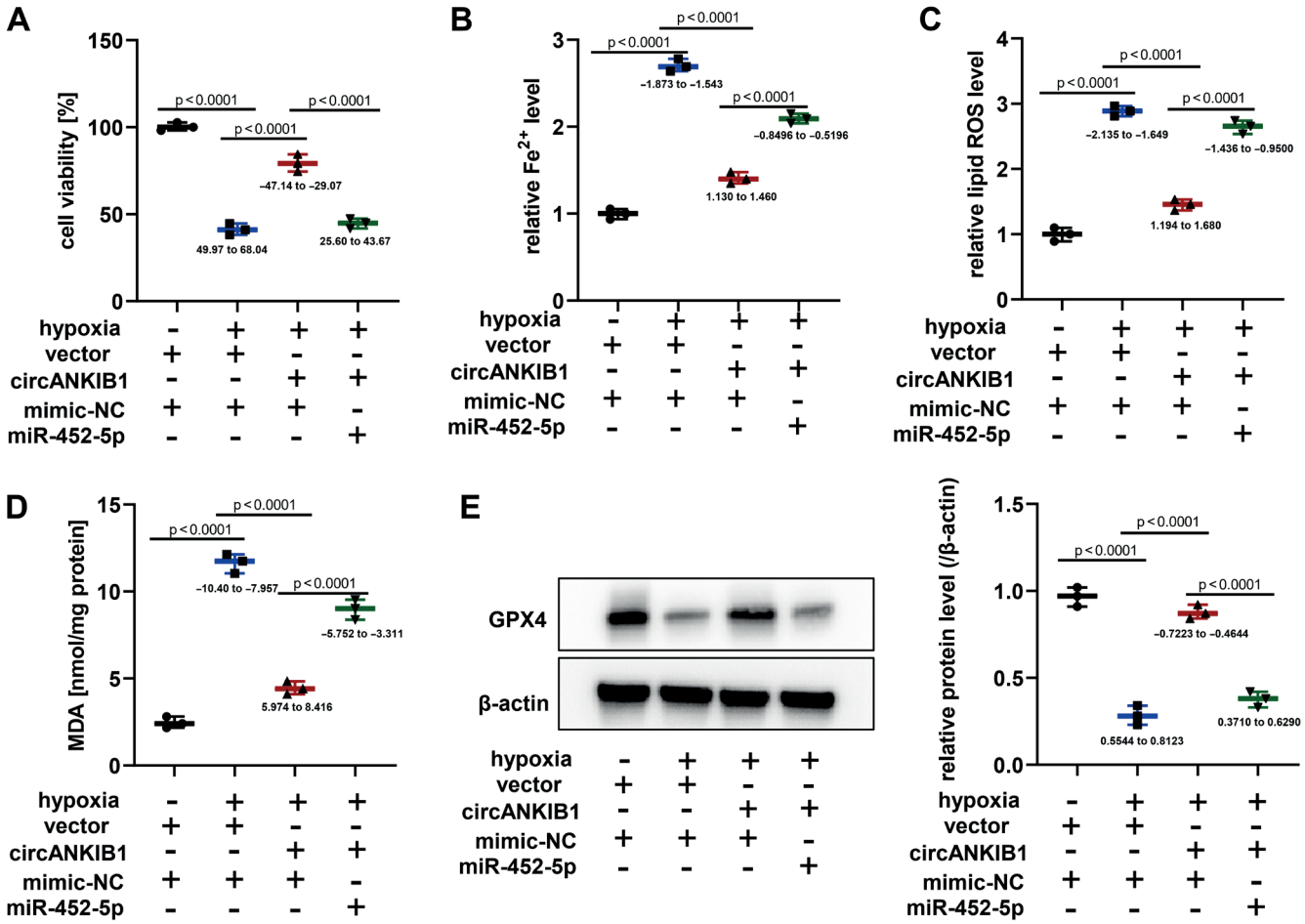


Fig. 4. MiR-452-5p mimic reversed the regulation of *circANKIB1* on hypoxia-induced cardiomyocyte injury and ferroptosis. A. Methyl thiazolyl tetrazolium (MTT) assay confirmed that cell viability induced in H9c2 cells by co-transfection with *circANKIB1* overexpression was effectively counteracted by miR-452-5p mimic (p = 0.001, n = 3, analysis of variance (ANOVA) test); B–D. Corresponding kits showed that the reduced levels of ferrous ion ($Fe^{2+}$) (B), reactive oxygen species (ROS) (C) and malondialdehyde (MDA) (D) were effectively counteracted by miR-452-5p mimic (p = 0.001, n = 3, ANOVA test); E. Western blotting analysis showed that GPX4 expression elevated by the overexpression of *circANKIB1* was eliminated by the miR-452-5p mimic (p = 0.001, n = 3, ANOVA test)

of hypoxia-treated H9c2 cells (Fig. 4A). Furthermore, the inhibitory effect of overexpressed *circANKIB1* on iron, ROS and MDA accumulation was notably reversed by miR-452-5p mimics in hypoxia-induced H9c2 cells (Fig. 4B–D). Moreover, the overexpression of *circANKIB1* elevated the expression of GPX4 in hypoxia-induced H9c2 cells, and this effect was significantly reduced by the miR-452-5p mimic (Fig. 4E). These data imply that circANKIB1 exerts its protective role in cardiomyocytes by mediating the expression of *miR-452-5p*.

## *SLC7A11* is a candidate target of *miR-452-5p* in hypoxia-treated H9c2 cells

A further analysis predicted that *miR-452-5p* would be able to bind to the 3'UTR of *SLC7A11* (Fig. 5A). Results collected from a dual-luciferase reporter gene assay suggested that the miR-452-5p mimic decreased luciferase activity in SLC7A11-WT, while the activity of SLC7A11-MUT was not affected (Fig. 5B). Furthermore, the expression level of *SLC7A11* was significantly decreased by hypoxia treatment in a time-dependent manner compared with normoxic H9c2 cells (Fig. 5C). The qPCR and western blotting analyses showed that hypoxia reduced SLC7A11 mRNA and protein expression, which was effectively restored by a miR-452-5p inhibitor (Fig. 5D,E). Moreover, to observe the regulatory influence of *circANKIB1* on *SLC7A11* expression, H9c2 cells were transfected with oe-circANKIB1 or vector, followed by an examination of SLC7A11 expression using western blot. The results highlighted that after the overexpression of *circANKIB1* in H9c2 cells, the expression of SLC7A11 was elevated, and this could be effectively restored by the miR-452-5p inhibitor (Fig. 5F).

## Silencing *SLC7A11* reversed the decreased cell apoptosis effect of *circANKIB1* overexpression on hypoxia-induced cardiomyocyte injury

To confirm the role of *SLC7A11* in hypoxia-treated cardiomyocyte injury, we constructed a vector with a *SLC7A11* knockdown for rescue experiments (Fig. 6A). Cell viability

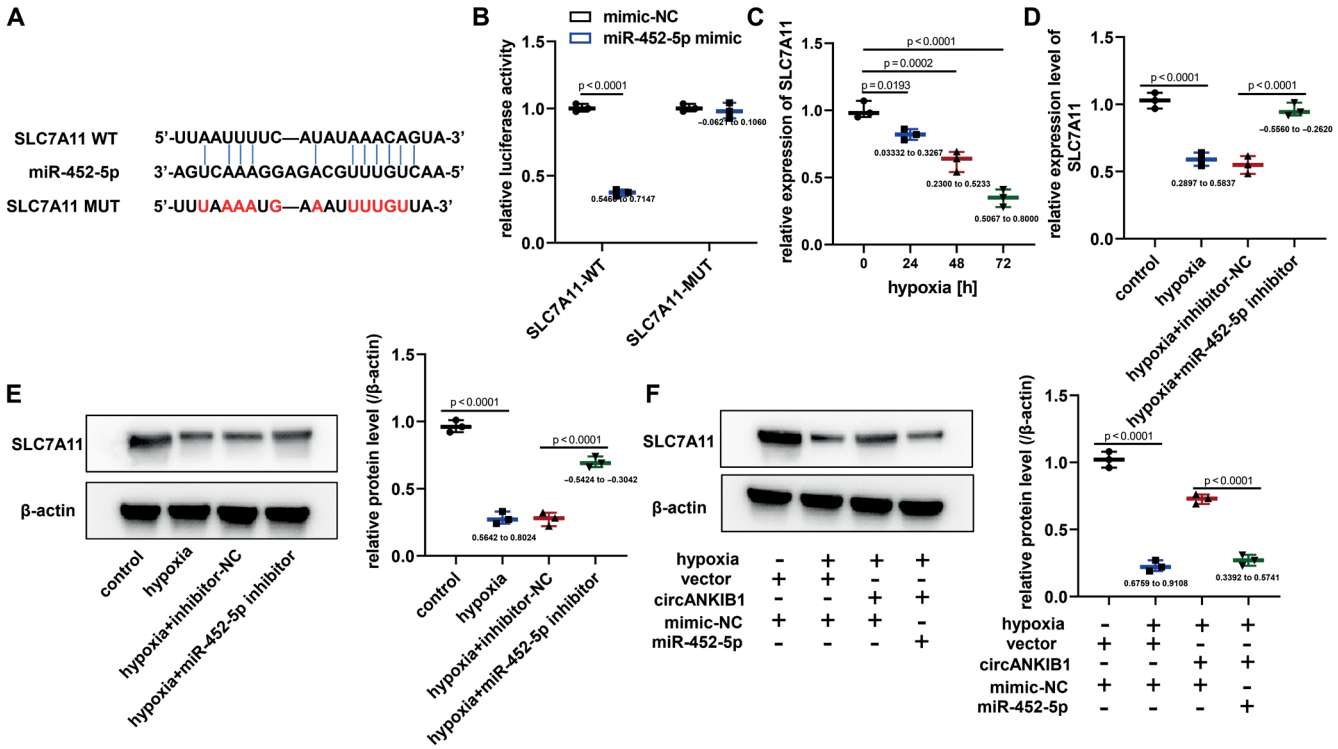


Fig. 5. *SLC7A11* is a candidate target of *miR-452-5p* in hypoxia-treated H9c2 cells. A. The binding sites between *miR-452-5p* and *SLC7A11* were forecast via the starBase database; B. The interaction between *miR-452-5p* and *SLC7A11* was verified using luciferase activity assay (p = 0.001, n = 3, analysis of variance (ANOVA) test); C. Decreased *SLC7A11* expression level in H9c2 cells after hypoxia treatment for 24 h, 48 h or 72 h was tested with quantitative real-time polymerase chain reaction (qPCR) assay (p = 0.001, n = 3, ANOVA test); D,E. Western blotting analysis and qPCR showed that hypoxia reduced SLC7A11 mRNA and protein expression, which was effectively restored by miR-452-5p inhibitor (p = 0.001, n = 3, ANOVA test); F. The increased protein level of *SLC7A11* expression in hypoxia-treated H9c2 cells transfected with *circANKIB1* overexpression was effectively restored by the miR-452-5p inhibitor and tested using western blotting analysis (p = 0.001, n = 3, ANOVA test)

restoration through *circANKIB1* overexpression was significantly reduced by *SLC7A11* silencing in hypoxic-treated H9c2 cardiomyocytes (Fig. 6B). Then, we explored the effect of *SLC7A11* downregulation in H9c2 cells with various treatments using si-SLC7A11. The number of TUNEL-postitive cells with transfected with si-SLC7A11 was markedly increased when compared with *circANKIB1* overexpression transfection in hypoxia-induced H9c2 cells (Fig. 6C,D).

## Downregulation of *SLC7A11* reversed the decreased ferroptosis effect of *circANKIB1* overexpression on hypoxia-induced H9c2 cardiomyocytes

The suppressive roles of overexpressed *circANKIB1* on the accumulation of iron, ROS and MDA were effectively counteracted by *SLC7A11* knockdown (Fig. 7A–C). In addition, the decreased $Fe^{2+}$ level in *circANKIB1* overexpression in H9c2 cells was markedly elevated after the transfection with si-SLC7A11 (Fig. 7D). Furthermore, the overexpression of *circANKIB1* increased GPX4 expression in H9c2 cells under hypoxic conditions, which was notably reversed by *SLC7A11* knockdown (Fig. 7E). Collectively, our findings demonstrated that *circANKIB1* protected cardiomyocytes from hypoxia-induced injury by mediating the *miR-452-5p*/*SLC7A11* axis.

# Discussion

Our research revealed that *circANKIB1* was a stable circRNA that was mainly distributed in the cytoplasm and decreased in hypoxia-treated H9c2 cells. The overexpression of *circANKIB1* significantly inhibited the progression of ferroptosis and protected H9c2 cardiomyocytes from hypoxia-induced injury. In addition, *miR-452-5p* is considered a direct target of *circANKIB1*, and a miR-452-5p mimic notably reversed the effect of *circANKIB1* overexpression on ferroptosis and injury in cardiomyocytes induced by hypoxia. Moreover, *SLC7A11* was a potential target for *miR-452-5p*, and *SLC7A11* silencing abolished the protective role of *circANKIB1* against hypoxia-induced cardiomyocyte injury.

Increasing evidence has shown that circRNAs exert vital roles in human CVDs.[9,34,35] For example, *circRbms1* is highly expressed in AMI, and the loss of circRbms1 effectively blocked $H_2O_2$-related cardiomyocyte apoptosis and ROS accumulation by mediating the *miR-92a*/*BCL2L11* axis.[36] Therefore, targeting circRNAs may be a promising approach for the treatment of AMI. In our previous study, we established a hypoxia model on H9c2 cardiomyocytes to simulate AMI in vitro, and tested the expression of several circRNAs associated with organ injury. The results suggested that hypoxia treatment increased the level of *circANKIB1* in H9c2 cells. The *circANKIB1* has been reported to promote Schwann cell proliferation,

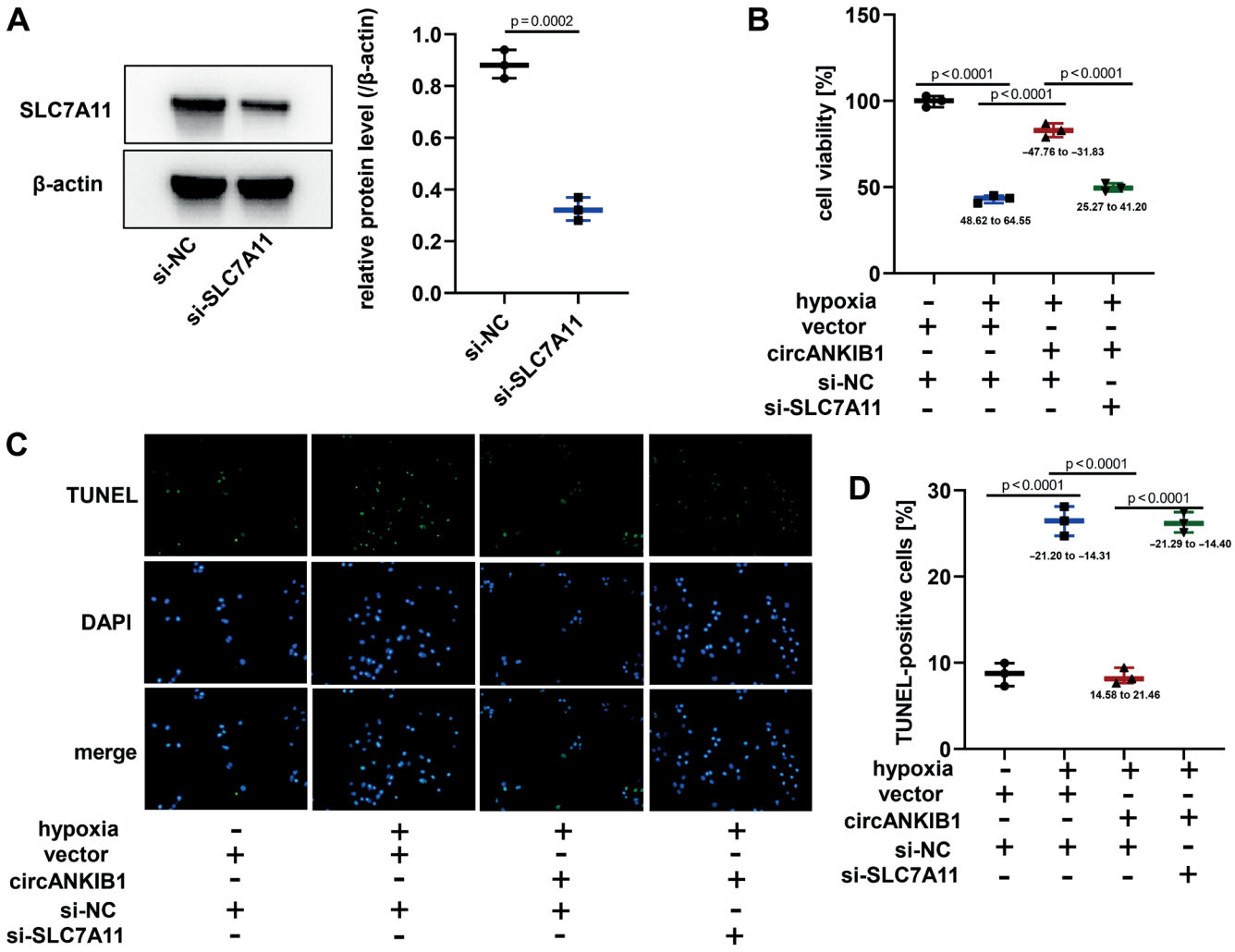


Fig. 6. *SLC7A11* silencing reversed the decreased apoptotic effects of *circANKIB1* overexpression on hypoxia-induced cardiomyocyte injury. A. The decreased protein level of *SLC7A11* was estimated via western blotting analysis (p = 0.001, n = 3, Student's t-test); B. Methyl thiazolyl tetrazolium (MTT) assay revealed that cell viability restored through *circANKIB1* overexpression was significantly reduced by *SLC7A11* silencing (p = 0.001, n = 3, analysis of variance (ANOVA) test); C,D. Terminal deoxynucleotidyl transferase dUTP nick end labeling (TUNEL) assay indicated that cell apoptosis was markedly increased when compared with *circANKIB1* overexpression transfection in hypoxia-induced H9c2 cells (p = 0.001, n = 3, ANOVA test)

thereby exerting a protective role in peripheral nerve injury.[15] However, whether *circANKIB1* affects hypoxia-induced cardiomyocytes remains unclear. This work demonstrated that *circANKIB1* was mainly localized in the cytoplasm of H9c2 cardiomyocytes and that the overexpression of *circANKIB1* effectively restored the viability of H9c2 cardiomyocytes that was reduced by hypoxia exposure.

Ferroptosis is a new cell death pattern, different from apoptosis, autophagy and pyrodeath, which is induced by iron-dependent MDA,[37] during which iron levels are notably elevated. An overload of ferrous ions causes ROS accumulation, which triggers the production of lipid peroxides such as MDA.[38] Furthermore, GPX4 acts as an effective terminator of ferroptosis, capable of converting toxic lipids into non-toxic lipids.[33] Accumulating evidence highlights that ferroptosis is tightly correlated to the occurrence of CVDs, including AMI.[37] Interestingly, the present study revealed that the overexpression of *circANKIB1* decreased the level of iron, ROS and MDA, but increased GPX4 expression in hypoxia-induced H9c2 cells. All these data indicated that *circANKIB1* suppressed ferroptosis in our in vitro model.

The circRNAs are regarded as the sponge of miRNAs, regulating their functional role.[39] Bioinformatics analysis illustrated that *miR-452-5p* was a potential miRNA target of *circANKIB1*, which was confirmed with luciferase activity that validated the interaction between *circANKIB1* and *miR-452-5p*. The *miR-452-5p* is a vital miRNA that participates in various intracellular activities, including tumorigenesis[40] and chronic contractile injury.[41] The present study demonstrated a significant upregulation of *miR-452-5p* in H9c2 cardiomyocytes after hypoxia exposure. The overexpression of *miR-452-5p* effectively eliminated the effect of *circANKIB1* on hypoxia-induced H9c2 cell injury and ferroptosis, indicating that *circANKIB1* protected cardiomyocytes from hypoxia by sponging *miR-452-5p*.

Recent studies have confirmed that miRNAs can block the expression of target genes by binding to the 3'UTR of mRNAs.[42] This study showed that *SLC7A11* was a direct

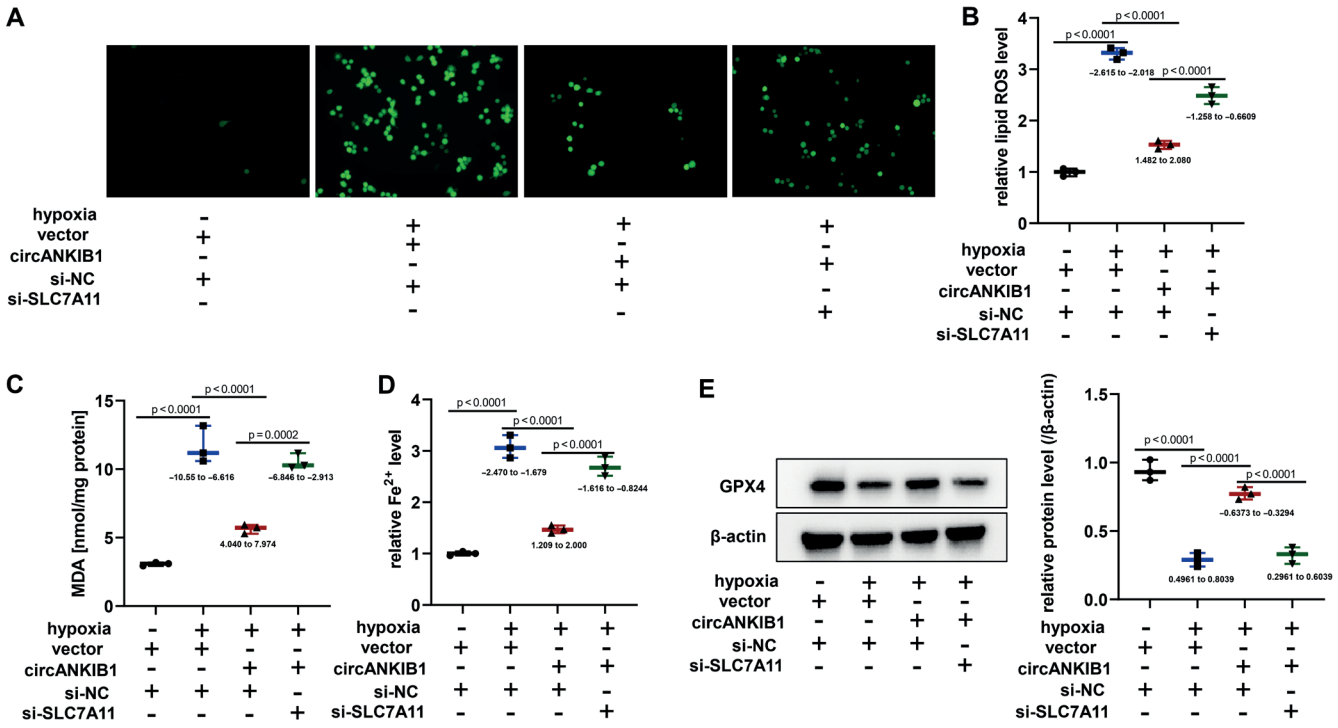


Fig. 7. Downregulation of *SLC7A11* reversed the decreased ferroptosis effect of *circANKIB1* overexpression on hypoxia-induced H9c2 cardiomyocytes. A–D. The levels of reactive oxygen species (ROS) (A,B), malondialdehyde (MDA) (C) and ferrous ion ($Fe^{2+}$) (D) were markedly decreased after transfection with si-SLC7A11 when tested using corresponding kits (p = 0.001, n = 3, analysis of variance (ANOVA) test); E. GPX4 expression increased by *circANKIB1* overexpression and was effectively counteracted by *SLC7A11* knockdown, as analyzed using western blotting analysis (p = 0.001, n = 3, ANOVA test)

target of *miR-452-5p*. The *SLC7A11* has previously been reported to inhibit oxidative stress and maintain GSH levels, thereby eliminating the occurrence of ferroptosis.[43] Emerging evidence showed that *SLC7A11* plays a positive role in protecting cardiomyocytes.[43] Our study showed that hypoxia significantly reduced *SLC7A11* expression in cardiomyocytes, which was notably counteracted by miR-452-5p inhibitors or *circANKIB1* overexpression. Additionally, the *SLC7A11* knockdown effectively eliminated the protective effect of *circANKIB1* overexpression on cardiomyocyte injury and hypoxia-induced ferroptosis.

## Limitations

There are some limitations to this study. First, there no animal experiments were conducted under the AMI model to verify whether *circANKIB1* exerts cardioprotective effects in vivo. In addition, human and mouse cardiomyocytes need to be introduced to further validate these findings. In terms of data analysis, the Shapiro–Wilk test and Levene's test have very low power at such a small sample size. In future studies, we will increase the sample size to ensure that the results of the statistical analysis are more accurate.

# Conclusions

In conclusion, this study revealed that *circANKIB1* alleviates hypoxia-induced cardiomyocyte injury and ferroptosis by modulating *miR-452-5p*/*SLC7A11* signaling, providing a potential therapeutic target for patients with AMI.

## ORCID iDs

Gang Li https://orcid.org/0009-0007-4604-2184
Xiaolei Tang https://orcid.org/0000-0002-3751-1643
Huaping Tang https://orcid.org/0009-0006-1191-3560

## References

1. Benjamin EJ, Virani SS, Callaway CW, et al. Heart Disease and Stroke Statistics – 2018 update: A report from the American Heart Association. *Circulation*. 2018;137(12):e67–e492. doi:10.1161/CIR.0000000000000558
2. Anderson JL, Morrow DA. Acute myocardial infarction. *N Engl J Med*. 2017;376(21):2053–2064. doi:10.1056/NEJMra1606915
3. Tang Q, Li MY, Su YF, et al. Absence of miR-223-3p ameliorates hypoxia-induced injury through repressing cardiomyocyte apoptosis and oxidative stress by targeting KLF15. *Eur J Pharmacol*. 2018;841:67–74. doi:10.1016/j.ejphar.2018.10.014
4. Huang L, Guo B, Liu S, Miao C, Li Y. Inhibition of the lncRNA Gpr19 attenuates ischemia–reperfusion injury after acute myocardial infarction by inhibiting apoptosis and oxidative stress via the miR-324-5p/Mtfr1 axis. *IUBMB Life*. 2020;72(3):373–383. doi:10.1002/iub.2187
5. Ebbesen KK, Kjems J, Hansen TB. Circular RNAs: Identification, biogenesis and function. *Biochim Biophys Acta*. 2016;1859(1):163–168. doi:10.1016/j.bbagrm.2015.07.007
6. Li X, Yang L, Chen LL. The biogenesis, functions, and challenges of circular RNAs. *Mol Cell*. 2018;71(3):428–442. doi:10.1016/j.molcel.2018.06.034
7. Patop IL, Wüst S, Kadener S. Past, present, and future of circRNAs. *EMBO J*. 2019;38(16):e100836. doi:10.15252/embj.2018100836
8. Gao JL, Chen G, He HQ, Wang J. CircRNA as a new field in human disease research [in Chinese]. *Zhongguo Zhong Yao Za Zhi*. 2018;43(3):457–462. doi:10.19540/j.cnki.cjcmm.20171106.012
9. Altesha M, Ni T, Khan A, Liu K, Zheng X. Circular RNA in cardiovascular disease. *J Cell Physiol*. 2019;234(5):5588–5600. doi:10.1002/jcp.27384

10. Wang Y, Liu B. Circular RNA in diseased heart. *Cells*. 2020;9(5):1240. doi:10.3390/cells9051240
11. Ren K, Li B, Jiang L, et al. Circ_0023461 silencing protects cardiomyocytes from hypoxia-induced dysfunction through targeting Mir-370-3p/Pde4d signaling. *Oxid Med Cell Longev*. 2021;2021:8379962. doi:10.1155/2021/8379962
12. Wang S, Cheng Z, Chen X, Lu G, Zhu X, Xu G. CircUBXN7 mitigates H/R-induced cell apoptosis and inflammatory response through the miR-622-MCL1 axis. *Am J Transl Res*. 2021;13(8):8711–8727. PMID:34539989.
13. Tang J, Duan G, Wang Y, Wang B, Li W, Zhu Z. Circular RNA_ANKIB1 accelerates chemo-resistance of osteosarcoma via binding microRNA-26b-5p and modulating enhancer of zeste homolog 2. *Bioengineered*. 2022;13(3):7351–7366. doi:10.1080/21655979.2022.2037869
14. Du YX, Guo LX, Pan HS, Liang YM, Li X. Circ_ANKIB1 stabilizes the regulation of miR-19b on SOCS3/STAT3 pathway to promote osteosarcoma cell growth and invasion. *Hum Cell*. 2020;33(1):252–260. doi:10.1007/s13577-019-00298-6
15. Mao S, Zhang S, Zhou S, et al. A Schwann cell-enriched circular RNA circ-Ankib1 regulates Schwann cell proliferation following peripheral nerve injury. *FASEB J*. 2019;33(11):12409–12424. doi:10.1096/fj.201900965R
16. Mirahmadi Y, Nabavi R, Taheri F, et al. MicroRNAs as biomarkers for early diagnosis, prognosis, and therapeutic targeting of ovarian cancer. *J Oncol*. 2021;2021:3408937. doi:10.1155/2021/3408937
17. Ma X, Liu C, Gao C, et al. circRNA-associated ceRNA network construction reveals the circRNAs involved in the progression and prognosis of breast cancer. *J Cell Physiol*. 2020;235(4):3973–3983. doi:10.1002/jcp.29291
18. Kobayashi M, Suhara T, Baba Y, Kawasaki NK, Higa JK, Matsui T. Pathological roles of iron in cardiovascular disease. *Curr Drug Targets*. 2018;19(9):1068–1076. doi:10.2174/1389450119666180605112235
19. Fang X, Wang H, Han D, et al. Ferroptosis as a target for protection against cardiomyopathy. *Proc Natl Acad Sci U S A*. 2019;116(7):2672–2680. doi:10.1073/pnas.1821022116
20. Stockwell BR, Friedmann Angeli JP, Bayir H, et al. Ferroptosis: A regulated cell death nexus linking metabolism, redox biology, and disease. *Cell*. 2017;171(2):273–285. doi:10.1016/j.cell.2017.09.021
21. Zheng J, Conrad M. The metabolic underpinnings of ferroptosis. *Cell Metab*. 2020;32(6):920–937. doi:10.1016/j.cmet.2020.10.011
22. Koppula P, Zhuang L, Gan B. Cystine transporter SLC7A11/xCT in cancer: Ferroptosis, nutrient dependency, and cancer therapy. *Protein Cell*. 2021;12(8):599–620. doi:10.1007/s13238-020-00789-5
23. Zhou Y, Li X, Zhao D, Li X, Dai J. Long non-coding RNA MEG3 knockdown alleviates hypoxia-induced injury in rat cardiomyocytes via the miR-325-3p/TRPV4 axis. *Mol Med Rep*. 2021;23(1):18. doi:10.3892/mmr.2020.11656
24. Tan J, Pan W, Chen H, et al. Circ_0124644 serves as a ceRNA for Mir-590-3p to promote hypoxia-induced cardiomyocytes injury via regulating Sox4. *Front Genet*. 2021;12:667724. doi:10.3389/fgene.2021.667724
25. Bustin SA, Benes V, Garson JA, et al. The MIQE guidelines: Minimum information for publication of quantitative real-time PCR experiments. *Clin Chem*. 2009;55(4):611–622. doi:10.1373/clinchem.2008.112797
26. Liu B, Guo K. CircRbms1 knockdown alleviates hypoxia-induced cardiomyocyte injury via regulating the miR-742-3p/FOXO1 axis. *Cell Mol Biol Lett*. 2022;27(1):31. doi:10.1186/s11658-022-00330-y
27. Zhang Y, Li Z, Wang J, Chen H, He R, Wu H. CircTRRAP knockdown has cardioprotective function in cardiomyocytes via the signal regulation of mir-370-3p/PAWR axis. *Cardiovasc Ther*. 2022;2022:7125602. doi:10.1155/2022/7125602
28. Lan Z, Wang T, Zhang L, Jiang Z, Zou X. CircSLC8A1 exacerbates hypoxia-induced myocardial injury via interacting with Mir-214-5p to upregulate TEAD1 expression. *Int Heart J*. 2022;63(3):591–601. doi:10.1536/ihj.21-547
29. Dai R, Yang X, He W, Su Q, Deng X, Li J. LncRNA AC005332.7 Inhibited ferroptosis to alleviate acute myocardial infarction through regulating mir-331-3p/CCND2 axis. *Korean Circ J*. 2023;53(3):151–167. doi:10.4070/kcj.2022.0242
30. Zhang Z, Yang W, Ma F, et al. Enhancing the chemotherapy effect of Apatinib on gastric cancer by co-treating with salidroside to reprogram the tumor hypoxia micro-environment and induce cell apoptosis. *Drug Deliv*. 2020;27(1):691–702. doi:10.1080/10717544.2020.1754528
31. Kietzmann T, Samoylenko A, Roth U, Jungermann K. Hypoxia-inducible factor-1 and hypoxia response elements mediate the induction of plasminogen activator inhibitor-1 gene expression by insulin in primary rat hepatocytes. *Blood*. 2003;101(3):907–914. doi:10.1182/blood-2002-06-1693
32. Ma S, Sun L, Wu W, Wu J, Sun Z, Ren J. USP22 protects against myocardial ischemia–reperfusion injury via the SIRT1-p53/SLC7A11-dependent inhibition of ferroptosis-induced cardiomyocyte death. *Front Physiol*. 2020;11:551318. doi:10.3389/fphys.2020.551318
33. Yang WS, SriRamaratnam R, Welsch ME, et al. Regulation of ferroptotic cancer cell death by GPX4. *Cell*. 2014;156(1–2):317–331. doi:10.1016/j.cell.2013.12.010
34. Gong X, Wu G, Zeng C. Role of circular RNAs in cardiovascular diseases. *Exp Biol Med (Maywood)*. 2019;244(2):73–82. doi:10.1177/1535370218822988
35. Lin F, Zhao G, Chen Z, et al. circRNA-miRNA association for coronary heart disease. *Mol Med Report*. 2019;19(4):2527–2536. doi:10.3892/mmr.2019.9905
36. Jin L, Zhang Y, Jiang Y, Tan M, Liu C. Circular RNA Rbms1 inhibited the development of myocardial ischemia–reperfusion injury by regulating miR-92a/BCL2L11 signaling pathway. *Bioengineered*. 2022;13(2):3082–3092. doi:10.1080/21655979.2022.2025696
37. Li M, Wang ZW, Fang LJ, Cheng SQ, Wang X, Liu NF. Programmed cell death in atherosclerosis and vascular calcification. *Cell Death Dis*. 2022;13(5):467. doi:10.1038/s41419-022-04923-5
38. Wang M, Liu CY, Wang T, et al. (+)–Clausenamide protects against drug-induced liver injury by inhibiting hepatocyte ferroptosis. *Cell Death Dis*. 2020;11(9):781. doi:10.1038/s41419-020-02961-5
39. Kulcheski FR, Christoff AP, Margis R. Circular RNAs are miRNA sponges and can be used as a new class of biomarker. *J Biotechnol*. 2016;238:42–51. doi:10.1016/j.jbiotec.2016.09.011
40. Lin X, Han L, Gu C, et al. MiR-452-5p promotes colorectal cancer progression by regulating an ERK/MAPK positive feedback loop. *Aging (Albany NY)*. 2021;13(5):7608–7626. doi:10.18632/aging.202657
41. Tian Y, Sun L, Qi T. Long noncoding RNA GAS5 ameliorates chronic constriction injury induced neuropathic pain in rats by modulation of the miR-452-5p/CELF2 axis. *Can J Physiol Pharmacol*. 2020;98(12):870–877. doi:10.1139/cjpp-2020-0036
42. Fabian MR, Sonenberg N, Filipowicz W. Regulation of mRNA translation and stability by microRNAs. *Annu Rev Biochem*. 2010;79:351–379. doi:10.1146/annurev-biochem-060308-103103
43. Li Y, Yan J, Zhao Q, Zhang Y, Zhang Y. ATF3 promotes ferroptosis in sorafenib-induced cardiotoxicity by suppressing Slc7a11 expression. *Front Pharmacol*. 2022;13:904314. doi:10.3389/fphar.2022.90431

# Transferrin receptor modulated by microRNA-497-5p suppresses cervical cancer cell malignant phenotypes

Xiangming Fang[A,E], Pei Hu[B], Ying Gao[C], Chuqiao Chen[C], Jianqing Xu[D]

Department of Gynecology, Shulan (Hangzhou) Hospital, Shulan International Medical College, Zhejiang Shuren University, Hangzhou, China

A – research concept and design; B – collection and/or assembly of data; C – data analysis and interpretation;
D – writing the article; E – critical revision of the article; F – final approval of the article

Advances in Clinical and Experimental Medicine, ISSN 1899–5276 (print), ISSN 2451–2680 (online) *Adv Clin Exp Med*. 2024;33(3):273–282

**Address for correspondence**
Xiangming Fang
E-mail: fang08_12xm@163.com

**Funding sources**
None declared

**Conflict of interest**
None declared

Received on October 21, 2022
Reviewed on January 29, 2023
Accepted on June 14, 2023

Published online on July 24, 2023

## Abstract

**Background.** Cervical cancer is prevalent throughout the world, and microRNA-497-5p (miR-497-5p) plays an important role in its development. However, the specific mechanism by which miR-497-5p targets the transferrin receptor (TFRC) during cervical cancer development has not been clarified.

**Objectives.** The aim of the study was to unravel TFRC expression and its role in cervical cancer cells, as well as the impact of the miR-497-5p/TFRC axis on cervical cancer cells.

**Materials and methods.** The target mRNA was determined through differential analysis, followed by the evaluation of its impact on survival and clinical staging. Then, quantitative real-time polymerase chain reaction (qPCR) was conducted to analyze the TFRC mRNA level in cervical cancer cells and normal cervical epithelial cells. Western blot (WB) was utilized to examine the expression levels of TFRC, cleaved caspase-3, cleaved caspase-9, and epithelial–mesenchymal transition (EMT)-related proteins. The miRNAs upstream of the target mRNA were predicted, and Pearson correlation analysis was performed, followed by the validation through the dual-luciferase reporter assay. The 3-(4,5-dimethylthiazol-2-yl)-2,5-diphenyltetrazolium bromide (MTT) and colony formation assays were performed to analyze cancer cell viability, followed by a transwell assay aimed at measuring cell migratory and invasive abilities. Finally, flow cytometry was conducted to examine cell apoptosis and cell cycle.

**Results.** The transferrin receptor was significantly increased in cervical cancer cells and positively associated with clinical T and N stages. Silencing TFRC could constrain cell proliferative, migratory and invasive abilities, arrest the cell cycle and facilitate cell apoptosis in cervical cancer cells. The bioinformatics analysis showed a significantly negative correlation between miR-497-5p and TFRC in cervical cancer. Moreover, upregulated miR-497-5p hampered cervical cancer progression and decreased TFRC expression. The overexpression of TFRC reversed the suppressive impact of miR-497-5p overexpression on cervical cancer progression.

**Conclusions.** The modulatory role of the miR-497-5p/TFRC axis was confirmed in cervical cancer cells. This axis may present a new avenue for the diagnosis of cervical cancer and provide a novel target for cervical cancer treatment.

**Key words:** miR-497-5p, TFRC, biological function, cervical cancer

**Cite as**
Fang X, Hu P, Gao Y, Chen C, Xu J. Transferrin receptor modulated by microRNA-497-5p suppresses cervical cancer cell malignant phenotypes. *Adv Clin Exp Med*. 2024;33(3):273–282. doi:10.17219/acem/168342

**DOI**
10.17219/acem/168342

# Background

Cervical cancer is a gynecological malignancy with increasing morbidity and mortality worldwide, especially in developing countries.[1] In China, cervical cancer mortality ranks 4$^{th}$ among all cancers, and 2$^{nd}$ among cancers in women. Furthermore, it is commonly reported in patients aged 40–50 years old in China,[2] and there are approx. 500,000 newly diagnosed cervical cancer cases each year.[3] Cervical cancer may be induced by a variety of modalities[4] and may develop complications during its progression,[5] making its treatment complex and difficult. Although novel diagnostic and therapeutic technologies for cervical cancer are underpinned by extensive clinical research,[6] leading to a 30–50% 5-year survival rate in patients at advanced stages,[7] the therapeutic efficacy is still poor due to tumor recurrence and metastasis.[8] Therefore, further investigation of effective targets for cervical cancer treatment is warranted.

The transferrin receptor (*TFRC*), namely CD71, participates in iron homeostasis and cell growth,[9,10] and TfR1 is often upregulated in tissue with a high proliferation index.[11] The TfR1/CD71 is overexpressed in several human malignancies, such as lymphoma, liver cancer,[12] colon cancer,[13] and endometrial cancer,[14] and may be associated with tumor stage and progression.[11] The iron uptake by *TFRC* is an essential approach for cellular iron absorption, and *TFRC* is significantly dysregulated in many malignant cell types.[15] However, the expression of *TFRC* in cervical cancer as well as its molecular mechanism are still not fully understood.

Aberrantly expressed microRNAs (miRNAs) are associated with tumorigenesis.[16] Some miRNAs can act as oncogenes to promote tumorigenesis, while others serve as tumor suppressor genes.[17,18] Numerous studies have demonstrated that miRNAs are a new class of tumor markers for cancer diagnosis, therapy and prognosis.[19] A previous study[20] unveiled that miRNAs repressed target gene expression by interfering with the genes or inhibiting mRNA translation. Accordingly, understanding the targets and regulatory mechanisms of miRNAs contributes to easier application of miRNAs in the cancer field. Recently, microRNA-497-5p (miR-497-5p) has been shown to be aberrantly expressed in several different cancers.[21–23] For example, miR-497-5p modulates FGF2 to hamper proliferative and invasive properties of non-small cell lung cancer (NSCLC).[24] Moreover, Zheng et al. proposed that miR-497-5p targeted HMGA2 to hinder hepatocellular carcinoma cell proliferation and metastasis.[25] Furthermore, miR-497-5p/PDK3 restrains gastric cancer cell proliferation and cell cycle.[26] However, the molecular mechanism of miR-497-5p in cervical cancer is lacking, and together with the lack of a targeted treatment represents an urgent research need.

# Objectives

The aim of this study was to explore the mechanism of miR-497-5p and its ability to modulate TFRC in cervical cancer. The findings will contribute to the application of miR-497-5p/TFRC in cervical cancer diagnosis and prognosis.

# Materials and methods

## Bioinformatics methods

Expression profiles of mature miRNAs (normal: 3, tumor: 309) and mRNAs (normal: 3, tumor: 306) as well as clinical data from cervical cancer patients were obtained from The Cancer Genome Atlas (TCGA) database. The "edgeR" package was employed for a differential analysis of miRNAs and mRNAs between normal and tumor groups ($|logFC| > 1.5$, $p_{adj} < 0.05$), allowing for the determination of differentially expressed miRNAs (DEmiRNAs) and mRNAs (DEmRNAs). The target mRNA was selected according to previous literature.[27,28] Pearson correlation analysis was conducted to determine upstream miRNA, and upstream regulatory miRNAs of the target mRNA were identified using starBase, TargetScan and mirDIP databases. Finally, the survival analysis was carried out on the target mRNA by using the "survival" package in R. The relationship between the clinical stage and differential gene expression of miRNA was also analyzed.

## Cell culture

Human normal cervical epithelial cell line HcerEpic (BNCC340374), and 4 human cervical cancer cell lines, namely Hela (BNCC337633), SiHa (BNCC102118), Caski (BNCC338223), and C33A (BNCC341097) were accessed from BeNa Culture Collection (Beijing, China). The HcerEpic, SiHa and C33A cells were cultured in Dulbecco's modified Eagle medium (DMEM) (Gibco, Grand Island, USA) with 10% fetal bovine serum (FBS) (Gibco), while the other cervical cells were kept in RPMI-1640 medium with 10% FBS. Penicillin and streptomycin were added to all the media, and all cultures were maintained with 5% $CO_2$ at 37°C.

## Cell transfection

The sh-TFRC (TFRC knockdown treatment) and sh-NC (control of TFRC knockdown), as well as pcDNA3.1-constructed oe-TFRC (TFRC overexpression treatment) and oe-NC (control of TFRC overexpression) plasmids were procured from GeneChem (Shanghai, China). Lipofectamine™ RNAiMAX (cat. No. 13778150; Invitrogen, Waltham, USA) was applied to perform the cell transfection. A miR-497-5p mimic (miR-497-5p overexpression

treatment) and NC-mimic (control of miR-497-5p overexpression) (GenePharma, Suzhou, China) were transfected into cervical cancer cells with Lipofectamine™ 2000 (cat. No. 11668019; Invitrogen). Samples were cultured for 2 days in the corresponding medium at 37°C with 5% $CO_2$. After culture, transfection efficiency was detected using quantitative real-time polymerase chain reaction (qPCR).

## qPCR

The *miR-497-5p* and *TFRC* mRNA expression levels in cervical cancer cells were assayed using qPCR. The TRIzol reagent (Thermo Fisher Scientific, Waltham, USA) was utilized for total RNA extraction, and the total RNA concentration was assessed with a NanoDrop ND-1000 instrument (NanoDrop Technologies, Wilmington, USA). Specific primers (RiboBio, Guangzhou, China) and prime script RT reagent kit (Takara, Kusatsu, Japan) were employed to reverse transcribe miRNA and mRNA into cDNA. Next, SYBR-Green PCR kit (Applied Biosystems, Waltham, USA) and SYBR® Premix Ex Taq™ II kit (Takara) were employed to quantify miRNA and mRNA expression, respectively. Finally, qRT-PCR was conducted on an ABI Prism 7500 fast real-time PCR system (Applied Biosystems). Endogenous references for *miR-497-5p* and *TFRC* were *U6* and *GAPDH*, respectively. The $2^{-\Delta\Delta Ct}$ method was utilized to quantify and compare relative expression levels of miR-497-5p or TFRC mRNA in control and experiment groups.[29] Primer sequences are detailed in Table 1.

Table 1. Primer sequences in quantitative real-time polymerase chain reaction (qPCR)

| Gene | Primer sequence | Amplicon size |
|---|---|---|
| *miR-497-5p* | F: 5′-ATCCAGTGCGTGTCGTG-3′ | 461 |
| | R: 5′-TGCTCAGCAGCACACTGT-3′ | |
| *U6* | F: 5′-GCTTCGGCAGCACATATACTAAAAT-3′ | 91 |
| | R: 5′-CGCTTCACGAATTTGCGTGTCAT-3′ | |
| *TFRC* | F: 5′-GGCTACTTGGGCTATTGTAAAGG-3′ | 156 |
| | R: 5′-CAGTTTCTCCGACAACTTTCTCT-3′ | |
| *GAPDH* | F: 5′-TGAAGGTCGGAGTCAACGGATT-3′ | 171 |
| | R: 5′-CCTGGAAGATGGTGATGGGATT-3′ | |

## Western blot

Cervical cancer cells in different transfection groups were lysed on ice for 30 min using a pre-cooled radioimmunoprecipitation reagent (Beyotime, Shanghai, China). The supernatant was removed and centrifuged at 14,000 rpm and 4°C, followed by collection. Total proteins were determined with a BCA protein concentration kit (RTP7102; Real-Times Biotechnology, Beijing, China). Next, protein samples (20 μg) were separated on a 10% sodium dodecyl-sulfate polyacrylamide gel electrophoresis (SDS-PAGE) and transferred onto polyvinylidene fluoride (PVDF) membranes (Corning Inc., Corning, USA). Then, the membranes were blocked with 5% skimmed milk at room temperature for 2 h, and probed with monoclonal antibodies; rabbit anti-TFRC (ab214039, 1:1000; Abcam, Cambridge, UK), rabbit anti-GAPDH (ab181602, 1:10000; Abcam), rabbit anti-cleaved caspase-3 (ab32042, 1:500; Abcam), rabbit anti-cleaved caspase-9 (SAB4503337, 1:500; Merck, Rahway, USA), rabbit anti-E-cadherin (ab40772, 1:5000; Abcam), rabbit anti-N-cadherin (ab76011, 1:5000; Abcam), and rabbit anti-vimentin (ab92547, 1:5000; Abcam) overnight at 4°C. Membranes were rinsed 3 times (15 min/time) with phosphate-buffered saline (PBS) and Tween-20, after which they were cultured with goat anti-rabbit IgG H&L (HRP) (ab6721, 1:2000; Abcam) at room temperature for 1 h. Afterward, images were acquired using a chemiluminescence detection kit (Sigma-Aldrich, St. Louis, USA) in the darkroom. ImageJ software (National Institutes of Health, Bethesda, USA) was used for statistical analysis of the results.

## MTT and colony formation assays

Cells were cultured in 96-well plates ($5\times10^3$ cells/well), and after transfection for 0, 24, 48, 72, and 96 h, 20 μL of 3-(4,5-dimethylthiazol-2-yl)-2,5-diphenyltetrazolium bromide (MTT) (5 g/L; Sigma-Aldrich) was added for another 4 h of cell incubation at 37°C. Then, 150 μL of dimethyl sulfoxide (DMSO) was supplemented to each well to dissolve crystal violet. Finally, a spectrophotometer was utilized to detect the absorbance at 570 nm.

The 6-well plates ($5\times10^2$ cells/well) were recommended for cell seeding, and the culture medium was replaced every 3 days. After 10 days, the cells were rinsed twice with 1×PBS, followed by 20 min of 4% paraformaldehyde and 5 min of crystal violet. Five fields were selected under an optical microscope (model CKX53; Olympus Corp., Tokyo, Japan). The number of colonies was counted.

## Cell migration and invasion assays

Mitomycin C (MedChemExpress, Monmouth Junction, USA) (10 μg/mL) was used to eliminate the influence of cell proliferation. The 24-well insert and polycarbonate membrane with 8.0-μm well (Millipore, Burlington, USA) was utilized for experiments. To assess cell migration, $5\times10^4$ cells were inoculated to the upper chamber with serum-free medium, while the lower chamber was supplemented with 800 μL medium plus 10% FBS. Then, the cells were kept for 24 h in this medium. Regarding the cell invasion assessment, the transwell upper chamber was covered with 30 μL Matrigel (BD Biosciences, Franklin Lakes, USA) at first. Next, $1\times10^5$ cells were inoculated as described above, followed by culturing for 24 h. Residues in the upper chamber were swabbed and cells outside the membrane were stained with 0.1% crystal violet. A microscope (model CKX53; Olympus Corp.) was used to observe 5 different fields of view.

## Cell apoptosis and cell cycle analysis

Apoptosis was analyzed using a cell apoptosis kit (BD Biosciences) according to the manufacturer's instructions. First, the cells were prepared into a single-cell suspension, which was re-suspended with PBS after centrifugation. Then, the negative and positive control groups were prepared. For the assessment of cell apoptosis, propidium iodide (PI) and Annexin V were used to stain the cells, followed by flow cytometry using a FACSCanto™ II (BD Biosciences). To analyze the cell cycle, staining was conducted with PI only, followed by flow cytometry.

## Dual-luciferase reporter gene assay

First, gene sequences of the 3'-untranslated region (3'-UTR) of wild-type (WT) or mutant (MUT) TFRC were cloned into pmir-GLO vector (Promega, Madison, USA), and named TFRC-WT and TFRC-MUT, respectively. The miR-497-5p mimic/NC mimic and TFRC-WT/TFRC-MUT vectors were transfected into cervical cancer cells with the use of Lipofectamine™ 2000 (Invitrogen). Then, luciferase activity was evaluated using a dual-luciferase reporter detection system (Promega).

## Statistical analyses

All collected data were processed using GraphPad Prism v. 6.0 (GraphPad Software, San Diego, USA), while the "edgeR" package and "survival" package were processed with R software v. 4.0.2 (MathSoft, Cambridge, USA). All in vitro experiments were repeated 9 times. Due to the limited statistical sample size, which was insufficient for normal distribution, the data did not meet the assumption of normal distribution. Therefore, Mann–Whitney U tests were used to make the comparison between the 2 groups, a Kruskal–Wallis test was used to test the comparison between more than 2 groups, and Dunn's test was applied as a post hoc test. The Kaplan–Meier curve was utilized to conduct survival analysis, and Pearson correlation analysis was utilized to determine upstream miRNAs of the target gene. All data are expressed as mean ± standard deviation (M ±SD), with $p < 0.05$ representing statistical significance, $p < 0.01$ indicating a significant difference and $p < 0.001$ denoting an extremely significant difference.

# Results

## *TFRC* expression is significantly increased in cervical cancer cells

To identify the differentially expressed genes in cervical cancer, mRNAs in the TCGA database were categorized, with $|\log FC| > 1.5$ and false discovery rate (FDR) <0.05 as cutoff standards. Through the differential expression analysis conducted using the "edgeR" package, a total of 2956 DEmRNAs were obtained, among which 1274 genes were upregulated (red dots), 1682 genes were differentially downregulated (green dots), and the black dots represented genes with insignificant differences (Fig. 1A). Although previous studies have reported that concomitant upregulation of *TFRC* in various tumor tissues is associated with poor prognosis and facilitates cancer cell proliferation and metastasis,[9,30] its role in cervical cancer is less understood. Therefore, *TFRC* was selected for follow-up investigations. The results of the differential expression analysis, as presented in Fig. 1B, revealed an increased *TFRC* expression in cervical cancer tissue compared to normal tissue ($p < 0.05$, Mann–Whitney U test). Meanwhile, clinical data demonstrated that *TFRC* expression displayed a significant difference in various clinical T/N stages with an increasing trend ($p < 0.01$, Kruskal–Wallis test; $p < 0.05$, Mann–Whitney U test) (Fig. 1C,D). The survival analysis further showed that the upregulation of *TFRC* in cervical cancer tissue influenced a patient's prognosis ($p < 0.050$, Mann–Whitney U test) (Fig. 1E), with the survival time of patients with decreased TFRC level being longer than those with increased TFRC expression. Relative to HcerEpic cells, TFRC expression was increased in Hela, SiHa, Caski, and C33A cells (Hela compared to HcerEpic: $p < 0.001$, SiHa compared to HcerEpic: $p < 0.001$, Caski compared to HcerEpic: $p < 0.01$, C33A compared to HcerEpic: $p < 0.05$, Kruskal–Wallis test with Dunn's post hoc test) (Fig. 1F). Therefore, Hela and SiHa cell lines with relatively high TFRC levels were chosen for further functional experiments.

## *TFRC* silencing contributes to attenuating cancer cell malignant phenotypes

To identify the impact of *TFRC* on cancer cells, sh-TFRC and sh-NC were transfected into Hela and SiHa cell lines. Transfection efficacy was verified using qPCR, showing that the *TFRC* level was significantly decreased in the sh-TFRC group ($p < 0.05$, Mann–Whitney U test) (Fig. 2A). To investigate whether *TFRC* expression affects cervical cell behaviors and phenotypes, several cell function experiments were introduced. Silencing TFRC restrained cervical cancer cell proliferation ($p < 0.05$, Mann–Whitney U test) (Fig. 2B), while colony formation assays demonstrated that silencing TFRC resulted in fewer colonies of Hela and SiHa cells relative to the sh-NC group ($p < 0.05$, Mann–Whitney U test) (Fig. 2C). To define the impact of *TFRC* expression on cell migration and invasion, a transwell assay was performed, showing that cell migration and invasion were significantly reduced in the sh-TFRC group compared to those in the sh-NC group ($p < 0.05$, Mann–Whitney U test) (Fig. 2D,E). Furthermore, the cell apoptosis assay illustrated that silencing *TFRC* significantly upregulated ($p < 0.05$, Mann–Whitney U test) the cell apoptosis rate (Fig. 2F). Considering the influence of *TFRC* on the cell cycle, flow cytometry was used to examine the cell cycle

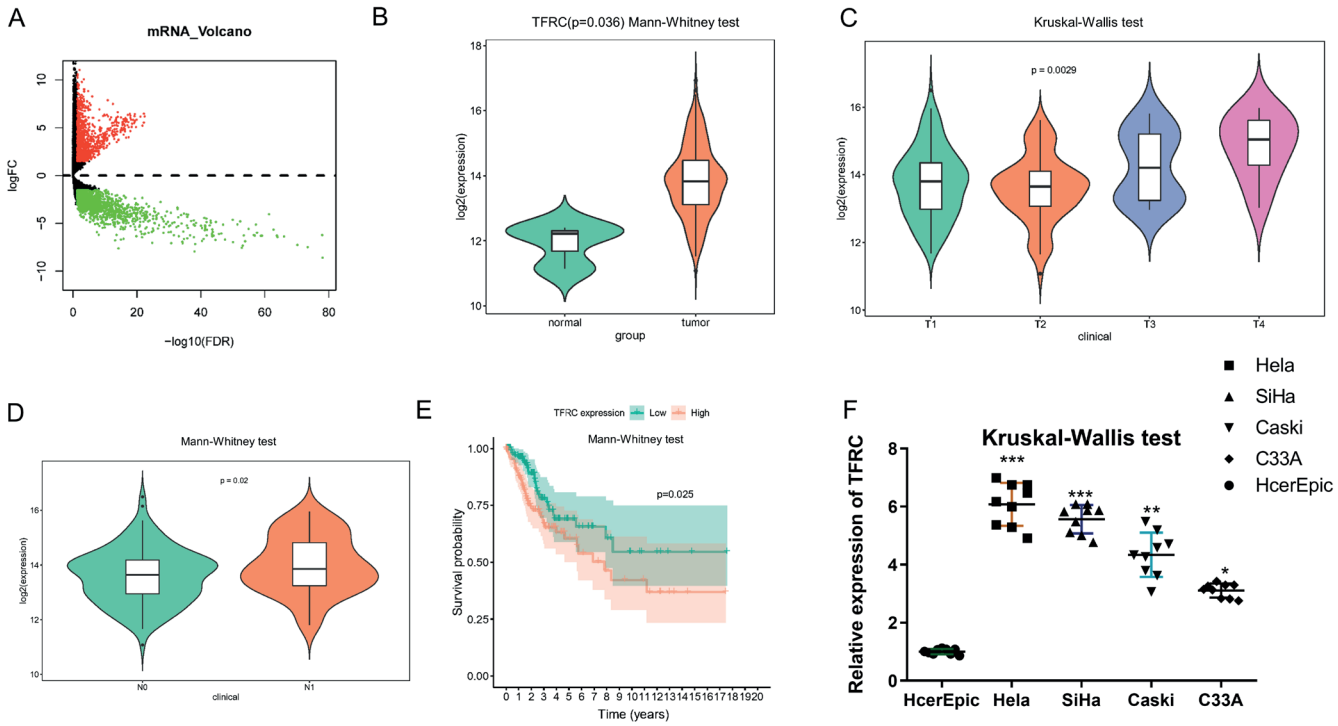


Fig. 1. Transferrin receptor (*TFRC*) level is increased in cervical cancer cells. A. Volcano map of differentially expressed (DE)mRNAs in normal and tumor samples in cervical cancer dataset (red dots: upregulated DEmRNAs, green dots: downregulated DEmRNAs); B. Violin plot of *TFRC* level in the normal (n = 3, green) and tumor (n = 306, red) samples (Mann–Whitney U test); C,D. Violin plot of *TFRC* level in varying T stages (T1–T4) (Kruskal–Wallis test) and varying N stages (N0, N1) (Mann–Whitney U test); E. Survival curves of high/low *TFRC* level on patient's prognosis (red line: high-TFRC level group; green line: low-TFRC level group (Mann–Whitney U test)); F. Quantitative real-time polymerase chain reaction (qPCR) measured *TFRC* expression in HcerEpic and Hela, SiHa, Caski, and C33A cells (Kruskal–Wallis test, Dunn's test was used for post-inspection)

*p < 0.05 indicated statistically significant values; **p < 0.01 indicated a significant difference; ***p < 0.001 indicated an extremely significant difference.

status between the differentially transfected cell lines. Inhibiting the expression of *TFRC* could arrest the cell cycle in cervical cancer cells in the G0/G1 phase (p < 0.05, Mann–Whitney U test) (Fig. 2G). These findings highlighted that silencing *TFRC* hampered the progression of cervical cancer cell phenotype in vitro.

## *miR-497-5p* inhibits the *TFRC* expression in cervical cancer cells

To screen potential upstream regulatory miRNAs for TFRC, miRNAs in the TCGA database were categorized, with |logFC| > 1.5 and FDR < 0.05 set as cutoff standards. A differential analysis was conducted using the "edgeR" package, highlighting 128 DEmiRNAs, among which 76 genes were upregulated (red dots), 52 genes were differentially downregulated (green dots), and the black dots represented miRNAs with insignificant differences (Fig. 3A). Next, the upstream regulatory miRNAs of TFRC were mined using bioinformatics databases. Predicted miRNAs overlapped with downregulated DEmiRNAs, and thus we obtained 8 DEmiRNAs with binding sites into *TFRC* (Fig. 3B). Then, the correlation analysis was conducted on *TFRC* and 8 DEmiRNAs, and a negative correlation was found between *miR-497-5p* and *TFRC*, along with the highest coefficient (p = −0.27) (Fig. 3C). Through bioinformatics analysis, we theorized that *miR-497-5p* level was lowered in cervical cancer tissue compared to normal tissue (p < 0.001, Mann–Whitney U test) (Fig. 3D). Therefore, *miR-497-5p* was selected for further analysis.

A binding site analysis demonstrated that *miR-497-5p* was a direct binding partner of *TFRC* (Fig. 3E). To investigate whether *miR-497-5p* targets *TFRC* by binding to its 3'UTR, WT or MUT TFRC luciferase reporter plasmid and miR-497-5p mimic or NC mimic were co-transfected into Hela and SiHa cells. The luciferase activity assay showed that luciferase activity of TFRC-WT in Hela and SiHa cell lines in the miR-497-5p mimic group was significantly reduced (p < 0.05, Mann–Whitney U test), and no substantial difference was observed in the TFRC-MUT group (p > 0.05, Mann–Whitney U test) (Fig. 3F). Furthermore, the upregulation of miR-497-5p significantly reduced TFRC mRNA (p < 0.05, Mann–Whitney U test) and protein levels, as assessed through qPCR and WB (Fig. 3G,H). Hence, it could be determined that *miR-497-5p* inhibited *TFRC* expression.

To investigate the influence of *miR-497-5p* on cervical cancer cells, a *miR-497-5p* overexpression cell line was established for cell function experiments. Western blot (WB) analysis revealed that when *miR-497-5p* was overexpressed, protein expression of apoptosis-related proteins, namely cleaved caspase-3 and cleaved caspase-9, was significantly elevated compared with the NC group

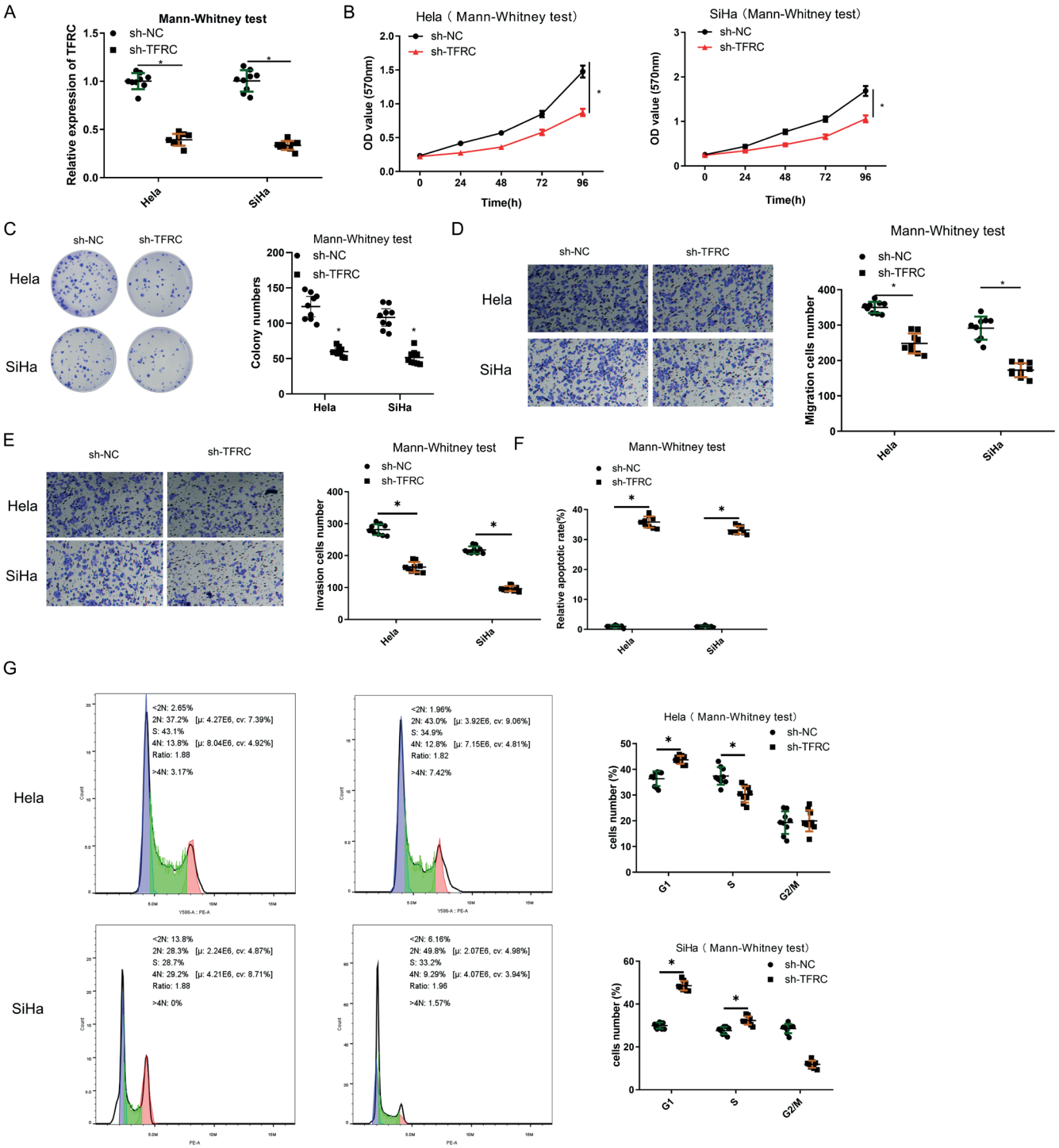


Fig. 2. Silencing transferrin receptor (TFRC) hinders cervical cancer cell phenotype progression. A. Transfection efficacy in Hela and SiHa cells (Mann–Whitney U test); B. Proliferative property of cervical cancer cells (Mann–Whitney U test); C. Cell colony formation of cervical cancer cells (Mann–Whitney U test); D,E. Cell migration and invasion in various treatment groups (100×) (Mann–Whitney U test); F. Apoptosis rate of cervical cancer cells in varying transfection groups (Mann–Whitney test); G. Cell cycle in differently transfected cell lines (Mann–Whitney U test)

*p < 0.05 indicated statistically significant values; OD – optical density.

(Supplementary Fig. 1). The transwell assay further demonstrated that the overexpression of miR-497-5p inhibited cervical cell migration and invasion compared with the NC group ($p < 0.05$, Mann–Whitney U test) (Supplementary Fig. 2). Next, we detected levels of epithelial–mesenchymal transition (EMT)-related proteins using WB, showing that the overexpression of miR-497-5p hampered N-cadherin and vimentin protein levels, and fostered E-cadherin protein levels compared with the NC group ($p < 0.050$, Mann–Whitney U test) (Supplementary Fig. 3). These results illustrated that miR-497-5p could hamper migration and invasion of cervical cancer cells, but foster cell apoptosis.

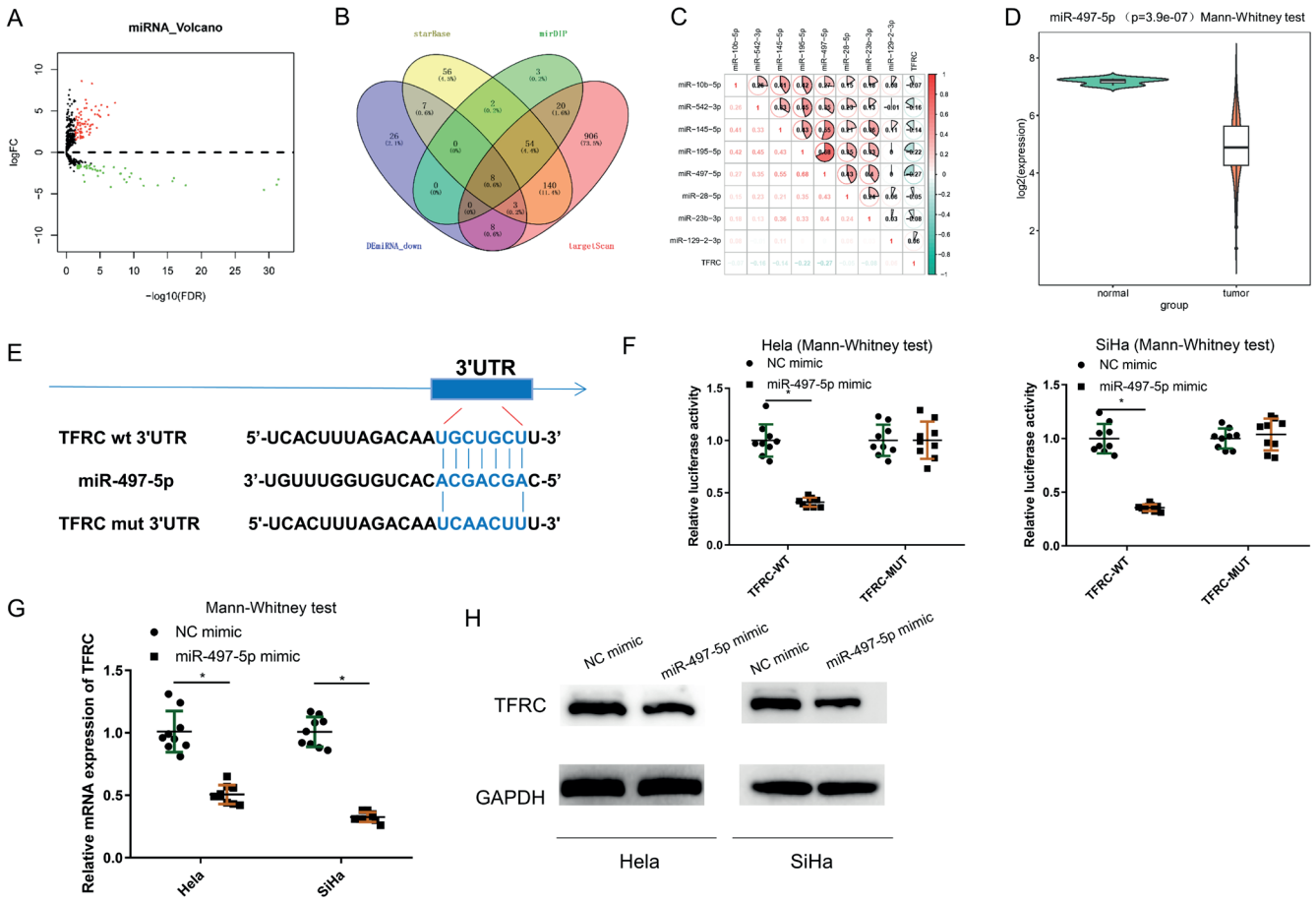


Fig. 3. MicroRNA-497-5p (miR-497-5p) hampers transferrin receptor (TFRC) in cervical cancer cells. A. Volcano map of differentially expressed (DE)miRNAs in normal and tumor groups in cervical cancer dataset (red dots: upregulated DEmiRNAs, green dots: downregulated DEmiRNAs); B. Venn diagram of the predicted upstream miRNAs of TFRC and downregulated DEmiRNAs; C. Pearson correlation analysis of 8 upstream regulatory miRNAs and *TFRC*; D. *miR-497-5p* level in normal (n = 3, green) and tumor (n = 309, red) samples (Mann–Whitney U test); E. Binding sites of *TFRC* and *miR-497-5p*; F. Luciferase activity of Hela and SiHa cells (Mann–Whitney U test); G,H. TFRC mRNA and protein levels in Hela and SiHa cells (Mann–Whitney U test)

*p < 0.05 indicated statistically significant values.

## *miR-497-5p* hampers malignant progression of cervical cancer cells by downregulating *TFRC*

To determine whether *miR-497-5p* modulates the development of cervical cancer cells via *TFRC*, a miR-497-5p mimic was utilized to upregulate miR-497-5p. Simultaneously, the miR-497-5p mimic and oe-TFRC were co-transfected into cervical cancer cells. Through qRT-PCR and WB, it was observed that the upregulation of *miR-497-5p* decreased *TFRC* expression compared to the NC mimic+oe-NC group, and *TFRC* level was elevated in the miR-497-5p mimic+oe-TFRC group compared with the miR-497-5p mimic group ($p < 0.05$, Mann–Whitney U test) (Fig. 4A,B). The MTT and colony formation assay unveiled that proliferation and colony formation of Hela and SiHa cells were hindered by transfecting the miR-497-5p mimic, but the inhibitory impact was partially eliminated by co-transfecting with oe-TFRC ($p < 0.05$, Mann–Whitney U test) (Fig. 4C,D). Moreover, migratory and invasive properties were weakened in cervical cancer cells that overexpressed miR-497-5p compared with the NC group, whereas TFRC overexpression reversed this inhibitory effect and returned to NC group levels ($p < 0.05$, Mann–Whitney U test) (Fig. 4E,F). Moreover, flow cytometry showed that increased miR-497-5p resulted in increased apoptosis of Hela and SiHa cells compared with the NC group, but simultaneous overexpression of *miR-497-5p* and *TFRC* reduced the apoptosis ($p < 0.05$, Mann–Whitney U test) (Fig. 4G). Similarly, miR-497-5p facilitated cell cycle arrest in the G0/G1 phase, but the cell cycle was restored in the NC group by additional transfection of oe-TFRC ($p < 0.05$, Mann–Whitney U test) (Fig. 4H). Together, these findings revealed that TFRC modulated cervical cancer cell progression via the restraining influence of miR-497-5p.

## Discussion

Patients with advanced cervical adenocarcinoma are largely incurable due to local recurrence and metastatic diffusion.[31] As reported previously, many mRNAs are

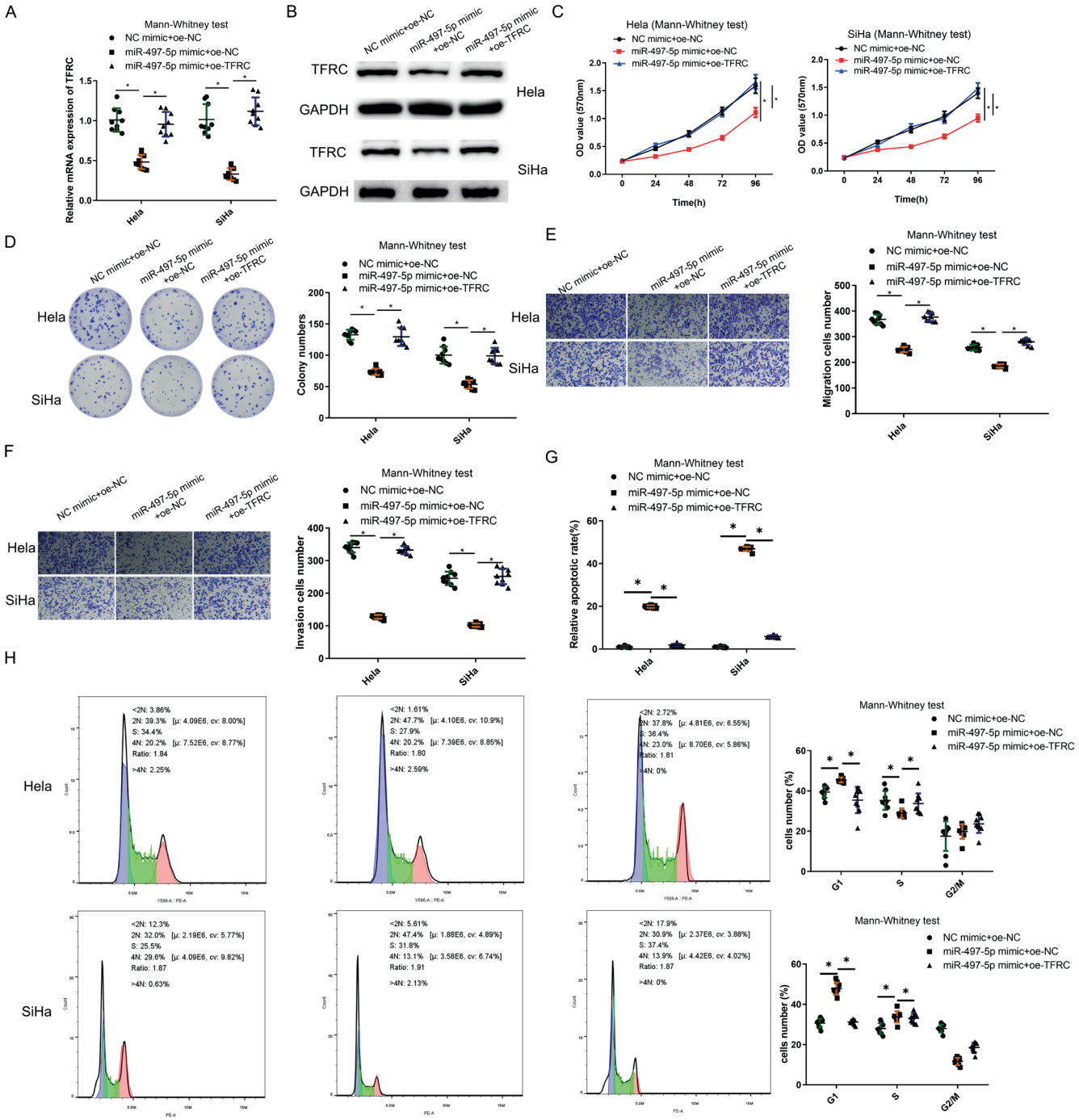


Fig. 4. MicroRNA-497-5p (*miR-497-5p*) represses cell phenotype progression in cervical cancer through transferrin receptor (*TFRC*) downregulation. A,B. TFRC mRNA and protein levels in cervical cancer cells (Hela and SiHa) (Mann–Whitney U test); C. Cell proliferation in varying groups (Mann–Whitney U test); D. Colony formation of cervical cancer cells in various treatment groups (Mann–Whitney U test); E,F. Cell migration and invasion in various treatment groups (100×) (Mann–Whitney U test); G. Cell apoptosis in various treatment groups (Mann–Whitney U test); H. Cell cycle statuses in various groups (Mann–Whitney U test)

*p < 0.05 indicated statistically significant values; OD – optical density.

aberrantly expressed in cervical cancer and are implicated in tumorigenesis and progression.[32] Of note, exploring the potential mechanism of cervical cancer may lead to its early diagnosis and effective therapy.[33] Transferrin receptor is present in almost all mammalian cells.[34] Herein, *TFRC* expression data in cervical cancer were analyzed for the mechanism of *TFRC* dysregulation in the pathogenesis of the disease, finding that *TFRC* was upregulated, and silencing *TFRC* repressed the progression of cervical cancer cell phenotype. Previous studies have uncovered that *TFRC* is increased in both colon and lung cancers. Specifically, Fu et al. highlighted that TFR1 was significantly increased and was essential in the malignant progression of colorectal cancer.[35] Furthermore, Whitney et al. confirmed that

*TFRC* was significantly increased in NSCLC.[36] Our work is concordant with an earlier report that compared the up-regulation of *TFRC* in cervical cancers to adjacent non-tumor tissue and correlated these results to progression stages, tumor status and lymph node involvement.[37] These findings show that *TFRC* may function as a direct and indirect target for the administration of therapeutics, presenting a potential prospect in treating cancer cell malignant progression.

This work uncovered the mechanism of *miR-497-5p* modulating *TFRC* in cervical cancer cells. Earlier studies have shown that *miR-497-5p*, *miR-320* and *miR-210* target *TFRC*.[38,39] Herein, we have demonstrated that *TFRC* was a direct target of *miR-497-5p*. Moreover, through bioinformatics analysis, a negative link between *miR-497-5p* and *TFRC* was uncovered. Our finding is congruous with previous evidence stating that the expression of *miR-497-5p* is reduced in gastric cancer,[26] while Li et al. proposed that *miR-497-5p* is significantly decreased in NSCLC.[40] Most importantly, increased *miR-497-5p* expression decreased *TFRC* in cervical cancer cells, while *miR-497-5p* and *TFRC* overexpression restored the repressive influence of overexpressing *miR-497-5p* on cervical cancer. This result was also supported by Chen et al.[41] Given that *miR-497-5p* targets *TFRC* to repress cervical cancer tumorigenesis and progression, it may represent a feasible therapeutic target for cervical cancer patients.

## Limitations

While the findings of the study are promising, an analysis of these aspects in animal models and clinical trials would be valuable. Therefore, future research will focus on the mechanism of the *miR-497-5p*/*TFRC* axis in cervical cancer from multiple perspectives in order to offer a theoretical foundation for potential therapies.

# Conclusions

Transferrin receptor knockdown could inhibit the proliferation, migration and invasion of cervical cancer cells while promoting apoptosis. Regarding the regulatory mechanism, concomitant upregulation of *TFRC* is caused by decreased *miR-497-5p* level, while the upregulation of *miR-497-5p* repressed the malignant phenotype of cervical cancer by modulating *TFRC*. This work has contributed to proposing more therapeutic regimens for cervical cancer.

## Supplementary data

The supplementary materials are available at https://doi.org/10.5281/zenodo.8032200. The package contains the following files:

Supplementary Fig. 1. Expression of apoptosis-related proteins, cleaved caspase-3 and cleaved caspase-9, as assayed by WB.

Supplementary Fig. 2. Cell migration and invasion abilities evaluated using transwell assay (Mann–Whitney U test).

Supplementary Fig. 3. Changes in expression of EMT-related proteins evaluated using WB (Mann–Whitney U test; *$p < 0.050$ represents statistically significant values).

## ORCID iDs

Xiangming Fang https://orcid.org/0000-0003-0757-2274
Pei Hu https://orcid.org/0009-0004-0576-367X
Ying Gao https://orcid.org/0009-0005-5529-8611
Chuqiao Chen https://orcid.org/0009-0008-4882-9017
Jianqing Xu https://orcid.org/0000-0001-7022-5369

## References

1. Ji X, Guo H, Yin S, Du H. miR-139-5p functions as a tumor suppressor in cervical cancer by targeting TCF4 and inhibiting Wnt/β-catenin signaling. *Onco Targets Ther*. 2019;12:7739–7748. doi:10.2147/OTT.S215796
2. Fu K, Zhang L, Liu R, Shi Q, Li X, Wang M. MiR-125 inhibited cervical cancer progression by regulating VEGF and PI3K/AKT signaling pathway. *World J Surg Oncol*. 2020;18(1):115. doi:10.1186/s12957-020-01881-0
3. Cohen PA, Jhingran A, Oaknin A, Denny L. Cervical cancer. *Lancet*. 2019;393(10167):169–182. doi:10.1016/S0140-6736(18)32470-X
4. Isik A, Wysocki AP, Memiş U, Sezgin E, Yezhikova A, Islambekov Y. Factors associated with the occurrence and healing of umbilical pilonidal sinus: A rare clinical entity. *Adv Skin Wound Care*. 2022;35(8):1–4. doi:10.1097/01.ASW.0000833608.27136.d1
5. Isik A, Soran A, Grasi A, Barry N, Sezgin E. Lymphedema after sentinel lymph node biopsy: Who is at risk? *Lymphat Res Biol*. 2022;20(2):160–163. doi:10.1089/lrb.2020.0093
6. Hill EK. Updates in cervical cancer treatment. *Clin Obstet Gynecol*. 2020;63(1):3–11. doi:10.1097/GRF.0000000000000507
7. Chopra S, Gupta M, Mathew A, et al. Locally advanced cervical cancer: A study of 5-year outcomes. *Indian J Cancer*. 2018;55(1):45–49. doi:10.4103/ijc.IJC_428_17
8. Bose CK. Balstilimab and other immunotherapy for recurrent and metastatic cervical cancer. *Med Oncol*. 2022;39(4):47. doi:10.1007/s12032-022-01646-7
9. Huang Y, Huang J, Huang Y, et al. TFRC promotes epithelial ovarian cancer cell proliferation and metastasis via up-regulation of AXIN2 expression. *Am J Cancer Res*. 2020;10(1):131–147. PMID:32064157.
10. Cui P, Dai X, Liu R, Cao H. LncRNA LINC00888 upregulation predicts a worse survival of laryngeal cancer patients and accelerates the growth and mobility of laryngeal cancer cells through regulation of miR-378g/TFRC. *J Biochem Mol Toxicol*. 2021;35(10):e22878. doi:10.1002/jbt.22878
11. Yang C, Li J, Guo Y, et al. Role of TFRC as a novel prognostic biomarker and in immunotherapy for pancreatic carcinoma. *Front Mol Biosci*. 2022;9:756895. doi:10.3389/fmolb.2022.756895
12. Muhammad JS, Bajbouj K, Shafarin J, Hamad M. Estrogen-induced epigenetic silencing of *FTH1* and *TFRC* genes reduces liver cancer cell growth and survival. *Epigenetics*. 2020;15(12):1302–1318. doi:10.1080/15592294.2020.1770917
13. Kim H, Villareal LB, Liu Z, et al. Transferrin receptor-mediated iron uptake promotes colon tumorigenesis. *Adv Sci (Weinh)*. 2023;10(10):e2207693. doi:10.1002/advs.202207693
14. Zhang J, Chen S, Wei S, et al. CircRAPGEF5 interacts with RBFOX2 to confer ferroptosis resistance by modulating alternative splicing of TFRC in endometrial cancer. *Redox Biol*. 2022;57:102493. doi:10.1016/j.redox.2022.102493
15. Shen Y, Li X, Dong D, Zhang B, Xue Y, Shang P. Transferrin receptor 1 in cancer: A new sight for cancer therapy. *Am J Cancer Res*. 2018;8(6):916–931. PMID:30034931. PMCID:PMC6048407.
16. He B, Zhao Z, Cai Q, et al. miRNA-based biomarkers, therapies, and resistance in cancer. *Int J Biol Sci*. 2020;16(14):2628–2647. doi:10.7150/ijbs.47203
17. Menon A, Abd-Aziz N, Khalid K, Poh CL, Naidu R. miRNA: A promising therapeutic target in cancer. *Int J Mol Sci*. 2022;23(19):11502. doi:10.3390/ijms231911502

18. Mou T, Xie F, Zhong P, et al. MiR-345-5p functions as a tumor suppressor in pancreatic cancer by directly targeting CCL8. *Biomed Pharmacother*. 2019;111:891–900. doi:10.1016/j.biopha.2018.12.121
19. Petrovic N, Ergun S. miRNAs as potential treatment targets and treatment options in cancer. *Mol Diagn Ther*. 2018;22(2):157–168. doi:10.1007/s40291-017-0314-8
20. Liang Z, Yang Y, Sun X, et al. Integrated analysis of microRNA and mRNA expression profiles in the fat bodies of MbMNPV-infected *Helicoverpa armigera*. *Viruses*. 2022;15(1):19. doi:10.3390/v15010019
21. Lu M, Gao Q, Wang Y, Ren J, Zhang T. LINC00511 promotes cervical cancer progression by regulating the miR-497-5p/MAPK1 axis. *Apoptosis*. 2022;27(11–12):800–811. doi:10.1007/s10495-022-01768-3
22. Wang L, Guo J, Zhou J, Wang D, Kang X, Zhou L. NF-κB maintains the stemness of colon cancer cells by downregulating miR-195-5p/497-5p and upregulating MCM2. *J Exp Clin Cancer Res*. 2020;39(1):225. doi:10.1186/s13046-020-01704-w
23. Liu C, Bordeaux A, Hettich S, Han S. MicroRNA-497-5p functions as a modulator of apoptosis by regulating metadherin in ovarian cancer. *Cell Transplant*. 2020;29:096368971989706. doi:10.1177/0963689719897061
24. Huang X, Wang L, Liu W, Li F. MicroRNA-497-5p inhibits proliferation and invasion of non-small cell lung cancer by regulating FGF2. *Oncol Lett*. 2019;17(3):3425–3431. doi:10.3892/ol.2019.9954
25. Zheng S, Hou J, Chang Y, Zhao D, Yang H, Yang J. CircRNA Circ-CCND1 aggravates hepatocellular carcinoma tumorigenesis by regulating the miR-497-5p/HMGA2 axis. *Mol Biotechnol*. 2022;64(2):178–186. doi:10.1007/s12033-021-00391-y
26. Feng L, Cheng K, Zang R, Wang Q, Wang J. miR-497-5p inhibits gastric cancer cell proliferation and growth through targeting PDK3. *Biosci Rep*. 2019;39(9):BSR20190654. doi:10.1042/BSR20190654
27. Hu J, Peng X, Du W, Huang Y, Zhang C, Zhang X. circSLC6A6 sponges miR-497-5p to promote endometrial cancer progression via the PI4KB/Hedgehog axis. *J Immunol Res*. 2021;2021:5512391. doi:10.1155/2021/5512391
28. Fridrichova I, Kalinkova L, Karhanek M, et al. miR-497-5p decreased expression associated with high-risk endometrial cancer. *Int J Mol Sci*. 2020;22(1):127. doi:10.3390/ijms22010127
29. Liu S, Wang L, Zhang R. Corylin suppresses metastasis of breast cancer cells by modulating miR-34c/LINC00963 target. *Libyan J Med*. 2021;16(1):1883224. doi:10.1080/19932820.2021.1883224
30. Ye J, Wang Z, Chen X, et al. YTHDF1-enhanced iron metabolism depends on TFRC $m^6A$ methylation. *Theranostics*. 2020;10(26):12072–12089. doi:10.7150/thno.51231
31. Liu X, Zhou Y, Ning YE, Gu H, Tong Y, Wang N. MiR-195-5p inhibits its malignant progression of cervical cancer by targeting YAP1. *Onco Targets Ther*. 2020;13:931–944. doi:10.2147/OTT.S227826
32. Li N, Yu K, Lin Z, Zeng D. Identifying a cervical cancer survival signature based on mRNA expression and genome-wide copy number variations. *Exp Biol Med (Maywood)*. 2022;247(3):207–220. doi:10.1177/15353702211053580
33. Díaz-González SDM, Deas J, Benítez-Boijseauneau O, et al. Utility of microRNAs and siRNAs in cervical carcinogenesis. *Biomed Res Int*. 2015;2015:374924. doi:10.1155/2015/374924
34. Thorstensen K, Romslo I. The transferrin receptor: Its diagnostic value and its potential as therapeutic target. *Scand J Clin Lab Invest Suppl*. 1993;215:113–120. doi:10.3109/00365519309090703
35. Fu Y, Lin L, Xia L. MiR-107 function as a tumor suppressor gene in colorectal cancer by targeting transferrin receptor 1. *Cell Mol Biol Lett*. 2019;24:31. doi:10.1186/s11658-019-0155-z
36. Whitney JF, Clark JM, Griffin TW, Gautam S, Leslie KO. Transferrin receptor expression in nonsmall cell lung cancer. Histopathologic and clinical correlates. *Cancer*. 1995;76(1):20–25. doi:10.1002/1097-0142(19950701)76:1<20::AID-CNCR2820760104>3.0.CO;2-3
37. Xu X, Liu T, Wu J, Wang Y, Hong Y, Zhou H. Transferrin receptor-involved HIF-1 signaling pathway in cervical cancer. *Cancer Gene Ther*. 2019;26(11–12):356–365. doi:10.1038/s41417-019-0078-x
38. Schaar DG, Medina DJ, Moore DF, Strair RK, Ting Y. miR-320 targets transferrin receptor 1 (CD71) and inhibits cell proliferation. *Exp Hematol*. 2009;37(2):245–255. doi:10.1016/j.exphem.2008.10.002
39. Yoshioka Y, Kosaka N, Ochiya T, Kato T. Micromanaging iron homeostasis: Hypoxia-inducible micro-RNA-210 suppresses iron homeostasis-related proteins. *J Biol Chem*. 2012;287(41):34110–34119. doi:10.1074/jbc.M112.356717
40. Li G, Wang K, Wang J, Qin S, Sun X, Ren H. miR-497-5p inhibits tumor cell growth and invasion by targeting SOX5 in non–small-cell lung cancer. *J Cell Biochem*. 2019;120(6):10587–10595. doi:10.1002/jcb.28345
41. Chen Y, Du J, Wang Y, et al. MicroRNA-497-5p induces cell cycle arrest of cervical cancer cells in S phase by targeting CBX4. *Onco Targets Ther*. 2019;12:10535–10545. doi:10.2147/OTT.S210059

# *LncRNA-LINC00472* suppresses the malignant progression of non-small cell lung cancer via modulation of the *miRNA-1275/Homeobox A2* axis

Meichen Jiang[1,D], Xiangli Ye[2,C], Dongliang Shi[1,B,C], Qili Lin[1,C], Feijian Huang[2,D], Yong Li[2,A,E]

[1] Department of Pathology, Fujian Medical University Union Hospital, Fuzhou, China
[2] Department of Respiration Medicine, Fujian Medical University Union Hospital, Fuzhou, China

A – research concept and design; B – collection and/or assembly of data; C – data analysis and interpretation;
D – writing the article; E – critical revision of the article; F – final approval of the article

Advances in Clinical and Experimental Medicine, ISSN 1899–5276 (print), ISSN 2451–2680 (online) *Adv Clin Exp Med*. 2024;33(3):283–297

**Address for correspondence**
Yong Li
E-mail: leo_liyong9@163.com

**Funding sources**
This study was sponsored by Fujian Provincial Health Technology Project (grant No. 2020GGB027), Natural Science Foundation of Fujian Province (grant No. 2021J01747) and Joint Funds for the Innovation of Science and Technology, Fujian province (grant No. 2021Y9043).

**Conflict of interest**
None declared

Received on June 29, 2022
Reviewed on November 24, 2022
Accepted on June 16, 2023

Published online on September 4, 2023

**Cite as**
Jiang M, Ye X, Shi D, Lin Q, Huang F, Li Y. *LncRNA-LINC00472* suppresses the malignant progression of non-small cell lung cancer via modulation of the *miRNA-1275/Homeobox A2* axis. *Adv Clin Exp Med*. 2024;33(3):283–297. doi:10.17219/acem/168431

**DOI**
10.17219/acem/168431



## Abstract

**Background.** Long non-coding RNAs (lncRNAs) are increasingly observed as regulatory factors for the initiation and progression of varying kinds of cancers. However, studies on lncRNAs in non-small cell lung cancer (NSCLC) progression are currently lacking.

**Objectives.** We intended to determine the role of lncRNA *LINC00472* and its downstream regulatory mechanism in NSCLC, thus providing novel ideas for targeted therapies for NSCLC.

**Materials and methods.** The target signaling axis comprising the lncRNA/microRNA/mRNA was identified through bioinformatics analysis. Subcellular localization of *LINC00472* was assessed with fluorescence in situ hybridization (FISH). Cellular function experiments were conducted to examine the proliferation, migration, invasion, and apoptosis of NSCLC cells, and dual-luciferase and RNA binding protein immunoprecipitation assays were performed to validate the binding relationship. Quantitative real-time polymerase chain reaction (qPCR) and western blot were utilized to assess the expression levels of the investigated gene and protein, respectively.

**Results.** The *LINC00472* expression was markedly decreased in NSCLC tissues and cells. The FISH, combined with nuclear–cytoplasm separation assay, demonstrated that *LINC00472* was mainly located in the cytoplasm. The overexpression of *LINC00472* restrained proliferation and metastasis of NSCLC in vitro. The *LINC00472* could target and repress *miR-1275* level, and overexpression of *LINC00472* reduced the *miR-1275*-dependent malignant cell phenotype in NSCLC. Further study revealed that *HOXA2* was a downstream target of *miR-1275* and was negatively modulated by *miR-1275*. Rescue assays exhibited that the overexpression of *miR-1275* or inhibition of *HOXA2* reversed the impact of *LINC00472* overexpression on the malignant progression of NSCLC cells. The *LINC00472* repressed the epithelial–mesenchymal transition (EMT) of NSCLC cells through *miR-1275/HOXA2*.

**Conclusions.** The *LINC00472* functioned as a competing endogenous RNA to modulate *HOXA2* level by sponging *miR-1275* in NSCLC. Simultaneously, the *LINC00472/miR-1275/HOXA2* axis may be a possible therapeutic target and biomarker for NSCLC.

**Key words:** NSCLC, *miR-1275*, malignant progression, *LINC00472*, *HOXA2*

# Background

Lung cancer (LC) reaches the highest mortality rates among cancers throughout the world,[1] and 85% of cases are categorized as non-small cell lung cancer (NSCLC).[1,2] Few NSCLC patients are diagnosed at an early stage,[3] and more than 60% of LC patients are already at an advanced stage or have tumor metastasis (stage III or IV) at the first diagnosis, precluding surgical resection. Until now, chemotherapy and radiotherapy have been the main treatment methods for this disease.[4] Despite progress in LC clinical diagnosis and therapy, neither new targeted therapy nor immunotherapy has been able to yield a desirable effect,[4] with the 5-year overall survival (OS) of less than 20%.[5,6] Therefore, elucidating the molecular mechanism underlying NSCLC progression and exposing potential diagnostic and treatment targets are essential.

Long non-coding RNAs (lncRNAs) have no or limited protein-coding potential.[7] They have been widely studied for their ability to sponge microRNA (miRNA) and regulate downstream gene expression, and lncRNA mutations or disorders play an important role in cancer.[8] The *LINC00472* is an intergenic lncRNA[9] located on chromosome 6q13, and its abnormal expression is implicated in many biological processes and tumor progression.[10] It is reported that *LINC00472* has an antitumor effect in breast cancer,[11,12] and is negatively correlated with the breast cancer tumor-node-metastasis (TNM) stage.[13] Moreover, the *LINC00472* level in epithelial ovarian cancer (EOC) is also related to TNM stage.[14] The *LINC00472* has been shown to repress proliferation and enhance apoptosis of colorectal cancer (CRC) cells by mediating the *miR-196a*/*PDCD4* axis.[9] In hepatocellular carcinoma (HCC), *LINC00472* can inhibit the malignant phenotype via regulating the *miR-93-5p*/*PDCD4* axis.[15] Although it has been reported that *LINC00472* has a potential regulatory role in LC[16] and NSCLC[17,18] and is a candidate biomarker for diagnosis and treatment, the role of *LINC00472* in NSCLC progression requires further investigation.

The miRNAs can modulate downstream targeted genes[19] through the complementary pairing of mRNA 3'-UTR ends at the post-transcriptional level. According to reports, *miR-21*,[20] *miR-1253*[21] and *miR-3607-3p*[22] participate in the progression of NSCLC through different cellular processes. The *miR-1275* is pivotal in different tumors, such as bladder cancer,[23] nasopharyngeal carcinoma (NPC)[24] and esophageal cancer.[25] In addition, *PGM5P4-AS1* can inhibit the malignant behavior of LC cells through sponging *miR-1275*.[26] However, investigations regarding *miR-1275* in NSCLC have been lacking.

*Homeobox A2* (*HOXA2*) belongs to the *HOX* family,[27] whose members are involved with multiple cancer types. For instance, *HOXB5* restrains NSCLC cell phenotype progression by inactivating the *Wnt/β-catenin* pathway,[28] and it also has an association with CRC,[29] NPC[30] and breast cancer.[31] The *HOXA2* can play a regulatory role in the malignant progression of glioma cells, and its elevated expression reflects a poor prognosis for glioma patients.[32] Furthermore, *HOXA2* is a common hypermethylation marker gene in squamous cell carcinoma and is associated with its prognosis.[33] However, the molecular mechanism of *HOXA2* and its effects on NSCLC have not been thoroughly studied.

# Objectives

This study combined bioinformatics analysis as well as molecular and cell function experiments to explore the influence of the lncRNA-*LINC00472*/*miR-1275*/*HOXA2* axis on the malignant progression of NSCLC, providing a theoretical basis for finding novel targeted treatment method.

# Materials and methods

## Bioinformatics analysis

The *NSCLC* gene expression chips GSE44077 and GSE102286 were obtained through the Gene Expression Omnibus (GEO) database, where GSE44077 contains mRNA expression data (normal: n = 66, tumor: n = 55) and GSE102286 is composed of miRNA expression data (normal: n = 88, tumor: n = 91). The R package "limma"[34] was introduced for differential analysis, with |logFC| > 1 and p-value <0.05 set as thresholds. Regulatory miRNAs downstream of *LINC00472* were predicted using the RNA22 database, and target genes downstream of *miR-1275* were predicted via TargetScan (https://www.targetscan.org), miRSearch (https://www.mirbase.org/search.shtml) and mirDIP (http://ophid.utoronto.ca/mirDIP).

## Cell culture

Cell line information is shown in Table 1. The normal human lung epithelial cell line BEAS-2B and NSCLC cell lines NCI-H1975, NCI-H157, NCI-H358, and NCI-H1299

**Table 1.** Cell lines used in the assay (all obtained from Cobioer, Nanjing, China)

| Cell line | Cell type | Product code |
|---|---|---|
| BEAS-2B | human lung (bronchus) epithelial cell line | CBP60577 |
| NCI-H1975 | human adenocarcinoma cell line | CBP60121 |
| NCI-H157 | human squamous cell carcinoma cell line | CBP60952 |
| NCI-H358 | human NSCLC cell line | CBP60136 |
| NCI-H1299 | human NSCLC cell line | CBP60053 |
| 293T | human embryonic kidney cell | CBP60440 |

NSCLC – non-small cell lung cancer.

were maintained in Roswell Park Memorial Institute-1640 (RPMI-1640) complete medium (cat. No. MFCD00217820; Sigma-Aldrich, St. Louis, USA). Human embryonic kidney cell line 293T was maintained in Dulbecco's modified Eagle's medium (DMEM, cat. No. M3942; Sigma-Aldrich). All media contained an additional 10% fetal bovine serum (FBS; cat. No. 10099141; Gibco, Grand Island, USA), 100 U/mL penicillin and 100 µg/mL streptomycin sulfate (cat. No. 30-002-CI; Corning Inc., Corning, USA), and cultures were maintained at 37°C with 5% $CO_2$. After sterilizing the purchased cell lines with 75% alcohol, we observed cell shape, adhesion and density under an inverted microscope (model CKX53; Olympus Corp., Tokyo, Japan). Then, we put cells in a 37°C and 5% $CO_2$ cell incubator (model BB150; Thermo Fisher Scientific, Waltham, USA) for 2–3 h to stabilize them before further experiments.

## Cell transfection

The sequence of *LINC00472* (full-length) was cloned using the SMARTer™ RACE cDNA kit (cat. No. 634858/59; Takara, Kusatsu, Japan). The *LINC00472* overexpression vector (oe-*LINC00472*) and empty pcDNA3.1 vector (cat. No. V79020, oe-NC) were obtained from Thermo Fisher Scientific, and following lentiviral transduction, infected cell lines NCI-H358 and NCI-H1299 were treated with 1 mg/mL puromycin to generate stably transfected cell lines. The *miR-1275* mimic (miR-mimic) and blank control (miR-NC) were obtained from RiboBio Co., Ltd. (Guangzhou, China), and *HOXA2* silencing plasmids (si-*HOXA2*) and pLenti vectors (si-NC) were purchased from Vigene Biosciences (Rockville, USA). Lipofectamine™ 3000 (cat. No. L3000015; Invitrogen, Waltham, USA) was employed for transfection. Cells were harvested 48 h after transfection, with the transfection efficiency being assessed using quantitative real-time polymerase chain reaction (qPCR).

## qPCR

The total RNA of each cell line (BEAS-2B, NCI-H1975, NCI-H157, NCI-H358, and NCI-H1299) was extracted and quantified. Total RNA was extracted using TRIzol™ reagent (cat. No. 10296010; Thermo Fisher Scientific), and the RNA concentration was assessed using a NanoDrop™ 2000 (Thermo Fisher Scientific). The miScript II RT kit (cat. No. 18064071; Qiagen, Hilden, Germany) was used to synthesize cDNA by reverse transcription from miRNA, miScript SYBR Green PCR Kit (cat. No. 4309155; Qiagen) was used for detection, and U6 was utilized as the internal reference. Using PrimeScript RT Master Mix (cat. No. RR036Q; Takara), lncRNA and mRNA were reverse transcribed into cDNA. Additionally, SYBR® Premix Ex Taq TM II (cat. No. RR820A; Takara) was utilized for assessment, and GAPDH was the endogenous control. All qPCR tests were performed on an Applied Biosystems® 7500 Real-Time PCR Systems (cat. No. 4362143; Thermo Fisher Scientific). Primer information is available in Table 2. The $2^{-\Delta\Delta Ct}$ method was applied for relative expression calculations, and the experiment was performed in triplicate.

Table 2. Primer sequence used in quantitative real-time polymerase chain reaction (qPCR)

| Gene | Sequence | |
|---|---|---|
| *LINC00472* | forward | 5′-GATGGCAGCTGTCTCTCTCC-3′ |
| | reverse | 5′-GGGCCTCTCTGACCGTATCT-3′ |
| *GAPDH* | forward | 5′-GGGCCAAAAGGGTCATCATC-3′ |
| | reverse | 5′-ATGACCTTGCCCACAGCCTT-3′ |
| *miR-1275* | forward | 5′-TGGGGGAGAGGCTGTC-3′ |
| | reverse | 5′-GAACATGTCTGCGTATCTC-3′ |
| *U6* | forward | 5′-CTCGCTTCGGCAGCACAT-3′ |
| | reverse | 5′-TTTGCGTGTCATCCTTGCG-3′ |
| *HOXA2* | forward | 5′-GGGTATTYGGGYGGTTGTAGG-3′ |
| | reverse | 5′-AATACCTAACATCTTTTCCCCCTATC-3′ |

## Fluorescence in situ hybridization and subcellular separation

The lncRNA *LINC00472* fluorescence in situ hybridization (FISH) probe was labeled with 5-carboxyfluorescein and synthesized by Biolite Corp (cat. No. 76823-03-5; Xi'an, China). Following protease K digestion, the tissue was denatured with formamide and hybridized overnight with the *LINC00472* probe at 42°C, followed by staining with 300 µL 4,6-diamino-2-phenyl indole (DAPI; cat. No. 28718-90-3; Solarbio, China). Samples were analyzed with the use of laser scanning confocal microscope (model LSM700; Carl Zeiss, Oberkochen, Germany), and the nucleus and cytoplasm of NCI-H358 and NCI-H1299 cells were separated using PARIS Kit (cat. No. AM1921; Thermo Fisher Scientific).

## Cell Counting Kit-8 assay

Cells were seeded into 96-well plates ($2\times10^4$ cells/well) under routine conditions and grown at 70% confluence. After 0, 24, 48, and 72 h, 10-microliter Cell Counting Kit-8 (CCK-8) solution (cat. No. CK04; Dojindo Laboratories, Kumamoto, Japan) was administered to each well, followed by a 2-hour incubation. The optical density was assessed at 450 nm using a microplate reader (Multiskan MK3; Thermo Fisher Scientific), and the experiment was performed 3 times.

## Transwell assay

### Cell invasion

Cells ($1\times10^4$ cells/well) were added to the upper insert of 24-well transwell chambers (8 µm in diameter; cat. No. 3428; Corning Inc.) coated with Matrigel. The lower chamber was filled with RPMI-1640 complete medium (cat.

No. R4130; Sigma-Aldrich) and 10% FBS (cat. No. 10099141; Gibco). Following 36 h of incubation at 37°C, we utilized a wet applicator to remove cells that did not pass the membrane, and cells on the lower surface underwent fixation with 4% paraformaldehyde and staining with 0.5% crystal violet. After staining, cells were imaged using an inverted microscope (model CKX53; Olympus Corp.).

### Cell migration

After 24 h of starvation, log phase cells were digested, centrifuged and resuspended the next day to a concentration of $2\times10^4$ cells/mL. A total of 0.2 mL of the cell suspension was seeded to the upper chamber, with the lower chamber being filled with 700 µL of precooled RPMI-1640 complete medium and 10% FBS. After maintaining cells in routine conditions for 36 h, we removed cells that did not migrate, and fixed the migrated cells with methanol for 30 min. Cells were stained with 0.5% crystal violet for 20 min, washed, inverted, and dried naturally, followed by imaging under an inverted microscope (model CKX53; Olympus Corp.). We selected 5 visual fields to count the visible cells.

## Annexin V/propidium iodide double staining assay

Trypsin without ethylenediamine tetra-acetic acid (EDTA) was used to treat log phase cells, which were centrifuged, and the supernatant was discarded. Cells were rinsed twice with phosphate-buffered saline (PBS), and then resuspended with 500 µL of precooled 1× binding buffer until the concentration reached $1\times10^6$ cells/mL. A total of 100 µL of cell suspension was added with 5 µL of Annexin-V-FITC (cat. No. C1062S; Beyotime, Shanghai, China) at room temperature for 15 min in the dark. After that, 2.5 µL of propidium iodide (PI) staining solution (cat. No. 25535-16-4; MedChemExpress, Belleville, USA) was added 5 min before the analysis using a flow cytometer (cat. No. A29003; Thermo Fisher Scientific). FlowJo v. 10 software (FlowJo LLC, Ashland, USA) was used to analyze apoptosis. The experiment was repeated 3 times.

## Dual-luciferase reporter gene analysis

The pmirGLO luciferase reporter vectors (cat. No. E1330; Promega, Madison, USA) inserted with wild-type (WT) and mutant (MUT) *LINC00472* or *HOXA2* 3'UTR were built, respectively. The 293T cells were maintained in 24-well plates and transfected based on the co-transfection groups (miR-mimic + *LINC00472*-WT or *LINC00472*-MUT; miR-NC + *LINC00472*-WT or *LINC00472*-MUT; miR-mimic + *HOXA2*-WT or *HOXA2*-MUT; miR-NC + *HOXA2*-WT or *HOXA2*-MUT). Then, 48 h after transfection, luciferase activity was measured with a dual-luciferase reporter system (cat. No. E1910; Promega).

## RNA binding protein radioimmunoprecipitation assay

Magna RNA immunoprecipitation kit (cat. No. 17-704; Millipore, Burlington, USA) was used according to the manufacturer's instructions. After being maintained in radioimmunoprecipitation (RIP) buffer with magnetic beads, cell lysates were combined with rabbit anti-Ago2 antibody. Input or rabbit immunoglobulin G (IgG) was utilized as the negative control (NC). Protease K (cat. No. HY-108717; MCE) was utilized to purify and immunoprecipitate the RNA of both the samples and the inputs. Next, RNA was isolated for qPCR analysis. Antibody information is displayed in Table 3.

Table 3. Antibody information used in the assay (all antibodies purchased from Abcam, Cambridge, UK)

| Antibody | Application | Dilution ratio | Product code | Specificity |
|---|---|---|---|---|
| Anti-*HOXA2* | western blot | 1:2000 | ab229960 | rabbit |
| Anti-*E-cadherin* | | 1:10,000 | ab40772 | rabbit |
| Anti-*N-cadherin* | | 1:10,000 | ab76011 | rabbit |
| Anti-*MMP2* | | 1:5000 | ab92536 | rabbit |
| Anti-*MMP9* | | 1:10,000 | ab76003 | rabbit |
| Anti-*Bax* | | 1:5000 | ab32503 | rabbit |
| Anti-*Bcl-2* | | 1:1000 | ab32124 | rabbit |
| Anti-*GAPDH* | | 1:10,000 | ab181602 | rabbit |
| Anti-*Argonaute-2* | RIP | – | ab32381 | rabbit |
| *IgG* | | – | ab172730 | rabbit |
| Anti-*HOXA2* | IHC | 1:2000 | ab229960 | rabbit |
| Anti-*Ki67* | | 1:500 | ab15580 | rabbit |
| *IgG* | | 1:1000 | ab6721 | goat anti-rabbit |

RIP – RNA immunoprecipitation; IHC – immunohistochemistry.

## Western blot assay

The extraction of total proteins from cells was performed using RIP assay (RIPA; cat. No. P0013B; Beyotime), and protein concentration was assessed with a bicinchoninic acid (BCA) protein assay kit (cat. No. P0011; Beyotime). After denaturation at a high temperature, proteins were isolated using sodium dodecyl sulfate–polyacrylamide gel electrophoresis (SDS-PAGE), followed by a transfer to polyvinylidene fluoride (cat. No. 24937-79-9; Millipore) membranes. Membranes were blocked with 5% bovine serum albumin (BSA) at room temperature for 2 h, and probed with primary antibodies overnight at 4°C. Relevant information about primary antibodies is shown in Table 3. Membranes were incubated with the secondary antibody goat anti-rabbit *IgG* H&L (HRP) (cat. No. ab205718; Abcam, Cambridge, UK) for 2 h at room temperature. The protein blots on the membrane were detected using an enhanced chemiluminescence kit (ECL; cat. No. P0018S; Beyotime).

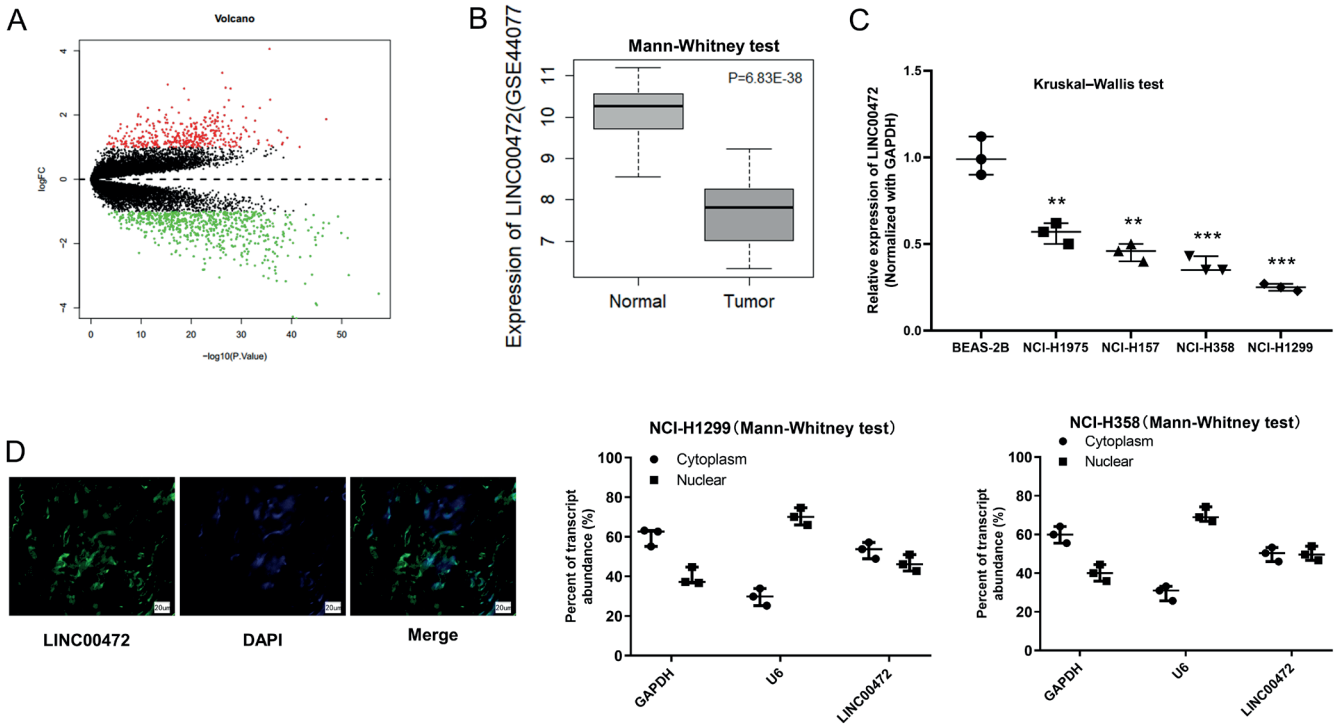


Fig. 1. *LINC00472* is downregulated in non-small cell lung cancer (NSCLC) and predominantly located in the cytoplasm. A. Volcano map of differential genes in NSCLC gene expression chip GSE44077. X-axis represents the $\log_{10}$ p-value, while Y-axis represents the logFC value; the red points represent significantly upregulated genes in the tumor, the green points represent markedly downregulated genes in the tumor, and the black points represent genes with no significant difference; B. *LINC00472* level in normal (left) and tumor (right) groups in GSE44077. X-axis: sample type, Y-axis: lncRNA expression value (Mann–Whitney U test (M–W)); C. *LINC00472* level in NSCLC cells (NCI-H1975, NCI-H157, NCI-H358, and NCI-H1299) and normal cells (BEAS-2B) was assayed using quantitative real-time polymerase chain reaction (qPCR) (Kruskal–Wallis test); D. Fluorescence in situ hybridization (FISH) (400×) was conducted to verify location of *LINC00472* in NSCLC tissues. After the nuclei and cytoplasm of NCI-H1299 and NCI-H358 cells were separated, the expression of *GAPDH* (cytoplasmic marker), *U6* (nuclear marker) and *LINC00472* was assessed (M–W; **p < 0.01; ***p < 0.001). The horizontal lines represent the medians

## Statistical analyses

GraphPad Prism v. 8.0.2 (GraphPad Software, San Diego, USA) was employed for data processing, and all experiments were performed in triplicate. All experimental data are shown as raw data, and due to limited sample size, all data were assessed with nonparametric tests. The Mann–Whitney U test (M–W) was used for a comparison between 2 groups, and the Kruskal–Wallis test was used for a comparison of 3 or more groups, followed by Dunn's post hoc test. The medians with 95% confidence interval (95% CI) whiskers are presented in results.[35] The reference sample shown in Fig. 1A and Fig. 1B is the normal group, the reference sample shown in Fig. 1C is the BEAS-2B cell line, the reference sample presented in Fig. 2 is the oe-NC group, and the reference sample displayed in Fig. 3 is the miR-NC group. In Fig. 4, the oe-NC+miR-NC group is the reference sample for the oe-NC+miR-mimic group, while the oe-NC+miR-mimic group is the reference sample for the oe-*LINC00472*+miR-mimic group. The reference sample in Fig. 5B is the normal group. The reference sample in Fig. 5D–F is the miR-NC group. Fig. 5A is the interaction of sets from 4 databases that down-regulate miRAN without reference groups, and Fig. 5C is sequence information without reference groups In Fig. 5G,H and Fig. 6, the NC group is the reference sample for the oe-*LINC00472* group, and the oe-*LINC00472* group is the reference sample for the oe-*LINC00472*+miR-mimic group and oe-*LINC00472*+si-*HOXA* group. All experiments were performed in triplicate. Statistical significance was determined at $p < 0.05$, while $p < 0.010$ suggested a significant difference and $p < 0.001$ indicated an extremely significant difference.

# Results

## *LINC00472* is downregulated and mainly located in the cytoplasm in NSCLC

The NSCLC gene expression chip GSE44077 was obtained from the GEO database, with differential analysis finding 1029 differentially expressed genes (Fig. 1A). The *LINC00472* was dramatically underexpressed in NSCLC tissues (Fig. 1B, $p < 0.001$, M–W), suggesting that *LINC00472* may be pivotal in NSCLC progression. In addition, the *LINC00472* level in BEAS-2B, NCI-H1975, NCI-H157, NCI-H358, and NCI-H1299 cells was assessed using qPCR. Compared with BEAS-2B, *LINC00472* expression was lower in 4 NSCLC cell lines,

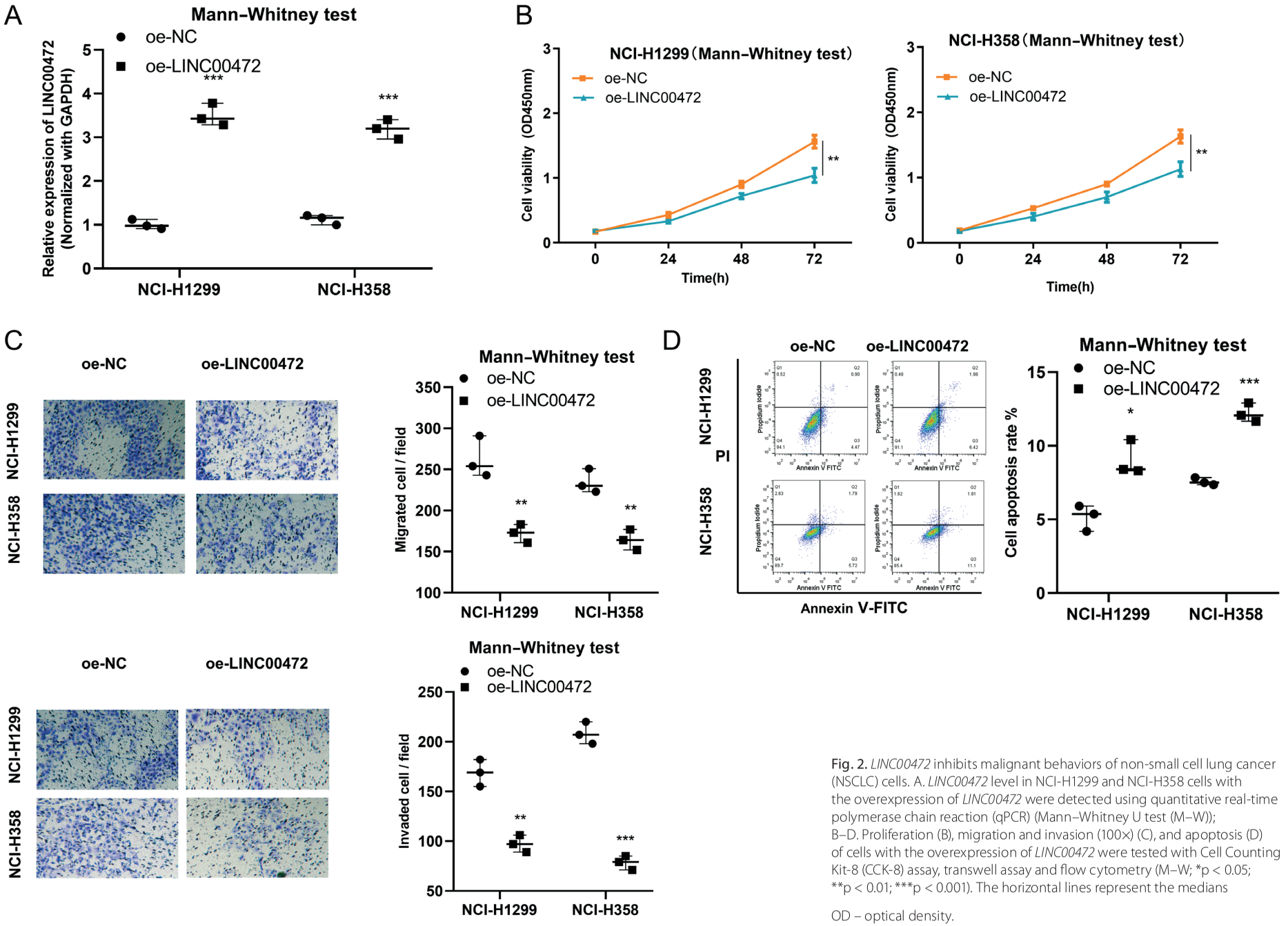


Fig. 2. *LINC00472* inhibits malignant behaviors of non-small cell lung cancer (NSCLC) cells. A. *LINC00472* level in NCI-H1299 and NCI-H358 cells with the overexpression of *LINC00472* were detected using quantitative real-time polymerase chain reaction (qPCR) (Mann–Whitney U test (M–W)); B–D. Proliferation (B), migration and invasion (100×) (C), and apoptosis (D) of cells with the overexpression of *LINC00472* were tested with Cell Counting Kit-8 (CCK-8) assay, transwell assay and flow cytometry (M–W; *p < 0.05; **p < 0.01; ***p < 0.001). The horizontal lines represent the medians

OD – optical density.

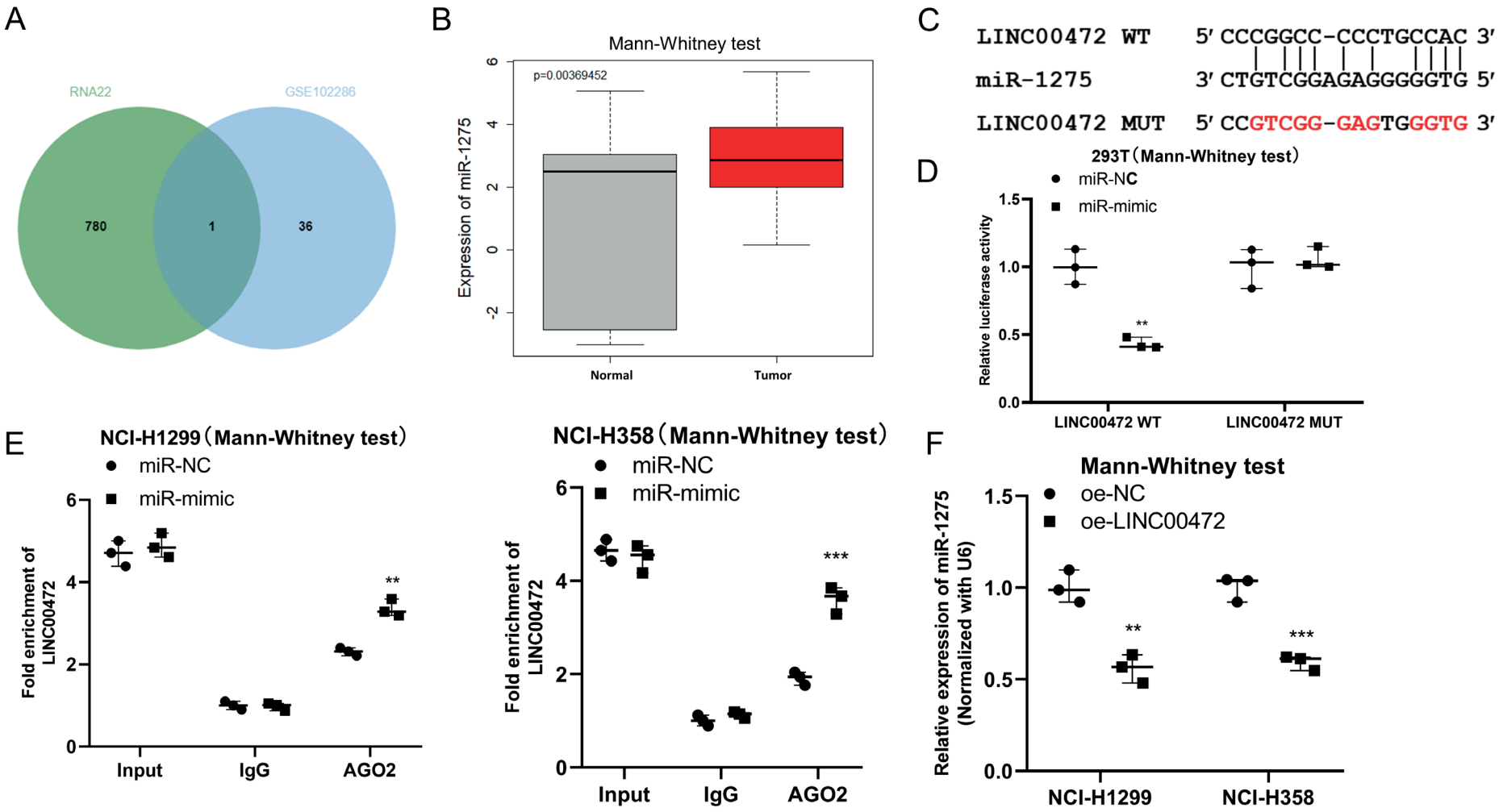


Fig. 3. *LINC00472* targets to inhibit *miR-1275* level in NSCLC cells. A. Identification of the downstream miRNA of *LINC00472*. The left side is the prediction result of the RNA22 database, the right side is the differential analysis result of the GSE102286 chip, and the overlapped part is the intersection of the 2 groups of data; B. *MiR-1275* level in normal (grey) and tumor (red) groups in GSE102286 (Mann–Whitney U test (M–W)); C. Binding sites between *LINC00472* and *miR-1275* were predicted; D. The relationship between *LINC00472* and *miR-1275* was confirmed using dual-luciferase assay (M–W); E. RNA immunoprecipitation (RIP) was used to validate the relationship between *LINC00472* and *miR-1275* in NCI-H1299 and NCI-H358 cells (M–W); F. *MiR-1275* level in cells after *LINC00472* was overexpressed (M–W; **p < 0.01; ***p < 0.001). The horizontal lines represent the medians

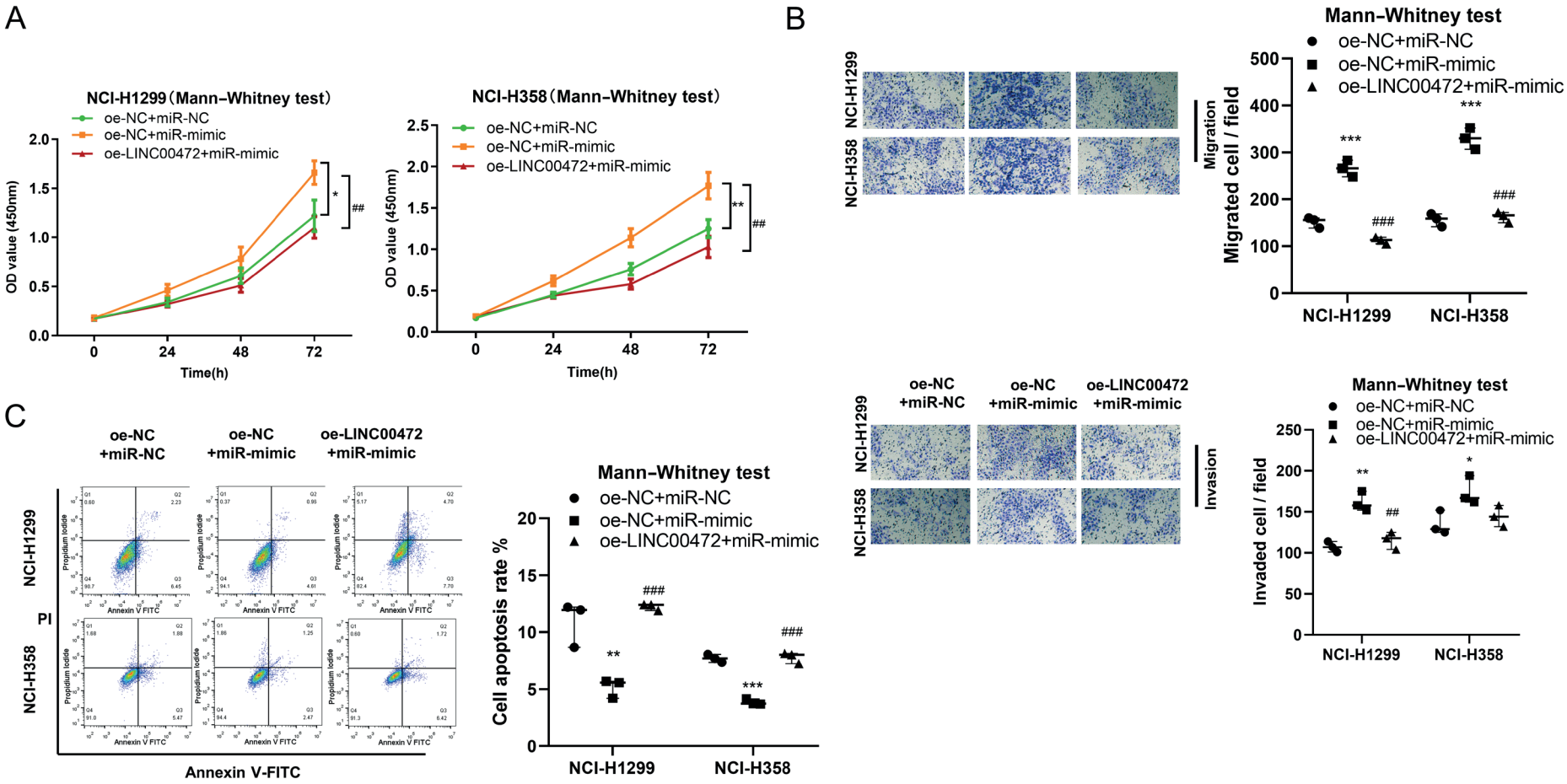


Fig. 4. *LINC00472* reverses the impact of *miR-1275* on the malignant phenotype of non-small cell lung cancer (NSCLC) cells. A–C. Proliferation (A), migration and invasion (100×) (B), and apoptosis (C) of NCI-H1299 and NCI-H358 cells were tested with Cell Counting Kit-8 (CCK-8) assay, transwell assay and flow cytometry in each group (Mann–Whitney U test). The horizontal lines represent the medians

OD – optical density; *compared to the NC group; #compared to the oe-NC+miR-mimic group; */#p < 0.05; **/##p < 0.01; ***/###p < 0.001.

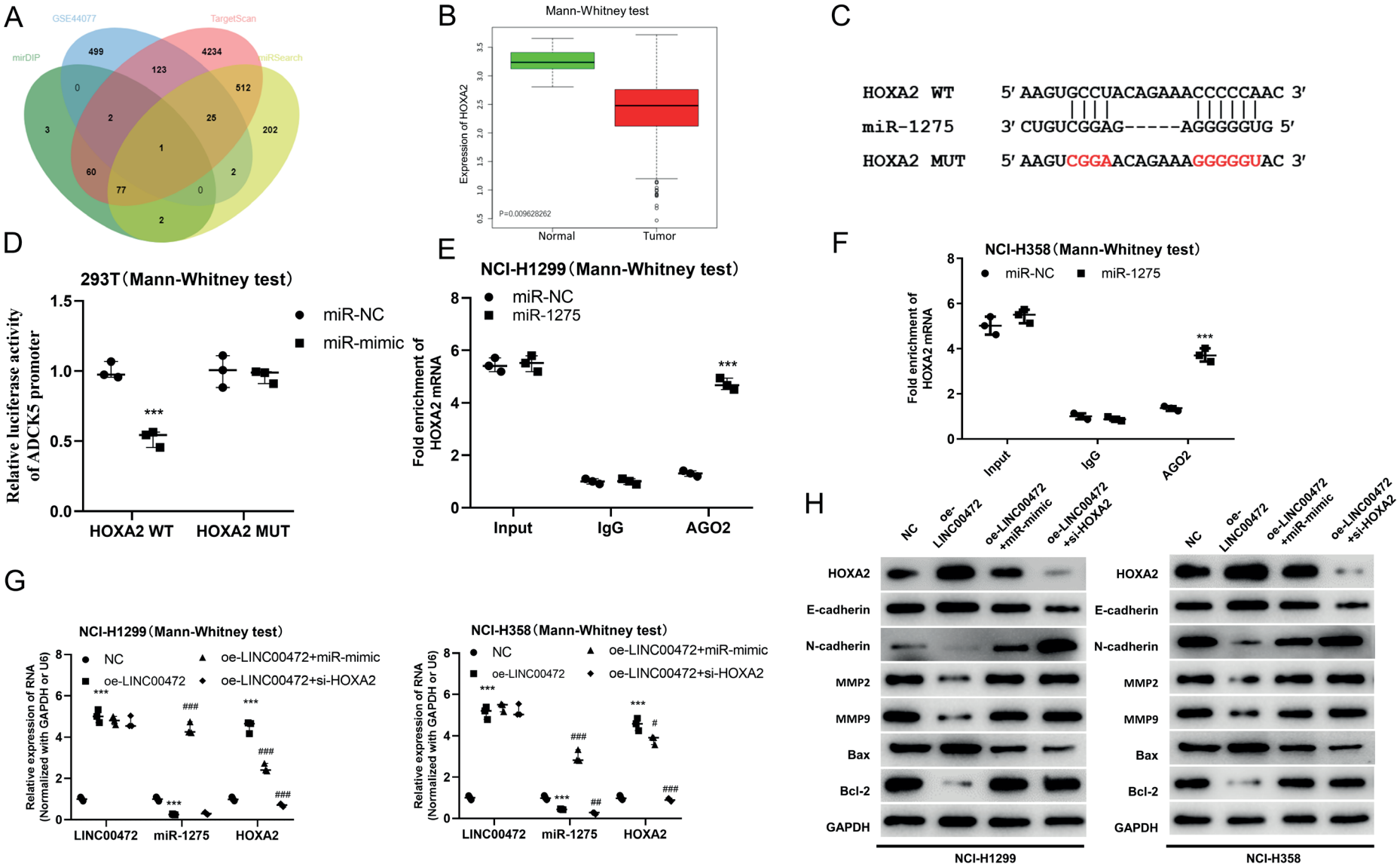


Fig. 5. *LINC00472* promotes *HOXA2* expression level and affects epithelial–mesenchymal transition (EMT), metastasis and apoptosis-related protein levels via inhibiting *miR-1275*. A. Identification of the downstream targeted gene of *miR-1275*. Four ellipses in the picture respectively represent differentially downregulated genes in GSE44077, prediction results of TargetScan database, mirDIP and miRSearch databases, and the overlapped part represents the intersection of data in 4 groups; B. Boxplot of *HOXA2* gene level in normal (green) and tumor (red) groups in GSE44077 (Mann–Whitney U test (M–W)); C. Predictive binding sites between *miR-1275* and *HOXA2*; D. The targeted relationship confirmed with dual luciferase analysis (M–W); E,F. The targeted relationship between *miR-1275* and *HOXA2* in NCI-H1299 and NCI-H358 cell lines were determined using RNA immunoprecipitation (RIP) assay (M–W); G. mRNA expression levels of *LINC00472*, *miR-1275* and *HOXA2* in each group were tested with the use of quantitative real-time polymerase chain reaction (qPCR) (M–W); H. The protein expression of *HOXA2*, *E-cadherin*, *N-cadherin*, *MMP2*, *MMP9*, *Bax*, and Bcl-2 proteins as determined using western blot. The horizontal lines represent the medians

*compared to the NC group; #compared to the oe-*LINC00472* group; */#p < 0.05; **/##p < 0.01; ***/###p < 0.001.

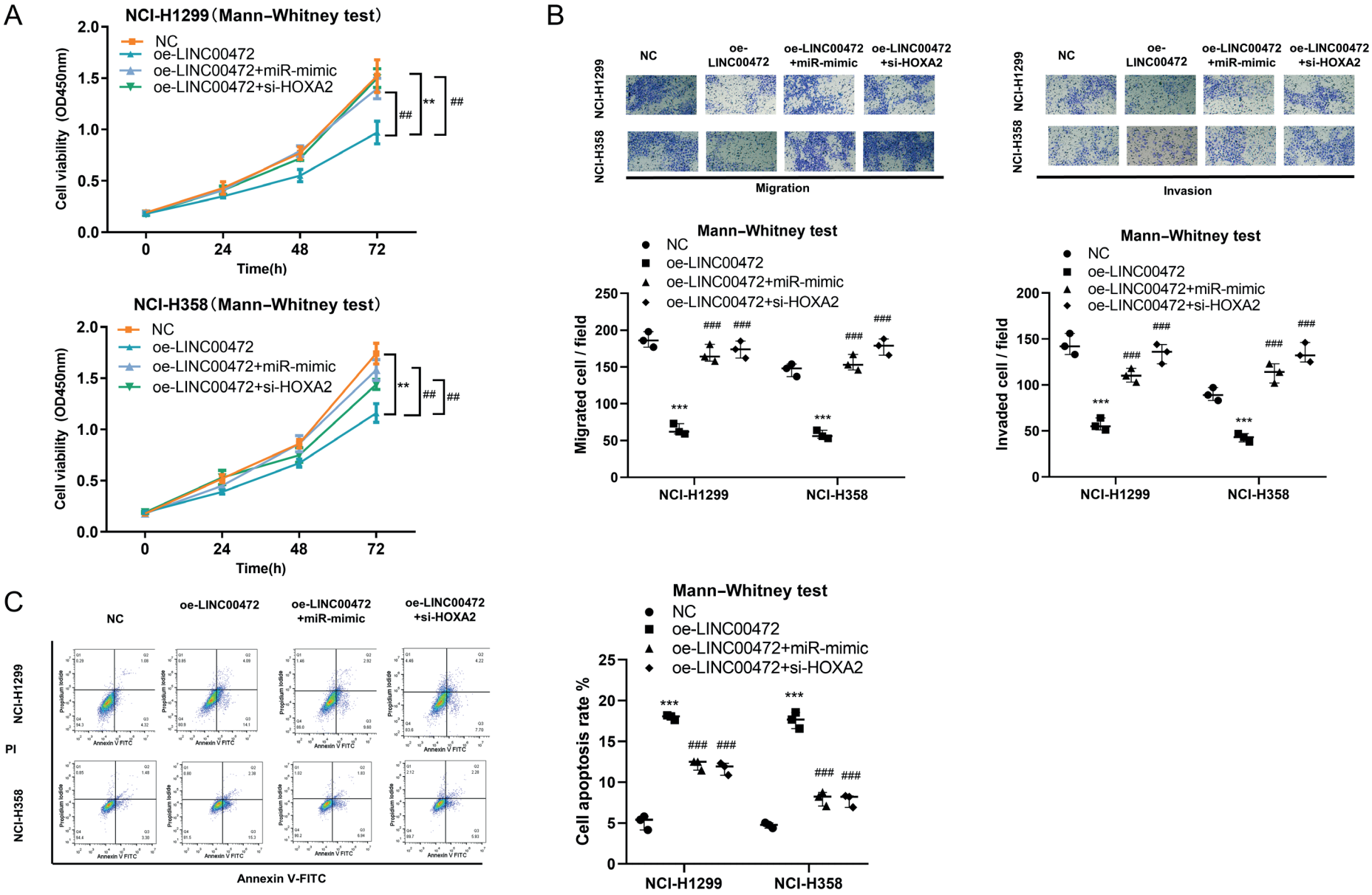


Fig. 6. *LINC00472/miR-1275/HOXA2* axis regulates the progression of non-small cell lung cancer (NSCLC) cell phenotype. A. Proliferation of NCI-H1299 and NCI-H358 cells in each treatment group was assayed using Cell Counting Kit-8 (CCK-8) assay (Mann–Whitney U test (M–W)); B. The migration and invasion of NCI-H1299 and NCI-H358 cells in each treatment group were tested using transwell assay (100×) (M–W); C. The apoptosis of NCI-H1299 and NCI-H358 cells in each treatment group was assayed using flow cytometry (M–W). The horizontal lines represent the medians

*compared to the NC group; #compared to the oe-*LINC00472* group; */#p < 0.05; **/##p < 0.01; ***/###p < 0.001.

especially in NCI-H358 and NCI-H1299 (NCI-H1975 compared to BEAS-2B, $p < 0.010$; NCI-H157 compared to BEAS-2B, $p < 0.010$; NCI-H358 compared to BEAS-2B, $p < 0.001$; NCI-H1299 compared to BEAS-2B, $p < 0.001$; Kruskal–Wallis test with Dunn's post hoc test) (Fig. 1C). Therefore, in vitro experiments were conducted on NCI-H1299 and NCI-H358 cell lines.

Previous studies have highlighted that *LINC00472* could play a modulatory role via the expression of ceRNA.[9,18] The FISH and nuclear–cytoplasm separation assays verified that *LINC00472* mainly existed in the cytoplasm (Fig. 1D, $p > 0.050$, M–W), and hence, *LINC00472*, as a ceRNA, may regulate the levels of downstream targeted genes by binding to miRNA.

## *LINC00472* represses malignant behaviors of NSCLC cells

Based on the *LINC00472* level in tumor tissues and cells, we hypothesized that *LINC00472* had a negative correlation with NSCLC progression. Therefore, we speculated that the overexpression of *LINC00472* in NSCLC cells could affect cancer progression. First, we overexpressed *LINC00472* in NCI-H1299 and NCI-H358 cells, and detected its transfection efficiency using qPCR (NCI-H1299, $p < 0.001$; NCI-H358, $p < 0.001$; M–W). Thus, the transfected cell lines could be utilized for subsequent experiments (Fig. 2A).

Then, we examined the impact of the overexpression of *LINC00472* on cell proliferation. The CCK-8 assay disclosed that the overexpression of *LINC00472* noticeably reduced the proliferative ability of both cell lines (NCI-H1299, $p < 0.010$; NCI-H358, $p < 0.010$; M–W) (Fig. 2B). Next, we assessed the influence of *LINC00472* on NSCLC cell migration and invasion, and we demonstrated notable repression (migration: NCI-H1299, $p < 0.010$; NCI-H358, $p < 0.010$; invasion: NCI-H1299, $p < 0.010$; NCI-H358, $p < 0.001$; M–W) (Fig. 2C). In addition, the cell apoptosis assay highlighted that the overexpression of *LINC00472* significantly upregulated cell apoptosis (NCI-H1299, $p < 0.050$; NCI-H358, $p < 0.001$; M–W) (Fig. 2D). Thus, *LINC00472* could be characterized as a tumor repressor by restraining malignant NSCLC cell behaviors.

## *LINC00472* sponges *miR-1275* in NSCLC cells

Modulatory miRNA downstream of *LINC00472* was predicted using the RNA22 database. Concurrently, significantly upregulated miRNAs were obtained through differential analysis of NSCLC miRNA chip GSE102286. Through the intersection of the predicted results and the differentially upregulated miRNAs (Fig. 3A), we identified *miR-1275* to be highly expressed in NSCLC tissues (Fig. 3B, $p < 0.010$, M–W).

To further understand the molecular regulatory mechanism of *LINC00472* and *miR-1275*, their binding sites were predicted through a bioinformatics analysis (Fig. 3C), which was then verified with a dual-luciferase analysis. The overexpression of *miR-1275* could inhibit luciferase activity of *LINC00472*-WT (293T, $p < 0.010$, M–W) but did not influence *LINC00472*-MUT (293T, $p > 0.050$, M–W), highlighting their targeted relationship (Fig. 3D). Subsequently, we conducted a RIP assay, which confirmed the targeted relationship (*AGO2*: NCI-H1299, $p < 0.01$; NCI-H358, $p < 0.001$; M–W) (Fig. 3E). Next, we tested *miR-1275* expression in NCI-H358 and NCI-H1299 cells after overexpressing *LINC00472*. The results demonstrated that the *miR-1275* level was significantly reduced after *LINC00472* overexpression (NCI-H1299, $p < 0.010$; NCI-H358, $p < 0.001$; M–W) (Fig. 3F). The above results unveiled a direct interaction between *LINC00472* and *miR-1275* in NSCLC, and *LINC00472* was able to be a molecular sponge of *miR-1275*.

## *LINC00472* mitigates the influence of *miR-1275* on NSCLC malignant phenotypes

To demonstrate that *LINC00472* could regulate the biological function of cells by binding to *miR-1275*, we carried out rescue experiments in NCI-H358 and NCI-H1299 cells. According to the results of the CCK-8 assay, proliferative potential of cells was significantly increased upon *miR-1275* overexpression, while it returned to normal level when *LINC00472* and *miR-1275* were overexpressed at the same time (NCI-H1299, oe-NC+miR-mimic compared to oe-NC+miR-NC, $p < 0.050$; oe-*LINC00472*+miR-mimic compared to oe-NC+miR-mimic, $p < 0.010$; NCI-H358, oe-NC+miR-mimic compared to oe-NC+miR-NC, $p < 0.010$; oe-*LINC00472*+miR-mimic compared to oe-NC+miR-mimic, $p < 0.010$; M–W) (Fig. 4A). Forced overexpression of *miR-1275* significantly enhanced cell migratory and invasive properties, while simultaneous overexpression of *LINC00472* and *miR-1275* significantly decreased these traits (migration: NCI-H1299, oe-NC+miR-mimic compared to oe-NC+miR-NC, $p < 0.001$; oe-*LINC00472*+miR-mimic compared to oe-NC+miR-mimic, $p < 0.001$; NCI-H358, oe-NC+miR-mimic compared to oe-NC+miR-NC, $p < 0.001$; oe-*LINC00472*+miR-mimic compared to oe-NC+miR-mimic, $p < 0.001$; invasion: NCI-H1299, oe-NC+miR-mimic compared to oe-NC+miR-NC, $p < 0.010$; oe-*LINC00472*+miR-mimic compared to oe-NC+miR-mimic, $p < 0.010$; NCI-H358, oe-NC+miR-mimic compared to oe-NC+miR-NC; $p < 0.050$, oe-*LINC00472*+miR-mimic compared to oe-NC+miR-mimic, $p > 0.050$; M–W) (Fig. 4B). The apoptosis assay showed that the concurrent overexpression of both *LINC00472* and *miR-1275* could reverse the repressive effect of *miR-1275* on apoptosis rate (NCI-H1299, oe-NC+miR-mimic compared to oe-NC+miR-NC, $p < 0.010$; oe-*LINC00472*+miR-mimic

compared to oe-NC+miR-mimic, $p < 0.001$; NCI-H358, oe-NC+miR-mimic compared to oe-NC+miR-NC, $p < 0.001$; oe-*LINC00472*+miR-mimic compared to oe-NC+miR-mimic, $p < 0.001$; M–W) (Fig. 4C). Therefore, *LINC00472* could reverse the influence of *miR-1275* on NSCLC malignant cell phenotype progression.

## *LINC00472* promotes *HOXA2* expression level by restraining *miR-1275*

Targeted genes downstream of *miR-1275* were predicted using miRSearch, TargetScan and mirDIP databases, and overlapped with differentially downregulated genes screened in the GSE44077 chip (Fig. 5A). The *HOXA2* was obtained, and its expression level in GSE44077 was noticeably downregulated (Fig. 5B, $p < 0.001$, M–W). Our bioinformatics approach showed that *miR-1275* and *HOXA2* had targeted binding sites (Fig. 5C), and the overexpression of *miR-1275* repressed luciferase activity of *HOXA2*-WT (293T, $p < 0.001$, M–W) but did not affect the luciferase activity of *HOXA2*-MUT (293T, $p > 0.05$, M–W) (Fig. 5D), indicating that *miR-1275* could target *HOXA2*. Concurrently, the experimental RIP results demonstrated a binding relationship between *HOXA2* and *miR-1275* (*AGO2*: NCI-H1299, $p < 0.001$; NCI-H358, $p < 0.001$; M–W) (Fig. 5E,F). The above results indicate that *LINC00472* competitively bound to *miR-1275* with *HOXA2*. Using qPCR assay, we denoted that when *LINC00472* was overexpressed, the mRNA level of *miR-1275* was significantly downregulated, while the *HOXA2* level was markedly increased. In addition to *LINC00472* overexpression, simultaneous upregulation of *miR-1275* or silencing of *HOXA2* partially rescued the impact of *LINC00472* overexpression on *HOXA2* mRNA expression level (details of statistical analysis are presented in Table 4). It is commonly known that matrix metalloproteinase (*MMP*) and epithelial–mesenchymal transition (EMT)-related proteins are vital biomarkers associated with tumor metastasis.[36–39] We used western blot analysis to investigate protein levels of EMT-related proteins in order to ascertain whether the *LINC00472*/*miR-1275*/*HOXA2* axis is related to EMT processes and apoptosis in NSCLC. After overexpressing *LINC00472*, the *E-cadherin* level was notably upregulated, but levels of *N-cadherin*, *MMP2* and *MMP9* were significantly decreased. Meanwhile, we explored protein levels of the apoptosis-related *Bax* and *Bcl-2*, and found that the overexpression of *LINC00472* enhanced pro-apoptotic *Bax* protein level but reduced anti-apoptotic protein *Bcl-2* level. Moreover, the overexpression of *miR-1275* or silencing of *HOXA2* partly rescued or even reversed the expression of the above proteins (Fig. 5H). These results highlight that *LINC00472* could promote *HOXA2* level and affect the expression of EMT, metastasis and apoptosis-related proteins by inhibiting *miR-1275*.

## *LINC00472*/*miR-1275*/*HOXA2* axis regulates NSCLC cell phenotype progression

To verify whether *LINC00472* exerted its anti-cancer effect by targeting *miR-1275* to regulate *HOXA2*, we conducted rescue experiments in NCI-H358 and NCI-H1299 cell lines. The overexpression of *LINC00472* repressed cell proliferation, migration and invasion, and promoted apoptosis, while further forced *miR-1275* expression offset the abovementioned suppressive effects (details of statistical analysis are presented in Table 5) (Fig. 6A–C). Interestingly, simultaneous overexpression of *LINC00472* and silencing of *HOXA2* also largely rescued the inhibition of *LINC00472* on malignant phenotype found in NSCLC cells (Fig. 6A–C). The above results show that the overexpression of *LINC00472* regulated *HOXA2* by targeting *miR-1275* to inhibit the proliferation, migration and invasion of NSCLC cells and promote apoptosis. These findings, combined with previous studies, demonstrate that *LINC00472* plays an essential role in regulating NSCLC cells by competitively sponging *miR-1275* with *HOXA2*.

# Discussion

Over the past 2 decades, NSCLC treatment has undergone tremendous changes. A deeper understanding of the mechanism of cancer pathogenesis has made early

**Table 4.** Statistical analysis of the expression levels of *LINC00472*, *miR-1275* and *HOXA2* in NCI-H1299 and NCI-H358 cells of each treatment group (Mann–Whitney U test; cf. Fig. 5G)

| Cell lines | Group | oe-LINC00472 compared to NC | oe-LINC00472+miR-mimic compared to oe-LINC00472 | oe-LINC00472+si-HOXA2 compared to oe-LINC00472 |
|---|---|---|---|---|
| NCI-H1299 | *LINC00472* | $p < 0.001$ | $p > 0.050$ | $p > 0.050$ |
| | *miR-1275* | $p < 0.001$ | $p < 0.001$ | $p > 0.050$ |
| | *HOXA2* | $p < 0.001$ | $p < 0.001$ | $p < 0.001$ |
| NCI-H358 | *LINC00472* | $p < 0.001$ | $p > 0.050$ | $p > 0.050$ |
| | *miR-1275* | $p < 0.001$ | $p < 0.001$ | $p < 0.010$ |
| | *HOXA2* | $p < 0.001$ | $p < 0.050$ | $p < 0.001$ |

NC – negative control.

**Table 5.** Statistical analysis of NCI-H1299 and NCI-H358 cell viability, migration, invasion, and apoptosis rate in each treatment group (Mann–Whitney U test; cf. Fig. 6A–C)

| Analysis project | Group | oe-LINC00472 compared to NC | oe-LINC00472+miR-mimic compared to oe-LINC00472 | oe-LINC00472+si-HOXA2 compared to oe-LINC00472 |
|---|---|---|---|---|
| Cell viability | NCI-H1299 | $p < 0.010$ | $p < 0.010$ | $p < 0.010$ |
| | NCI-H358 | $p < 0.010$ | $p < 0.010$ | $p < 0.010$ |
| Migration | NCI-H1299 | $p < 0.001$ | $p < 0.001$ | $p < 0.001$ |
| | NCI-H358 | $p < 0.001$ | $p < 0.001$ | $p < 0.001$ |
| Invasion | NCI-H1299 | $p < 0.001$ | $p < 0.001$ | $p < 0.001$ |
| | NCI-H358 | $p < 0.001$ | $p < 0.001$ | $p < 0.001$ |
| Apoptosis rate | NCI-H1299 | $p < 0.001$ | $p < 0.001$ | $p < 0.001$ |
| | NCI-H358 | $p < 0.001$ | $p < 0.001$ | $p < 0.001$ |

NC – negative control.

diagnosis and the development of new targeted therapies possible.[40] Precision medicine is the trend of the times, so it is urgent to uncover novel NSCLC biomarkers. Mounting evidence shows that lncRNAs are involved in cancer growth, differentiation, metastasis, and apoptosis.[8,41] We investigated the role of *LINC00472* in the progression of NSCLC and explored its regulatory mechanism.

Herein, we demonstrated that *LINC00472* and *HOXA2* expression was reduced, and *miR-1275* level was elevated in NSCLC tissues and cells. According to previous studies, *LINC-PINT*[42] and *FENDRR*[43] also have reduced expression in NSCLC similar to *LINC00472*, and act as antitumor lncRNAs, able to inhibit the progression of NSCLC. However, other lncRNAs such as LINC01561,[44] *HOTAIR*[45] and *H19*[46] are overexpressed in NSCLC and promote its progression. Lung cancer progression is closely related to changes in *HOX* gene expression, and the *HOXA* family of genes is usually downregulated in primary NSCLC.[47] For example, *HOXA9* is directly downregulated by *miR-196b*, and regulates NSCLC invasion potential by regulating *nuclear factor-kappa B* (*NF-κB*) activity.[48] The *HOXC* and *HOXD* family genes (such as *HOXC4*, *HOXC8*, *HOXC9*, *HOXC13*, *HOXD8*, and *HOXD10*) are highly expressed in LC[47,49] and are pivotal in promoting cancer. Following the previous studies on *HOXA* family genes, we found that *HOXA2* was downregulated in NSCLC and can act as a tumor repressor of cell malignant progression. Deng et al. disclosed that *LINC00472* represses EMT in lung adenocarcinoma, but the overexpression of *YBX1* restores the EMT phenotype.[50] Our results showed that *LINC00472* constrained EMT, but further overexpression of *miR-1275* or knockdown of *HOXA2* restored EMT, in agreement with the findings of the previous studies.

To further explore the regulatory role of *LINC00472* in NSCLC, we conducted a bioinformatics analysis on *LINC00472* and found the downstream gene *miR-1275*. One study has found that *miR-1275* is upregulated in lung adenocarcinoma, which can play a tumorigenic role by co-activating the *Wnt/β-catenin* and Notch signaling pathways in lung adenocarcinoma.[51] Another study shows that lncRNA *FAM225A* can promote the occurrence and metastasis of nasopharyngeal carcinoma by targeting *miR-590-3p*/*miR-1275* and upregulating *ITGB3*.[24] Our study demonstrated that *miR-1275* was highly expressed in NSCLC. The *LINC00472* could regulate the proliferation, migration and invasion of NSCLC cells by targeting *miR-1275*, which is consistent with and builds upon previous research. Our data enrich the known regulatory network of *miR-1275* in NSCLC.

Furthermore, we found that *LINC00472* could combine with *miR-1275*, while *miR-1275* targeted *HOXA2* directly. The overexpression of *LINC00472* constrained *miR-1275* expression and increased *HOXA2* level, while the overexpression of *miR-1275* restrained *HOXA2* levels. In a study regarding the lncRNA–miRNA–mRNA signaling axis, Zhang et al. found that a low expression of *LINC00472* in osteosarcoma can control the expression of *FOXO1* by targeting *miR-300*, to regulate the occurrence of osteosarcoma.[52] Ye et al. displayed the stimulatory effect of *LINC00472* on apoptosis in CRC cells.[9] We elucidated that the overexpression of *LINC00472* facilitated apoptosis of NSCLC cancer cells, but the upregulation of *miR-1275* or silencing of *HOXA2* repressed this occurrence. To the best of our knowledge, this study is the first investigation regarding the *LINC00472*/*miR-1275* axis in NSCLC. The *HOXA2* is targeted by several miRNAs in a variety of cell types. For example, miR-135 in adipose tissue-derived stem cells targets *HOXA2* to promote bone and skeleton regeneration,[53] and in vascular smooth muscle cells (VSMCs), *miR-3960* targets *HOXA2* to promote osteogenic trans-differentiation.[54] The current study is our first investigation on the targeted relationship between *miR-1275* and *HOXA2*.

Furthermore, we found that *LINC00472* could restrain NSCLC malignant cell phenotype, while forced expression of *miR-1275* or silencing of *HOXA2* partially rescued or even reversed the impact of *LINC00472* upregulation alone on NSCLC cell biological behaviors. According to the report by Zhang et al., *LINC-PINT* displays reduced expression in NSCLC. The *LINC-PINT*, as a sponge

of *miR-543*, increases *PTEN* level, thereby inhibiting NSCLC growth and migration, blocking cells in the G1 phase and promoting apoptosis.[42] After a critical review of the above studies, we believe that *LINC00472* also functions as a sponge of *miR-1275* to affect *HOXA2* levels, thus inhibiting the progression of NSCLC. The lncRNA *HOTAIR* is an important indicator of NSCLC diagnosis and treatment, and it can facilitate the malignant procession of LC cells.[55] Our study also provides possible molecular markers for NSCLC diagnosis and therapy. Moreover, *miR-1275* can facilitate the proliferation, invasion and migration of squamous cell head and neck carcinoma by increasing *IGF-1R* and *CCR7*.[56] Conversely, silencing *miR-1275* can significantly restrain the growth of gliomas by increasing the *Claudin11* protein level.[57] Furthermore, *miR-1275* can also target *ELK1* to suppress the differentiation of human visceral preadipocytes and inhibit obesity.[58] The methylation level of *miR-1275* is closely related to the pathogenesis of NSCLC, and *HOXA2* is a gene that is specifically methylated in NSCLC tumors.[59] Based on previous research results and the results of this study, we reasonably speculated that the *LINC00472*/*miR-1275*/*HOXA2* axis may be a candidate therapeutic target in NSCLC.

## Limitations

The sample size of this study was limited, and future research would benefit from a larger, more diverse study population.

# Conclusions

This study shows that the overexpression of *LINC00472* can enhance *HOXA2* level via the repression of *miR-1275* level, thus regulating proliferation, migration, invasion, apoptosis, and EMT progression of NSCLC cells. Our research provided evidence for the connection between *LINC00472*, *miR-1275* and *HOXA2*, but also offered a novel path for NSCLC therapy.

## Supplementary data

The supplementary materials are available at https://doi.org/10.5281/zenodo.8053329. The package contains the following files:

Supplementary Materials. Analysis of normal distribution of genes.

### ORCID iDs

Meichen Jiang https://orcid.org/0009-0007-7326-9480
Xiangli Ye https://orcid.org/0009-0001-5596-5120
Dongliang Shi https://orcid.org/0009-0003-1263-4529
Qili Lin https://orcid.org/0009-0009-8998-3202
Feijian Huang https://orcid.org/0009-0000-4904-677X
Yong Li https://orcid.org/0000-0002-5842-3722

## References

1. Siegel RL, Miller KD, Jemal A. Cancer statistics, 2019. *CA Cancer J Clin*. 2019;69(1):7–34. doi:10.3322/caac.21551
2. Rabe KF. Precision diagnosis and treatment for advanced non-small-cell lung cancer. *N Engl J Med*. 2017;377(9):849–861. doi:10.1056/NEJMra1703413
3. Travis WD, Brambilla E, Burke AP, Marx A, Nicholson AG. Introduction to The 2015 World Health Organization Classification of Tumors of the Lung, Pleura, Thymus, and Heart. *J Thorac Oncol*. 2015;10(9):1240–1242. doi:10.1097/JTO.0000000000000663
4. Osmani L, Askin F, Gabrielson E, Li QK. Current WHO guidelines and the critical role of immunohistochemical markers in the subclassification of non-small cell lung carcinoma (NSCLC): Moving from targeted therapy to immunotherapy. *Semin Cancer Biol*. 2018;52(Pt 1):103–109. doi:10.1016/j.semcancer.2017.11.019
5. Travis WD, Brambilla E, Nicholson AG, et al. The 2015 World Health Organization Classification of Lung Tumors: Impact of genetic, clinical and radiologic advances since the 2004 classification. *J Thorac Oncol*. 2015;10(9):1243–1260. doi:10.1097/JTO.0000000000000630
6. Hirsch FR, Scagliotti GV, Mulshine JL, et al. Lung cancer: Current therapies and new targeted treatments. *Lancet*. 2017;389(10066):299–311. doi:10.1016/S0140-6736(16)30958-8
7. Fang Y, Fullwood MJ. Roles, functions, and mechanisms of long noncoding RNAs in cancer. *Genomics Proteomics Bioinformatics*. 2016;14(1):42–54. doi:10.1016/j.gpb.2015.09.006
8. Bhan A, Soleimani M, Mandal SS. Long noncoding RNA and cancer: A new paradigm. *Cancer Res*. 2017;77(15):3965–3981. doi:10.1158/0008-5472.CAN-16-2634
9. Ye Y, Yang S, Han Y, et al. Linc00472 suppresses proliferation and promotes apoptosis through elevating PDCD4 expression by sponging miR-196a in colorectal cancer. *Aging (Albany NY)*. 2018;10(6):1523–1533. doi:10.18632/aging.101488
10. Sanchez Calle A, Kawamura Y, Yamamoto Y, Takeshita F, Ochiya T. Emerging roles of long non-coding RNA in cancer. *Cancer Sci*. 2018;109(7):2093–2100. doi:10.1111/cas.13642
11. Shen Y, Wang Z, Loo LW, et al. LINC00472 expression is regulated by promoter methylation and associated with disease-free survival in patients with grade 2 breast cancer. *Breast Cancer Res Treat*. 2015;154(3):473–482. doi:10.1007/s10549-015-3632-8
12. Wang Z, Katsaros D, Biglia N, et al. ERα upregulates the expression of long non-coding RNA LINC00472 which suppresses the phosphorylation of NF-κB in breast cancer. *Breast Cancer Res Treat*. 2019;175(2):353–368. doi:10.1007/s10549-018-05108-5
13. Shen Y, Katsaros D, Loo LWM, et al. Prognostic and predictive values of long non-coding RNA *LINC00472* in breast cancer. *Oncotarget*. 2015;6(11):8579–8592. doi:10.18632/oncotarget.3287
14. Fu Y, Biglia N, Wang Z, et al. Long non-coding RNAs, ASAP1-IT1, FAM215A, and LINC00472, in epithelial ovarian cancer. *Gynecol Oncol*. 2016;143(3):642–649. doi:10.1016/j.ygyno.2016.09.021
15. Chen C, Zheng Q, Kang W, Yu C. Long non-coding RNA LINC00472 suppresses hepatocellular carcinoma cell proliferation, migration and invasion through miR-93-5p/PDCD4 pathway. *Clin Res Hepatol Gastroenterol*. 2019;43(4):436–445. doi:10.1016/j.clinre.2018.11.008
16. Chen Y, Pan Y, Ji Y, Sheng L, Du X. Network analysis of differentially expressed smoking-associated mRNAs, lncRNAs and miRNAs reveals key regulators in smoking-associated lung cancer. *Exp Ther Med*. 2018;16(6):4991–5002. doi:10.3892/etm.2018.6891
17. Zhu TG, Xiao X, Wei Q, Yue M, Zhang LX. Revealing potential long non-coding RNA biomarkers in lung adenocarcinoma using long non-coding RNA-mediated competitive endogenous RNA network. *Braz J Med Biol Res*. 2017;50(9):e6297. doi:10.1590/1414-431x20176297
18. Sui J, Li YH, Zhang YQ, et al. Integrated analysis of long non-coding RNA-associated ceRNA network reveals potential lncRNA biomarkers in human lung adenocarcinoma. *Int J Oncol*. 2016;49(5):2023–2036. doi:10.3892/ijo.2016.3716
19. Liu J, Song S, Lin S, et al. Circ-SERPINE2 promotes the development of gastric carcinoma by sponging miR-375 and modulating *YWHAZ*. *Cell Prolif*. 2019;52(4):e12648. doi:10.1111/cpr.12648
20. Bica-Pop C, Cojocneanu-Petric R, Magdo L, Raduly L, Gulei D, Berindan-Neagoe I. Overview upon miR-21 in lung cancer: Focus on NSCLC. *Cell Mol Life Sci*. 2018;75(19):3539–3551. doi:10.1007/s00018-018-2877-x

21. Liu M, Zhang Y, Zhang J, et al. MicroRNA-1253 suppresses cell proliferation and invasion of non-small-cell lung carcinoma by targeting WNT5A. *Cell Death Dis*. 2018;9(2):189. doi:10.1038/s41419-017-0218-x
22. Gao P, Wang H, Yu J, et al. miR-3607-3p suppresses non-small cell lung cancer (NSCLC) by targeting TGFBR1 and CCNE2. *PLoS Genet*. 2018;14(12):e1007790. doi:10.1371/journal.pgen.1007790
23. Xie H, Huang H, Huang W, Xie Z, Yang Y, Wang F. LncRNA miR143HG suppresses bladder cancer development through inactivating Wnt/β-catenin pathway by modulating miR-1275/AXIN2 axis. *J Cell Physiol*. 2019;234(7):11156–11164. doi:10.1002/jcp.27764
24. Zheng ZQ, Li ZX, Zhou GQ, et al. Long noncoding RNA FAM225A promotes nasopharyngeal carcinoma tumorigenesis and metastasis by acting as ceRNA to sponge miR-590-3p/miR-1275 and upregulate ITGB3. *Cancer Res*. 2019;79(18):4612–4626. doi:10.1158/0008-5472.CAN-19-0799
25. Xie C, Wu Y, Fei Z, Fang Y, Xiao S, Su H. MicroRNA-1275 induces radiosensitization in oesophageal cancer by regulating epithelial-to-mesenchymal transition via Wnt/β-catenin pathway. *J Cell Mol Med*. 2020;24(1):747–759. doi:10.1111/jcmm.14784
26. Feng J, Li J, Qie P, Li Z, Xu Y, Tian Z. Long non-coding RNA (lncRNA) PGM5P4-AS1 inhibits lung cancer progression by up-regulating leucine zipper tumor suppressor (LZTS3) through sponging microRNA miR-1275. *Bioengineered*. 2021;12(1):196–207. doi:10.1080/21655979.2020.1860492
27. Li L, Zhang X, Liu Q, et al. Emerging role of HOX genes and their related long noncoding RNAs in lung cancer. *Crit Rev Oncol Hematol*. 2019;139:1–6. doi:10.1016/j.critrevonc.2019.04.019
28. Zhang B, Li N, Zhang H. Knockdown of homeobox B5 (HOXB5) inhibits cell proliferation, migration, and invasion in non-small cell lung cancer cells through inactivation of the Wnt/beta-Catenin pathway. *Oncol Res*. 2018;26(1):37–44. doi:10.3727/096504017X14900530835262
29. Li D, Bai Y, Feng Z, et al. Study of promoter methylation patterns of HOXA2, HOXA5, and HOXA6 and its clinicopathological characteristics in colorectal cancer. *Front Oncol*. 2019;9:394. doi:10.3389/fonc.2019.00394
30. Li HP, Peng CC, Chung IC, et al. Aberrantly hypermethylated homeobox A2 derepresses metalloproteinase-9 through TBP and promotes invasion in nasopharyngeal carcinoma. *Oncotarget*. 2013;4(11):2154–2165. doi:10.18632/oncotarget.1367
31. Tapia-Carrillo D, Tovar H, Velazquez-Caldelas TE, Hernandez-Lemus E. Master regulators of signaling pathways: An application to the analysis of gene regulation in breast cancer. *Front Genet*. 2019;10:1180. doi:10.3389/fgene.2019.01180
32. Liu Z, Shen F, Wang H, et al. Abnormally high expression of HOXA2 as an independent factor for poor prognosis in glioma patients. *Cell Cycle*. 2020;19(13):1632–1640. doi:10.1080/15384101.2020.1762038
33. Hata A, Nakajima T, Matsusaka K, et al. A low DNA methylation epigenotype in lung squamous cell carcinoma and its association with idiopathic pulmonary fibrosis and poorer prognosis. *Int J Cancer*. 2020;146(2):388–399. doi:10.1002/ijc.32532
34. Ritchie ME, Phipson B, Wu D, et al. limma powers differential expression analyses for RNA-sequencing and microarray studies. *Nucleic Acids Res*. 2015;43(7):e47. doi:10.1093/nar/gkv007
35. Venkatesh B, Finfer S, Cohen J, et al. Adjunctive glucocorticoid therapy in patients with septic shock. *N Engl J Med*. 2018;378(9):797–808. doi:10.1056/NEJMoa1705835
36. Wang W, Li D, Xiang L, et al. TIMP-2 inhibits metastasis and predicts prognosis of colorectal cancer via regulating MMP-9. *Cell Adh Migr*. 2019;13(1):272–283. doi:10.1080/19336918.2019.1639303
37. Zhang S, Yang Y, Huang S, et al. SIRT1 inhibits gastric cancer proliferation and metastasis via STAT3/MMP-13 signaling. *J Cell Physiol*. 2019;234(9):15395–15406. doi:10.1002/jcp.28186
38. Tian S, Peng P, Li J, et al. SERPINH1 regulates EMT and gastric cancer metastasis via the Wnt/β-catenin signaling pathway. *Aging (Albany NY)*. 2020;12(4):3574–3593. doi:10.18632/aging.102831
39. Zhang H, Wang J, Yin Y, Meng Q, Lyu Y. The role of EMT-related lncRNA in the process of triple-negative breast cancer metastasis. *Biosci Rep*. 2021;41(2):BSR20203121. doi:10.1042/BSR20203121
40. Herbst RS, Morgensztern D, Boshoff C. The biology and management of non-small cell lung cancer. *Nature*. 2018;553(7689):446–454. doi:10.1038/nature25183
41. Fatica A, Bozzoni I. Long non-coding RNAs: New players in cell differentiation and development. *Nat Rev Genet*. 2014;15(1):7–21. doi:10.1038/nrg3606
42. Wang S, Jiang W, Zhang X, et al. LINC-PINT alleviates lung cancer progression via sponging miR-543 and inducing PTEN. *Cancer Med*. 2020;9(6):1999–2009. doi:10.1002/cam4.2822
43. Zhang G, Wang Q, Zhang X, Ding Z, Liu R. LncRNA FENDRR suppresses the progression of NSCLC via regulating miR-761/TIMP2 axis. *Biomed Pharmacother*. 2019;118:109309. doi:10.1016/j.biopha.2019.109309
44. Gao W, Qi C, Feng M, Yang P, Liu L, Sun S. SOX2-induced upregulation of lncRNA LINC01561 promotes non-small-cell lung carcinoma progression by sponging miR-760 to modulate SHCBP1 expression. *J Cell Physiol*. 2020;235(10):6684–6696. doi:10.1002/jcp.29564
45. Jiang C, Yang Y, Yang Y, et al. Long noncoding RNA (lncRNA) HOTAIR affects tumorigenesis and metastasis of non-small cell lung cancer by upregulating miR-613. *Oncol Res*. 2018;26(5):725–734. doi:10.3727/096504017X15119467381615
46. Huang Z, Lei W, Hu H, Zhang H, Zhu Y. H19 promotes non-small-cell lung cancer (NSCLC) development through STAT3 signaling via sponging miR-17. *J Cell Physiol*. 2018;233(10):6768–6776. doi:10.1002/jcp.26530
47. Bhatlekar S, Fields JZ, Boman BM. HOX genes and their role in the development of human cancers. *J Mol Med (Berl)*. 2014;92(8):811–823. doi:10.1007/s00109-014-1181-y
48. Yu SL, Lee DC, Sohn HA, et al. Homeobox A9 directly targeted by miR-196b regulates aggressiveness through nuclear factor-kappa B activity in non-small cell lung cancer cells. *Mol Carcinog*. 2016;55(12):1915–1926. doi:10.1002/mc.22439
49. Omatu T. Overexpression of human homeobox gene in lung cancer A549 cells results in enhanced motile and invasive properties [in Japanese]. *Hokkaido Igaku Zasshi*. 1999;74(5):367–376. PMID:10495851.
50. Deng X, Xiong W, Jiang X, et al. LncRNA LINC00472 regulates cell stiffness and inhibits the migration and invasion of lung adenocarcinoma by binding to YBX1. *Cell Death Dis*. 2020;11(11):945. doi:10.1038/s41419-020-03147-9
51. Jiang N, Zou C, Zhu Y, et al. HIF-1α-regulated miR-1275 maintains stem cell-like phenotypes and promotes the progression of LUAD by simultaneously activating Wnt/β-catenin and Notch signaling. *Theranostics*. 2020;10(6):2553–2570. doi:10.7150/thno.41120
52. Zhang J, Zhang J, Zhang D, Ni W, Xiao H, Zhao B. Down-regulation of LINC00472 promotes osteosarcoma tumorigenesis by reducing FOXO1 expressions via miR-300. *Cancer Cell Int*. 2020;20:100. doi:10.1186/s12935-020-01170-6
53. Xie Q, Wang Z, Zhou H, et al. The role of miR-135-modified adipose-derived mesenchymal stem cells in bone regeneration. *Biomaterials*. 2016;75:279–294. doi:10.1016/j.biomaterials.2015.10.042
54. Xia ZY, Hu Y, Xie PL, et al. Runx2/miR-3960/miR-2861 positive feedback loop is responsible for osteogenic transdifferentiation of vascular smooth muscle cells. *Biomed Res Int*. 2015;2015:624037. doi:10.1155/2015/624037
55. Loewen G, Jayawickramarajah J, Zhuo Y, Shan B. Functions of lncRNA HOTAIR in lung cancer. *J Hematol Oncol*. 2014;7:90. doi:10.1186/s13045-014-0090-4
56. Liu MD, Wu H, Wang S, et al. MiR-1275 promotes cell migration, invasion and proliferation in squamous cell carcinoma of head and neck via up-regulating IGF-1R and CCR7. *Gene*. 2018;646:1–7. doi:10.1016/j.gene.2017.12.049
57. Katsushima K, Shinjo K, Natsume A, et al. Contribution of microRNA-1275 to Claudin11 protein suppression via a polycomb-mediated silencing mechanism in human glioma stem-like cells. *J Biol Chem*. 2012;287(33):27396–27406. doi:10.1074/jbc.M112.359109
58. Pang L, You L, Ji C, et al. miR-1275 inhibits adipogenesis via ELK1 and its expression decreases in obese subjects. *J Mol Endocrinol*. 2016;57(1):33–43. doi:10.1530/JME-16-0007
59. Heller G, Babinsky VN, Ziegler B, et al. Genome-wide CpG island methylation analyses in non-small cell lung cancer patients. *Carcinogenesis*. 2013;34(3):513–521. doi:10.1093/carcin/bgs363

# Long COVID and its cardiovascular consequences: What is known?

Justyna Aleksandra Składanek[1,A–F], Michał Leśkiewicz[1,A–F], Karolina Gumiężna[1,B–D,F], Piotr Baruś[1,B,E,F], Adam Piasecki[1,C,E,F], Dominika Klimczak-Tomaniak[2,3,C,E,F], Grażyna Sygitowicz[4,C,E,F], Janusz Kochman[1,C,E,F], Marcin Grabowski[1,C,E,F], Mariusz Tomaniak[1,A–F]

[1] First Department of Cardiology, Medical University of Warsaw, Poland
[2] Department of Cardiology, Hypertension and Internal Medicine, Medical University of Warsaw, Poland
[3] Department of Immunology, Transplantation and Internal Medicine, Medical University of Warsaw, Poland
[4] Department of Clinical Chemistry and Laboratory Diagnostics, Medical University of Warsaw, Poland

A – research concept and design; B – collection and/or assembly of data; C – data analysis and interpretation; D – writing the article; E – critical revision of the article; F – final approval of the article

Advances in Clinical and Experimental Medicine, ISSN 1899–5276 (print), ISSN 2451–2680 (online) *Adv Clin Exp Med*. 2024;33(3):299–308

**Address for correspondence**
Mariusz Tomaniak
E-mail: tomaniak.mariusz@gmail.com

**Funding sources**
None declared

**Conflict of interest**
None declared

Received on February 21, 2023
Reviewed on April 26, 2023
Accepted on June 6, 2023

Published online on June 30, 2023

## Abstract

The severe acute respiratory syndrome coronavirus 2 (SARS-CoV-2) pandemic has caused high morbidity and mortality and has been a source of substantial challenges for healthcare systems globally. Despite a full recovery, a significant proportion of patients demonstrate a broad spectrum of cardiovascular, pulmonary and neurological symptoms that are believed to be caused by long-term tissue damage and pathological inflammation, which play a vital role in disease development. Microvascular dysfunction also causes significant health problems. This review aimed to critically appraise the current data on the long-term cardiovascular sequelae of coronavirus disease 2019 (COVID-19), with a primary focus on cardiovascular symptoms such as chest pain, fatigue, palpitations, and breathlessness, and more significant disease entities including myocarditis, pericarditis and postural tachycardia syndrome. Potential risk factors identified in recent studies that contribute towards the development of long COVID are also included alongside a summary of recent advances in diagnostics and putative treatment options.

**Key words:** COVID-19, inflammation, microcirculation, SARS-CoV-2

**Cite as**
Składanek JA, Leśkiewicz M, Gumiężna K, et al. Long COVID and its cardiovascular consequences: What is known?. *Adv Clin Exp Med*. 2024;33(3):299–308. doi:10.17219/acem/167482

**DOI**
10.17219/acem/167482

# Introduction

The term "long COVID" was first used by a patient as a hashtag on Twitter shortly after the pandemic spread in May 2020,[1] and quickly gained popularity within the scientific community. Even though long coronavirus disease (COVID), also known as post-coronavirus disease 2019 (COVID-19) or chronic COVID syndrome, affects many patients each year, it is a poorly understood illness, and its definition is not entirely clear. This is because the syndrome includes several hundred complications with completely different degrees of severity that impact functioning with varying duration. The disorder also affects psychophysical performance and nearly every organ within the human body. The World Health Organization (WHO) defines long COVID as a condition that "occurs in individuals with a history of probable or confirmed severe acute respiratory syndrome coronavirus 2 (SARS-CoV-2) infection, usually 3 months from the onset of COVID-19 with symptoms that last for at least 2 months and cannot be explained by an alternative diagnosis".[2] However, researchers often use the revised criteria, which makes it difficult to determine the frequency at which it occurs. In a recently published meta-analysis, the global prevalence of long COVID was estimated at 0.43 and was higher for hospitalized than non-hospitalized patients. Researchers also described heterogeneity of the results of the included studies (from 0.09 to 0.81).[3]

# Objectives

Since long COVID is a new disease entity with a short observation period, this review aimed to present possible pathophysiological mechanisms, risk factors, cardiovascular manifestations, diagnostics, and treatments using the limited literature available. A complete understanding of this disease is crucial to providing adequate evidence-based patient care.

# Materials and methods

The literature search used the PubMed, medRxiv and Google Scholar databases, references from relevant articles, and internet sources, including WHO reports and the web pages of the British Medical Journal (BMJ) and Office for National Statistics (Cardiff, UK). Search terms included "post-COVID-19", "post-COVID syndrome", "long COVID", "chronic COVID syndrome", "post-acute COVID-19 syndrome", "myocarditis", "pericarditis", "arrhythmia", and "post-COVID-19 tachycardia syndrome". No filters were applied for the starting dates, with the last literature search performed on March 22, 2023. The authors screened the titles and abstracts to identify relevant papers.

## Risk factors

The currently available data show that the most prominent risk factors for long COVID are acute COVID-19 with admission to the intensive care unit (ICU) and/or ventilator support, female sex, and more than 5 symptoms during the 1st week of illness.[4–6] There was no difference in morbidity between patients treated with oxygen alone, invasive ventilation or continuous positive airway pressure.[5,7] The risk of developing long COVID increases when the patient smokes tobacco or has underlying comorbidities such as diabetes, hypertension, obesity, cardiovascular diseases (CVDs), chronic alcoholism, and chronic kidney disease (CKD).[8–10] However, many patients with light/mild acute symptoms who were not hospitalized also develop long COVID symptoms.[5,11,12] Some studies show that a history of depression, anxiety or antidepressant use can influence the likelihood of developing long COVID.[4,13,14] Reports also suggest that older age groups are at risk of developing long COVID and that children may experience symptoms similar to adults.[15] Evidence is also available indicating that the virus variant affects the risk of developing long COVID, with a higher risk associated with Delta than with Omicron BA.1 or Omicron BA.2 variants. Studies on the effects of vaccines on long COVID risk are inconclusive, with some researchers demonstrating a significant risk reduction in vaccinated patients; the recent data do not support these findings and claim that there is only a 15% risk reduction. Nonetheless, even though vaccination does not eliminate the risk, it reduces it to some extent.[16,17]

# Putative pathophysiology

The mechanisms of long COVID are likely multifactorial, and there seems to be a continuity of pathogenesis of acute illness. The etiology may include pathological inflammation leading to long-term tissue damage, dysregulation of the renin–angiotensin–aldosterone system (RAAS) and the kinin–kallikrein system (KKS), a virus-induced cytokine and bradykinin storm, dysregulated immune responses, endothelialitis, and mast cell activation syndrome (MCAS).

## Pathological inflammation and dysregulated immune responses

The SARS-CoV-2 persistence in the body is a possible consequence of deoxyribonucleic acid (DNA) integration of the viral genome[18,19] and its presence in immunologically privileged sites.[20] These mechanisms contribute to the phenomenon in which patients who recovered from COVID-19 continuously obtain positive polymerase chain reaction (PCR) results.[18,19] Viral ribonucleic acid (RNA) and antigens may prompt some level of immune activation leading to the development of long COVID,[4]

with the process of presenting antigens to autoreactive dysfunctional T-cells by antigen-presenting cells making long COVID pathophysiology similar to autoimmunity.[4,21] Furthermore, some studies have shown that B-cells produce antibodies against neutrophils, interferons, cell nuclei, cyclic citrullinated peptides, and connective tissues, indicative of autoimmunity.[4,22]

Hyperinflammatory syndrome, which can contribute to long COVID, results from dysregulated host innate immune responses and decreased absolute lymphocyte count.[23] Endothelialitis, which takes part in cardiovascular system dysfunction and its symptomatology, is caused by viral elements within endothelial cells and inflammatory cell infiltration of the myocardium.[20,24]

## Dysfunction of the renin–angiotensin–aldosterone system and the kinin–kallikrein system

Adherence of the viral S protein to angiotensin-converting enzyme 2 (ACE2) is a primary route for SARS-CoV-2 cellular entry. Locations such as the intestines, kidneys and heart have high expression of ACE2, while its expression is moderate in blood vessels. There are studies showing the downregulation of ACE2[25,26] and its disintegrin and metalloproteinase domain-containing protein 17 (ADAMS17)-mediated shedding from the cell surface[27] caused by SARS-CoV-2, which leads to RAAS dysregulation and plays a significant role in long COVID development. Under normal physiological conditions, RAAS consists of the angiotensin II (Ang II) type 1 receptors ($AT_1R$) (via which signaling components can intensify cardiac fibrosis and hypertrophy, vasoconstriction, endothelial dysfunction, and vascular inflammation) and Ang II type 2 receptors ($AT_2R$) (which promote vasodilatation, cardioprotection and decreased platelet aggregation).[25] Due to ACE2 downregulation and cytokine-induced hyperinflammation, elevated Ang II/AT1R axis activity contributes to myocardial injury, microvascular thrombosis and dysfunction of numerous organs, as shown in Fig. 1. In addition, ACE2 shedding initiates a cytokine storm by aggravating the response of tumor necrosis factor alpha (TNF-α) and interleukin (IL)-6R.[27,28] Some have theorized that MCAS and the resultant cytokine storm are associated with long COVID.[8,29]

The KKS exerts biological effects through bradykinin-1 ($B_1$) and bradykinin-2 ($B_2$) receptor activation. While $B_2$ receptors are present in all tissues, $B_1$ receptor expression increases during cellular stress and inflammation. Elevated expression of ACE contributes to the downregulation of the KKS as well as suppresses its cardioprotective activity, and hyperinflammation causes moderate stimulation of $B_1$ receptors, leading to a cytokine storm. A bradykinin storm causes myocardial and endothelial dysfunction due to fibrotic accumulations, and may be a consequence of ACE2 reduction and downregulation of des-Arg$^9$-bradykinin (DABK) degradation.[25,30]

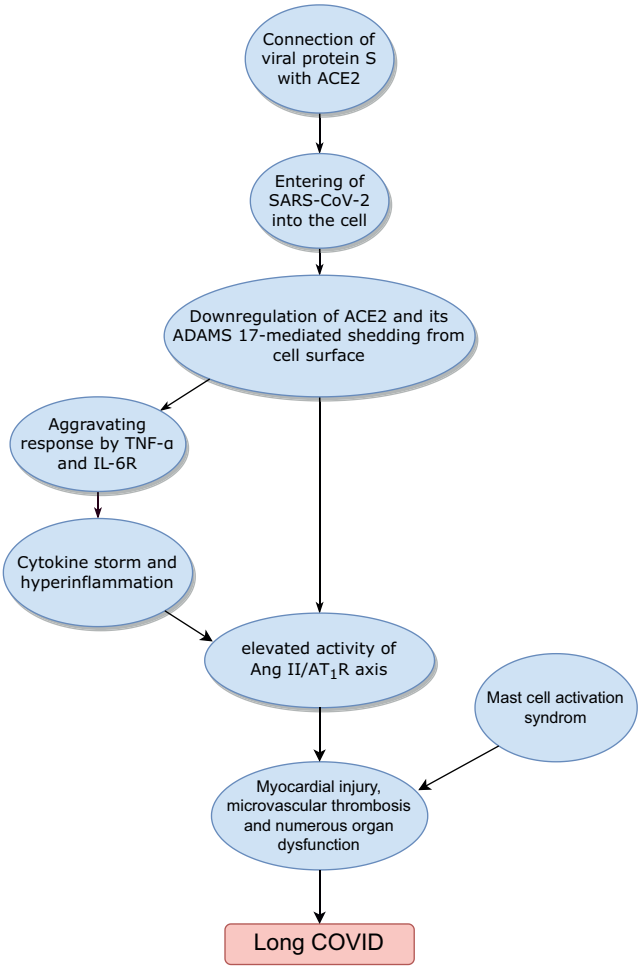


Fig. 1. Dysfunction of the renin–angiotensin–aldosterone system (RAAS) and kinin–kallikrein system (KKS)

Ang II/$AT_1R$ – angiotensin II/type 1 receptors; ACE2 – angiotensin-converting enzyme 2; ADAMS17 – disintegrin and metalloprotease 17; TNF-α – tumor necrosis factor alpha; IL-6 – interleukin 6; COVID – coronavirus disease; SARS-CoV-2 – severe acute respiratory syndrome coronavirus 2.

## Mast cell activation syndrome

Mast cell activation syndrome is an inflammatory disease caused by mast cells mistakenly releasing excessive amounts of inflammatory cytokines. Some have theorized that a connection exists between prolonged COVID-19 symptomatology and hyperactive mast cells in patients with underlying primary MCAS. Due to the expression of ACE2, mast cells become an easy target for SARS-CoV-2. Nevertheless, there is a lack of experimental studies confirming this hypothesis.[31,32]

# Microvascular dysfunction

Microcirculation analysis, related to the development and improvement of research techniques that allow for microvascular assessment, is continuously gaining more attention. Great hopes are placed on functional diagnosis

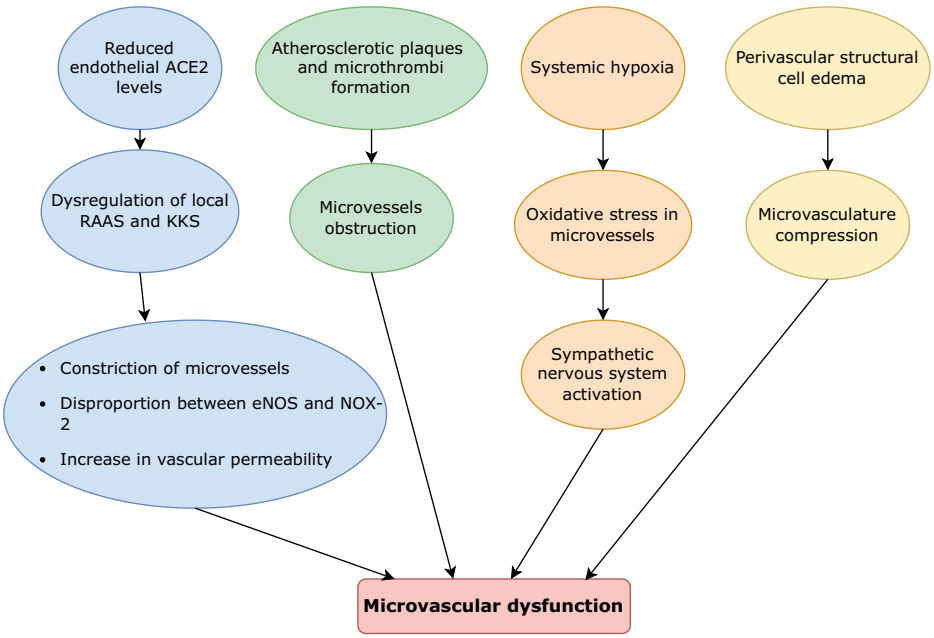


**Fig. 2.** Processes leading to microvascular dysfunction

ACE2 – angiotensin-converting enzyme 2; RAAS – renin–angiotensin–aldosterone system; KKS – kinin–kallikrein system; eNOS – endothelial nitric oxide synthase; NOX-2 – nicotinamide adenine dinucleotide phosphate (NADPH) oxidase 2.

in coronary microcirculation, as it would allow for the detection of changes in the small arteries of the heart and help determine whether coronary microcirculation dysfunction causes symptoms. Microcirculatory responses to hypoxia can be a prognostic factor for COVID-19, with hypoxia-inducible factor (HIF) playing a critical role in the response. Its actions induce protective molecules that are vital to maintaining a well-functioning response to hypoxia.[33]

Coronavirus disease 2019 disturbs blood flow in the microcirculation, which results in a high mortality rate. The pathomechanism is complex and consists of many elements acting together to significantly dysregulate homeostasis. The RAAS system is mainly responsible for maintaining optimal blood pressure, though overactivation of this endocrine system causes proliferation and inflammation.[34] The ACE2 is a central part of the RAAS system, and its imbalance leads to hypertension, obesity, inflammation, thrombosis, and insulin resistance. Its reduced activity is due to the fact that the virus uses the receptor to enter the cells,[35] and as ACE2 levels drop, the Ang II/$AT_1R$ axis becomes overactive. The release of complement factors and the endothelial expression of tissue factor (TF) and plasminogen activator inhibitor-1 (PAI-1) increase, leading to a hypercoagulable state.[36] Moreover, higher expression of ACE2 was demonstrated in pericytes of patients with underlying heart failure, meaning they may have a greater risk of progressing to severe disease during COVID-19 infection.[37]

Systemic inflammation, as a result of immune responses to COVID-19 infection, causes dysregulation of the entire immune system, leading to a cytokine storm activating T-cells and macrophages.[35] Another important aspect of the pathophysiology of microvascular dysfunction is oxidative stress, which leads to a type 2 myocardial infarction due to a supply and demand mismatch. Another effect of oxidative stress is the activation of the sympathetic nervous system, with subsequent catecholamine release resulting in vasoconstriction and increased cardiomyocyte oxygen demand.[34]

Increased blood viscosity and decreased red blood cell deformability is an important risk factor that occurs due to low estrogen levels (one of the causes of higher male mortality), obesity, vitamin D deficiency, diabetes, and hypertension.[38] Furthermore, a crucial part of microcirculation disorders is the damaged endothelium leading to an imbalance between endothelial nitric oxide synthase (eNOS) and nicotinamide adenine dinucleotide phosphate (NADPH) oxidase 2 (NOX-2). Production of nitric oxide (NO) has a vasodilating effect and is dependent on eNOS. Low concentrations of NO cause hypertension, thrombosis and vascular inflammation. In contrast, NOX-2 activity increases the number of free radicals that further damage the endothelium.[34–36,39] It was also found that perivascular cells (myocytes, pericytes and adipocytes) damaged by coronavirus cause the compression of the coronary microcirculation and can release toxic agents.[34] In summary, disturbances in the microcirculation occur during SARS-CoV-2 infection, with the virus damaging the endothelium, causing its remodeling and loss of function. Microcirculation disorders may persist after the infection and be the basis for the development of many long COVID disorders. The summary of the processes leading to microvascular dysfuntion is presented in Fig. 2.

## Cardiovascular manifestations

The association between SARS-CoV-2 infection and an increased risk of late cardiovascular problems was

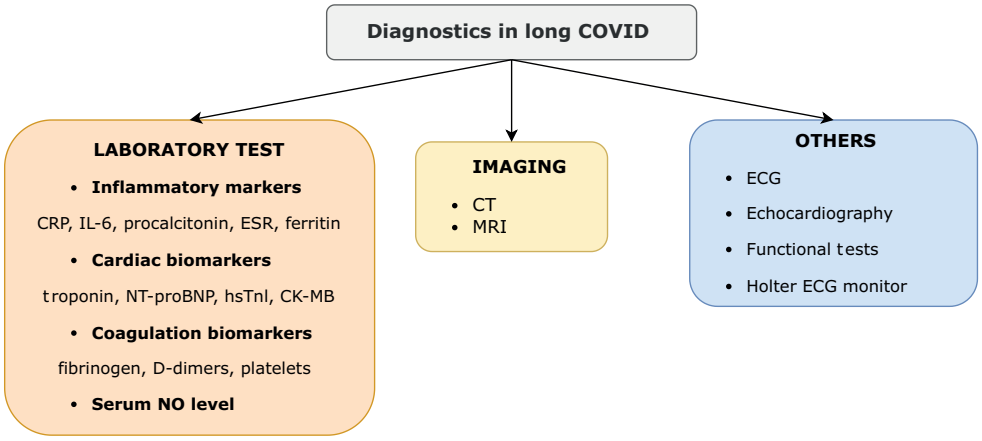


**Fig. 3.** Diagnostic methods for identifying long coronavirus disease (COVID)

ESR – erythrocyte sedimentation rate; CK-MB – creatine kinase myocardial band; hsTnI – high sensitivity troponin I; CT – computed tomography; MRI – magnetic resonance imaging; ECG – electrocardiography; CRP – C-reactive protein; NT-proBNP – N-terminal pro B-type natriuretic peptide; NO – nitric oxide; IL-6 – interleukin 6.

observed early in the pandemic. A recent study on a large group showed that people who had contracted COVID-19 were more likely to develop incident CVDs, including cerebrovascular disorders, dysrhythmias, inflammatory heart disease, ischemic heart disease, heart failure, thromboembolic disease, and other cardiac disorders, within 12 months of illness. The increased risk was independent of other factors and confirmed previously conducted research.

Cardiovascular long COVID most often manifests as long-lasting symptoms, of which the most persistent include palpitations, fatigue, chest pain, and back pain. The complications can also occur in patients who seem to have fully recovered from infection and whose symptoms were relatively mild. Thus, there is a need to develop diagnostic and therapeutic strategies for post-infection patients.[40–42]

## Myocarditis

Myocarditis is an inflammation of the heart muscle, most commonly being a consequence of viral infection. The pathogenesis of COVID-related myocarditis is unknown, yet the main hypotheses assume the involvement of molecular mimicry mechanisms and the effect of viruses on ACE2 regulation.[43] Even though there is evidence of SARS-CoV-2 genomes in endomyocardial biopsies, it is suspected that myocarditis is caused in most patients by the hyperinflammatory response triggered by the virus.[44,45] Moreover, heart muscle injury was assessed using biochemical and imaging tests soon after the infection and was present in most patients. Due to the destruction of myocytes, this condition deteriorates cardiac function, causing heart failure, cardiomyopathy and sudden cardiac death. There have been multiple studies on myocarditis after COVID-19 infection, with Puntmann et al. showing cardiac involvement in 78% of patients and ongoing myocardial inflammation in 60% after a median time of 71 days.[46] Cardiac involvement was also present in later studies showing that cardiac magnetic resonance (CMR) is useful for patient monitoring.[47] Further research established that myocardial injury, assessed using troponin levels during infection, can be predictive of later CMR abnormalities.[48]

The impact of the SARS-CoV-2 virus on the cardiac muscle of professional athletes has yet to be established. The studies show discrepant results, though all available research was performed in small patient groups.[49–51] Vaccination seems to be the only effective method for preventing COVID-19 and its complications. However, post-vaccination myopericarditis should not be overlooked.[52–54] Recommendations for CMR imaging criteria of active myocarditis provided by the *Journal of the American College of Cardiology* scientific expert panel consists of an increase in at least 1 T1-based method, including T1 mapping, and 1 T2-based method, including T2 mapping.[55] This method of imaging, in addition to clinical manifestations of myocarditis, is currently the gold standard non-invasive diagnostic modality.[56]

## Pericarditis

Pericarditis is common in acute SARS-CoV-2 infection but can also occur after recovery. There are minimal data concerning its epidemiology, though it seems to be a common manifestation of long COVID[57] and is thought to be associated with the ongoing inflammation that results from the persistence of viral nucleic acid. In most cases, it is diagnosed by exclusion and 2 of the following symptoms: pericardial effusion, chest pain, electrographic changes, and pericardial friction. Isolated, small pericardial effusion is much more common than pericarditis.[31,46,58] One study demonstrated that 30.9% of patients had myocarditis and/or pericarditis 10 weeks after COVID-19 pneumonia. Therefore, some refer to both as myopericarditis (pericarditis with associated myocarditis on CMR without left ventricular wall motion abnormalities) or perimyocarditis (when left ventricular wall motion abnormalities are present), depending on the dominating clinical image.[59] A study by Dini et al. reported a high prevalence (22%) of pericarditis in patients previously affected by COVID-19 after at least 12 weeks from the end of the infection.[57]

## Long COVID tachycardia syndrome and other arrhythmias

Tachycardia is thought to be a common feature following acute SARS-CoV-2 infection. Persistent, symptomatic tachycardia constitutes a syndrome called long COVID tachycardia syndrome, which presents clinically as postural orthostatic tachycardia syndrome (POTS), inappropriate sinus tachycardia or sinus tachycardia, with 54% of patients reporting persistent symptoms and an increased resting heart rate. Holter monitoring and other devices measuring the heart rhythm may allow for diagnosis and monitoring of progress in an outpatient setting. Moreover, tachycardia can be a valuable quantitative indicator of long COVID severity and reflects not only autonomic dysfunction and possible damage to the heart but also the general condition of the patient.[31,60–62]

The first studies comparing the available treatments for long COVID tachycardia syndrome have already appeared, with one showing that ivabradine, which acts on the sinus node, was more effective than carvedilol.[63] Knowledge of the prevalence of POTS and inappropriate sinus tachycardia in patients suffering from long COVID is limited, as most studies retrospective or have small sample sizes.[64] Based on the available data, the proportion of COVID-19 survivors developing POTS and inappropriate sinus tachycardia is estimated at 2–22% and 4–20%, respectively.[65–67]

In addition to sinus tachycardia, long COVID may include other arrhythmias such as atrial fibrillation (AF), ventricular tachyarrhythmias (VT), bradyarrhythmias, and conduction defects. It is suspected that multiple mechanisms may lead to this complication, though the primary pathophysiology is driven by the inflammatory response. Cytokines, especially TNF-α, IL-1 and IL-6, may cause myocardial damage or systemic effects that indirectly influence the heart muscle.[68] A slightly different mechanism has been described for VT, in which patients who limited their physical activity due to infection had a higher incidence of VT.[69] Ingul et al. found cardiac arrhythmias of unknown clinical importance 3 months after hospitalization due to COVID-19 in 27% of participants, premature ventricular contractions in 18% and non-sustained ventricular tachycardia in 5%.[70]

Another problem faced by patients is arterial pressure dysregulation. In one study, the hazard ratios for high blood pressure persisted for up to 6 months after infection.[71] A summary of the studies on cardiovascular consequences is presented in Table 1.

# Diagnostics

Long COVID diagnosis is currently based on reported symptoms and a history of confirmed SARS-CoV-2 infection. Many studies suggest that diagnostic tests should be performed to assess long COVID cardiovascular manifestations. The American College of Cardiology expert panel recommends performing basic cardiac tests (electrocardiography, cardiac troponin levels and echocardiography) as a minimum in patients at risk of developing CVD after COVID-19, which includes those with a moderate to severe disease course, CVD history, or risk factors such as age, obesity, hypertension, diabetes, and other comorbidities. The current state of knowledge leaves the physician with broad discretion. A better understanding of the epidemiology and pathomechanisms could contribute to creating more universal management guidelines.[72,73]

# Laboratory tests

One study showed that patients presenting long COVID symptoms had increased N-terminal pro B-type natriuretic peptide (NT-proBNP) and NO levels, while troponin remained within normal limits. There was no statistically significant difference in other oxidative stress markers between people with and without symptoms.[74] Some studies revealed no difference in systemic inflammatory biomarkers, such as C-reactive protein (CRP), procalcitonin and IL-6, between patients who recovered from COVID-19 with and without persistent symptoms.[4,14,75–78] However, another study demonstrated a connection between these biomarkers and radiological abnormalities of the heart at 2-to 3-month follow-up of discharged patients.[4,79] Patients with long COVID had elevated levels of endothelin-1, which indicates endothelial hypoperfusion.[80] Furthermore, some symptomatic patients continued to display increased D-dimer levels 2 months after hospital discharge following acute SARS-CoV-2 infection.[81]

# Imaging and others

Numerous articles have evaluated the role of electrocardiogram (ECG), magnetic resonance imaging (MRI) and echocardiography in screening patients with cardiac manifestations of long COVID.[55] One study showed that patients presenting long COVID symptoms had sinus tachycardia in resting ECG or atrial tachycardia in 24-hour Holter monitoring.[74] Other indicators of myocardial damage on ECG are ST-segment and T wave changes.[82] Noninvasive examination methods, such as computed tomography (CT), MRI and echocardiography, can help rule out coronary artery disease (CAD), myopericarditis or congestive heart failure, and assess left/right ventricle function and regional wall motion.[83–86] In transthoracic echocardiography of 102 long COVID patients, there were 4 patterns of abnormalities, including impaired left ventricular function (LVF) in 35 subjects, increased estimated systolic pulmonary artery pressure in 51, diastolic dysfunction with normal LVF in 66, and pericardial effusion/thickening in 23.[85] The summary of diagnostic methods helpful in identifying long COVID is shown in Fig. 3.

**Table 1.** Studies on COVID-19-related cardiovascular consequences

| Study, reference | Study population | Findings |
|---|---|---|
| Myocarditis | | |
| Puntmann et al.[46] | 100 patients who recently recovered from COVID-19 | CMR revealed cardiac involvement in 78 patients (78%) and ongoing myocardial inflammation in 60 patients (60%). |
| Wang et al.[47] | 44 patients who recovered from COVID-19 and 31 healthy controls | Myocardial injury is present in nearly 1/3 of COVID-19 patients at 3 months. |
| Kotecha et al.[48] | 148 patients with troponin elevation | Myocardial injury during COVID-19 infection is associated with a CMR abnormality in approx. 50% of patients. |
| Vago et al.[49] | 12 professional elite athletes | No signs of cardiac involvement on CMR in elite athletes who underwent COVID-19. |
| Małek et al.[50] | 26 consecutive elite athletes | CMR did not reveal any case of acute myocarditis. Cardiac abnormalities were found in 5 (19%) athletes. |
| Rajpal et al.[51] | 26 competitive athletes | 15% of athletes had CMR findings suggestive of myocarditis and 30.8% exhibited late gadolinium enhancement. |
| Pericarditis | | |
| Dini et al.[57] | 180 patients previously diagnosed with COVID-19 | Acute pericarditis was diagnosed in 39 patients (22%). |
| Eiros et al.[59] | 139 healthcare workers with confirmed past SARS-CoV-2 infection | Isolated pericarditis was diagnosed in 5.8%, myopericarditis in 7.9% and isolated myocarditis in 17.3% of workers. |
| Long COVID tachycardia syndrome | | |
| Monaghan et al.[65] | 85 adults reporting long COVID symptoms | Postural orthostatic tachycardia syndrome was diagnosed in 1 (2%) out of 53 adults who had a 10-minute tilt test. |
| Shouman et al.[66] | 27 patients with autonomic symptoms developed at or after the SARS-CoV-2 infection | Postural orthostatic tachycardia was diagnosed in 6 patients (22%) and inappropriate sinus tachycardia in 1 person (4%). |
| Aranyó et al.[67] | 200 patients with persistent symptoms beyond the 3rd month of acute infection | 40 patients (20%) fulfilled the diagnostic criteria for inappropriate sinus tachycardia. |
| Other arrhythmias | | |
| Ingul et al.[70] | 204 patients 3 months after the hospitalization for COVID-19, and 204 controls | In patients with COVID-19, premature ventricular contractions (18%) and non-sustained ventricular tachycardia (5%) were found. |
| Hypertension | | |
| Daugherty et al.[71] | total 2020 population: 9,247,505 people; 2020 comparator group: 8,980,919 people; 2019 comparator group: 9,722,381 people | The absolute risk for hypertension in young adults aged 18–34 was significantly elevated. |

CMR – cardiac magnetic resonance; COVID-19 – coronavirus disease 2019; SARS-CoV-2 – severe acute respiratory syndrome coronavirus 2.

# Treatment

Since long COVID is a relatively new condition, pilot studies are primarily available. As such, all administered drugs should be used with the utmost care. Initially, it was assumed that therapy with drugs that inhibit RAAS could cause increased cellular ACE2 expression, which may facilitate virus entry and exacerbate the infection. However, several studies found that these drugs had no negative effect on mortality and should not be discontinued.[87–89] Moreover, some studies indicate their positive impact in the context of SARS-CoV-2 infection, which is related to their antioxidant and anti-inflammatory effects.[90] Sulodexide is a promising drug for endothelial disorders, and a small study showed that it can reduce long COVID symptoms, such as chest pain, palpitations and fatigue, after a 21-day follow-up.[91] In addition, the hypothetical positive effects of anticoagulants on long COVID are being increasingly discussed. However, no scientifically robust evidence exists to recommend their use in this population at this stage.[92,93]

Guidelines for implementing rehabilitation into long COVID treatment plans, as well as inclusion and exclusion criteria to adapt it to patients' individual needs are under development. Nonetheless, most patients will benefit from light aerobic and breathing exercises.[4]

## Limitations

The primary limitation that may affect the conclusions of this study is that COVID-19 and the associated long COVID are new disease entities. For this reason, the short observation period limits the results and conclusions drawn. Larger studies are required in the future to determine the precise influence of long COVID on health, particularly for putative treatments based on small pilot studies. No relevant recommendations exist, and treatment is based on hypotheses and clinical practices.

## Conclusions

The COVID-19 outbreak has proven to be a substantial challenge for healthcare systems. Although the media interest focused on acute disease, the long-term effects of the epidemic will continue to affect citizens' health for a long time. Unfortunately, the literature and research on long COVID are still scarce, making it challenging to plan appropriate patient care and treatment. In our article, we focused on the cardiovascular aspects of long COVID and devoted a large part to its pathogenesis because, in the absence of research and standards for diagnosis and treatment, it is crucial to primarily understand the mechanisms in order to implement an optimal therapeutic strategy. Patients with risk factors such as diabetes, hypertension, obesity, CVDs, and CKD require special attention and should be closely monitored.

Myocarditis, pericarditis and tachycardia syndrome are the main cardiovascular manifestations of long COVID. Research is ongoing in the fields of vasculitis, CAD and thromboembolism to better understand their role in long COVID. Continuously developing imaging techniques and laboratory tests allow for the detection of patients who may suffer from long COVID. Treatment is mainly based on symptoms and includes both pharmacological and non-pharmacological approaches. Hopefully, precise therapeutic methods will emerge as research on the pathophysiology and diagnostic processes continues, resulting in better clinical outcomes.

### ORCID iDs

Justyna Aleksandra Składanek https://orcid.org/0009-0003-0547-6841
Michał Leśkiewicz https://orcid.org/0009-0000-0890-2672
Karolina Gumiężna https://orcid.org/0000-0002-3423-9832
Piotr Baruś https://orcid.org/0000-0003-2567-5349
Adam Piasecki https://orcid.org/0000-0002-5088-169X
Dominika Klimczak-Tomaniak https://orcid.org/0000-0001-8825-511X
Grażyna Sygitowicz https://orcid.org/0000-0002-0057-4253
Janusz Kochman https://orcid.org/0000-0001-8239-8726
Marcin Grabowski https://orcid.org/0000-0003-3306-0301
Mariusz Tomaniak https://orcid.org/0000-0003-0966-3313

### References

1. Perego E, Callard F, Stras L, Melville-Jóhannesson B, Pope R, Alwan N. Why we need to keep using the patient made term "long Covid".; BMJ Blogs;2020. https://blogs.bmj.com/bmj/2020/10/01/why-we-need-to-keep-using-the-patient-made-term-long-covid/#content. Accessed December 20, 2022.
2. World Health Organization (WHO). A clinical case definition of post COVID-19 condition by a Delphi consensus, 6 October 2021. Geneva, Switzerland: World Health Organization (WHO); 2021. https://www.who.int/publications/i/item/WHO-2019-nCoV-Post_COVID-19_condition-Clinical_case_definition-2021.1. Accessed February 4, 2023.
3. Chen C, Haupert SR, Zimmermann L, Shi X, Fritsche LG, Mukherjee B. Global prevalence of post-coronavirus disease 2019 (COVID-19) condition or long COVID: A meta-analysis and systematic review. *J Infect Dis*. 2022;226(9):1593–1607. doi:10.1093/infdis/jiac136
4. Yong SJ. Long COVID or post-COVID-19 syndrome: Putative pathophysiology, risk factors, and treatments. *Infect Dis (London)*. 2021;53(10):737–754. doi:10.1080/23744235.2021.1924397
5. Crook H, Raza S, Nowell J, Young M, Edison P. Long COVID: Mechanisms, risk factors, and management. *BMJ*. 2021:n1648. doi:10.1136/bmj.n1648
6. Charfeddine S, Ibn Hadj Amor H, Jdidi J, et al. Long COVID 19 syndrome: Is it related to microcirculation and endothelial dysfunction? Insights from TUN-EndCOV study. *Front Cardiovasc Med*. 2021;8:745758. doi:10.3389/fcvm.2021.745758
7. Mandal S, Barnett J, Brill SE, et al. 'Long-COVID': A cross-sectional study of persisting symptoms, biomarker and imaging abnormalities following hospitalisation for COVID-19. *Thorax*. 2021;76(4):396–398. doi:10.1136/thoraxjnl-2020-215818
8. Garg M, Maralakunte M, Garg S, et al. The conundrum of 'Long-COVID-19': A narrative review. *Int J Gen Med*. 2021;14:2491–2506. doi:10.2147/IJGM.S316708
9. Ojo AS, Balogun SA, Williams OT, Ojo OS. Pulmonary fibrosis in COVID-19 survivors: Predictive factors and risk reduction strategies. *Pulm Med*. 2020;2020:6175964. doi:10.1155/2020/6175964
10. Halpin S, O'Connor R, Sivan M. Long COVID and chronic COVID syndromes. *J Med Virol*. 2021;93(3):1242–1243. doi:10.1002/jmv.26587
11. Dennis A, Wamil M, Alberts J, et al. Multiorgan impairment in low-risk individuals with post-COVID-19 syndrome: A prospective, community-based study. *BMJ Open*. 2021;11(3):e048391. doi:10.1136/bmjopen-2020-048391
12. Förster C, Colombo MG, Wetzel AJ, Martus P, Joos S. Persisting symptoms after COVID-19. *Dtsch Arztebl Int*. 2022;119(10):167–174. doi:10.3238/arztebl.m2022.0147
13. Poyraz BÇ, Poyraz CA, Olgun Y, et al. Psychiatric morbidity and protracted symptoms after COVID-19. *Psychiatry Res*. 2021;295:113604. doi:10.1016/j.psychres.2020.113604
14. Townsend L, Dyer AH, Jones K, et al. Persistent fatigue following SARS-CoV-2 infection is common and independent of severity of initial infection. *PLoS One*. 2020;15(11):e0240784. doi:10.1371/journal.pone.0240784
15. Ludvigsson JF. Case report and systematic review suggest that children may experience similar long-term effects to adults after clinical COVID-19. *Acta Paediatr*. 2021;110(3):914–921. doi:10.1111/apa.15673
16. Ayoubkhani D, Bosworth M. Self-reported long COVID after infection with the Omicron variant in the UK: 18 July 2022. Cardiff, UK: Office for National Statistics; 2022. https://www.ons.gov.uk/peoplepopulationandcommunity/healthandsocialcare/conditionsanddiseases/bulletins/selfreportedlongcovidafterinfectionwiththeomicronvariant/18july2022#main-points. Accessed January 9, 2022.
17. Flemming A. Vaccines only partially protect against long COVID. *Nat Rev Immunol*. 2022;22(7):410. doi:10.1038/s41577-022-00749-6
18. Di Toro A, Bozzani A, Tavazzi G, et al. Long COVID: Long-term effects? *Eur Heart J Suppl*. 2021;23(Suppl E):E1–E5. doi:10.1093/eurheartj/suab080
19. Zhang L, Richards A, Barrasa MI, Hughes SH, Young RA, Jaenisch R. Reverse-transcribed SARS-CoV-2 RNA can integrate into the genome of cultured human cells and can be expressed in patient-derived tissues. *Proc Natl Acad Sci U S A*. 2021;118(21):e2105968118. doi:10.1073/pnas.2105968118
20. Amenta EM, Spallone A, Rodriguez-Barradas MC, El Sahly HM, Atmar RL, Kulkarni PA. Postacute COVID-19: An overview and approach to classification. *Open Forum Infect Dis*. 2020;7(12):ofaa509. doi:10.1093/ofid/ofaa509
21. Ehrenfeld M, Tincani A, Andreoli L, et al. Covid-19 and autoimmunity. *Autoimmun Rev*. 2020;19(8):102597. doi:10.1016/j.autrev.2020.102597
22. Gao ZW, Zhang HZ, Liu C, Dong K. Autoantibodies in COVID-19: Frequency and function. *Autoimmun Rev*. 2021;20(3):102754. doi:10.1016/j.autrev.2021.102754
23. Gustine JN, Jones D. Immunopathology of hyperinflammation in COVID-19. *Am J Pathol*. 2021;191(1):4–17. doi:10.1016/j.ajpath.2020.08.009
24. Tschöpe C, Ammirati E, Bozkurt B, et al. Myocarditis and inflammatory cardiomyopathy: Current evidence and future directions. *Nat Rev Cardiol*. 2021;18(3):169–193. doi:10.1038/s41569-020-00435-x
25. Cooper SL, Boyle E, Jefferson SR, et al. Role of the renin-angiotensin-aldosterone and kinin-kallikrein systems in the cardiovascular complications of COVID-19 and long COVID. *Int J Mol Sci*. 2021;22(15):8255. doi:10.3390/ijms22158255

26. Li MY, Li L, Zhang Y, Wang XS. Expression of the SARS-CoV-2 cell receptor gene *ACE2* in a wide variety of human tissues. *Infect Dis Poverty*. 2020;9(1):45. doi:10.1186/s40249-020-00662-x
27. Cenko E, Badimon L, Bugiardini R, et al. Cardiovascular disease and COVID-19: A consensus paper from the ESC Working Group on Coronary Pathophysiology & Microcirculation, ESC Working Group on Thrombosis and the Association for Acute CardioVascular Care (ACVC), in collaboration with the European Heart Rhythm Association (EHRA). *Cardiovasc Res*. 2021;117(14):2705–2729. doi:10.1093/cvr/cvab298
28. Mehta P, McAuley DF, Brown M, Sanchez E, Tattersall RS, Manson JJ. COVID-19: Consider cytokine storm syndromes and immunosuppression. *Lancet*. 2020;395(10229):1033–1034. doi:10.1016/S0140-6736(20)30628-0
29. Afrin LB, Weinstock LB, Molderings GJ. Covid-19 hyperinflammation and post-Covid-19 illness may be rooted in mast cell activation syndrome. *Int J Infect Dis*. 2020;100:327–332. doi:10.1016/j.ijid.2020.09.016
30. Calixto JB, Medeiros R, Fernandes ES, Ferreira J, Cabrini DA, Campos MM. Kinin B1 receptors: Key G-protein-coupled receptors and their role in inflammatory and painful processes. *Br J Pharmacol*. 2004;143(7):803–818. doi:10.1038/sj.bjp.0706012
31. Dixit NM, Churchill A, Nsair A, Hsu JJ. Post-acute COVID-19 syndrome and the cardiovascular system: What is known? *Am Heart J Plus*. 2021;5:100025. doi:10.1016/j.ahjo.2021.100025
32. Afrin LB, Self S, Menk J, Lazarchick J. Characterization of mast cell activation syndrome. *Am J Med Sci*. 2017;353(3):207–215. doi:10.1016/j.amjms.2016.12.013
33. Gebicki J, Katarzynska J, Marcinek A. Can the microcirculatory response to hypoxia be a prognostic factor for Covid-19? *Respir Physiol Neurobiol*. 2020;280:103478. doi:10.1016/j.resp.2020.103478
34. Yin J, Wang S, Liu Y, Chen J, Li D, Xu T. Coronary microvascular dysfunction pathophysiology in COVID-19. *Microcirculation*. 2021;28(7):e12718. doi:10.1111/micc.12718
35. Gencer S, Lacy M, Atzler D, Van Der Vorst EPC, Döring Y, Weber C. Immunoinflammatory, thrombohaemostatic, and cardiovascular mechanisms in COVID-19. *Thromb Haemost*. 2020;120(12):1629–1641. doi:10.1055/s-0040-1718735
36. Del Turco S, Vianello A, Ragusa R, Caselli C, Basta G. COVID-19 and cardiovascular consequences: Is the endothelial dysfunction the hardest challenge? *Thromb Res*. 2020;196:143–151. doi:10.1016/j.thromres.2020.08.039
37. Chen L, Li X, Chen M, Feng Y, Xiong C. The ACE2 expression in human heart indicates new potential mechanism of heart injury among patients infected with SARS-CoV-2. *Cardiovasc Res*. 2020;116(6):1097–1100. doi:10.1093/cvr/cvaa078
38. Farber PL. Can erythrocytes behavior in microcirculation help the understanding the physiopathology and improve prevention and treatment for COVID-19? *Clin Hemorheol Microcirc*. 2021;78(1):41–47. doi:10.3233/CH-201082
39. Colantuoni A, Martini R, Caprari P, et al. COVID-19 sepsis and microcirculation dysfunction. *Front Physiol*. 2020;11:747. doi:10.3389/fphys.2020.00747
40. Madjid M, Safavi-Naeini P, Solomon SD, Vardeny O. Potential effects of coronaviruses on the cardiovascular system: A review. *JAMA Cardiol*. 2020;5(7):831–840. doi:10.1001/jamacardio.2020.1286
41. Clerkin KJ, Fried JA, Raikhelkar J, et al. COVID-19 and cardiovascular disease. *Circulation*. 2020;141(20):1648–1655. doi:10.1161/CIRCULATIONAHA.120.046941
42. Xie Y, Xu E, Bowe B, Al-Aly Z. Long-term cardiovascular outcomes of COVID-19. *Nat Med*. 2022;28(3):583–590. doi:10.1038/s41591-022-01689-3
43. Oudit GY, Kassiri Z, Jiang C, et al. SARS-coronavirus modulation of myocardial ACE2 expression and inflammation in patients with SARS. *Eur J Clin Invest*. 2009;39(7):618–625. doi:10.1111/j.1365-2362.2009.02153.x
44. Escher F, Pietsch H, Aleshcheva G, et al. Detection of viral SARS-CoV-2 genomes and histopathological changes in endomyocardial biopsies. *ESC Heart Fail*. 2020;7(5):2440–2447. doi:10.1002/ehf2.12805
45. Castiello T, Georgiopoulos G, Finocchiaro G, et al. COVID-19 and myocarditis: A systematic review and overview of current challenges. *Heart Fail Rev*. 2022;27(1):251–261. doi:10.1007/s10741-021-10087-9
46. Puntmann VO, Carerj ML, Wieters I, et al. Outcomes of cardiovascular magnetic resonance imaging in patients recently recovered from coronavirus disease 2019 (COVID-19). *JAMA Cardiol*. 2020;5(11):1265–1273. doi:10.1001/jamacardio.2020.3557
47. Wang H, Li R, Zhou Z, et al. Cardiac involvement in COVID-19 patients: Mid-term follow up by cardiovascular magnetic resonance. *J Cardiovasc Magn Reson*. 2021;23(1):14. doi:10.1186/s12968-021-00710-x
48. Kotecha T, Knight DS, Razvi Y, et al. Patterns of myocardial injury in recovered troponin-positive COVID-19 patients assessed by cardiovascular magnetic resonance. *Eur Heart J*. 2021;42(19):1866–1878. doi:10.1093/eurheartj/ehab075
49. Vago H, Szabo L, Dohy Z, Merkely B. Cardiac magnetic resonance findings in patients recovered from COVID-19: Initial experiences in elite athletes. *JACC Cardiovasc Imaging*. 2021;14(6):1279–1281. doi:10.1016/j.jcmg.2020.11.014
50. Małek ŁA, Marczak M, Miłosz-Wieczorek B, et al. Cardiac involvement in consecutive elite athletes recovered from Covid-19: A magnetic resonance study. *J Magn Reson Imaging*. 2021;53(6):1723–1729. doi:10.1002/jmri.27513
51. Rajpal S, Tong MS, Borchers J, et al. Cardiovascular magnetic resonance findings in competitive athletes recovering from COVID-19 infection. *JAMA Cardiol*. 2020;6(1):116–118. doi:10.1001/jamacardio.2020.4916
52. Szarpak L, Pruc M, Filipiak KJ, et al. Myocarditis: A complication of COVID-19 and long-COVID-19 syndrome as a serious threat in modern cardiology. *Cardiol J*. 2022;29(1):178–179. doi:10.5603/CJ.a2021.0155
53. Boehmer TK, Kompaniyets L, Lavery AM, et al. Association between COVID-19 and myocarditis using hospital-based administrative data – United States, March 2020 –January 2021. *MMWR Morb Mortal Wkly Rep*. 2021;70(35):1228–1232. doi:10.15585/mmwr.mm7035e5
54. Nygaard U, Holm M, Bohnstedt C, et al. Population-based incidence of myopericarditis after COVID-19 vaccination in Danish adolescents. *Pediatr Infect Dis J*. 2022;41(1):e25–e28. doi:10.1097/INF.0000000000003389
55. Raman B, Bluemke DA, Lüscher TF, Neubauer S. Long COVID: Post-acute sequelae of COVID-19 with a cardiovascular focus. *Eur Heart J*. 2022;43(11):1157–1172. doi:10.1093/eurheartj/ehac031
56. Friedrich MG, Marcotte F. Cardiac magnetic resonance assessment of myocarditis. *Circ Cardiovasc Imaging*. 2013;6(5):833–839. doi:10.1161/CIRCIMAGING.113.000416
57. Dini FL, Baldini U, Bytyçi I, Pugliese NR, Bajraktari G, Henein MY. Acute pericarditis as a major clinical manifestation of long COVID-19 syndrome. *Int J Cardiol*. 2023;374:129–134. doi:10.1016/j.ijcard.2022.12.019
58. Carubbi F, Alunno A, Leone S, et al. Pericarditis after SARS-CoV-2 infection: Another pebble in the mosaic of long COVID? *Viruses*. 2021;13(10):1997. doi:10.3390/v13101997
59. Eiros R, Barreiro-Pérez M, Martín-García A, et al. Pericardial and myocardial involvement after SARS-CoV-2 infection: A cross-sectional descriptive study in healthcare workers. *Rev Esp Cardiol (Engl Ed)*. 2022;75(9):734–746. doi:10.1016/j.rec.2021.11.001
60. Raj SR, Arnold AC, Barboi A, et al. Long-COVID postural tachycardia syndrome: An American Autonomic Society statement. *Clin Auton Res*. 2021;31(3):365–368. doi:10.1007/s10286-021-00798-2
61. Ståhlberg M, Reistam U, Fedorowski A, et al. Post-COVID-19 tachycardia syndrome: A distinct phenotype of post-acute COVID-19 syndrome. *Am J Med*. 2021;134(12):1451–1456. doi:10.1016/j.amjmed.2021.07.004
62. Kanjwal K, Jamal S, Kichloo A, Grubb B. New-onset postural orthostatic tachycardia syndrome following coronavirus disease 2019 infection. *J Innov Cardiac Rhythm Manag*. 2020;11(11):4302–4304. doi:10.19102/icrm.2020.111102
63. Jadhav K, Jariwala P. 'Ivabradin' versus 'Carvedilol' in the management of post-COVID-19 palpitation with sinus tachycardia. *Indian Heart J*. 2020;72:S33. doi:10.1016/j.ihj.2020.11.092
64. Ormiston CK, Świątkiewicz I, Taub PR. Postural orthostatic tachycardia syndrome as a sequela of COVID-19. *Heart Rhythm*. 2022;19(11):1880–1889. doi:10.1016/j.hrthm.2022.07.014
65. Monaghan A, Jennings G, Xue F, Byrne L, Duggan E, Romero-Ortuno R. Orthostatic intolerance in adults reporting long COVID symptoms was not associated with postural orthostatic tachycardia syndrome. *Front Physiol*. 2022;13:833650. doi:10.3389/fphys.2022.833650
66. Shouman K, Vanichkachorn G, Cheshire WP, et al. Autonomic dysfunction following COVID-19 infection: An early experience. *Clin Auton Res*. 2021;31(3):385–394. doi:10.1007/s10286-021-00803-8
67. Aranyó J, Bazan V, Lladós G, et al. Inappropriate sinus tachycardia in post-COVID-19 syndrome. *Sci Rep*. 2022;12(1):298. doi:10.1038/s41598-021-03831-6

68. Lazzerini PE, Laghi-Pasini F, Boutjdir M, Capecchi PL. Inflammatory cytokines and cardiac arrhythmias: The lesson from COVID-19. *Nat Rev Immunol*. 2022;22(5):270–272. doi:10.1038/s41577-022-00714-3
69. Diemberger I, Vicentini A, Cattafi G, et al. The impact of COVID-19 pandemic and lockdown restrictions on cardiac implantable device recipients with remote monitoring. *J Clin Med*. 2021;10(23):5626. doi:10.3390/jcm10235626
70. Ingul CB, Grimsmo J, Mecinaj A, et al. Cardiac dysfunction and arrhythmias 3 months after hospitalization for COVID-19. *J Am Heart Assoc*. 2022;11(3):e023473. doi:10.1161/JAHA.121.023473
71. Daugherty SE, Guo Y, Heath K, et al. Risk of clinical sequelae after the acute phase of SARS-CoV-2 infection: Retrospective cohort study. *BMJ*. 2021;373:n1098. doi:10.1136/bmj.n1098
72. Gluckman TJ, Bhave NM, Allen LA, et al. 2022 ACC Expert Consensus Decision Pathway on Cardiovascular Sequelae of COVID-19 in Adults: Myocarditis and Other Myocardial Involvement, Post-Acute Sequelae of SARS-CoV-2 Infection, and Return to Play. *J Am Coll Cardiol*. 2022;79(17):1717–1756. doi:10.1016/j.jacc.2022.02.003
73. Phelan D, Kim JH, Elliott MD, et al. Screening of potential cardiac involvement in competitive athletes recovering from COVID-19: An expert consensus statement. *JACC Cardiovasc Imaging*. 2020;13(12):2635–2652. doi:10.1016/j.jcmg.2020.10.005
74. Sarıçam E, Dursun AD, Türkmen Sarıyıldız G, et al. Laboratory and imaging evaluation of cardiac involvement in patients with post-acute COVID-19. *Int J Gen Med*. 2021;14:4977–4985. doi:10.2147/IJGM.S321156
75. Van Den Borst B, Peters JB, Brink M, et al. Comprehensive health assessment 3 months after recovery from acute coronavirus disease 2019 (COVID-19). *Clin Infect Dis*. 2021;73(5):e1089–e1098. doi:10.1093/cid/ciaa1750
76. Moreno-Pérez O, Merino E, Leon-Ramirez JM, et al. Post-acute COVID-19 syndrome. Incidence and risk factors: A Mediterranean cohort study. *J Infect*. 2021;82(3):378–383. doi:10.1016/j.jinf.2021.01.004
77. Salmon-Ceron D, Slama D, De Broucker T, et al. Clinical, virological and imaging profile in patients with prolonged forms of COVID-19: A cross-sectional study. *J Infect*. 2021;82(2):e1–e4. doi:10.1016/j.jinf.2020.12.002
78. Zhao YM, Shang YM, Song WB, et al. Follow-up study of the pulmonary function and related physiological characteristics of COVID-19 survivors three months after recovery. *EClinicalMedicine*. 2020;25:100463. doi:10.1016/j.eclinm.2020.100463
79. Raman B, Cassar MP, Tunnicliffe EM, et al. Medium-term effects of SARS-CoV-2 infection on multiple vital organs, exercise capacity, cognition, quality of life and mental health, post-hospital discharge. *EClinicalMedicine*. 2021;31:100683. doi:10.1016/j.eclinm.2020.100683
80. Haffke M, Freitag H, Rudolf G, et al. Endothelial dysfunction and altered endothelial biomarkers in patients with post-COVID-19 syndrome and chronic fatigue syndrome (ME/CFS). *J Transl Med*. 2022;20(1):138. doi:10.1186/s12967-022-03346-2
81. Pasini E, Corsetti G, Romano C, et al. Serum metabolic profile in patients with long-covid (PASC) syndrome: Clinical implications. *Front Med (Lausanne)*. 2021;8:714426. doi:10.3389/fmed.2021.714426
82. Elseidy SA, Awad AK, Vorla M, et al. Cardiovascular complications in the post-acute COVID-19 syndrome (PACS). *Int J Cardiol Heart Vasc*. 2022;40:101012. doi:10.1016/j.ijcha.2022.101012
83. Cau R, Faa G, Nardi V, et al. Long-COVID diagnosis: From diagnostic to advanced AI-driven models. *Eur J Radiol*. 2022;148:110164. doi:10.1016/j.ejrad.2022.110164
84. Paterson I, Ramanathan K, Aurora R, et al. Long COVID-19: A primer for cardiovascular health professionals, on behalf of the CCS Rapid Response Team. *Can J Cardiol*. 2021;37(8):1260–1262. doi:10.1016/j.cjca.2021.05.011
85. Tudoran C, Tudoran M, Cut TG, et al. Evolution of echocardiographic abnormalities identified in previously healthy individuals recovering from COVID-19. *J Pers Med*. 2022;12(1):46. doi:10.3390/jpm12010046
86. Borlotti A, Thomaides-Brears H, Georgiopoulos G, et al. The additive value of cardiovascular magnetic resonance in convalescent COVID-19 patients. *Front Cardiovasc Med*. 2022;9:854750. doi:10.3389/fcvm.2022.854750
87. Mancia G, Rea F, Ludergnani M, Apolone G, Corrao G. Renin-angiotensin-aldosterone system blockers and the risk of Covid-19. *N Engl J Med*. 2020;382(25):2431–2440. doi:10.1056/NEJMoa2006923
88. Hu J, Zhang X, Zhang X, et al. COVID-19 is more severe in patients with hypertension: ACEI/ARB treatment does not influence clinical severity and outcome. *J Infect*. 2020;81(6):979–997. doi:10.1016/j.jinf.2020.05.056
89. Lopes RD, Macedo AVS, De Barros E Silva PGM, et al. Continuing versus suspending angiotensin-converting enzyme inhibitors and angiotensin receptor blockers: Impact on adverse outcomes in hospitalized patients with severe acute respiratory syndrome coronavirus 2 (SARS-CoV-2). The BRACE CORONA Trial. *Am Heart J*. 2020;226:49–59. doi:10.1016/j.ahj.2020.05.002
90. Gao C, Cai Y, Zhang K, et al. Association of hypertension and antihypertensive treatment with COVID-19 mortality: A retrospective observational study. *Eur Heart J*. 2020;41(22):2058–2066. doi:10.1093/eurheartj/ehaa433
91. Charfeddine S, Ibn Hadjamor H, Torjmen S, et al. Sulodexide in the treatment of patients with long COVID 19 symptoms and endothelial dysfunction: The results of TUN-EndCOV study. *Arch Cardiovasc Dis Suppl*. 2022;14(1):127. doi:10.1016/j.acvdsp.2021.10.007
92. Wang C, Yu C, Jing H, et al. Long COVID: The nature of thrombotic sequelae determines the necessity of early anticoagulation. *Front Cell Infect Microbiol*. 2022;12:861703. doi:10.3389/fcimb.2022.861703
93. Pretorius E, Venter C, Laubscher GJ, et al. Prevalence of symptoms, comorbidities, fibrin amyloid microclots and platelet pathology in individuals with long COVID/post-acute sequelae of COVID-19 (PASC). *Cardiovasc Diabetol*. 2022;21(1):148. doi:10.1186/s12933-022-01579-5

# Application of machine learning in predicting frailty syndrome in patients with heart failure

Remigiusz Szczepanowski[1,A,C–F], Izabella Uchmanowicz[2,3,A,C–F], Aleksandra H. Pasieczna-Dixit[4,A,C–F], Janusz Sobecki[1,C,D], Radosław Katarzyniak[1,C,D], Grzegorz Kołaczek[1,C,D], Wojciech Lorkiewicz[1,C,D], Maja Kędras[1,C,D], Anant Dixit[1,C,D], Jan Biegus[3,5,C,D], Marta Wleklik[2,3,C,D], Robbert J.J. Gobbens[6,7,C,D], Loreena Hill[8,C,D], Tiny Jaarsma[9,C,D], Amir Hussain[10,C,D], Mario Barbagallo[11,C,D], Nicola Veronese[11,C,D], Francesco C. Morabito[12,C,D], Aleksander Kahsin[13,C,D]

[1] Department of Computer Science and Systems Engineering, Wroclaw University of Science and Technology, Poland
[2] Department of Nursing and Obstetrics, Faculty of Health Sciences, Wroclaw Medical University, Poland
[3] Institute of Heart Diseases, University Hospital, Wrocław, Poland
[4] Socio-Economic Department, Pomeranian Higher School, Starogard Gdański, Poland
[5] Institute for Heart Diseases, Wroclaw Medical University, Poland
[6] Faculty of Health, Sports and Social Work, Inholland University of Applied Sciences, Amsterdam, the Netherlands
[7] Zonnehuisgroep Amstelland, Amstelveen, the Netherlands
[8] Department Family Medicine and Population Health, Faculty of Medicine and Health Sciences, University of Antwerp, Belgium
[9] Tranzo, Tilburg University, the Netherlands
[10] School of Computing, Edinburgh Napier University, UK
[11] Geriatric Unit, Department of Internal Medicine and Geriatrics, University of Palermo, Italy
[12] Mediterranea University of Reggio Calabria (DICEAM), Italy
[13] Faculty of Medicine, Medical University of Gdansk, Poland

A – research concept and design; B – collection and/or assembly of data; C – data analysis and interpretation;
D – writing the article; E – critical revision of the article; F – final approval of the article

Advances in Clinical and Experimental Medicine, ISSN 1899–5276 (print), ISSN 2451–2680 (online) *Adv Clin Exp Med*. 2024;33(3):309–315

**Address for correspondence**
Izabella Uchmanowicz
E-mail: izabella.uchmanowicz@umw.edu.pl

**Funding sources**
This research was partially funded by the National Science Centre (Poland) under grant No. 2021/41/B/NZ7/01698.

**Conflict of interest**
None declared

Received on August 20, 2023
Reviewed on January 30, 2024
Accepted on February 13, 2024

Published online on March 26, 2024

## Abstract

Prevention and diagnosis of frailty syndrome (FS) in patients with heart failure (HF) require innovative systems to help medical personnel tailor and optimize their treatment and care. Traditional methods of diagnosing FS in patients could be more satisfactory. Healthcare personnel in clinical settings use a combination of tests and self-reporting to diagnose patients and those at risk of frailty, which is time-consuming and costly. Modern medicine uses artificial intelligence (AI) to study the physical and psychosocial domains of frailty in cardiac patients with HF. This paper aims to present the potential of using the AI approach, emphasizing machine learning (ML) in predicting frailty in patients with HF. Our team reviewed the literature on ML applications for FS and reviewed frailty measurements applied to modern clinical practice. Our approach analysis resulted in recommendations of ML algorithms for predicting frailty in patients. We also present the exemplary application of ML for FS in patients with HF based on the Tilburg Frailty Indicator (TFI) questionnaire, taking into account psychosocial variables.

**Key words:** heart failure, medical personnel, machine learning, frailty syndrome, artificial intelligence

**DOI**
10.17219/acem/184040



**Cite as**
Szczepanowski R, Uchmanowicz I, Pasieczna AH, et al. Application of machine learning in predicting frailty syndrome in patients with heart failure. *Adv Clin Exp Med*. 2024;33(3):309–315. doi:10.17219/acem/184040

# Introduction

Frailty syndrome (FS) is broadly defined as the premature or abnormal aging of elderly patients, indicated by a set of symptoms associated with a higher risk of mortality, lower quality of life and increased healthcare utilization.[1,2] Understanding the contributions of physical, social or psychological factors in the prevalence of frailty is an important research problem in contemporary medicine. Addressing this challenge should result in novel frailty measurements that help healthcare personnel promptly indentify and optimally manage patients with FS.

In clinical literature, frailty is often associated with terms such as weakness and fatigue.[3] Most definitions consider frailty to be a clinically recognizable condition resulting from aging that reduces the ability to cope with daily or severe stressors.[4] However, frailty is also linked to post-surgery complications and other consequences of stress associated with prolonged hospitalization and the risk of death.[5] Until recently, the frailty concept was defined as closely linked to old age, but there are indications that younger patients can also develop this syndrome.[6,7]

Frailty is an increasingly well-recognized clinical syndrome in cardiology that extends beyond the physiological aging process and commonly co-occurs with many cardiovascular diseases as disease-related frailty.[7] Frailty is more common in patients with heart failure (HF) than in the general population.[8] Heart failure is a clinical syndrome in which the heart is not able to pump enough blood to meet the demand of the body. The condition leads to symptoms (e.g., dyspnea, swelling in the ankles and fatigue) that may be accompanied by signs (e.g., elevated jugular venous pressure, pulmonary crackles and peripheral edema) The number of patients with HF is increasing due to the aging of the population and the therapeutic advancements that improve the survival of patients with heart disease.[7]

The prevalence of FS in patients with HF is approx. 45%.[9] The Cardiovascular Health Study showed that frailty is significantly associated with HF, affecting 1 in 2 adults, independent of age or the New York Heart Association (NYHA) classification.[10,11] A diagnosis of HF indicates the additional loss of biological reserves and increased vulnerability to several adverse clinical consequences.[12] Frailty increases the risk of HF and, in patients already diagnosed, contributes to increased mortality, rehospitalization and decreased quality of life.[13–16] The clinical identification of frailty can play an important role in developing preventive strategies against age-related conditions. Stressors that may affect a patient with frailty, and may predispose the patient to adverse health consequences, as well as lend themselves to modification or control, are divided into 4 groups: clinical, physical-functional, psychological, and social. These stressors can be clinical or non-clinical, acute or chronic, reversible or irreversible, and require supportive care.[8]

# Objectives

This paper presents the potential of using an artificial intelligence (AI) approach, specifically machine learning (ML), to predict frailty in patients with HF.

## Measurement instruments of frailty

There are several measures to diagnose frailty and identify the potential risk of developing FS. These measures differ in their approach to detecting frailty, which is historically consistent with the long-discussed ambiguity in effectively operationalizing the definition of FS.[17] The operationalization of FS focuses on the accumulation of deficits or embraces multidimensionality of the FS. The first approach assumes that more health deficits indicate higher frailty.[18,19] On the contrary, the multidimensional approach describes frailty as a dynamic state affecting an individual who experiences losses in 1 or more domains of human functioning (physical, psychological, social).[19] Here, we present selected frailty measures based on either deficit's accumulation or multidimensional approaches[19]:

- The Tilburg Frailty Indicator (TFI) is a self-report questionnaire that consists of 15 questions related to physical, psychological and social deficits to identify frailty.[20] The TFI measures losses caused by the influence of a range of variables, and losses which increase the risk of adverse outcomes.
- The Electronic Frailty Index (eFI) includes the diagnosis of 36 deficits (symptoms, diseases, disabilities, and abnormal laboratory results) to classify patients into 4 groups: no frailty, low frailty, moderate frailty, and high frailty.[21]
- The FI-CD index (Frailty Index based on Clinical Deficits, or Frailty Index of Cumulative Deficits) is based on clinical deficits, including at least 30 comorbidities, symptoms, diseases, and disabilities.[18]
- The frailty phenotype developed by Fried et al. includes the assessment of unintentional weight loss of over 5 kg in the past year, fatigue, lower grip strength, slower walking gait, and lower physical activity to classify older people.[22]
- The frailty Index based on Biomarkers (FI-B) is innovative but time-consuming and costly compared to the questionnaire-based approaches.[18]
- The Frailty Trait Scale (FTS) consists of 12 elements covering 7 dimensions: energy balance and nutrition, activity, nervous system, circulatory system, weakness, endurance, and slowing down.[23]
- A simplified FTS5 (based on 5 elements) was developed from the full FTS.[24]

The Heart Failure Association (HFA) of the European Society of Cardiology advocated that a holistic, multidimensional approach was more reliable than a physical approach only in identifying those patients with HF who have coexisting FS.[8] According to these assumptions, frailty in patients with HF should be defined as a multidimensional and dynamic condition independent of age, making

a person diagnosed with HF more vulnerable to stressors. As frailty in HF is viewed as a dynamic and partially reversible condition, recognizing those modifiable components is important to guide management and improve HF outcomes. Focusing on the reversible components of frailty in HF may reduce the risk of adverse clinical effects, such as increased morbidity, increased healthcare needs (hospitalization, prolonged recovery and institutionalization) and increased dependency and higher mortality risk.[8] Early recognition of frailty in older adults with HF is needed to target interventions to slow functional decline and improve patient-centered outcomes.

## Artificial intelligence in clinical decision-making

Artificial intelligence is gaining popularity and recognition as a feasible tool to support clinical decisions. There is a noticeable trend in the number of publications on AI in biomedicine, including topics such as living assistance, information processing, research, and the most urgent need in medicine: disease diagnostics and prediction.[25] Currently, the most popular AI method is ML, which is a particular subclass of AI methods. In short, ML is a data-driven approach which uses algorithms to learn, instead of using explicit programming, complex patterns from existing data and uses these patterns to make predictions on unseen data to make increasingly better decisions.[26] Support-vector machines (SVM) are one of the most popular options in the broadly understood medical applications,[27] whereas convolutional neural networks (CNN) are the most popular in the case of disease diagnosis.[28] Most cases of disease detection methods using AI are based on data in the form of diagnostic imaging,[27,29] and the 3 most common disorders detected are cardiovascular disease, sensory system disease and cancer.[29]

As noted, cardiology is at the forefront of AI applications in medicine. Machine learning is used in various parts of this field, and this connection is gaining popularity, which can be observed in the number of papers published on this subject.[30] Usage of AI includes echocardiography, nuclear cardiology, electrophysiology-enhanced diagnosis, prediction of treatment, and prognosis of disease development.[31] There is a great need to improve the algorithms for detecting patients at risk of hospital admission, apart from the possibility of analyzing patient data from devices such as pacemakers or smartwatches.[31] AI-based models for cardiology can also be divided by the type of task they are designed to perform, respectively: diagnosis, classification and prediction. Although the classification was presented as more challenging than the diagnosis, better results were obtained for this purpose. In contrast, the prediction task proved to be the most difficult and produced the worst outcomes, which may be due to the variety of factors that influence disease development and mortality.[32] The most frequently used models were neural networks (including deep and convolutional networks), obtaining the most accurate results. Among other valuable algorithms, we can distinguish Random Forest, Naïve Bayes, Support Vector Machines, k-Nearest Neighbors, and Gradient Boosting Machines.[32] It is also worth mentioning that during the COVID-19 pandemic, AI-supported cardiological research methods were developed that allowed for better medical examination, especially for patients infected with the coronavirus.[33]

Since frailty is an interdisciplinary issue, there is a need for multidisciplinary frailty definitions and their corresponding measures. Recent technological advances allow for much more extensive data to be collected, integrated and processed in a more complex way, resulting in a significant understanding of frailty. A recent approach to predict frailty is the application of ML. Machine learning algorithms are designed to apply ML to extract knowledge from available data.[34]

The explainable AI (XAI) approach could be considered a suitable method for dealing with frailty problems and evaluating the relations between different syndromes, which cannot be seen directly from separate questionnaires. The XAI facilitates the diagnosis and treatment of frailty as we can determine the importance of input features, enabling interpretation of the results obtained, dependencies between inputs and their values, and identification of data and concept drift. An example of such methods is tree-based algorithms applied in healthcare due to their property of explainability. Among all possibilities, XGBoost implementation can be considered a reasonable choice as it naturally deals with continuous, binary/discrete and missing data consistently.

## Benefits of applying ML in managing frail patients with HF

From a medical perspective, ML brings potential advantages in predicting FS. These potential benefits are following[35,36]:

- Employing an explainable ML model may help clinicians to gain new insight into the possible determinants of frailty. While some features are non-modifiable, e.g., age and height, other factors may be directly modifiable through lifestyle changes, physical exercise or cognitive stimulation (e.g., weight, smoking and mobility). As a result, it may be possible to ensure that a patient avoids reaching critical threshold values associated with frailty for some features. Conversely, those threshold values may be set as the targets to achieve a more stable state if engaging in rehabilitation.
- Facilitating a patient's diagnosis in the event of incomplete data about the patient (e.g., for a patient from another country or a patient who has not previously used medical services).
- Possibility of indicating significant relations between the frailty variables. Many frailty measures are based on highly correlated variables (e.g., see the Frailty Index (FI) of FI-CD measure). As indicated above, frailty includes dozens of measures, e.g., physical health, behavioral risks,

cognitive function, and mental health, which are also highly correlated (e.g., age and marital status). In practice, these measures do not provide new information important from the standpoint of frailty diagnosis. Machine learning algorithms can effectively identify the most representative associations between frailty variables. Here are the most prominent benefits for managing frail HF patients with a machine-learning approach:

- Developing a semi-open system with sufficient data, where AI system is screening patients based on specific diagnostic taxonomy with confidence intervals (frail status, pre-frail condition/endangered/healthy).
- Determination of diagnostic importance of frailty components and their contribution to the FS and other comorbid diseases (e.g., assessing the importance of frailty measures for frail patients with HF). For instance, one can target those who suffer from multiple diseases, e.g., frailty and hypertension. There may be synergy effects where co-existing diseases can be linked to an increased risk of the condition under study. This will probably be more specific for this subgroup than for both diseases separately (nonlinearity, in addition to the nonlinearity concerning age groups and gender). Subgroup-specific "diagnostic importance of variables" could be used to diagnose patients, for example, in precision and holistic medicine.
- Identification of the FS and its importance (see below) based on incomplete data. Healthcare professionals can benefit from this functionality when facing extensive historical data, as well as a shortage of resources.
- Panel data mining from long-term observation. Possibility to have a more advanced predictive model for prophylaxis (preventive care).
- Updating and expanding the AI systems by including existing clinical data and demographics of a given region and country.
- Possibility of screening pre-frail patients (non-binary output).
- Limiting human error caused by tiredness, subjectivity, abundance of data, or other factors.
- The AI system supports the selection of therapeutic strategies, i.e., personalization of multidisciplinary care in HF, building health literacy and patient empowerment, and personalization of educational recommendations for patients with HF and FS.
- The AI system provides support for multimorbid patients with FS in a modern, holistic manner. This allows patients to gain greater insight into their disease and improve their self-care.

## Applying ML algorithms to predict frailty

There are recent reports on applying ML algorithms to facilitate the integration of existing, traditional frailty diagnosis tools. For instance, one group used ML algorithms to develop predictive models for hospitalization, fracture occurrence, disability, and mortality as proxies for frailty.[37] In another work, different combinations of indicator variables were used to predict frailty with the results compared to eFI diagnoses.[38] Their results hinted that the support vector machines (SVM) outperformed k-nearest neighbors and the decision tree algorithms. The results of these studies were promising, but the number of explanatory variables used in the most effective SVM model was 70. The accuracy of this model was 93.5%, with a very promising Cohen's kappa index of 87%. At the same time, the models containing 10 and 11 explanatory variables turned out to be better than some of the more numerous explanatory variables of the models, which suggests significant possibilities of using various combinations of variables. However, this work only concerned patients over 75 years of age and did not focus on any specific disease.

In the context of frailty prediction, research on biomarkers has also been used to identify and classify patients with no frailty, risk of frailty and suffering from frailty.[39] These works highlight the effectiveness of ML methods to extract relevant information. The AI-based framework applies both supervised and non-supervised learning methods. Non-supervised learning is involved in the classification or grouping methods using, for example, k-means, k-nearest neighbors, decision tree algorithms, or other such as the stochastic gradient descent (SGD) or naïve Bayes classifiers applied depending on the size of data. Supervised learning uses the following methods: SVM, neural networks (NN), convolution neural networks (CNN), or other deep learning methods.

Our review also highlights several recent studies where AI, particularly ML algorithms like XGBoost and SVM, have shown effectiveness in frailty prediction using electronic medical records (EMRs), with evidence of high sensitivity and specificity.[38,40] These studies demonstrate the potential of AI to enhance the accuracy and efficiency of frailty screening compared to traditional methods.[38] Additionally, AI has been shown to improve the predictive performance of frailty indices in patients with HF, outperforming conventional models.[41,42]

Several recent studies have demonstrated the effectiveness of ML techniques in cardiovascular and ageing domains. A study utilized a gradient-boosting decision-tree method, showing the robustness of ML models in analyzing vascular function, cardiac motion and myocardial fibrosis, as well as conduction traits for cardiovascular ageing prediction.[43] Another research on ML algorithms for heart disease prediction highlighted how feature selection in ML models can enhance prediction accuracy, indicating that these models are capable of identifying and utilizing redundant information effectively.[44] Furthermore, a study using ML model demonstrated how ML techniques, including random forest models, can be employed to impute missing values in datasets.[45] This work identified a set of pre-frail indicators in middle-aged, community-dwelling adults. A recent work using SVM for identifying frailty in elderly individuals concluded that it is feasible

to use incomplete and imbalanced medical data for developing predictive models for FS. This not only reinforces the adaptability of ML models to diverse data conditions but also underscores their ability to discover potential predictive factors that are clinically relevant.[46] In summary, the application of ML in healthcare holds significant promise, particularly in understanding and addressing frailty conditions in aged individuals.

One of the main problems in ML methods application is appropriate data preparation and feature extraction. Data that will be used to feed AI-based FS prediction system can be divided into 2 main categories:

- Data that are possible to be joined, i.e., standard identifiers, are available => these are the data on which the analysis will be performed.
- Data that feed the model irrespective of patients => there are the data that will help create models and validate hypotheses.

We do not require a standard model for all patient-specific data on the level of data lakes. However, joining data from different sources should be feasible using known identifiers. While many AI methods have proven to be efficient, deep NN have shown remarkable improvements in big data marts and offer the best efficiency in many application areas. Most neural models, such as networks of simple non-linear, enable exchanging information via fixed connections, adapting simple parameters to learn vector mappings. However, complex neurons, microcircuits and small neural cortical ensembles with structural connections (fixed or slowly changing) can also be applied to model complex network states, which contain rich internal knowledge in modules interacting flexibly. The most straightforward model suitable for a given data and easy to handle should be used, as simpler models generalize better and are easier to interpret. A proper hybrid cloud approach should be considered to carry out efficient AI calculations. Some personal data points are susceptible and should not leave local infrastructure. Anonymization techniques should be utilized here, or maybe only data summaries should be processed in the cloud.[47]

## Predicting importance of frailty components in heart failure: Analysis of TFI measure

Our research team analyzed the diagnostic importance of individual psychosocial and physical criteria in the diagnosis of FS in elderly patients with HF.[48] Based on the AI approach and the TFI questionnaire, including physical, psychological and social components, ML models were constructed using a decision tree, random decision forest and AdaBoost classifier. These models were trained, validated and tested on 3 separated subsets of the full dataset.

To find the feature importance of the explanatory variables in ML classifying models, it was necessary to choose an appropriate method of evaluating these variables. The permutation method compares the accuracy of the model with its accuracy when we shuffle the values of specific variables. The procedure was performed separately for each of the 15 TFI explanatory variables, with many permutations. The calculations were made for 10,000 permutations and a single variable in our case. The greater the number of respondents (and their answers to a given TFI question) in the sample's subsets, the more permutations should be made to obtain more accurate results. Machine learning models were built and verified in a sample of patients with HF. To determine the diagnostic validity and verify the hypotheses, selected components of the physical domain were compared with all the psychological and social domain components within the TFI questionnaire.

The models with the highest classification accuracy were selected from the 3 ML algorithms, i.e., the random decision forest and the AdaBoost classifier (Table 1). The conducted ML analysis showed that none of the variables within the social domain was more diagnostically important than the physical variables (i.e., experiencing difficulties due to difficulties in walking, lack of strength in the hands and physical fatigue). In the case of psychological criteria for the diagnosis of FS, the variable related to irritability (i.e., feeling excited or nervous in the last month) was diagnostically more important than all considered physical variables, while the variable related to depressive mood (i.e., a decrease in mood in the previous month) was diagnostically more important than the physical variables: lack of strength in the hands and physical fatigue.

Table 1. Results from testing phase for selected machine learning (ML) – true positives and true negatives

| ML model | True positives | True negatives |
|---|---|---|
| Decision tree | 79.07 | 87.50 |
| Random forest | 93.02 | 100.00 |
| AdaBoost | 100.00 | 93.75 |

## Limitations

Our review has some limitations. First, from the perspective of model development, it is essential to generalize the frailty ML model to different healthcare settings and patient populations. Because the models were validated in a few studies and available datasets, the model's real-world applicability in clinical conditions may be limited. Second, our paper discusses some general aspects of feature selection and interpretability related to the ML approach. However, this review does not elaborate on the specific features, their combinations or how they relate to the frailty concept. Therefore, the interpretability of the chosen features and their clinical relevance may be a limitation. Additionally, whereas particular ML models of frailty show promising results in accuracy, it would be essential to examine their performance on independent datasets to validate practical claims rigorously. We also know

that the ML model's generalizability to a broader age range should be considered. The present work focuses on elderly patients, and the findings may not apply to younger patients with HF. Finally, the work suggests the potential benefits of using AI-based approaches in predicting frailty and the possibility of integrating these predictions into clinical practice. In fact, the real-world implementation of the frailty ML model and its acceptance by healthcare staff might be challenging.

# Conclusions

Identifying, interpreting and managing patients with both FS and HF requires a significant amount of information, resulting in a time-consuming and costly process. Artificial intelligence, specifically ML, can aid in parsing this data. Machine learning can be used to develop new diagnostic measurements of frailty and support research on improving classic measures, as well as addressing the theoretical issue of the operational definition of this clinical syndrome. These ML computations can aid in providing personalized care for patients at risk of the consequences of FS, improving diagnostic tools for examining this syndrome and facilitating effective collaboration between psychologists and healthcare professionals. This approach is applicable in holistic and patient-centered medicine, which requires knowledge from various disciplines to enable causal and symptomatic treatment while considering the patient's different domains of life and behavior. Future development should include a discussion on the compatibility of clinical patient data sources and privacy.

## ORCID iDs

Remigiusz Szczepanowski https://orcid.org/0000-0003-2989-2172
Izabella Uchmanowicz https://orcid.org/0000-0001-5452-0210
Aleksandra H. Pasieczna https://orcid.org/0000-0001-6867-3584
Janusz Sobecki https://orcid.org/0000-0001-7444-2627
Radosław Katarzyniak https://orcid.org/0000-0002-8941-9638
Grzegorz Kołaczek https://orcid.org/0000-0001-7125-0988
Wojciech Lorkiewicz https://orcid.org/0000-0002-4624-5180
Maja Kędras https://orcid.org/0000-0002-8306-8769
Anant Dixit https://orcid.org/0000-0001-8968-1938
Jan Biegus https://orcid.org/0000-0001-9977-7722
Marta Wleklik https://orcid.org/0000-0001-9574-4448
Robbert J.J. Gobbens https://orcid.org/0000-0003-0689-4191
Loreena Hill https://orcid.org/0000-0001-5232-0936
Tiny Jaarsma https://orcid.org/0000-0002-4197-4026
Amir Hussain https://orcid.org/0000-0002-8080-082X
Mario Barbagallo https://orcid.org/0000-0002-1349-6530
Francesco C. Morabito https://orcid.org/0000-0003-0734-9136
Aleksander Kahsin https://orcid.org/0000-0003-2802-4963

## References

1. Łęgosz P, Krzowski B, Płatek AE, et al. Zespół kruchości w gabinecie lekarza praktyka: O czym należy pamiętać? *Fol Cardiol*. 2018;13(2):137–143. doi:10.5603/FC.2018.0025
2. Vitale C, Jankowska E, Hill L, et al. Heart Failure Association of the European Society of Cardiology position paper on frailty in patients with heart failure. *Eur J Heart Fail*. 2019;21(11):1299–1305. doi:10.1002/ejhf.1611
3. Uchmanowicz I, Lisiak M, Jankowska-Polańska B. Research instruments used in the assessment of the frailty syndrome. *Gerontol Pol*. 2014;22(1):1–8. https://gerontologia.org.pl/wp-content/uploads/2016/05/2014-01-1.pdf. Accessed September 19, 2023.
4. Xue QL. The frailty syndrome: Definition and natural history. *Clin Geriatr Med*. 2011;27(1):1–15. doi:10.1016/j.cger.2010.08.009
5. Morley JE, Perry HM, Miller DK. Editorial: Something about frailty. *J Gerontol A Biol Sci Med Sci*. 2002;57(11):M698–M704. doi:10.1093/gerona/57.11.M698
6. Ness KK, Armstrong GT, Kundu M, Wilson CL, Tchkonia T, Kirkland JL. Frailty in childhood cancer survivors. *Cancer*. 2015;121(10):1540–1547. doi:10.1002/cncr.29211
7. McDonagh J, Ferguson C, Newton PJ. Frailty assessment in heart failure: An overview of the multi-domain approach. *Curr Heart Fail Rep*. 2018;15(1):17–23. doi:10.1007/s11897-018-0373-0
8. Uchmanowicz I, Łoboz-Rudnicka M, Szeląg P, Jankowska-Polańska B, Łoboz-Grudzień K. Frailty in heart failure. *Curr Heart Fail Rep*. 2014;11(3):266–273. doi:10.1007/s11897-014-0198-4
9. Chen MA. Frailty and cardiovascular disease: Potential role of gait speed in surgical risk stratification in older adults. *J Geriatr Cardiol*. 2015;12(1):44–56. doi:10.11909/j.issn.1671-5411.2015.01.006
10. Vitale C, Spoletini I, Rosano GM. Frailty in heart failure: Implications for management. *Card Fail Rev*. 2018;4(2):104. doi:10.15420/cfr.2018.22.2
11. Denfeld QE, Winters-Stone K, Mudd JO, Gelow JM, Kurdi S, Lee CS. The prevalence of frailty in heart failure: A systematic review and meta-analysis. *Int J Cardiol*. 2017;236:283–289. doi:10.1016/j.ijcard.2017.01.153
12. Bottle A, Kim D, Hayhoe B, et al. Frailty and co-morbidity predict first hospitalisation after heart failure diagnosis in primary care: Population-based observational study in England. *Age Ageing*. 2019;48(3):347–354. doi:10.1093/ageing/afy194
13. Wleklik M, Denfeld Q, Lisiak M, Czapla M, Kałużna-Oleksy M, Uchmanowicz I. Frailty syndrome in older adults with cardiovascular diseases: What do we know and what requires further research? *Int J Environ Res Public Health*. 2022;19(4):2234. doi:10.3390/ijerph19042234
14. Uchmanowicz I, Kuśnierz M, Wleklik M, Jankowska-Polańska B, Jaroch J, Łoboz-Grudzień K. Frailty syndrome and rehospitalizations in elderly heart failure patients. *Aging Clin Exp Res*. 2018;30(6):617–623. doi:10.1007/s40520-017-0824-6
15. Uchmanowicz I, Pasieczna AH, Wójta-Kempa M, et al. Physical, psychological and social frailty are predictive of heart failure: A cross-sectional study. *J Clin Med*. 2022;11(3):565. doi:10.3390/jcm11030565
16. Uchmanowicz I, Lee CS, Vitale C, et al. Frailty and the risk of all-cause mortality and hospitalization in chronic heart failure: A meta-analysis. *ESC Heart Fail*. 2020;7(6):3427–3437. doi:10.1002/ehf2.12827
17. Rodríguez-Mañas L, Féart C, Mann G, et al. Searching for an operational definition of frailty: A Delphi method based consensus statement. The Frailty Operative Definition-Consensus Conference Project. *J Gerontol A Biol Sci Med Sci*. 2013;68(1):62–67. doi:10.1093/gerona/gls119
18. Mitnitski A, Collerton J, Martin-Ruiz C, et al. Age-related frailty and its association with biological markers of ageing. *BMC Med*. 2015;13(1):161. doi:10.1186/s12916-015-0400-x
19. Dent E, Kowal P, Hoogendijk EO. Frailty measurement in research and clinical practice: A review. *Eur J Intern Med*. 2016;31:3–10. doi:10.1016/j.ejim.2016.03.007
20. Gobbens RJJ, Van Assen MALM, Luijkx KG, Wijnen-Sponselee MTh, Schols JMGA. The Tilburg Frailty Indicator: Psychometric properties. *J Am Med Dir Assoc*. 2010;11(5):344–355. doi:10.1016/j.jamda.2009.11.003
21. Clegg A, Bates C, Young J, et al. Development and validation of an electronic frailty index using routine primary care electronic health record data. *Age Ageing*. 2016;45(3):353–360. doi:10.1093/ageing/afw039
22. Fried LP, Tangen CM, Walston J, et al. Frailty in older adults: Evidence for a phenotype. *J Gerontol A Biol Sci Med Sci*. 2001;56(3):M146–M157. doi:10.1093/gerona/56.3.M146
23. García-García FJ, Carcaillon L, Fernandez-Tresguerres J, et al. A new operational definition of frailty: The Frailty Trait Scale. *J Am Med Dir Assoc*. 2014;15(5):371.e7–371.e13. doi:10.1016/j.jamda.2014.01.004

24. García-García FJ, Carnicero JA, Losa-Reyna J, et al. Frailty Trait Scale–Short Form: A frailty instrument for clinical practice. *J Am Med Dir Assoc*. 2020;21(9):1260–1266.e2. doi:10.1016/j.jamda.2019.12.008
25. Rong G, Mendez A, Bou Assi E, Zhao B, Sawan M. Artificial intelligence in healthcare: Review and prediction case studies. *Engineering*. 2020;6(3):291–301. doi:10.1016/j.eng.2019.08.015
26. Huyen C. *Designing Machine Learning Systems: An Iterative Process for Production-Ready Applications*. Sebastopol, USA: O'Reilly Media, Inc; 2022. ISBN:978-1-09-810796-3.
27. Jiang F, Jiang Y, Zhi H, et al. Artificial intelligence in healthcare: Past, present and future. *Stroke Vasc Neurol*. 2017;2(4):230–243. doi:10.1136/svn-2017-000101
28. Shen J, Zhang CJP, Jiang B, et al. Artificial intelligence versus clinicians in disease diagnosis: Systematic review. *JMIR Med Inform*. 2019;7(3):e10010. doi:10.2196/10010
29. Komal, Sethi GK, Ahmad N, Rehman MB, Ibrahim Dafallaa HME, Rashid M. Use of artificial intelligence in healthcare systems: State-of-the-art survey. In: 2021 2nd International Conference on Intelligent Engineering and Management (ICIEM). London, UK: IEEE; 2021:243–248. doi:10.1109/ICIEM51511.2021.9445391
30. Marques De Souza Filho E, De Amorim Fernandes F, Lacerda De Abreu Soares C, et al. Artificial intelligence in cardiology: Concepts, tools and challenges (The horse is the one who runs, you must be the jockey). *ABC Cardiol*. 2019;114(4):718–725. doi:10.36660/abc.20180431
31. Lopez-Jimenez F, Attia Z, Arruda-Olson AM, et al. Artificial intelligence in cardiology: Present and future. *Mayo Clin Proc*. 2020;95(5):1015–1039. doi:10.1016/j.mayocp.2020.01.038
32. Seckanovic A, Sehovac M, Spahic L, et al. Review of artificial intelligence application in cardiology. In: 2020 9th Mediterranean Conference on Embedded Computing (MECO). Budva, Montenegro: IEEE; 2020:1–5. doi:10.1109/MECO49872.2020.9134333
33. Haleem A, Javaid M, Singh RP, Suman R. Applications of artificial intelligence (AI) for cardiology during COVID-19 pandemic. *Sustainable Operations and Computers*. 2021;2:71–78. doi:10.1016/j.susoc.2021.04.003
34. Marr B. What is the difference between artificial intelligence and machine learning. *Forbes*. December 6, 2016. https://www.forbes.com/sites/bernardmarr/2016/12/06/what-is-the-difference-between-artificial-intelligence-and-machine-learning/. Accessed September 19, 2023.
35. Iniesta R, Stahl D, McGuffin P. Machine learning, statistical learning and the future of biological research in psychiatry. *Psychol Med*. 2016;46(12):2455–2465. doi:10.1017/S0033291716001367
36. Mijwil M. Artificial neural networks advantages and disadvantages. *LinkedIn*. January 27, 2018. www.linkedin.com/pulse/artificial-neural-networks-advantages-disadvantages-maad-m-mijwel/. Accessed September 19, 2023.
37. Tarekegn A, Ricceri F, Costa G, Ferracin E, Giacobini M. Predictive modeling for frailty conditions in elderly people: Machine learning approaches. *JMIR Med Inform*. 2020;8(6):e16678. doi:10.2196/16678
38. Ambagtsheer RC, Shafiabady N, Dent E, Seiboth C, Beilby J. The application of artificial intelligence (AI) techniques to identify frailty within a residential aged care administrative data set. *Int J Med Inform*. 2020;136:104094. doi:10.1016/j.ijmedinf.2020.104094
39. Gomez-Cabrero D, Walter S, Abugessaisa I, et al. A robust machine learning framework to identify signatures for frailty: A nested case-control study in four aging European cohorts. *GeroScience*. 2021;43(3):1317–1329. doi:10.1007/s11357-021-00334-0
40. Aponte-Hao S, Wong ST, Thandi M, et al. Machine learning for identification of frailty in Canadian primary care practices. *Int J Popul Data Sci*. 2021;6(1):1650. doi:10.23889/ijpds.v6i1.1650
41. Ju C, Zhou J, Lee S, et al. Derivation of an electronic frailty index for predicting short-term mortality in heart failure: A machine learning approach. *ESC Heart Fail*. 2021;8(4):2837–2845. doi:10.1002/ehf2.13358
42. Tohyama T, Ide T, Ikeda M, et al. Machine learning-based model for predicting 1 year mortality of hospitalized patients with heart failure. *ESC Heart Fail*. 2021;8(5):4077–4085. doi:10.1002/ehf2.13556
43. Shah M, De A. Inácio MH, Lu C, et al. Environmental and genetic predictors of human cardiovascular ageing. *Nat Commun*. 2023;14(1):4941. doi:10.1038/s41467-023-40566-6
44. Noroozi Z, Orooji A, Erfannia L. Analyzing the impact of feature selection methods on machine learning algorithms for heart disease prediction. *Sci Rep*. 2023;13(1):22588. doi:10.1038/s41598-023-49962-w
45. Sajeev S, Champion S, Maeder A, Gordon S. Machine learning models for identifying pre-frailty in community dwelling older adults. *BMC Geriatr*. 2022;22(1):794. doi:10.1186/s12877-022-03475-9
46. Hassler AP, Menasalvas E, García-García FJ, Rodríguez-Mañas L, Holzinger A. Importance of medical data preprocessing in predictive modeling and risk factor discovery for the frailty syndrome. *BMC Med Inform Decis Mak*. 2019;19(1):33. doi:10.1186/s12911-019-0747-6
47. Rithani M, Kumar RP, Doss S. A review on big data based on deep neural network approaches. *Artif Intell Rev*. 2023;56(12):14765–14801. doi:10.1007/s10462-023-10512-5
48. Pasieczna AH, Szczepanowski R, Sobecki J, et al. Importance analysis of psychosociological variables in frailty syndrome in heart failure patients using machine learning approach. *Sci Rep*. 2023;13(1):7782. doi:10.1038/s41598-023-35037-3